



# Aero-Thermal Calibration of the NASA Glenn Icing Research Tunnel (2004 and 2005 Tests)

*E. Allen Arrington and Christine M. Pastor  
Sierra Lobo, Inc., Cleveland, Ohio*

*Jose C. Gonzalez and Monroe R. Curry III  
QSS Group, Inc., Cleveland, Ohio*

## NASA STI Program . . . in Profile

Since its founding, NASA has been dedicated to the advancement of aeronautics and space science. The NASA Scientific and Technical Information (STI) program plays a key part in helping NASA maintain this important role.

The NASA STI Program operates under the auspices of the Agency Chief Information Officer. It collects, organizes, provides for archiving, and disseminates NASA's STI. The NASA STI program provides access to the NASA Aeronautics and Space Database and its public interface, the NASA Technical Reports Server, thus providing one of the largest collections of aeronautical and space science STI in the world. Results are published in both non-NASA channels and by NASA in the NASA STI Report Series, which includes the following report types:

- **TECHNICAL PUBLICATION.** Reports of completed research or a major significant phase of research that present the results of NASA programs and include extensive data or theoretical analysis. Includes compilations of significant scientific and technical data and information deemed to be of continuing reference value. NASA counterpart of peer-reviewed formal professional papers but has less stringent limitations on manuscript length and extent of graphic presentations.
- **TECHNICAL MEMORANDUM.** Scientific and technical findings that are preliminary or of specialized interest, e.g., quick release reports, working papers, and bibliographies that contain minimal annotation. Does not contain extensive analysis.
- **CONTRACTOR REPORT.** Scientific and technical findings by NASA-sponsored contractors and grantees.

- **CONFERENCE PUBLICATION.** Collected papers from scientific and technical conferences, symposia, seminars, or other meetings sponsored or cosponsored by NASA.
- **SPECIAL PUBLICATION.** Scientific, technical, or historical information from NASA programs, projects, and missions, often concerned with subjects having substantial public interest.
- **TECHNICAL TRANSLATION.** English-language translations of foreign scientific and technical material pertinent to NASA's mission.

Specialized services also include creating custom thesauri, building customized databases, organizing and publishing research results.

For more information about the NASA STI program, see the following:

- Access the NASA STI program home page at <http://www.sti.nasa.gov>
- E-mail your question via the Internet to [help@sti.nasa.gov](mailto:help@sti.nasa.gov)
- Fax your question to the NASA STI Help Desk at 443-757-5803
- Telephone the NASA STI Help Desk at 443-757-5802
- Write to:  
NASA Center for AeroSpace Information (CASI)  
7115 Standard Drive  
Hanover, MD 21076-1320



# Aero-Thermal Calibration of the NASA Glenn Icing Research Tunnel (2004 and 2005 Tests)

*E. Allen Arrington and Christine M. Pastor  
Sierra Lobo, Inc., Cleveland, Ohio*

*Jose C. Gonzalez and Monroe R. Curry III  
QSS Group, Inc., Cleveland, Ohio*

Prepared under Contracts NAS3-00145 and NNC05CA95C

National Aeronautics and  
Space Administration

Glenn Research Center  
Cleveland, Ohio 44135

*Level of Review:* This material has been technically reviewed by expert reviewer(s).

Available from

NASA Center for Aerospace Information  
7115 Standard Drive  
Hanover, MD 21076-1320

National Technical Information Service  
5301 Shawnee Road  
Alexandria, VA 22312

Available electronically at <http://gltrs.grc.nasa.gov>

# Contents

Summary .....	1
Introduction.....	1
Symbols .....	2
Subscripts .....	3
Description of Facility .....	4
Test Hardware, Instrumentation and Data Systems .....	5
9-ft Survey Rake.....	5
2-D RTD Array.....	8
Facility Instrumentation .....	10
Steady-State Data Acquisition System.....	11
Thermal Anemometry Instrumentation .....	11
Test Procedures and Execution .....	12
Test Matrix .....	12
Test Procedures .....	13
Data Reduction and Analysis.....	15
Facility Instrumentation .....	15
9-ft Survey Rake Calculations.....	16
Basic Flow Parameters.....	16
Flow Angularity .....	17
Turbulence Intensity.....	18
2-D RTD Array Calculations.....	20
Measurement and Data Uncertainty .....	20
Data Analysis .....	20
Discussion of Results.....	21
Aero-Thermal Calibration Curves.....	21
Updates Based on 2004 Calibration Test .....	21
Inputs to IRTAT .....	22
Test Section Conditions; Calibrated Values.....	23
Test Section Conditions; Calculated Values .....	24
Updates Based on 2005 Interim Calibration .....	24
Aero-Thermal Flow Quality Data .....	24
Total Pressure.....	25
Mach Number.....	32
Total Temperature.....	32
Flow Angularity .....	55
Turbulence .....	55
Summary of Test Results .....	70
Recommendations.....	70
Appendix A.—Uncertainty Estimates.....	71
A.1 General Uncertainty Analysis .....	71
A.2 Hardware RTD Temperature Uncertainty.....	71
A.3 Hardware Pressure Uncertainty .....	72
A.3.1 Total Pressure.....	72
A.3.2 Dynamic Pressure .....	73
A.3.3 Static Pressure .....	74
A.4 Airspeed Calculations .....	74
A.5 Mach Number Calculations .....	76
A.6 Flow Angle Calculations.....	76

Appendix B.—RTD Probe Flow Recovery Coefficients.....	79
Appendix C.—Calculated Test Section Conditions.....	81
Appendix D.—2005 Interim Aero-Thermal Calibration of the IRT.....	83
D.1 Total Temperature Calibration.....	84
D.2 Flow Quality Comparison.....	85
D.3 Calibration Curve Comparison.....	87
References.....	115

## List of Tables

Table 1.—Test matrix for the IRT aero-thermal calibration using the 9-ft survey rake (2004 test).....	12
Table 2.—Temperature calibration test matrix using the 2–D RTD array (2004 test). .....	13
Table 3.—Typical test conditions in the IRT during the 9-ft survey rake testing as part of the 2004 aero-thermal calibration .....	14
Table 4.—Aero-thermal flow quality goals for an icing tunnel test section.....	25
Table A.1.—RTD total temperature probe system component uncertainties. ....	72
Table A.2.—Total Pressure Component Bias uncertainties.....	72
Table A.3.—Total Pressure Component Precision uncertainties.....	73
Table A.4.—Facility Uncertainties.....	77
Table B.1.—Flow recovery correction coefficients for the RTD probes mounted on the 2–D RTD Arra.....	79
Table C.1.—Summary of the parameters used to determine the test section aero-thermal conditions in the IRT.....	82
Table D.1.—Test matrix for the IRT aero-thermal calibration using the 9-ft survey rake (2005 interim calibration). .....	83
Table D.2.—Temperature calibration test matrix using the 2–D RTD array (2005 interim calibration). .....	84
Table D.3.—General equation and curve fit coefficients used in the calculation of the calibrated test section total temperature.....	85

## List of Figures

Figure 1.—Layout of the NASA Glenn Icing Research Tunnel.....	4
Figure 2.—Installation photo of the replacement inlet guide vanes (IGV) upstream of the IRT drive fan.....	5
Figure 3.—Photograph of the 9-ft horizontal survey rake installed in the IRT test section. ....	6
Figure 4.—Plan view of the IRT test section showing the installed location of the 9-ft survey rake.....	6
Figure 5.—Plan and elevation views of the 9-ft survey rake.....	7
Figure 6.—Cross section of the 9-ft survey rake showing flow probes details. ....	7
Figure 7.—Details of RTD probes used on the 2–D RTD array (dimensions in inches).....	8
Figure 8.—7x7 grid arrangement of the RTD probes in the IRT test section.....	9
Figure 9.—RTD Array installed in the IRT test section. (a) View looking downstream. (b) View looking upstream. ....	9
Figure 10.—RTD array vertical member cross sectional details.....	10
Figure 11.—Typical total temperature flow recovery curve for the 2–D RTD array probes.....	10
Figure 12.—Total temperature flow recovery data for RTD probes 1 through 23 with average curve fit. ....	10
Figure 13.—Layout of the RTD probes mounted on the D corner turning vanes.....	11
Figure 14.—Schematic depicting terminology on one wire of X probe.....	19

Figure 15.—Aero-thermal calibration curves based on the 2004 full calibration test .....	22
Figure 16.—Total pressure distribution data from the IRT test section. Data collected using the 9-ft survey rake mounted at 11 vertical positions over several tunnel runs. The test section total pressure data is normalized using the bellmouth total pressure measurement. Data from the 66-in. vertical position has been omitted due to boundary layer influence. Each y-axis grid (0.0002 total pressure ratio) represents approximately 0.003 psia. (a) $U_{ts}=50$ mph (43 knots), $P_{air}=0$ psig. (b) $U_{ts}=50$ mph (43 knots), $P_{air}=70$ psig. (c) $U_{ts}=100$ mph (87 knots), $P_{air}=0$ psig. (d) $U_{ts}=100$ mph (87 knots), $P_{air}=70$ psig. ....	26
Figure 16.—Continued. (e) $U_{ts}=115$ mph (100 knots), $P_{air}=0$ psig. (f) $U_{ts}=115$ mph (100 knots), $P_{air}=70$ psig. (g) $U_{ts}=150$ mph (130 knots), $P_{air}=0$ psig. (h) $U_{ts}=150$ mph (130 knots), $P_{air}=70$ psig. ....	27
Figure 16.—Continued. (i) $U_{ts}=175$ mph (152 knots), $P_{air}=0$ psig. (j) $U_{ts}=175$ mph (152 knots), $P_{air}=5$ psig. (k) $U_{ts}=175$ mph (152 knots), $P_{air}=20$ psig. (l) $U_{ts}=175$ mph (152 knots), $P_{air}=70$ psig. ....	28
Figure 16.—Continued. (m) $U_{ts}=200$ mph (174 knots), $P_{air}=0$ psig. (n) $U_{ts}=200$ mph (174 knots), $P_{air}=70$ psig. (o) $U_{ts}=250$ mph (217 knots), $P_{air}=0$ psig. (p) $U_{ts}=250$ mph (217 knots), $P_{air}=70$ psig. ....	29
Figure 16.—Continued. (q) $U_{ts}=225$ mph (195 knots), $P_{air}=0$ psig. (r) $U_{ts}=225$ mph (195 knots), $P_{air}=20$ psig (no $z=36$ -in. vertical position data). (s) $U_{ts}=225$ mph (195 knots), $P_{air}=70$ psig. ....	30
Figure 16.—Concluded. (t) $U_{ts}=300$ mph (261 knots), $P_{air}=0$ psig. (u) $U_{ts}=300$ mph (261 knots), $P_{air}=70$ psig. (v) $U_{ts}=350$ mph (304 knots), $P_{air}=0$ psig. (w) $U_{ts}=350$ mph (304 knots), $P_{air}=70$ psig. ....	31
Figure 17.—Mach number distribution data from the IRT test section. Data collected using the 9-ft survey rake mounted at 11 vertical positions over several tunnel runs. The test section Mach number data was normalized using the bellmouth Mach number measurement. Data from the 66-in. vertical position was been omitted due to boundary layer influence. Approximate Mach number delta is indicated for each test section setting. ( a) $U_{ts}=50$ mph, $M_{ts}=0.066$ , $P_{air}=0$ psig. (b) $U_{ts}=50$ mph, $M_{ts}=0.066$ , $P_{air}=70$ psig. (c) $U_{ts}=100$ mph, $M_{ts}=0.133$ , $P_{air}=0$ psig. (d) $U_{ts}=100$ mph, $M_{ts}=0.133$ , $P_{air}=70$ psig. ....	33
Figure 17.—Continued. (e) $U_{ts}=115$ mph, $M_{ts}=0.152$ , $P_{air}=0$ psig. (f) $U_{ts}=115$ mph, $M_{ts}=0.152$ , $P_{air}=70$ psig. (g) $U_{ts}=150$ mph, $M_{ts}=0.199$ , $P_{air}=0$ psig. (h) $U_{ts}=150$ mph, $M_{ts}=0.199$ , $P_{air}=70$ psig. ....	34
Figure 17.—Continued. (i) $U_{ts}=175$ mph, $M_{ts}=0.232$ , $P_{air}=0$ psig. (j) $U_{ts}=175$ mph, $M_{ts}=0.232$ , $P_{air}=5$ psig. (k) $U_{ts}=175$ mph, $M_{ts}=0.232$ , $P_{air}=20$ psig. (l) $U_{ts}=175$ mph, $M_{ts}=0.232$ , $P_{air}=70$ psig. ....	35
Figure 17.—Continued. (m) $U_{ts}=200$ mph, $M_{ts}=0.265$ , $P_{air}=0$ psig. (n) $U_{ts}=200$ mph, $M_{ts}=0.265$ , $P_{air}=70$ psig. (o) $U_{ts}=250$ mph, $M_{ts}=0.332$ , $P_{air}=0$ psig. (p) $U_{ts}=250$ mph, $M_{ts}=0.332$ , $P_{air}=70$ psig. ....	36
Figure 17.—Continued. (q) $U_{ts}=225$ mph, $M_{ts}=0.305$ , $P_{air}=0$ psig. (r) $U_{ts}=225$ mph, $M_{ts}=0.265$ , $P_{air}=20$ psig. (s) $U_{ts}=225$ mph, $M_{ts}=0.305$ , $P_{air}=70$ psi. ....	37
Figure 17.—Concluded. (t) $U_{ts}=300$ mph, $M_{ts}=0.399$ , $P_{air}=0$ psig. (u) $U_{ts}=300$ mph, $M_{ts}=0.399$ , $P_{air}=70$ psig. (v) $U_{ts}=350$ mph, $M_{ts}=0.464$ , $P_{air}=0$ psig. (w) $U_{ts}=350$ mph, $M_{ts}=0.464$ , $P_{air}=70$ psig. ....	38
Figure 18.—Total temperature distribution along the D-corner turning vanes as measured by the D-corner RTD probes. See Figure 13 for location of probes relative to the heat exchanger. (a) $T_{T,davg}>4$ °C. (b) $-0.5>T_{T,davg}>-3$ °C. (c) $-3>T_{T,davg}>-9$ °C. ....	40
Figure 18.—Concluded. (d) $-11>T_{T,davg}>-22$ °C. (e) $-22>T_{T,davg}>-31$ °C. ....	41
Figure 19.—IRT test section total temperature distribution data collected using the 2-D RTD Array (a) $U_{ts}=50.1$ mph (43.5 knots), $T_{T,davg}=4.3$ °C, $P_{air}=0$ psig. (b) $U_{ts}=50.4$ mph (43.8 knots), $T_{T,davg}=5.2$ °C, $P_{air}=70$ psig. (c) $U_{ts}=50.6$ mph (44.0 knots), $T_{T,davg}=0.2$ °C, $P_{air}=0$ psig. (d) $U_{ts}=50.5$ mph (43.9 knots), $T_{T,davg}=0.2$ °C, $P_{air}=70$ psig. ....	42

Figure 19.—Continued. (e) $U_{ts}=50.4$ mph (43.8 knots), $T_{T,davg}=-5.4$ °C, $P_{air}=0$ psig. (f) $U_{ts}=49.9$ mph (43.3 knots), $T_{T,davg}=-5.3$ °C, $P_{air}=70$ psig. (g) $U_{ts}=49.9$ mph (43.4 knots), $T_{T,davg}=-17.6$ °C, $P_{air}=0$ psig. (h) $U_{ts}=49.9$ mph (43.4 knots), $T_{T,davg}=-17.6$ °C, $P_{air}=70$ psig.....	43
Figure 19.—Continued. (i) $U_{ts}=50.0$ mph (43.5 knots), $T_{T,davg}=-29.7$ °C, $P_{air}=0$ psig. (j) $U_{ts}=50.2$ mph (43.7 knots), $T_{T,davg}=-29.6$ °C, $P_{air}=70$ psig. (k) $U_{ts}=115.6$ mph (100.5 knots), $T_{T,davg}=4.8$ °C, $P_{air}=0$ psig. (l) $U_{ts}=116.4$ mph (101.2 knots), $T_{T,davg}=5.3$ °C, $P_{air}=70$ psig.....	44
Figure 19.—Continued. (m) $U_{ts}=116.8$ mph (101.5 knots), $T_{T,davg}=1.3$ °C, $P_{air}=0$ psig. (n) $U_{ts}=116.5$ mph (101.2 knots), $T_{T,davg}=1.3$ °C, $P_{air}=70$ psig. (o) $U_{ts}=116.4$ mph (101.1 knots), $T_{T,davg}=-4.2$ °C, $P_{air}=0$ psig. (p) $U_{ts}=117.0$ mph (101.7 knots), $T_{T,davg}=-4.2$ °C, $P_{air}=70$ psig.....	45
Figure 19.—Continued. (q) $U_{ts}=116.8$ mph (101.5 knots), $T_{T,davg}=-16.4$ °C, $P_{air}=0$ psig. (r) $U_{ts}=116.7$ mph (101.4 knots), $T_{T,davg}=-16.4$ °C, $P_{air}=70$ psig. (s) $U_{ts}=116.6$ mph (101.3 knots), $T_{T,davg}=-28.4$ °C, $P_{air}=0$ psig. (t) $U_{ts}=116.4$ mph (101.2 knots), $T_{T,davg}=-28.6$ °C, $P_{air}=70$ psig.....	46
Figure 19.—Continued. (u) $U_{ts}=151.5$ mph (131.7 knots), $T_{T,davg}=2.1$ °C, $P_{air}=0$ psig. (v) $U_{ts}=151.8$ mph (131.9 knots), $T_{T,davg}=2.3$ °C, $P_{air}=70$ psig. (w) $U_{ts}=152.3$ mph (132.4 knots), $T_{T,davg}=-3.5$ °C, $P_{air}=0$ psig. (x) $U_{ts}=151.8$ mph (131.9 knots), $T_{T,davg}=-3.3$ °C, $P_{air}=70$ psig.....	47
Figure 19.—Continued. (y) $U_{ts}=152.2$ mph (132.3 knots), $T_{T,davg}=-15.4$ °C, $P_{air}=0$ psig. (z) $U_{ts}=151.6$ mph (131.6 knots), $T_{T,davg}=-15.6$ °C, $P_{air}=70$ psig. (aa) $U_{ts}=151.8$ mph (131.9 knots), $T_{T,davg}=-27.9$ °C, $P_{air}=0$ psig. (bb) $U_{ts}=152.5$ mph (132.5 knots), $T_{T,davg}=-27.7$ °C, $P_{air}=70$ psig.....	48
Figure 19.—Continued. (cc) $U_{ts}=233.1$ mph (202.5 knots), $T_{T,davg}=5.1$ °C, $P_{air}=0$ psig. (dd) $U_{ts}=234.8$ mph (204.0 knots), $T_{T,davg}=5.5$ °C, $P_{air}=70$ psig. (ee) $U_{ts}=233.9$ mph (203.3 knots), $T_{T,davg}=-0.4$ °C, $P_{air}=0$ psig. (ff) $U_{ts}=234.0$ mph (203.4 knots), $T_{T,davg}=-0.2$ °C, $P_{air}=70$ psig.....	49
Figure 19.—Continued. (gg) $U_{ts}=232.8$ mph (202.3 knots), $T_{T,davg}=-12.5$ °C, $P_{air}=0$ psig. (hh) $U_{ts}=232.7$ mph (202.2 knots), $T_{T,davg}=-12.5$ °C, $P_{air}=70$ psig. (ii) $U_{ts}=233.6$ mph (203.0 knots), $T_{T,davg}=-24.7$ °C, $P_{air}=0$ psig. (jj) $U_{ts}=232.5$ mph (202.0 knots), $T_{T,davg}=-24.7$ °C, $P_{air}=70$ psig.....	50
Figure 19.—Continued. (kk) $U_{ts}=254.7$ mph (221.3 knots), $T_{T,davg}=4.9$ °C, $P_{air}=0$ psig. (ll) $U_{ts}=254.5$ mph (221.2 knots), $T_{T,davg}=4.8$ °C, $P_{air}=70$ psig. (mm) $U_{ts}=253.9$ mph (220.6 knots), $T_{T,davg}=0.6$ °C, $P_{air}=0$ psig. (nn) $U_{ts}=253.7$ mph (220.5 knots), $T_{T,davg}=0.7$ °C, $P_{air}=70$ psig.....	51
Figure 19.—Continued. (oo) $U_{ts}=253.3$ mph (220.1 knots), $T_{T,davg}=-11.4$ °C, $P_{air}=0$ psig. (pp) $U_{ts}=253.3$ mph (219.9 knots), $T_{T,davg}=-11.3$ °C, $P_{air}=70$ psig. (qq) $U_{ts}=254.1$ mph (220.8 knots), $T_{T,davg}=-23.7$ °C, $P_{air}=0$ psig. (rr) $U_{ts}=252.9$ mph (219.7 knots), $T_{T,davg}=-23.7$ °C, $P_{air}=70$ psig.....	52
Figure 19.—Continued. (ss) $U_{ts}=304.7$ mph (264.8 knots), $T_{T,davg}=5.3$ °C, $P_{air}=0$ psig. (tt) $U_{ts}=304.6$ mph (264.7 knots), $T_{T,davg}=5.0$ °C, $P_{air}=70$ psig. (uu) $U_{ts}=303.3$ mph (264.6 knots), $T_{T,davg}=-8.8$ °C, $P_{air}=0$ psig. (vv) $U_{ts}=303.8$ mph (264.0 knots), $T_{T,davg}=-8.9$ °C, $P_{air}=70$ psig.....	53
Figure 19.—Concluded. (ww) $U_{ts}=302.9$ mph (263.2 knots), $T_{T,davg}=-20.3$ °C, $P_{air}=0$ psig. (xx) $U_{ts}=303.8$ mph (264.0 knots), $T_{T,davg}=-20.2$ °C, $P_{air}=70$ psig.....	54
Figure 20.—Flow angle data from the IRT test section collected using the 9-ft survey rake mounted at 11 vertical positions over several tunnel runs. Nominal conditions are used to denote each data set. (a) $U_{ts}=50$ mph (43 knots), $P_{air}=0$ psig. (b) $U_{ts}=50$ mph (43 knots), $P_{air}=70$ psig. (c) $U_{ts}=100$ mph (87 knots), $P_{air}=0$ psig. (d) $U_{ts}=100$ mph (87 knots), $P_{air}=70$ psig.....	56
Figure 20.—Continued. (e) $U_{ts}=115$ mph (100 knots), $P_{air}=0$ psig. (f) $U_{ts}=115$ mph (100 knots), $P_{air}=70$ psig. (g) $U_{ts}=150$ mph (130 knots), $P_{air}=0$ psig. (h) $U_{ts}=150$ mph (130 knots), $P_{air}=70$ psig.....	57

Figure 20.—Continued. (i) $U_{ts}=175$ mph (152 knots), $P_{air}=0$ psig. (j) $U_{ts}=175$ mph (152 knots), $P_{air}=5$ psig. (k) $U_{ts}=175$ mph (152 knots), $P_{air}=20$ psig. (l) $U_{ts}=175$ mph (152 knots), $P_{air}=70$ psig. ....	58
Figure 20.—Continued. (m) $U_{ts}=200$ mph (174 knots), $P_{air}=0$ psig. (n) $U_{ts}=200$ mph (174 knots), $P_{air}=70$ psig. (o) $U_{ts}=250$ mph (217 knots), $P_{air}=0$ psig. (p) $U_{ts}=250$ mph (217 knots), $P_{air}=70$ psig. ....	59
Figure 20.—Continued. (q) $U_{ts}=225$ mph (195 knots), $P_{air}=0$ psig. (r) $U_{ts}=225$ mph (195 knots), $P_{air}=20$ psig. (s) $U_{ts}=225$ mph (195 knots), $P_{air}=70$ psig. ....	60
Figure 20.—Concluded. (t) $U_{ts}=300$ mph (261 knots), $P_{air}=0$ psig. (u) $U_{ts}=300$ mph (261 knots), $P_{air}=70$ psig. (v) $U_{ts}=350$ mph (304 knots), $P_{air}=0$ psig. (w) $U_{ts}=350$ mph (304 knots), $P_{air}=70$ psig. ....	61
Figure 21.—Average flow angularity vector magnitude in the core (center 4.5- by 3- ft area) of the IRT test section at various $P_{air}$ settings. ....	62
Figure 22.—Summary of the axial and transverse turbulence levels in the IRT test section as measured by probes mounted on the 9-ft survey rake. The probes were arrayed laterally across the span of the rake as follows: Probe 1 was 31.8 in. from the inside wall, probe 2 was 53.7 in. and probe 3 was 76.2 in. (a) Test section airspeed of 50 mph ....	63
Figure 22.—Continued. (b) 100 mph. ....	64
Figure 22.—Continued. (c) 115 mph. ....	65
Figure 22.—Continued. (d) 150 mph. ....	66
Figure 22.—Continued. (e) 175 mph, 0 and 70 psi. ....	67
Figure 22.—Continued. (f) 175 mph, 5 and 20 psi. ....	68
Figure 22.—Concluded. (g) 200 mph. ....	69
Figure D.1.—Total temperature calibration curves for the IRT based on the 2005 aero-thermal interim calibration data. ....	88
Figure D.2.—Total temperature calibration curve coefficients for $U_{ts} < 50$ knots. This information is used to interpolate slope and intercept values for spray bar air pressure settings between 0 and 40 and between 40 and 70 psig. ....	89
Figure D.3.—Comparison of Mach number ratio distribution data across the tunnel at test section centerline. (a) $M_{nom}=0.066$ , $U_{nom}=43$ knots. (b) $M_{nom}=0.100$ , $U_{nom}=65$ knots. (c) $M_{nom}=0.133$ , $U_{nom}=87$ knots. (d) $M_{nom}=0.152$ , $U_{nom}=100$ knots. ....	90
Figure D.3.—Continued. (e) $M_{nom}=0.200$ , $U_{nom}=130$ knots. (f) $M_{nom}=0.234$ , $U_{nom}=150$ knots. (g) $M_{nom}=0.266$ , $U_{nom}=175$ knots. (h) $M_{nom}=0.306$ , $U_{nom}=200$ knots. ....	91
Figure D.3.—Continued. (i) $M_{nom}=0.336$ , $U_{nom}=220$ knots. (j) $M_{nom}=0.370$ , $U_{nom}=240$ knots. (k) $M_{nom}=0.402$ , $U_{nom}=260$ knots. (l) $M_{nom}=0.435$ , $U_{nom}=280$ knots. ....	92
Figure D.3.—Concluded. (m) $M_{nom}=0.470$ , $U_{nom}=300$ knots. ....	93
Figure D.4.—IRT test section total temperature distribution data collected using the 2-D RTD Array. (a) $U_{ts}=49.02$ mph (42.6 knots), $T_{T,davg}=-29.8$ °C, $P_{air}=0$ psig. (b) $U_{ts}=55.2$ mph (48.0 knots), $T_{T,davg}=-29.8$ °C, $P_{air}=70$ psig. (c) $U_{ts}=49.14$ mph (42.7 knots), $T_{T,davg}=-17.6$ °C, $P_{air}=0$ psig. (d) $U_{ts}=54.89$ mph (47.7 knots), $T_{T,davg}=-17.5$ °C, $P_{air}=70$ psig. ....	94
Figure D.4.—Continued. (e) $U_{ts}=49.71$ mph (43.2 knots), $T_{T,davg}=0.2$ °C, $P_{air}=0$ psig. (f) $U_{ts}=49.94$ mph (43.4 knots), $T_{T,davg}=0.3$ °C, $P_{air}=40$ psig. (g) $U_{ts}=49.59$ mph (43.1 knots), $T_{T,davg}=0.2$ °C, $P_{air}=70$ psig. ....	95
Figure D.4.—Continued. (h) $U_{ts}=116.46$ mph (101.2 knots), $T_{T,davg}=-28.4$ °C, $P_{air}=0$ psig. (i) $U_{ts}=118.76$ mph (103.2 knots), $T_{T,davg}=-28.4$ °C, $P_{air}=70$ psig. (j) $U_{ts}=116.46$ mph (101.2 knots), $T_{T,davg}=-16.3$ °C, $P_{air}=0$ psig. (k) $U_{ts}=118.30$ mph (102.8 knots), $T_{T,davg}=-16.3$ °C, $P_{air}=70$ psig. ....	96
Figure D.4.—Continued. (l) $U_{ts}=116.57$ mph (101.3 knots), $T_{T,davg}=-4.3$ °C, $P_{air}=0$ psig. (m) $U_{ts}=116.80$ mph (101.5 knots), $T_{T,davg}=-4.2$ °C, $P_{air}=70$ psig. (n) $U_{ts}=116.34$ mph (101.1 knots), $T_{T,davg}=1.3$ °C, $P_{air}=0$ psig. (o) $U_{ts}=116.34$ mph (101.1 knots), $T_{T,davg}=1.3$ °C, $P_{air}=70$ psig. ....	97

Figure D.4.—Continued. (p) $U_{ts}=151.91$ mph (132.01 knots), $T_{T,davg}=-15.4$ °C, $P_{air}=0$ psig. (q) $U_{ts}=174.53$ mph (151.6 knots), $T_{T,davg}=0.06$ °C, $P_{air}=0$ psig. ....	98
Figure D.4.—Continued. (r) $U_{ts}=233.38$ mph (202.8 knots), $T_{T,davg}=-24.4$ °C, $P_{air}=0$ psig. (s) $U_{ts}=233.61$ mph (203.0 knots), $T_{T,davg}=-24.7$ °C, $P_{air}=70$ psig. (t) $U_{ts}=235.10$ mph (204.3 knots), $T_{T,davg}=-12.3$ °C, $P_{air}=0$ psig. (u) $U_{ts}=234.87$ mph (204.1 knots), $T_{T,davg}=-12.4$ °C, $P_{air}=70$ psig. ....	99
Figure D.4.—Continued. (v) $U_{ts}=230.5$ mph (200.3 knots), $T_{T,davg}=0.0$ °C, $P_{air}=0$ psig. (w) $U_{ts}=231.19$ mph (200.9 knots), $T_{T,davg}=0.0$ °C, $P_{air}=70$ psig. ....	100
Figure D.4.—Continued. (x) $U_{ts}=253.11$ mph (219.95 knots), $T_{T,davg}=0.67$ °C, $P_{air}=0$ psig. (y) $U_{ts}=292.07$ mph (253.8 knots), $T_{T,davg}=0.8$ °C, $P_{air}=0$ psig. (z) $U_{ts}=291.61$ mph (253.4 knots), $T_{T,davg}=0.7$ °C, $P_{air}=70$ psig. ....	101
Figure D.4.—Concluded. (aa) $U_{ts}=338.33$ mph (294.0 knots), $T_{T,davg}=-17.4$ °C, $P_{air}=0$ psig. (bb) $U_{ts}=338.1$ mph (293.8 knots), $T_{T,davg}=-17.7$ °C, $P_{air}=70$ psig. (cc) $U_{ts}=338.9$ mph (294.5 knots), $T_{T,davg}=-5.5$ °C, $P_{air}=0$ psig. (dd) $U_{ts}=339.6$ mph (295.1 knots), $T_{T,davg}=-5.6$ °C, $P_{air}=70$ psig. ....	102
Figure D.5.—IRT test section total temperature standard deviation data collected using the 2–D RTD Array at the center line of the RTD Array. ....	103
Figure D.5.—Concluded. IRT test section total temperature standard deviation data collected using the 2–D RTD Array for the full RTD Array. ....	104
Figure D.6.—Comparison of test section centerline flow angularity vectors from the 2004 full calibration and 2005 interim calibration at various $P_{air}$ settings. (a) $M_{nom} = 0.066$ , $V_{nom} = 43$ knots. (b) $M_{nom} = 0.100$ , $V_{nom} = 65$ knots. (c) $M_{nom} = 0.133$ , $V_{nom} = 87$ knots. (d) $M_{nom} = 0.152$ , $V_{nom} = 100$ knots. ....	105
Figure D.6.—Continued. (e) $M_{nom} = 0.200$ , $V_{nom} = 130$ knots. (f) $M_{nom} = 0.234$ , $V_{nom} = 150$ knots. (g) $M_{nom} = 0.266$ , $V_{nom} = 178$ knots. (h) $M_{nom} = 0.306$ , $V_{nom} = 200$ knots. ....	106
Figure D.6.—Continued. (i) $M_{nom} = 0.336$ , $V_{nom} = 220$ knots. (j) $M_{nom} = 0.370$ , $V_{nom} = 240$ knots. (k) $M_{nom} = 0.402$ , $V_{nom} = 260$ knots. (l) $M_{nom} = 0.435$ , $V_{nom} = 280$ knots. ....	107
Figure D.6.—Concluded. (m) $M_{nom} = 0.470$ , $V_{nom} = 300$ knots. ....	108
Figure D.7.—Comparison of average data from flow angularity measurements made in the IRT test section (horizontal survey at centerline) during the 2004 and 2005 test entries. (a) Full-span data (all eleven probes included). (b) Core data (center seven probes only). ....	109
Figure D.8.—Comparison of standard deviation data from flow angularity measurements made in the IRT test section (horizontal survey at centerline) during the 2004 and 2005 test entries. (a) Full-span data (all eleven probes included). (b) Core data (center seven probes only). ....	110
Figure D.9.—Comparison of 2004 and 2005 turbulence data (horizontal survey at centerline). ....	111
Figure D.10.—Comparison of the aero-thermal calibration curves created based on the 2004 and 2005 test results. (a): Mach number calibration curve comparison with 2004 and 2005 test data. ....	112
Figure D.10.—Continued. (b) Static Pressure calibration curves for the IRT based on the 2004 and 2005 calibration data. ....	113
Figure D.10.—Concluded. (c) Total temperature calibration curves for the IRT based on the 2004 and 2005 calibration data. ....	114

# **Aero-Thermal Calibration of the NASA Glenn Icing Research Tunnel (2004 and 2005 Tests)**

E. Allen Arrington and Christine M. Pastor  
Sierra Lobo, Inc.  
Cleveland, Ohio 44135

Jose C. Gonzalez and Monroe R. Curry III  
QSS Group, Inc.  
Cleveland, Ohio 44135

## **Summary**

A full aero-thermal calibration of the NASA Glenn Icing Research Tunnel was completed in 2004 following the replacement of the inlet guide vanes upstream of the tunnel drive system and improvement to the facility total temperature instrumentation. This calibration test provided data used to fully document the aero-thermal flow quality in the IRT test section and to construct calibration curves for the operation of the IRT. The 2004 test was also the first to use the 2-D RTD array, an improved total temperature calibration measurement platform.

## **Introduction**

Updating and maintaining the icing cloud and aero-thermal calibration and flow quality data are critical tasks in the NASA Glenn Icing Research Tunnel (IRT). Establishing and maintaining the calibrations is the only way to insure that correct test section operating conditions are being set for a given set of facility control inputs. Without knowledge of the calibration and flow quality data, it is impossible to provide high-quality test data for customers and researchers. To insure that the data quality from the IRT is always at the highest standards, IRT staff and wind tunnel calibration personnel have developed and continue to refine the calibration methodologies used.

The aero-thermal calibration test program provides the calibration relationships needed to accurately determine the test section operating conditions for total pressure, airspeed (comparable Mach number) and total temperature. Once these calibrated conditions are determined, all other aero-thermal operating conditions can be calculated. In addition to the calibration information, detailed flow quality data (spatial uniformity) is also collected. The collected calibration and flow quality data provide a complete description of the aero-thermal operation of the IRT.

The current aero-thermal calibration methodology and instrumentation has evolved based on lessons learned by the calibration team over the past 15 years, input from IRT customers, in-house research staff, IRT facility personnel, and recommendations from References 1 and 2. Reference 1 defines a time table and level of calibration that should be conducted following modifications to an icing tunnel. Correspondingly, Reference 1 recommends that short check calibrations should be conducted multiple times each year to insure repeatable operation of the wind tunnel. Based on these recommendations, the following aero-thermal calibration tests have been defined:

- **Full calibration:** Includes collection of aero-thermal calibration data over the entire operating range of the IRT as well as a complete mapping of the IRT flow quality at one cross section of the test section, typically at the centerline of the turntable. A full calibration should be conducted every 5 years or following a major facility modification. The full calibration provides all of the information needed to develop the aero-thermal calibration relationships, or calibration curves, for the facility and provides extensive detailed information on the aero-thermal flow quality characteristics of the test section.

- Interim calibration: Includes collection of aero-thermal calibration data over the entire operating range of the IRT, however, data is only required from the test section centerline. An interim calibration is conducted one year following a full calibration. The interim calibration is used to validate the data collected during the full calibration, therefore, if the full calibration and interim calibration data match then the facility is operating properly, however if not, then an investigation must commence immediately to rectify the discrepancies.
- Check calibration: Ideally a one-day test using a very simple rake. Check calibration testing covers the entire operating range, but the test matrix is not as extensive as a full or interim calibration. This calibration should be conducted 2 to 3 times per year. The check calibration data is used in a statistical process control analysis to monitor the stability and repeatability of the facility operation.

This paper provides a detailed description of the full aero-thermal calibration conducted in the IRT in 2004. This calibration was required due to replacement of the drive system inlet guide vanes, which is detailed in the subsequent Description of Facility section. The 2004 full calibration was also needed to update the total temperature calibration based on improvements to facility instrumentation (Ref. 3). Previous to the 2004 calibration, the most recent full calibration was completed in 2000 following the replacement of the facility heat exchanger (Ref. 4).

The goals for the 2004 aero-thermal full calibration are listed below:

- Qualify for operation the 2–D RTD array as the new measurement platform for total temperature calibration and flow quality data in the IRT test section.
- Complete data collection and construct aero-thermal calibration curves for the IRT. The three calibration relationships used are total pressure, Mach number and total temperature.
- Complete detailed flow quality surveys using the 9-ft survey rake and 2–D RTD array.

While the bulk of this report focuses on the full aero-thermal calibration conducted in 2004, a discussion of the 2005 interim calibration is included in an appendix. The 2005 interim calibration provided additional information on the total temperature calibration of the IRT and allowed an opportunity to verify additional planned improvements to the total temperature calibration.<sup>1</sup>

## Symbols

$a$	speed of sound, ft/sec
$A_0, A_1, A_2$	Hot wire curve fit coefficients
$C_0, C_1, C_2$	RTD probe total temperature flow recovery curve fit coefficients
$C_\alpha$	Pitch angle pressure coefficient
$C_\beta$	Yaw angle pressure coefficient
$C_{TT,0}, C_{TT,1}$	Test section total temperature calibration curve fit coefficients
$C_o$	Total pressure coefficient (9-ft rake pressure probes)
$C_q$	Static pressure coefficient (9-ft rake pressure probes)
$C_t$	Total temperature recovery coefficient (9-ft rake total temperature probes)
$E$	Hot wire anemometer output voltage, volts
$K_0$ to $K_2$	Flow angle prediction coefficients, degrees
$l$	characteristic length, ft
$M$	Mach number
$N$	Number of data points
$P$	Pressure, psia

---

<sup>1</sup>Check calibration data are collected as part of both full and interim calibration test entries, as well as during dedicated check calibration test entries. However, the check calibration tests are not covered in this report.

$P_1$ to $P_9$	Flow angle probe pressures, psia
$P_{air}$	Spray bar air pressure, psig
$P_{avg}$	Average of $P_1$ , $P_2$ , $P_3$ , and $P_4$ , psia
$P_{rat}$	Ratio of static to total pressure
$P_S$	Static pressure, psia (psf)
$P_{S,rake}$	Average of $P_6$ , $P_7$ , $P_8$ , and $P_9$ (probe static pressure), psia
$P_T$	Total pressure, psia (psf)
$P_{T,rake}$	Equal to $P_5$ (probe total pressure), psia
$q$	Dynamic pressure, psi
$R$	Specific gas constant for air, 1716 ft <sup>2</sup> /(sec <sup>2</sup> °R)
Re	Reynolds number
RSS	Root-sum-squared uncertainty estimate
$T$	Temperature, °C (°F)
$TI_u$	Axial turbulence intensity, percent
$TI_v$	Transverse turbulence intensity, percent
$T_S$	Static temperature, °C (°F)
$T_T$	Total temperature, °C (°F)
$T_{T,davg}$	Average of the 24 D-corner total temperature measurements, °C (°F)
$T_{T,dc}$	D-corner total temperature measurement, °C (°F)
$U$	Velocity, knots (ft/sec, mph)
$u$	Hot wire axial velocity, ft/sec
$v$	Hot wire transverse velocity, ft/sec
$V_m$	Flow angle resultant vector magnitude, degrees
$V_\phi$	Flow angle resultant vector orientation, degrees
$X$	Axial coordinate with axis origin at bellmouth/test section weld seam, in.
$Y$	Spanwise coordinate with axis origin at the test section inner wall, in.
$Z$	Vertical coordinate with axis origin at the test section floor, in.
$\alpha$	Pitch flow angle, degrees
$\beta$	Yaw flow angle, degrees
$\gamma$	Ratio of specific heats, 1.4
$\Delta$	Measured pitch or yaw angle offset, degrees
$\overline{\Delta T_{DC}}$	D-Corner average temperature, °C (°F)
$\sigma$	Standard deviation
$\sigma_{TT,DC}$	Standard deviation of the D-corner total temperature, °C (°F)
$\theta$	Hot wire sensor inclination angle, degrees
$\phi$	Parameter used to calculate flow angle resultant vector orientation, degrees

### Subscripts

<i>arm</i>	Pertaining to the 6 degree-of-freedom digitizing arm
<i>array</i>	Pertaining to the 2-D RTD array
<i>avg</i>	Average
<i>bm</i>	Bellmouth conditions
<i>bm,north</i>	Measured by the north bellmouth rake
<i>bm,south</i>	Measured by the south bellmouth rake
<i>eff</i>	Pertaining to hot wire effective velocities
<i>HW</i>	Pertaining to a hot wire probe
<i>i</i>	Data point index or hot wire sensor index
<i>level</i>	Pertaining to a digital level

<i>local</i>	Pertaining to parameters in the test section after all probe calibration coefficients have been taken into account
<i>nom</i>	Nominal test section condition or setting
<i>rake</i>	Pertaining to the 9-ft survey rake
<i>ruler</i>	Pertaining to a tape measure or ruler
<i>ts</i>	Test section conditions (based on calibration data)

## Description of Facility

The NASA Glenn Icing Research Tunnel (IRT) is a closed-loop atmospheric tunnel illustrated in Figure 1. The airflow is driven by a 25-ft diameter twelve blade fan that is powered by a 5000-hp electric motor. The test section, shown at the bottom center of Figure 1, is 6-ft high, 9-ft wide, and 20-ft long, with no divergence along any of the test section surfaces. The velocity in the empty test section can be varied between 25 and 340 knots at  $-17.8\text{ }^{\circ}\text{C}$  (37 to 575 ft/sec at  $0\text{ }^{\circ}\text{F}$ ). A pair of heat exchangers located in the C-D leg of the tunnel loop, seen at the left of Figure 1, allow for total temperature settings as low as  $-30\text{ }^{\circ}\text{C}$ . A set of ten horizontally oriented spray bars, located in the settling chamber at the bellmouth inlet prior to the test section, inject atomized water into the airflow to create icing conditions. The IRT has been in service since 1944 and has undergone several major upgrades and modifications over the years to insure that it remains the lead ground test facility for icing research (Refs. 5 and 6). In 2004, the inlet guide vanes (IGVs) upstream of the drive fan were replaced, primarily for structural reasons, but also to improve aerodynamic performance. Figure 2 shows the final configuration of the replacement IGVs upstream of the IRT drive fan prior to being painted. The view in Figure 2 looks downstream from Corner B showing the inlet and outlet guide vanes, fan blades, and floor drain. During the downtime for the IGV replacement, the new facility instrumentation for total temperature measurement was installed in D-corner, consisting of 24 RTD probes. More information about the IRT is located in Reference 7.

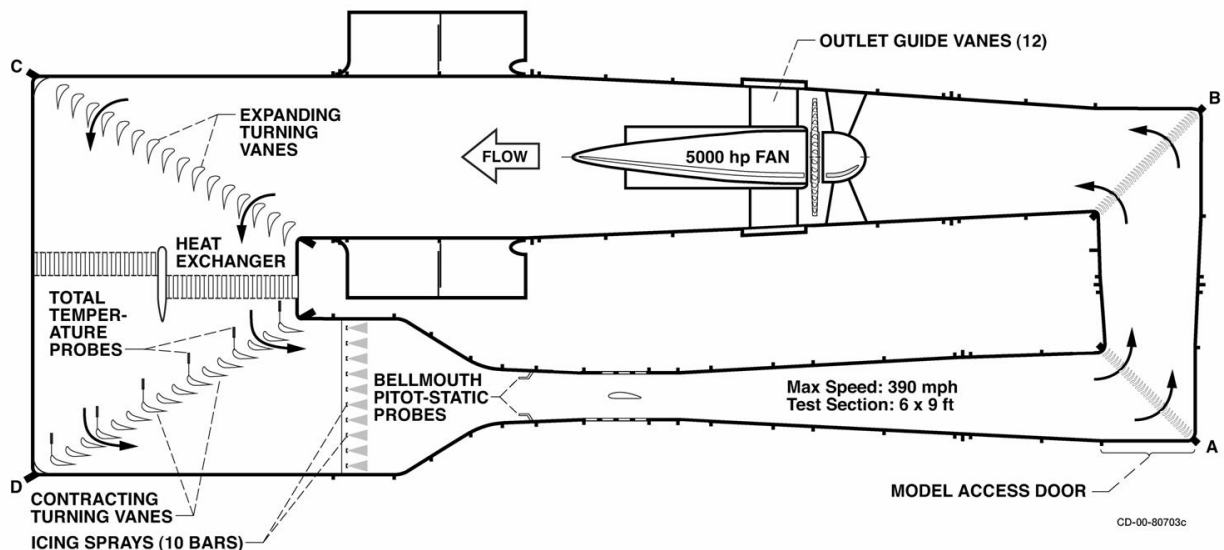


Figure 1.—Layout of the NASA Glenn Icing Research Tunnel.

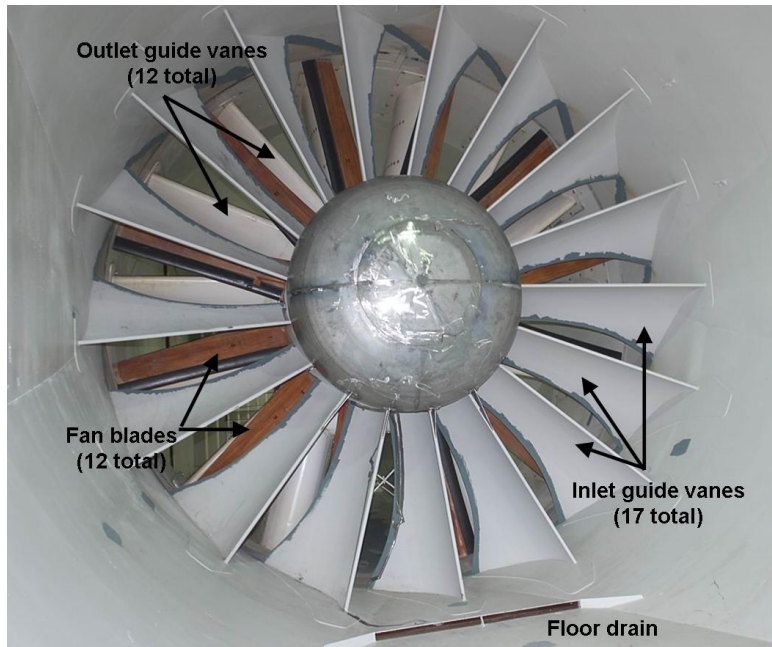


Figure 2.—Installation photo of the replacement inlet guide vanes (IGV) upstream of the IRT drive fan.

## Test Hardware, Instrumentation and Data Systems

The 9-ft survey rake and the 2-D RTD array are two pieces of test hardware used to complete the aero-thermal calibration of the IRT. The 9-ft survey rake is used to collect pressure, flow angle, turbulence calibration, and flow quality data. The 2-D RTD array is used to collect total temperature calibration and flow quality data<sup>2</sup>. Detailed descriptions of the hardware, instrumentation and data systems are included in this section.

### 9-ft Survey Rake

Figure 3 shows the 9-ft horizontal survey rake installed in the IRT test section at the vertical centerline, a height of  $Z=36$ -in. The flow angle pressure probes, total temperature probes, and hot wire probes mounted on the 9-ft survey rake in Figure 3, will be discussed in more detail later in this section. The reference axis is also defined in Figure 3 depicting the vertical direction as the  $Z$ -axis, the horizontal direction as the  $Y$ -direction, and the axial direction as the  $X$ -axis. The origin of the left-handed  $X$ - $Y$ - $Z$  coordinate system is as follows: the  $X$  axis origin is at the bellmouth/test section weld seam as seen in Figure 4, the  $Y$  axis origin is at the inner wall as seen in Figure 4, and the  $Z$  axis origin is at the floor as seen in Figure 3. This rake is used to collect calibration and flow quality data for pressure, airspeed, flow angle and turbulence in the IRT test section.

Figure 4 illustrates the plan view of the IRT test section with the survey rake installed. The rake was installed at an axial position of  $X=179.3$ -in. This was also the axial location of the cross-sectional plane surveyed during the 2004 test program as well as the test program in 1997. Figure 5 shows the plan and front views of the survey rake. The following illustration, Figure 6 details a cross-section of the survey rake with exploded views of the flow angle pressure probe ports.

<sup>2</sup>Prior to the 2004 calibration, the 9-ft survey rake was used to collect all calibration data, including total temperature data. Starting in 2004, an improved total temperature measurement platform, the 2-D RTD Array, was introduced for calibration and flow quality data collection.

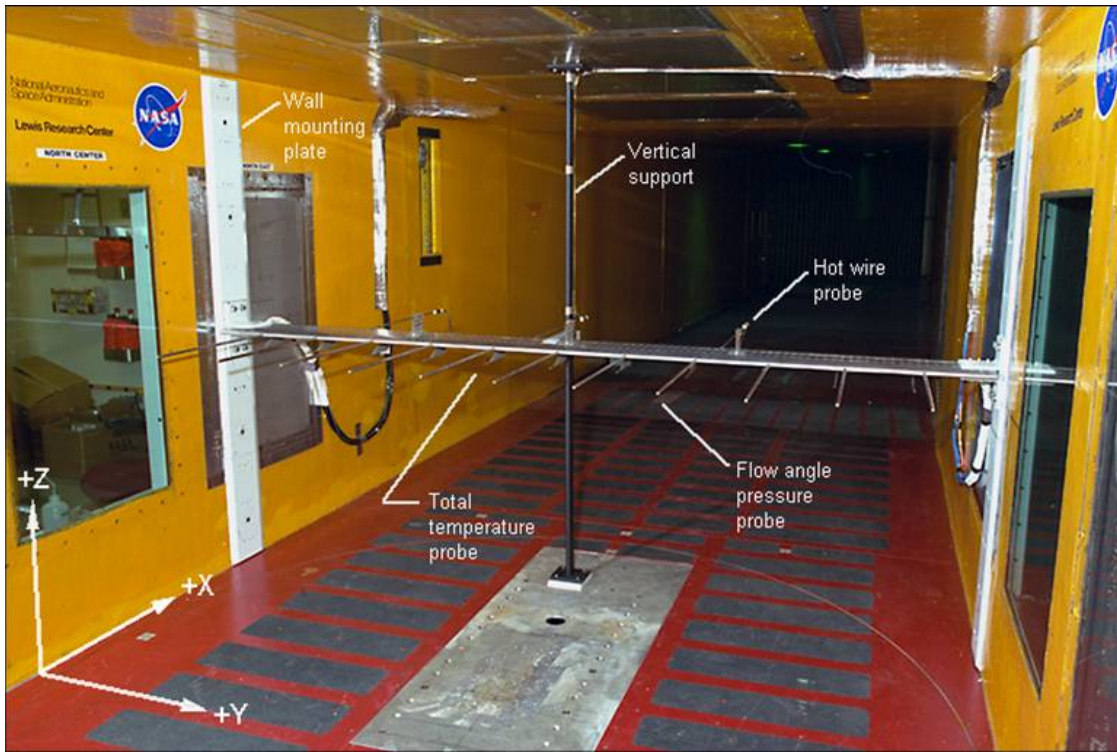


Figure 3.—Photograph of the 9-ft horizontal survey rake installed in the IRT test section.

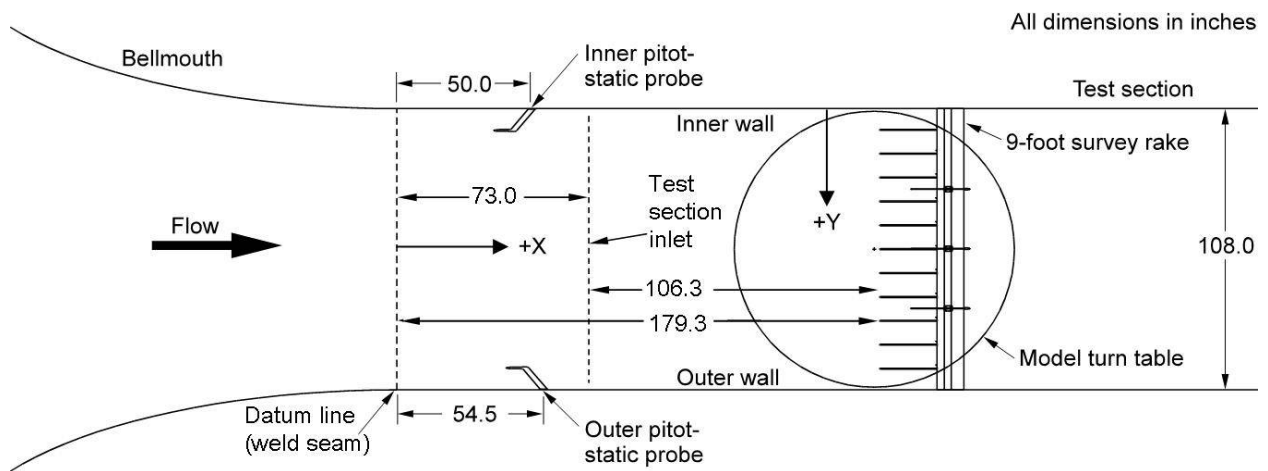
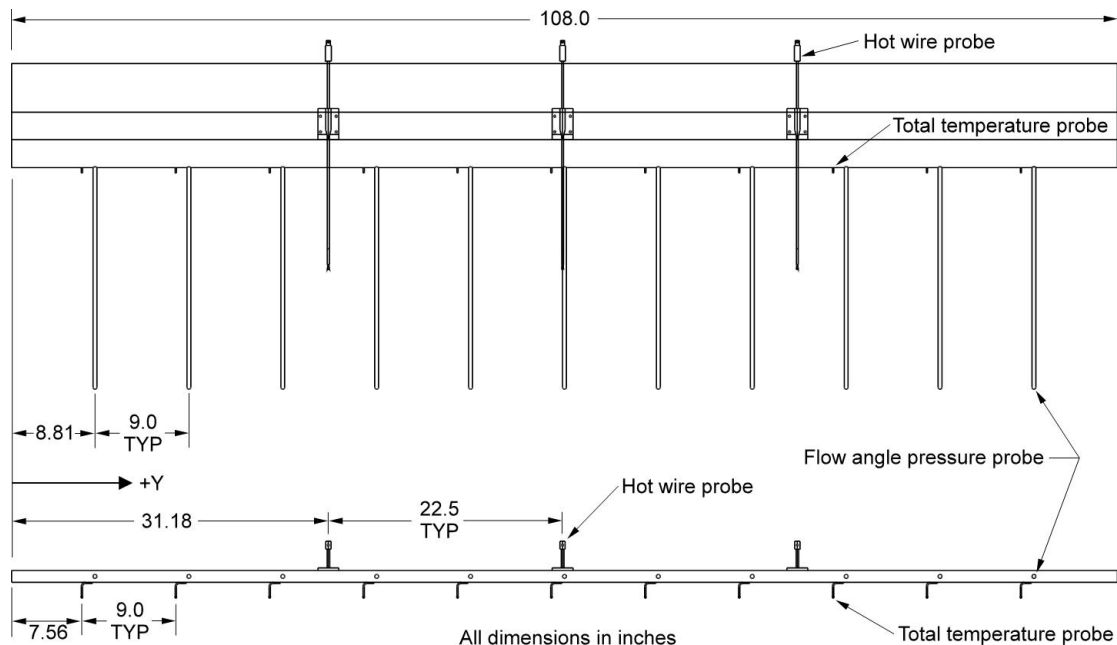
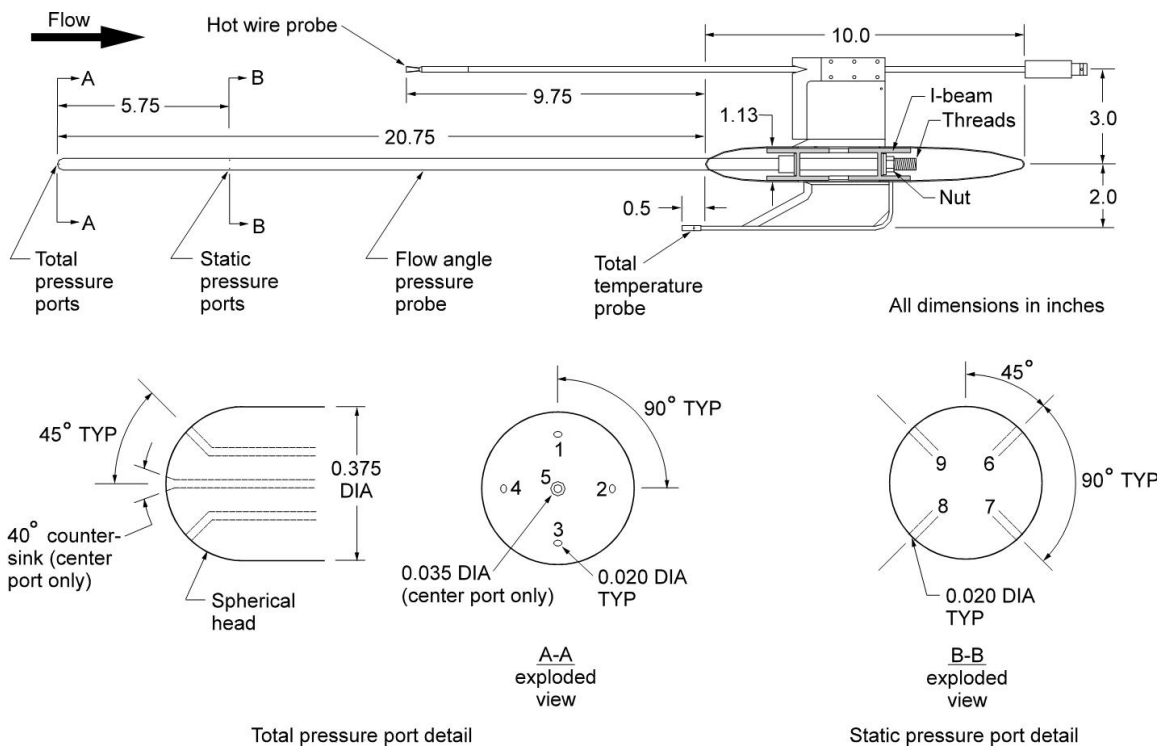


Figure 4.—Plan view of the IRT test section showing the installed location of the 9-ft survey rake.



All dimensions in inches  
 Figure 5.—Plan and elevation views of the 9-ft survey rake.



Total pressure port detail  
 Static pressure port detail  
 Figure 6.—Cross section of the 9-ft survey rake showing flow probes details.

The instrumentation mounted on the 9-ft survey rake includes eleven flow angle pressure probes, eleven total temperature thermocouple probes, and three thermal anemometry probes. The spanwise, *Y* positions of all probes with respect to the test section inner wall are defined in Figure 5. The survey rake was supported at both ends by bolting the rake to wall mounted support plates as seen in Figure 3. These support plates are 6-ft tall and have a bolt pattern that allows the rake to be positioned vertically every

6-in. above or below the test section centerline. A vertical strut, shown in Figure 3, was also used to support the rake in the center. As seen in Figure 6, the main body of the rake is formed by two aluminum I-beams and thin aluminum plates riveted together. Thin sheets of aluminum were bent to form the leading and trailing edge of the rake body.

The flow angle pressure probes are bolted to the rake body I-beams as illustrated in Figure 6. These probes are of hemi-spherical head design, bottom left Figure 6, and have five total pressure ports in the head. The bottom center Figure 6 shows the center port in the hemi-spherical head design which measures total pressure, and the four circumferential total pressure ports which measure pitch and yaw angle. Four static pressure ports are located downstream of the head depicted bottom right Figure 6. Top Figure 6, shows the heads of the probes located 20.75-in. upstream of the rake leading edge and the static pressure taps on each probe located 5.75-in. downstream of the head. The probes were calibrated for Mach numbers between 0.1 and 0.6 in the NASA Glenn 3.5-in. diameter free jet calibration facility. Details of the probe calibration can be found in Reference 8.

Aspirated total temperature type T thermocouple probes with copper/constantan wires were used to monitor test section temperature. These probes are also depicted in Figure 3, Figure 5, and Figure 6. The probes are mounted to the bottom surface of the survey rake with the tips of the probes approximately 0.5-in. upstream of the rake leading edge and 2.0-in. below the rake centerline. The total temperature probes were calibrated for total temperature recovery in the NASA Glenn 3.5-in. diameter free jet calibration facility.

Three single sensor and dual sensor (cross-wire) hot-wire probes with 0.00015-in. diameter tungsten wires, were used to measure the turbulence levels in the test section. The probes were mounted to the upper surface of the rake body as shown in Figure 3, Figure 5, and Figure 6. The top of Figure 6 more clearly illustrates the probe tips were located 9.75 in. upstream of the rake body leading edge and 3.0-in. above the rake centerline.

## 2-D RTD Array

The 2-D RTD Array was designed and built to provide a more accurate total temperature calibration and temperature mapping of the test section, with the benefit of reducing overall test time and cost. The total temperature probes used on the array are 4-wire resistive temperature device (RTD) with a ceramic capsule sensor. Figure 7 shows the details of the RTD probe. See Reference 3 for a discussion of the thought process used to arrive at the design of the array and selection of the probes.

Reference 1 was utilized to determine the number and arrangement of probes on the array. Figure 8 shows the resulting layout is a 7-by-7 grid with the probes spaced at 0,  $\pm 25$ ,  $\pm 50$  and  $\pm 75$  percent of the test section dimension from the horizontal and vertical centerlines. The intersections of the dotted lines in this figure indicate the probe positions. The 7-by-7 grid arrangement provided the test section coverage required without incurring an unreasonable cost for the RTD probes.

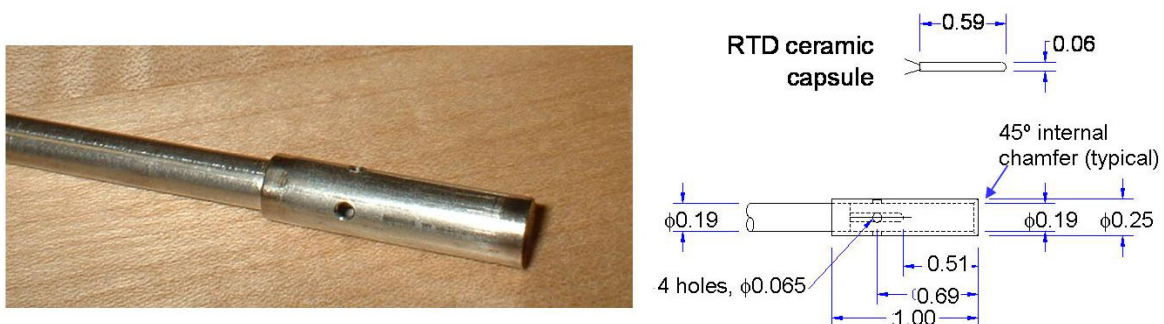


Figure 7.—Details of RTD probes used on the 2-D RTD array (dimensions in inches).

Figure 9 shows the 2-D RTD array installed in the IRT test section (views looking downstream and upstream). The structure of the 2-D RTD array includes a set of seven vertical members and horizontal members. Each vertical member houses seven RTD probes and instrumentation wiring, while the four horizontal members provide structural rigidity. The vertical members seen in Figure 9 are 0.75 in. thick by 4 in. wide and have a round leading edge. Figure 10 illustrates the cross section of an array vertical member assembly. Also, Figure 10 shows how the tips of the RTDs extend 7 in. forward of the leading edge, and the 0.75 in. deep channel that was attached to the trailing edge to house the instrumentation lines. The horizontal members seen in Figure 9 are 0.5 in. thick by 3 in. wide and also have a round leading edge. The array was secured to the test section walls, floor and ceiling, with allowances made to account for thermal expansion of the array. The tips of the RTD probes were positioned 194.5 in. downstream of the tunnel datum line or 121.5 in. from the inlet of the test section (the thermocouples on the 9-ft survey rake were 199.5 in. downstream of the datum line).

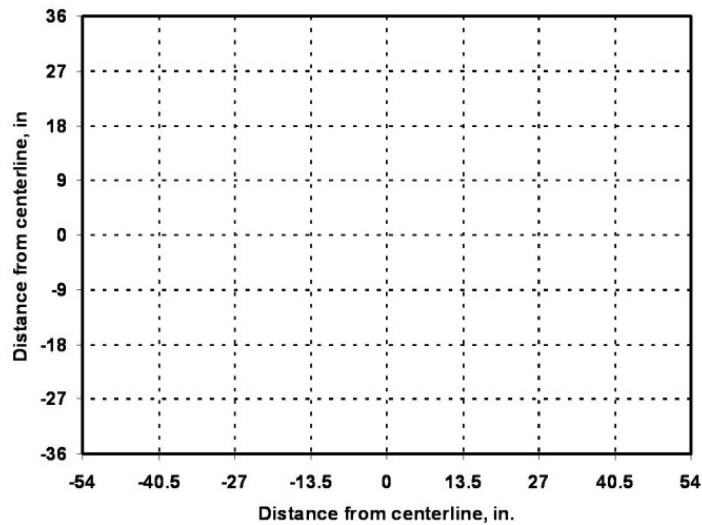


Figure 8.—7x7 grid arrangement of the RTD probes in the IRT test section.

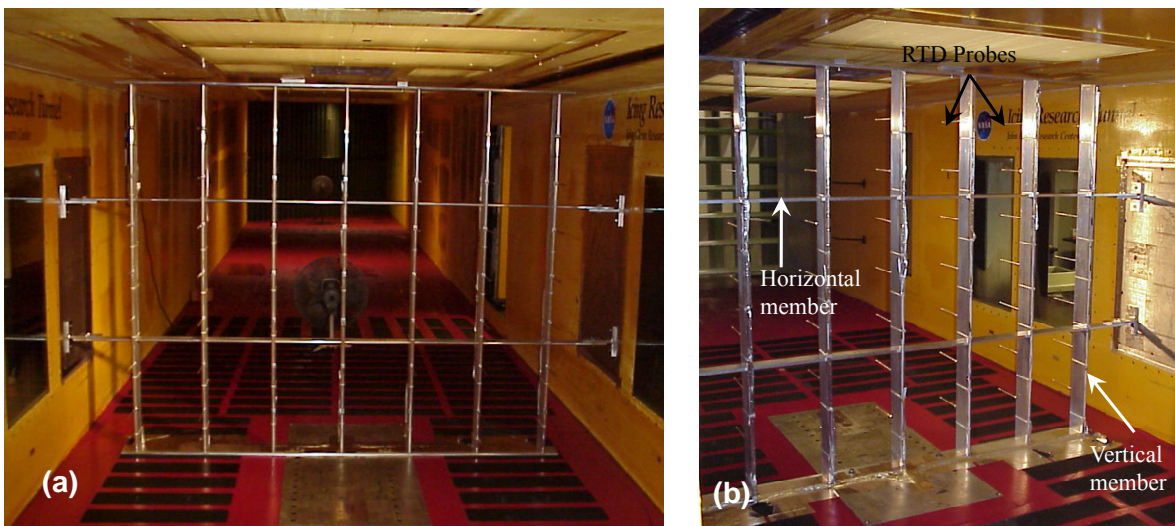


Figure 9.—RTD Array installed in the IRT test section. (a) View looking downstream. (b) View looking upstream.

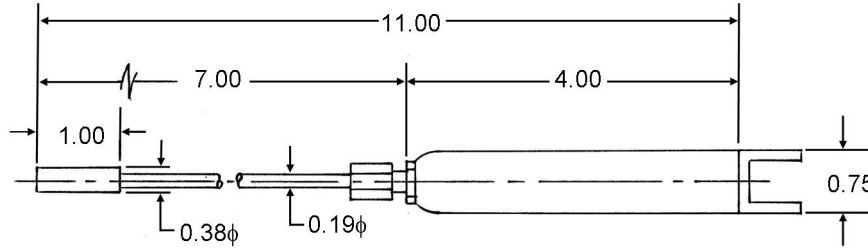


Figure 10.—RTD array vertical member cross sectional details.

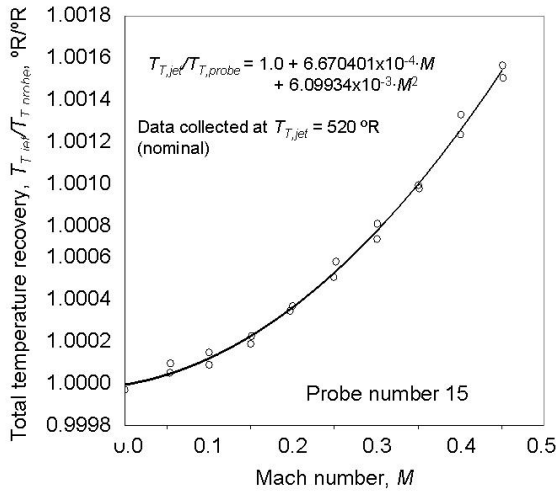


Figure 11.—Typical total temperature flow recovery curve for the 2-D RTD array probes.

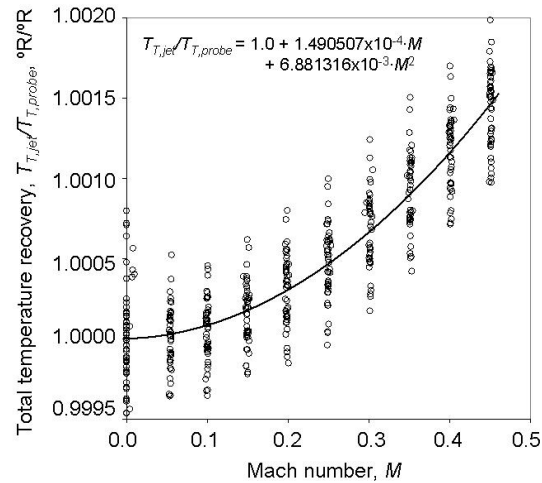


Figure 12.—Total temperature flow recovery data for RTD probes 1 through 23 with average curve fit.

A portion of the RTD probes (serial numbers 1 through 23) were calibrated for temperature flow recovery in the 3.5-in. Diameter Free Jet Facility. The recovery testing was conducted to determine how well the probes sense the total temperature over a range of airflow conditions. During the testing, the free jet air temperature was set to a nominal condition of about 520 °R (60.33 °F) and held constant while the free jet Mach number was varied from 0 to 0.5. Figure 11 shows the total temperature recovery results for a typical probe (serial number 15) with its individual flow recovery curve. The recovery curves were subsequently used to correct data collected in the IRT. The 20 RTD probes that were individually calibrated for flow recovery were mounted in the center of the 2-D RTD array. The probes not measured directly for their recovery characteristics were mounted around the periphery of the array and used the average recovery from all the calibrated probes, seen in Figure 12. The probes have an absolute measurement uncertainty of  $\pm 0.10$  °C ( $\pm 0.18$  °F) for a probe that was individually calibrated for total temperature flow recovery or  $\pm 0.16$  °C ( $\pm 0.29$  °F) for a probe that was not specifically calibrated for recovery (uses the average recovery values). The details of this uncertainty analysis are found in Appendix A. A summary of the flow recovery correction coefficients is provided in Appendix B.

## Facility Instrumentation

The following standard facility instrumentation was used during this test program.

- 1) Bellmouth pitot-static probes: A probe is mounted on the south and north wall near the exit of the bellmouth. Transducers associated with these probes measure the total and differential pressures. These measurements are used to arrive at  $P_{T,bm}$  and  $P_{S,bm}$ . The location of these probes is shown in Figure 4, as the outer (north) probe and the inner (south) probe.

- 2) Total temperature probes in D-corner: Twenty-four RTD probes are arrayed on the leading edges of the turning vanes in D-corner to measure the temperature profile exiting the facility cooler. The distribution of the measured temperatures and the average of these twenty-four probes,  $T_{T,davg}$ , is used to monitor the operation of the heat exchanger. The locations of these probes are shown in Figure 13.

### Steady-State Data Acquisition System

Real-time steady-state data acquisition and data display are provided by the NASA Glenn Escort Alpha system. This is the standard data acquisition and data display system used in the large test facilities at NASA Glenn. The system accommodates inputs from the Electronically Scanned Pressure System (ESP), the facility distributed process control system, and any analog devices such as thermocouples, RTDs and pressure transducers. This system records all steady-state pressures and temperatures from the 9-ft survey rake, 2-D RTD array, the tunnel bellmouth pitot-static probes, and the total temperature probes in the D-corner. It also records important facility parameters such as fan rotational speed and spray bar air pressure. The Escort program, designated D046, used for data collection, online data analysis and display was developed specifically for the aero-thermal calibration testing.

The Electronically Scanned Pressure system used during this test program utilized plug-in modules that each contained 32 individual transducers with individual ports. Each transducer/port can be addressed separately and scanned at a rate of 10,000 ports per second. Calibration of all ESP transducers was performed automatically by the system at least every 2 hr. For this test program,  $\pm 5$  psid modules were used. The accuracy in the pressure measurements made with the ESP system is 0.1 percent of full-scale of the module, or 0.005 psia for the  $\pm 5$  psid modules used.

### Thermal Anemometry Instrumentation

Commercially available constant temperature hot wire anemometers were used for the turbulence intensity measurements. Three anemometers were required for the three single sensor probes used. Each anemometer was equipped with its own signal conditioner for low-pass filtering, DC offsetting, and amplifying. A commercial off the shelf (COTS) 3-channel 12-bit analog to digital converter with an input range of  $\pm 5$  V was used to digitize the signal conditioned anemometer bridge voltages. A COTS personal computer with COTS software was used to control the data acquisition process and to store the digitized data on computer hard disk.

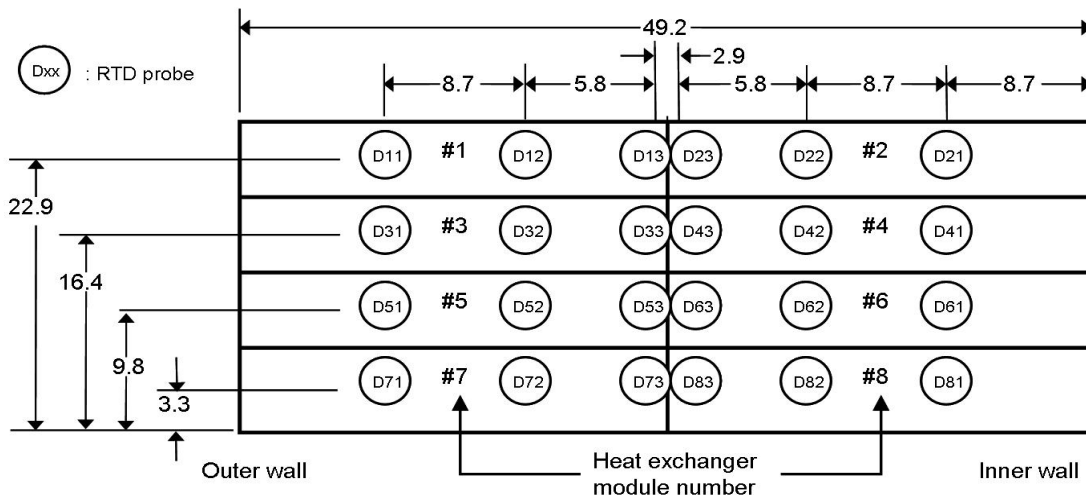


Figure 13.—Layout of the RTD probes mounted on the D corner turning vanes.

The hot wire probes were calibrated in place using the velocities measured by the flow angle pressure probes. Data was acquired at small enough velocity increments to generate calibration curves for the hot wires. The probes were generally used from 50 mph to 175 mph, i.e., within the incompressible range. Over this speed range, the bridge output voltage varied between 1.3 and 1.8 V.

## Test Procedures and Execution

This section and the subsequent subsections describe aspects of the test planning, setup and execution that were critical to the success of the aero-thermal calibration in the IRT. As indicated in Reference 2, it is important that tunnel calibration tests are given proper attention to detail and with respect to project management. Also, customer requirements must be considered when developing the tunnel calibration test plan, test matrix and hardware. This specific test considered needs from both internal and external customers requiring improved total temperature measurement accuracy, correspondingly improving total temperature calibration. These requirements had a direct impact on the development of the new test hardware as well as the test planning and execution.

### Test Matrix

The recommendations made following the 2000 aero-thermal calibration (Ref. 4) were implemented for the 2004 full aero-thermal calibration. The “aero” and “thermal” data collection were separated; the 9-ft survey rake was used to collect the “aero” data at ambient temperature conditions and the 2-D RTD array was used to collect all temperature calibration data. The “aero” test matrix, seen in Table 1 was completed in 3 test days. Only 1 day was needed to complete the RTD array test matrix, seen in Table 2.

Table 2 also shows the update in how the temperature calibration test matrix was constructed. In previous tests, the total temperature calibration test matrix was set up to cover the operating range of the IRT by selecting test points at minimum and maximum conditions and at regular intervals in between based on the D-corner total temperature. Starting in 2004, the temperature calibration test matrix was based on the test section static temperature as outlined in the guidelines provided in Reference 1. The actual test points are still the test section airspeed and D-corner total temperature, but the total temperature setting is determined from the airspeed and desired test section static temperature. The order of test points were arranged from highest to lowest in order to more efficiently use the available test time.

TABLE 1.—TEST MATRIX FOR THE IRT AERO-THERMAL CALIBRATION USING THE 9-ft SURVEY RAKE (2004 TEST)

Rake height, $Y$ , in.	Total temperature, $T_{T,davg}$ , °C	Test section airspeed, $U_{ts}$ , knots	Spraybar air pressure, $P_{air}$ , psig
36	Ambient (nominally 5 °C)	0, 43, 65, 87, 100, 130, 152, 173, 200, 217, 240, 260, 282, 304, 339	0, 70
6, 12, 18, 24, 30, 42, 48, 54, 60, 66	ambient	0, 43, 87, 100, 130, 173, 200, 217, 260, 304	0

TABLE 2.—TEMPERATURE CALIBRATION TEST MATRIX USING THE 2–D RTD ARRAY (2004 TEST).

Test section static temperature, $T_{S,ts}$ , °C	Test section airspeed, $U_{ts}$ , knots	D-corner total temperature, $T_{T,davg}$ , °C	Spraybar air pressure, $P_{air}$ , psig	Test section static temperature, $T_{S,ts}$ , °C	Test section airspeed, $U_{ts}$ , knots	D-corner total temperature, $T_{T,davg}$ , °C	Spraybar air pressure, $P_{air}$ , psig
-30	43	-29.8	0, 70	-5.6	43	-5.3	0, 70
-30	100	-28.7	0, 70	-5.6	100	-4.2	0, 70
-30	130	-27.8	0, 70	-5.6	130	-3.3	0, 70
-30	200	-24.5	0, 70	-5.6	200	-0.3	0, 70
-30	217	-23.8	0, 70	-5.6	217	0.7	0, 70
-30	304	-17.8	0, 70	0	43	0.2	0, 70
-17.8	43	-17.6	0, 70	0	100	1.3	0, 70
-17.8	100	-16.4	0, 70	0	130	2.2	0, 70
-17.8	130	-15.6	0, 70	-0.6	200	4.7	0, 70
-17.8	200	-12.5	0, 70	-1.7	217	4.6	0, 70
-17.8	217	-11.6	0, 70	-7.2	304	4.9	0, 70
-17.8	304	-5.6	0, 70	4.4	43	4.7	0, 70
				3.3	100	4.7	0, 70

One area where the test matrices deviate from the recommendations in Reference 1 was at the higher airspeed and temperature settings because it was not possible to set static temperatures of 4.4 °C at 174 and 260 knots. The total temperatures were 8.3 and 13.3 °C, respectively, since temperature control is not available at total temperature settings above about 4 °C). Therefore, the total temperature (D-corner temperature) was set at 5 °C with the lower related static temperatures in the test section as listed in Table 2.

Test points were added to the 2–D RTD Array test matrix to cover static temperature conditions around the freezing point, 0 °C, since this is an important operating range for the icing community. Test points were also added to the test matrices corresponding to airspeed settings of 100, 200 and 300 knots so that flow quality information would be available at these specific settings.

### Test Procedures

For the 2004 test entry, testing using the 9-ft survey rake was completed in May. Testing using the 2–D RTD array was delayed until July due to additional time allowed for icing cloud calibration.

The first test configuration was with the 9-ft survey rake positioned at the test section centerline. Prior to the first tunnel run, the flow angle probe, pitch and yaw offset angles were measured with respect to the tunnel centerline using a six-degree of freedom digitizing arm. Providing a check, in addition to these measurements pitch and yaw offset angles were verified with a digital level, tape measure or ruler. The combination of these measurements formed the baseline pitch and yaw offset angles. For each change in Z, vertical rake height change, the flow angle probe pitch and yaw offset angles were measured again with the digital level and tape measure and compared to the baseline values. All changes from the baseline were recorded and were later used to correct the pitch and yaw angles generated by the data reduction process. Table 3 shows the typical test conditions encountered during the 9-ft survey rake testing. The values listed in Table 3 are the average of all readings collected for each nominal setting across all test runs. It is important to note that all testing using the 9-ft survey rake was conducted at temperatures of approximately 4 °C ( $T_{T,bm} \geq 4$  °C). This is done to avoid having the tips of the pressure probes freeze during tunnel operation and to decrease the possibility of getting water in the instrumentation lines.

TABLE 3.—TYPICAL TEST CONDITIONS IN THE IRT DURING THE 9-ft SURVEY  
RAKE TESTING AS PART OF THE 2004 AERO-THERMAL CALIBRATION

Test section airspeed, $U_{ts}$ (knots)	Spray bar air pressure, $P_{air}$ (psig)	Bellmouth Mach number, $M_{bm}$	Bellmouth total pressure, $P_{T,bm}$ (psia)	Bellmouth static pressure, $P_{S,bm}$ (psia)	D-corner average total temperature, $T_{T,davg}$		Drive system fan speed (rpm)
					(°R)	(°C)	
43.5	0	0.067	14.308	14.264	510.3	5.4	76
51.3	70	0.079	14.315	14.252	502.7	6.1	76
64.5	0	0.099	14.310	14.213	505.7	7.8	109
70.1	70	0.107	14.314	14.200	507.1	8.6	109
87.3	0	0.134	14.308	14.131	507.9	9.0	143
90.4	70	0.139	14.311	14.120	504.1	6.9	143
99.4	0	0.153	14.305	14.074	504.7	7.2	163
101.6	70	0.156	14.310	14.070	505.7	7.8	163
131.0	0	0.201	14.299	13.902	507.5	8.8	212
131.5	70	0.202	14.304	13.905	508.0	9.0	212
150.9	0	0.232	14.296	13.770	505.8	7.9	242
150.6	5	0.232	14.300	13.775	506.0	8.0	242
151.1	20	0.233	14.301	13.771	503.9	6.8	242
152.1	70	0.234	14.301	13.768	507.3	8.7	242
172.2	0	0.265	14.299	13.618	507.2	8.6	275
173.4	70	0.268	14.306	13.611	503.9	6.8	275
198.8	0	0.306	14.290	13.394	510.5	10.4	315
200.1	70	0.309	14.295	13.381	507.5	8.8	315
216.4	0	0.334	14.290	13.230	509.1	9.7	342
218.6	70	0.337	14.293	13.212	509.3	9.8	342
237.3	0	0.365	14.291	13.037	515.1	13.0	373
237.9	70	0.366	14.294	13.032	514.4	12.6	373
257.6	0	0.397	14.284	12.817	515.4	13.2	404
259.0	70	0.399	14.287	12.803	515.0	13.0	404
280.3	0	0.430	14.280	12.573	521.1	16.4	439
281.8	70	0.434	14.283	12.552	519.0	15.2	439
300.9	0	0.466	14.270	12.296	515.2	13.1	473
302.9	70	0.468	14.271	12.283	518.0	14.6	472

The Escort system was used to collect data for both the 9-ft survey rake and the 2-D RTD array. For each test condition, two to three readings were taken at a scan rate of one per second, for 20 sec, and averaged to generate the final reading.

All three probe types were recorded simultaneously by individual analog-to-digital converter data acquisition boards integrated into a personal computer. The data acquisition boards were configured to sample three or six channels simultaneously, depending on whether a single sensor or dual sensor X probe was used. The sensors were set to acquire data at a rate of 10,000 samples per second and 100,000 data points per channel. This is the equivalence of 10 sec of data for each channel. The signal conditioners for each hot wire probe were configured to a low pass filter at 4000 Hz, DC offset of -1 V, and a gain of 5.

The addition of the 2-D RTD array increased efficiency of gathering total temperature calibration and flow quality data. The array is mounted at the test section test plane and requires minimal documentation of axial station and probe measurement prior to operation. Unlike the 9 ft survey rake no detailed alignment procedure of the RTD probes is required when using the 2-D RTD array. Checks of the RTD

array instrumentation connections and structure are completed prior to the tunnel run. The most efficient way to complete the RTD array test matrix is to start at the coldest bellmouth total temperature condition and work through the matrix toward the higher conditions. This is done because it is faster and easier to change airspeed settings at a given total temperature, rather than hold the airspeed constant and change temperature. The order of test points for the RTD array test matrix, seen in Table 2, is listed by increasing total temperature.

## Data Reduction and Analysis

This section provides a detailed description of the steps taken in the reduction and analysis of all data collected using the 9-ft survey rake and the 2-D RTD array. Included in this section are instrumentation calibrations, data corrections and conversion equations. The conversion equations were used to convert the measured pressures and temperatures into Mach number, flow angle and turbulence data. For all of the equations listed, the specific heat ratio,  $\gamma$ , is 1.4 and the specific gas constant for air,  $R$ , is equal to  $1716 \text{ ft}^2 / (\text{sec}^2 \text{ }^\circ\text{R})$ .

U.S. customary units of measurement are used in the following data reduction. However, the icing community prefers a mixed set of units including airspeed in knots and temperature in degrees Celsius ( $^\circ\text{C}$ ). Therefore, the details on the data reduction are presented as they are carried out in English units. The final results have been converted to and are presented in the units used by the icing community.

### Facility Instrumentation

The measured and calculated facility parameters that are of greatest importance to the IRT aerothermal calibration are the bellmouth total pressure, bellmouth static pressure, and the D-corner total temperature. The bellmouth total pressure is the average of the two measured total pressures from the north wall and south wall

$$P_{T,bm} = (P_{T,north} + P_{T,south})/2$$

In the IRT, the total pressure and differential pressures are measured. The static pressure for each bellmouth probe is calculated from their difference. The north and south probe are each calculated using the equation

$$P_S = P_T - \Delta P$$

The bellmouth static pressure is again the average of the two probe calculations

$$P_{S,bm} = (P_{S,north} + P_{S,south})/2$$

The facility total temperature,  $T_{T,davg}$  is the average of the 24 RTDs mounted on the leading edge of the D-corner turning vanes

$$T_{T,davg} = \frac{1}{24} \sum_{i=1}^{24} T_{T,d,i}$$

In addition to the basic parameters, some calculated parameters were also needed based on the bellmouth total and static pressure measurements,  $P_{T,bm}$  and  $P_{S,bm}$ , respectively. The calculated bellmouth Mach number is

$$M_{bm} = \sqrt{\frac{2}{\gamma-1} \left[ \left( \frac{P_{T,bm}}{P_{S,bm}} \right)^{\frac{\gamma-1}{\gamma}} - 1 \right]}$$

The dynamic pressure based on bellmouth conditions is

$$q_{bm} = \frac{\gamma}{2} \cdot P_{S,bm} \cdot M_{bm}^2$$

### 9-ft Survey Rake Calculations

Data collected by the 9-ft survey rake is used to construct calibration curves for total pressure and Mach number. Additionally, the collected data provides flow quality information on total pressure, static pressure, Mach number, flow angularity and turbulence. For the following calculations, subscript “*bm*” refers to measured or calculated parameters associated with the two bellmouth pitot-static probes located on the inner and outer tunnel walls at the exit of the bellmouth, as shown in Figure 4. The subscript “*rake*” refers to measured or calculated parameters associated with any of the probes on the 9-ft survey rake. Additionally, the subscript “*local*” refers to the measured or calculated corrected “*rake*” parameters, which have been corrected by individual probe calibration coefficients and represent the true “*local*” properties in the test section. Note that all “*local*” total pressures, static pressures, and Mach numbers are normalized by bellmouth (“*bm*”) parameters to arrive at recovery ratios. All of the compressible flow equations used in the data reduction can be found in Reference 9.

#### Basic Flow Parameters

The average static pressure sensed by each pressure probe was calculated by averaging the four static pressure taps on the probe body

$$P_{S,rake} = \frac{(P_6 + P_7 + P_8 + P_9)}{4}$$

The probe total pressure is simply the pressure measured by port  $P_5$  ( $P_{T,rake} = P_5$ ). Mach number is calculated using the ratio of the static to total pressure measured by each probe

$$M_{rake} = \sqrt{\frac{2}{\gamma-1} \left[ \left( \frac{P_{T,rake}}{P_{S,rake}} \right)^{\frac{\gamma-1}{\gamma}} - 1 \right]}$$

The correction equations for total and static pressure are based on the rake Mach number.  $C_o$  and  $C_q$  are functions of  $M_{rake}$  and are experimentally determined during calibration of the pressure probe flow angle. Values for these coefficients can be found in Reference 8.

$$P_{T,local} = P_{T,rake} - C_o(M_{rake}) \cdot [P_{T,rake} - P_{S,rake}]$$

$$P_{S,local} = P_{T,local} - \frac{(P_{T,rake} - P_{S,rake})}{C_q(M_{rake})}$$

The local test section Mach number for each probe is determined using the  $P_{T,local}$  and  $P_{S,local}$  calculated above

$$M_{local} = \sqrt{\frac{2}{\gamma-1} \left[ \left( \frac{P_{T,local}}{P_{S,local}} \right)^{\frac{\gamma-1}{\gamma}} - 1 \right]}$$

Local dynamic pressure in the test section is then determined

$$q_{local} = \frac{\gamma}{2} \cdot P_{S,local} \cdot M_{local}^2$$

The thermocouples on the 9-ft survey rake are only used to monitor the temperature during the aero portion of the calibration. Total temperature calibration and flow quality data are collected using the 2-D RTD array. The following equations are used to reduce the collected temperature data. The equations containing “local” and “rake” parameters apply to all eleven individual total temperature probes mounted on the 9-ft survey rake. The corrected local total temperature,  $T_{T,local}$ , is calculated as a function of  $T_{T,rake}$  and  $M_{local}$

$$T_{T,local} = C_t(M_{local}) \cdot T_{T,rake}$$

$C_t$  is the recovery coefficient for each individual total temperature probe and is a function of  $M_{local}$ . These coefficients were determined experimentally when the probes were calibrated in the NASA Glenn 3.5-in. diameter free jet calibration facility. The total temperature probes gradually predict temperatures lower than the actual temperature as the local Mach number increases. For example, at a local Mach number of 0.1, typical values of  $C_t$  are 1.001 and at a local Mach number of 0.6, the values of  $C_t$  are generally around 1.005. The values of  $C_t$  are listed in Reference 10. The local static temperature was calculated to monitor data and conditions during the test

$$T_{S,local} = T_{T,local} \cdot \left( 1 + \frac{\gamma-1}{2} M_{local}^2 \right)^{-1}$$

The local airspeed is based on a matched set of one pressure probe and one thermocouple from the 9-ft survey rake. Each pressure probe was matched to the thermocouple mounted directly under it on the rake. The local airspeed for each set of probes was calculated using the following equation

$$U_{local} = M_{local} \cdot \sqrt{\gamma R T_{S,local}}$$

### Flow Angularity

The equations in this section were used to generate pitch and yaw flow angle data from the raw pressure data obtained from the flow angle pressure probes (recall Figure 6). The average of the four flow angle pressure measurements is used as part of the calculation for both pitch and yaw flow angles

$$P_{avg} = \frac{P_1 + P_2 + P_3 + P_4}{4}$$

Pressure coefficients are calculated for both the pitch angle and yaw angle based on the five pressure ports on the hemispherical head of each probe. The pitch angle is related to the pressure difference between the ports in the pitch plane, ports  $P_1$  and  $P_3$ , while the yaw angle is related to the difference between the yaw plane ports,  $P_2$  and  $P_4$ , as shown in the following equations

$$C_\alpha = \frac{(P_3 - P_1)}{(P_5 - P_{avg})} \text{ and } C_\beta = \frac{(P_4 - P_2)}{(P_5 - P_{avg})}$$

The pitch angle,  $\alpha$ , and yaw angle,  $\beta$ , are calculated as a function of  $M_{rake}$ ,  $C_\alpha$  and  $C_\beta$ .

$$\alpha = K_{0,\alpha}(M_{rake}) + K_{1,\alpha}(M_{rake}) \cdot C_\alpha + \Delta_{\alpha,arm} + \Delta_{\alpha,level}$$

$$\beta = K_{0,\beta}(M_{rake}) + K_{2,\beta}(M_{rake}) \cdot C_\beta + \Delta_{\beta,arm} + \Delta_{\beta,ruler}$$

Pressures  $P_1$  through  $P_5$  are measured directly from the flow angle pressure probes. The coefficients  $K_{0,\alpha}$ ,  $K_{1,\alpha}$ ,  $K_{0,\beta}$ , and  $K_{2,\beta}$  were experimentally determined when the flow angle pressure probes were calibrated in the NASA Glenn 3.5-in. diameter free jet calibration facility and are all functions of  $M_{rake}$ . Values for these coefficients are documented in Reference 8. The  $\Delta_{\alpha,arm}$  and  $\Delta_{\beta,arm}$  values were determined by measuring the pitch and yaw offset angles for the probes with a 6 degree of freedom digitizing arm and were constant for every  $Z$  elevation. The  $\Delta_{\alpha,level}$  and  $\Delta_{\beta,ruler}$  values were equal to  $0^\circ$  for the  $Z=36$ -in. elevation since this elevation is where the baseline measurements were taken and were different for every other  $Z$  elevation. These values were determined by taking measurements with a digital level and a ruler and comparing these measurements to the baseline values. Deviations from the baseline numbers were entered as  $\Delta_{\alpha,level}$  and  $\Delta_{\beta,ruler}$ .

### Turbulence Intensity

As was previously indicated, the hot wire probes were calibrated *in situ* in the IRT. This is because it is difficult to match the temperature and static pressure conditions of the IRT with those in the probe calibration facility. Data were acquired so that calibration curves could be constructed after acquisition was completed. Time averaged bridge voltages were matched to time averaged airspeeds from the flow angle pressure probes from the 9-ft survey rake for the same condition. Calibration curves, exponential functions with effective air velocity as a function of hot wire bridge voltage, were generated for each hot wire probe sensor. The equations used in this curve-fit process are from Reference 11<sup>3</sup> and are given below,

$$U_{HW,eff,i} = U_{local} \cdot \cos \theta_{HW,i} \text{ and } U_{HW,eff,i} = A_{0,i} \cdot E_{HW,i} + A_{1,i} \cdot e^{A_{2,i} \cdot E_{HW,i}}$$

where  $i = 1$  for a single, straight-wire sensor and  $i = 1$  to  $2$  for a dual cross-wire sensor (X probe).  $\theta_{HW,i}$  is the angle of the hot wire sensor relative to the freestream velocity vector minus  $90^\circ$ . For a single sensor probe, the sensor is normal to the velocity vector and  $\theta_{HW,1}$  is  $(90^\circ - 90^\circ =) 0^\circ$  for this case. For a dual sensor X probe at  $0^\circ$  angle of attack, one sensor is at  $45^\circ$  and the other is at  $135^\circ$  relative to the velocity vector. For these two sensors,  $\theta_{HW,1}$  is  $(45^\circ - 90^\circ =) -45^\circ$  and  $\theta_{HW,2}$  is  $(135^\circ - 90^\circ =) +45^\circ$ .  $U_{local}$  is the freestream velocity, and  $U_{HW,eff,i}$  is the velocity component normal to the hot-wire sensor.  $E_{HW,i}$  is the hot-wire voltage measured by the anemometer. Once the values of  $U_{HW,eff,i}$  are computed, these values along with the corresponding values of hot wire anemometer bridge voltage,  $E_{HW,i}$  can be used to arrive at values of  $A_{0,i}$ ,  $A_{1,i}$ , and  $A_{2,i}$  via non-linear least squares curve-fitting using the exponential equation given above.

<sup>3</sup>The procedure was changed in subsequent calibrations to use the King's Law equation and single-wire probes.

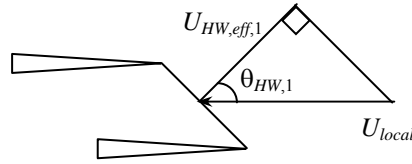


Figure 14.—Schematic depicting terminology on one wire of X probe.

The reader may be wondering how accurate flow angles and transverse velocities can be computed by the dual sensor X probe if no angular calibration data is used. To answer this question, two key assumptions are called upon. The first key assumption is that the X probes will only be used to assess the unsteadiness in flow angle and will not be used to quantify the absolute flow angle. The resulting flow angles and transverse velocities will all be centered around zero and have averages essentially at zero. This should work fine in the IRT test section since we know that the flow angles will be small, typically  $\pm 2^\circ$  or less, and will be centered about zero. The second key assumption is that the X probes used in this test behave like other X probes previously calibrated through various flow angles. The results for an X probe calibrated through various flow angles show that the calibration map will collapse down to one curve when effective velocity is plotted versus hot wire anemometer bridge voltage. This typically holds true for angles between  $\pm 20^\circ$ .

Given the exponential curve fit equation used to relate hot wire effective velocity to hot wire anemometer bridge voltage, data reduction can continue with the equations given below for a dual sensor hot wire X probe.

$$\text{Test section airspeed: } U_{HW} = \sqrt{U_{HW,eff,1}^2 + U_{HW,eff,2}^2}$$

$$\text{Pitch flow angle: } \alpha_{HW} = 45^\circ - \tan^{-1}\left(\frac{U_{HW,eff,2}}{U_{HW,eff,1}}\right)$$

$$\text{Axial velocity component: } u_{HW} = U_{HW} \cdot \cos(\alpha_{HW})$$

$$\text{Transverse velocity component: } v_{HW} = U_{HW} \cdot \sin(\alpha_{HW})$$

For a single sensor hot wire probe, the following equalities are used instead of the four equations above.

$$u_{HW} = U_{HW} = U_{HW,eff,1}$$

Once  $u_{HW}$  is available for a single sensor probe, and  $u_{HW}$  and  $v_{HW}$  are available for dual sensor X probe, statistics necessary for computing turbulence intensity can be calculated using the equations given below. The value of  $N$  was 100,000. The average axial and transverse air velocity components are determined using the following equations.

$$u_{HW,avg} = \frac{1}{N} \sum_{i=1}^N u_{HW,i} \quad \text{and} \quad v_{HW,avg} = \frac{1}{N} \sum_{i=1}^N v_{HW,i}$$

The magnitude of the velocity vector, also known as airspeed, is determined by combining the axial and transverse velocity components.

$$U_{HW,avg} = \sqrt{u_{HW,avg}^2 + v_{HW,avg}^2}$$

The standard deviation of the axial and transverse velocity components are calculated using the following standard statistical equations.

$$\sigma_{u_{HW}} = \sqrt{\frac{1}{N-1} \sum_{i=1}^N (u_{HW,i} - u_{HW,avg})^2} \quad \text{and} \quad \sigma_{v_{HW}} = \sqrt{\frac{1}{N-1} \sum_{i=1}^N (v_{HW,i} - v_{HW,avg})^2}$$

Finally, the turbulence intensity for the axial and transverse velocity components are defined as

$$TI_u = \frac{\sigma_{u_{HW}}}{U_{HW,avg}} \times 100\% \quad \text{and} \quad TI_v = \frac{\sigma_{v_{HW}}}{U_{HW,avg}} \times 100\%$$

Since in-situ calibration curves were generated, there was no need to correct for changes in temperature or static pressure. The calibration curves took care of these inherent variations. In addition, new calibration curves were generated for every velocity sweep.

## 2-D RTD Array Calculations

The total temperature measurements made by the 49 RTD probes on the 2-D RTD array only required a correction of flow recovery. The determination of the total temperature flow recovery correction was described in a previous section of this report. The resulting correction equation is

$$T_{T,local} = (C_0 + C_1 \cdot M_{ts} + C_2 \cdot M_{ts}^2) \cdot T_{T,array}$$

Where  $T_{T,array}$  is the total temperature measured by each probe and  $T_{T,local}$  is the corrected total temperature. The correction coefficients are listed in Appendix B. Only 20 of the 49 probes on the array were directly calibrated for flow recovery and therefore have specific coefficients. These 20 probes were mounted in the interior portion of the array. The remaining 29 RTD probes used the average of the correction coefficients as listed in Appendix B.

## Measurement and Data Uncertainty

Details of the data uncertainty analysis are contained in Appendix A. The uncertainty analysis follows the standard procedure set in Reference 12.

## Data Analysis

Standard test procedure was to collect three data readings for each test condition listed in the test matrices for the 9-ft survey rake and the 2-D RTD array. Each data reading was the average of 20 scans of data, at a data acquisition rate of 1 scan per second. The data readings were used in two combinations for development of calibration curves versus assessment of test section flow quality.

- For the construction of the calibration curves, the readings were used as they were collected (average of 20 scans). So, each test condition would contribute three individual readings to the development of the calibration curves.
- Flow quality distribution data plots were created by averaging the three data readings collected at each test condition. For data from the 9-ft survey rake, the data represented at each rake position, or height, is the average of three separate data readings collected at one test condition over the course of 11 tunnel runs (one run for each of the 11 vertical rake positions). For the 2-D RTD

array, the data is again plotted by height of the RTD probes above the test section floor and each data set of the average of three readings collected at a given test setting. However, unlike the 9-ft rake, for the array, only one tunnel run was needed to collect all the data for a given test setting.

- To combine data collected using the 9-ft survey rake over several test runs to show the composite flow quality in the test section, the pressure, Mach number and airspeed data were normalized using data collected simultaneously by the facility bellmouth rakes.
- The corrected pitch and yaw flow angle data were converted into flow angle vectors to more easily visualize the flow direction. The length of the vector represents the resultant flow angle magnitude and the orientation of the vector shows the resultant flow direction. The magnitude and orientation were calculated as shown below.

$$\text{Vector magnitude, } V_m \quad V_m = \sqrt{\alpha^2 + \beta^2}$$

$$\text{Vector orientation, } V_\phi \quad \phi = \tan^{-1} \left| \frac{\alpha}{\beta} \right| \quad \text{and} \quad V_\phi = \begin{cases} \phi, & \text{if } \alpha \geq 0 \text{ and } \beta \geq 0 \\ 180 - \phi, & \text{if } \alpha \geq 0 \text{ and } \beta < 0 \\ \phi + 180, & \text{if } \alpha < 0 \text{ and } \beta < 0 \\ 360 - \phi, & \text{if } \alpha < 0 \text{ and } \beta \geq 0 \end{cases}$$

## Discussion of Results

There are three sets of results described in this section: (1) the aero-thermal calibration curves for determining the operating conditions in the IRT, (2) detailed aero-thermal flow quality mapping data for the IRT test section and (3) uncertainty estimates for the measured and calculated data.

### Aero-Thermal Calibration Curves

As indicated, one of the primary goals of this test entry was to update the aero-thermal calibration curves used to set operating conditions in the IRT test section. A computer program subroutine was created following the 2000 calibration. This subroutine contained the calibration relationships and additional calculations to fully describe the test section aero-thermal operating point. This subroutine is the IRT Aero-Thermal, and abbreviated as IRTAT. The data collected during the 2004 calibration test were used to update the IRTAT.

#### Updates Based on 2004 Calibration Test

The existing calibration curves, based on 2000 calibration data, were compared to calibration curves developed from the 2004 data. It was not expected that the 2000 and 2004 curves would match due to the changes made to the facility, but large variations were also not anticipated. Figure 15 shows the four calibration relationships that were created based on the 2004 data, total pressure, static pressure, Mach number and total temperature. The primary calibration relationships were changed after review of the 2004 calibration curves and comparison to the existing year 2000 calibration curves. This change was completed by replacing the total pressure curve with the Mach number calibration curve, due to a reduced sensitivity on spraybar air injection effects. The 2000 calibration curves do not include spraybar air injection. Spraybar air injection and high temperature test points, above 37 °F or 3 °C, were not included in the total temperature calibration curve. The computing requirements for IRTAT were updated per the new calibration curves (Revision 4, dated July 29, 2004).<sup>4</sup> The calculations used in IRTAT (Revision 4) are described below.

<sup>4</sup>Additional corrections were made to IRTAT so the final version based on the 2004 data was Revision 5, dated August 13, 2004.

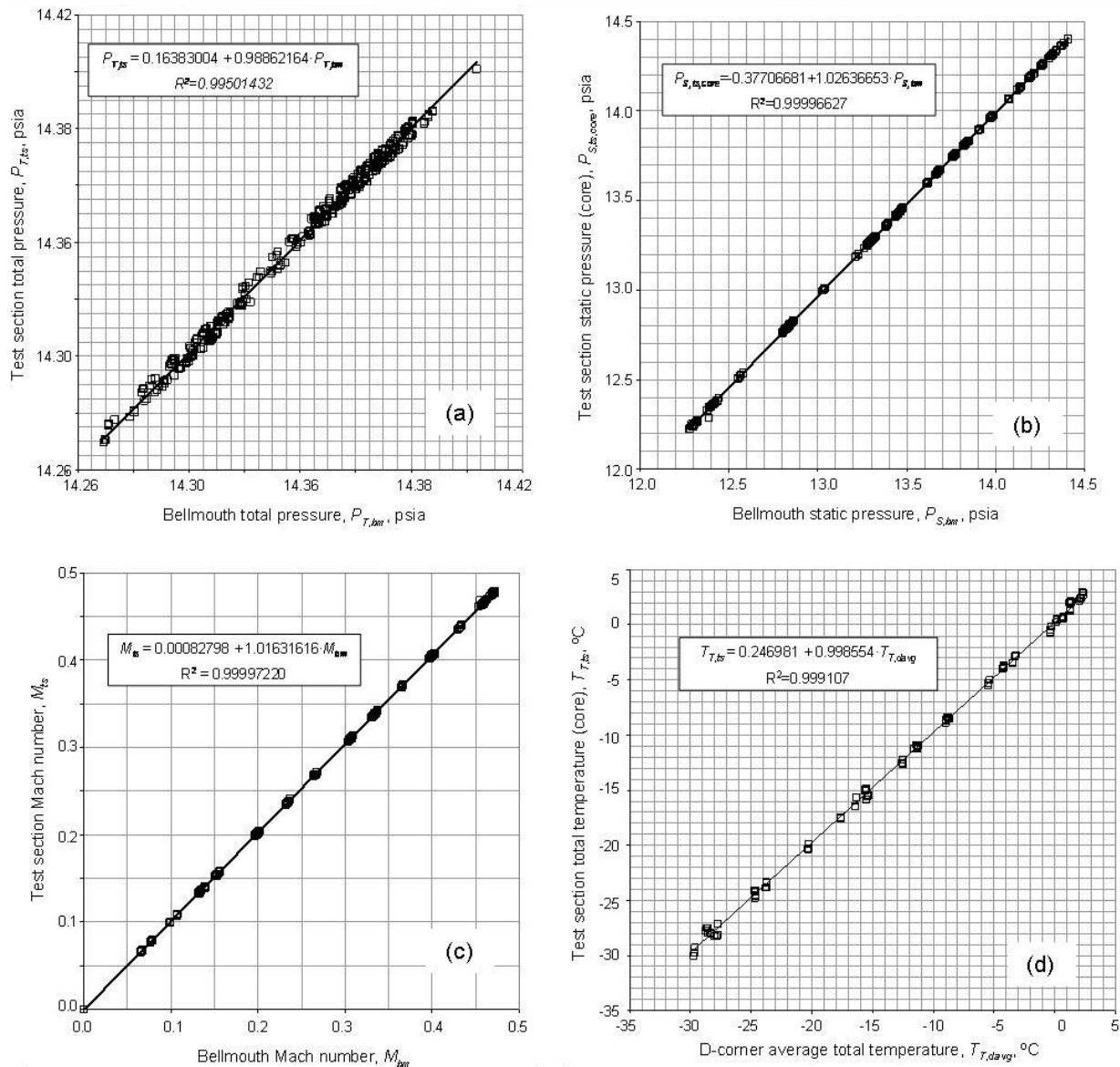


Figure 15.—Aero-thermal calibration curves based on the 2004 full calibration test

### Inputs to IRTAT

The measured inputs for determining the calibrated test section aero-thermal conditions are acquired from two areas. The first area is the north and south bellmouth, or test section inlet, pitot-static probes, and the second area is the 24 D-corner RTD probes. Details and definitions on these inputs and their use for determining the calibrated parameters are listed below, with the appropriate units listed in parenthesis.

Bellmouth total pressure (psia),  $P_{T,bm}$ , is the average of the two measured pressures, one each from the north and south bellmouth rakes

$$P_{T,bm} = \frac{1}{2} (P_{T,bm,n} + P_{T,bm,s})$$

Likewise, the bellmouth delta-pressure (psid),  $\Delta P_{bm}$ , is the average of the two delta-pressure transducers

$$\Delta P_{bm} = \frac{1}{2}(\Delta P_{bm,n} + \Delta P_{bm,s})$$

The bellmouth static pressure (psia),  $P_{s,bm}$ , is calculated from the measured total and differential pressures. First the static pressure for each bellmouth rake is determined

$$P_{S,bm,n} = P_{T,bm,n} - \Delta P_{bm,n} \text{ and } P_{S,bm,s} = P_{T,bm,s} - \Delta P_{bm,s}$$

The bellmouth static pressure is then the average of the static pressure calculated from each bellmouth probe

$$P_{S,bm} = \frac{1}{2}(P_{S,bm,n} + P_{S,bm,s})$$

The facility total temperature is the average of the 24 D-corner total temperature RTD measurements ( $^{\circ}\text{C}$ ),  $T_{T,davg}$

$$T_{T,davg} = \sum_{i=1}^{24} T_{T,D,i}$$

The Mach number based on bellmouth conditions,  $M_{bm}$ , is calculated from the ratio of the bellmouth static to bellmouth total pressure using the standard isentropic flow equation (Eq. 44 from Ref. 9 with  $\gamma=1.4$ )

$$M_{bm} = \sqrt{5 \left[ \left( \frac{P_{S,bm}}{P_{T,bm}} \right)^{-0.2857} - 1 \right]}$$

### Test Section Conditions; Calibrated Values

The test section calibrated values, Mach number, static pressure and total temperature, are determined from calibration curves based on bellmouth pitot-static probes and D-corner RTD measurements. Figure 15 shows the above mentioned calibration curves. The relationships for the test section conditions are listed in the subsequent section. The calibration relationships were based on data collected using the 9-ft survey rake and the RTD Array. The 9-ft survey rake measured total and static pressure which is used to compute Mach number and the RTD Array measured the total temperature. The calibrated test section values are based on conditions measured at the test section turntable centerline and represent average flow field values at the core of the test section (the center 25 measurement locations from both the aerodynamic and thermal surveys). The pressure and Mach number calibration curves include data for all airspeed and spraybar air pressure settings, however, the total temperature calibration curve based on the 2004 calibration excludes data at the following conditions:  $T_{T,davg} > 3^{\circ}\text{C}$ , airspeed  $< 50$  knots,  $P_{air} > 0$  psig. The calibrated test section static pressure (psia),  $P_{s,ts}$ , is determined from the static pressure calibration curve, seen in

Figure 15(b), based on the least squares curve fit to the data

$$P_{S,ts} = -0.37706681 + 1.02636653 \cdot P_{S,bm}$$

The calibrated test section Mach number,  $M_{ts}$ , is likewise calculated from the Mach number calibration curve, shown in

Figure 15(c), and best fit line

$$M_{ts} = 0.00082798 + 1.01631617 \cdot M_{bm}$$

Test section total temperature ( $^{\circ}\text{C}$ ),  $T_{T,ts}$ , is determined from the calibration curve shown in

Figure 15(d) and calculated from the following equation

$$T_{T,ts} = 0.246981 + 0.998554 \cdot T_{T,davg}$$

It is important to note that the units for the calibrated test section conditions are not in a consistent set of engineering units. For subsequent calculations, the total temperature was converted from metric to English

$$T_{T,ts} (^{\circ}\text{F}) = \left( T_{T,ts} (^{\circ}\text{C}) \cdot \frac{9}{5} \right) + 32 \quad \text{and} \quad T_{T,ts} (^{\circ}\text{R}) = T_{T,ts} (^{\circ}\text{F}) + 459.67$$

### Test Section Conditions; Calculated Values

The remaining test section aero-thermal operating conditions are calculated based on the values of the calibrated parameters ( $P_{S,ts}$ ,  $M_{ts}$  and  $T_{T,ts}$ ). The calculated parameters include the total pressure, static temperature, airspeed and Reynolds number. The details of these calculations are included in Appendix C.

### Updates Based on 2005 Interim Calibration

As described in Appendix D of the IRT and Reference 3, the total temperature calibration was improved in 2005. The improved total temperature calibration was incorporated into IRTAT as Revision 6 (dated April 11, 2005). These updates are documented in Appendix D.

### Aero-Thermal Flow Quality Data

In addition to creating the aero-thermal calibration relationships, the data collected using the 9-ft survey rake and the 2-D RTD array are also used to construct detailed descriptions of the test section flow field. The flow quality data for total and static pressure, total temperature, airspeed and Mach number are presented in x-y plots (rather than contour plots) to provide as much detail as possible about the flow field. Pitch and yaw flow angle data were combined to create flow vectors that provide a combined flow angle magnitude and direction. Note that for most of the data presented, the data collected with the 9-ft survey rake at 66-in. above the test section floor (maximum height) was omitted as this data was affected by boundary layer (either the rake was in the boundary layer or tripped the boundary layer). Also, in some cases, data near the test section walls has been truncated due to the choice of y-axis scale; this was done in order to show the details of the flow field in the test section core. The total pressure measurement on probe number two (18 in. from the inside test section wall) was inoperative during testing (plugged tube). These data were omitted from the flow quality plots and account for the gap in the total pressure and Mach number distribution data at the position 18 in. from the wall. As noted earlier, 9-ft survey rake data were collected at bellmouth total temperature settings greater than  $4^{\circ}\text{C}$  (about  $40^{\circ}\text{F}$ ).

Aero-thermal flow quality goals for an icing tunnel are defined in Reference 1 and are summarized here in Table 4. In general, the IRT flow quality is very good in terms of the pressure, temperature and Mach number (airspeed) distributions and meets or exceeds the goals listed in Table 4 (as will be discussed in subsequent sections). While the IRT does not have any conventional flow field manipulators (i.e. turbulence reduction screens or flow straightening honeycomb), the heat exchanger does act a flow

manipulator and provides a significant pressure drop that evens the flow field in the tunnel. The flow angularity in the IRT test section is rather high compared with an aerodynamic wind tunnel of similar operating range. This is due to the lack of flow straightening and also the presence of the spraybars in the settling chamber upstream of the test section. The IRT is a classic example of the trade-offs made in ground testing; in order to create icing conditions, test section aerodynamic flow quality is somewhat sacrificed by the omission of normal flow field manipulators since those devices would collect ice and effect operation and icing performance of the tunnel.

TABLE 4.—AERO-THERMAL FLOW QUALITY GOALS FOR AN ICING TUNNEL TEST SECTION

Parameter	Measurement Uncertainty	Test section spatial uniformity	Tunnel centerline temporal stability
Airspeed	±1%	±2%	±2%
Static air temperature between -30 and +5 °C	±2 °C	±1 °C	±0.5 °C
Flow angularity	±0.25°	±2°	N/A
Turbulence ( $P_{air}=0$ psig)	±0.25%	<2%	±2%
Turbulence ( $P_{air}=70$ psig)	±0.25%	<2%	±2%

### Total Pressure

Figure 16 shows the total pressure flow quality data over the operating range of the IRT. As described above, the total pressure data from the 9-ft survey rake were divided by the corresponding bellmouth total pressure to remove the run-to-run variations. The data collected from various rake heights for like operating conditions were then combined to provide a representation of the test section flow quality in a plane located axially at the centerline of the test section turntable.

With the spraybar air off ( $P_{air} = 0$  psig), the total pressure data show a very uniform distribution across the test section with very little variation in the core of the test section. At the lower airspeed settings ( $U_{ts} \leq 150$  mph or 130 knots) the total pressure variation throughout the entire surveyed area of the test section is 0.003 psia or less. At about 200 mph (174 knots) a very slight gradient trend begins to form in the test section, with higher total pressures recorded near the inside test section wall. Worst case is at the 350 mph (304 knots) setting, where the total pressure variation is about 0.006 psia.

Adding spraybar air into the tunnel airflow has a measurable effect on the total pressure distribution over the entire airspeed range of the facility. In order to gage the worst case effect, data were collected with the spraybar air at 70 psig, although there was some data collected at lower air pressure settings. The effects of the spraybar air injection are larger at lower test section airspeeds. The largest effects are also seen near the test section boundaries, so the spraybar air injection appears to have an effect on the test section boundary layer. The flow in the core of the test section is affected minimally. For example, at 100 mph (87 knots) the total pressure variation in the central 5-ft core area is about 0.003 psia for both the 0 and 70 psig spraybar air injection cases. The difference is seen in the 2-ft area near each test section wall where larger variations were measured (about 0.010 psia near the outside tunnel wall). Similar results are seen at higher test section airspeeds. The spraybar air injection also increases the total pressure gradient recorded in the test section at airspeeds above 200 mph. At the 300 mph (261 knots), the gradient increases from about 0.003 psia at 0 psig spraybar air to about 0.006 psia at 70 psig spraybar air.

Overall, the IRT test section flow quality is excellent for the total pressure distributions. The magnitude of the variations discussed above is quite small and should not have any significant impact of the testing conducted in the IRT.

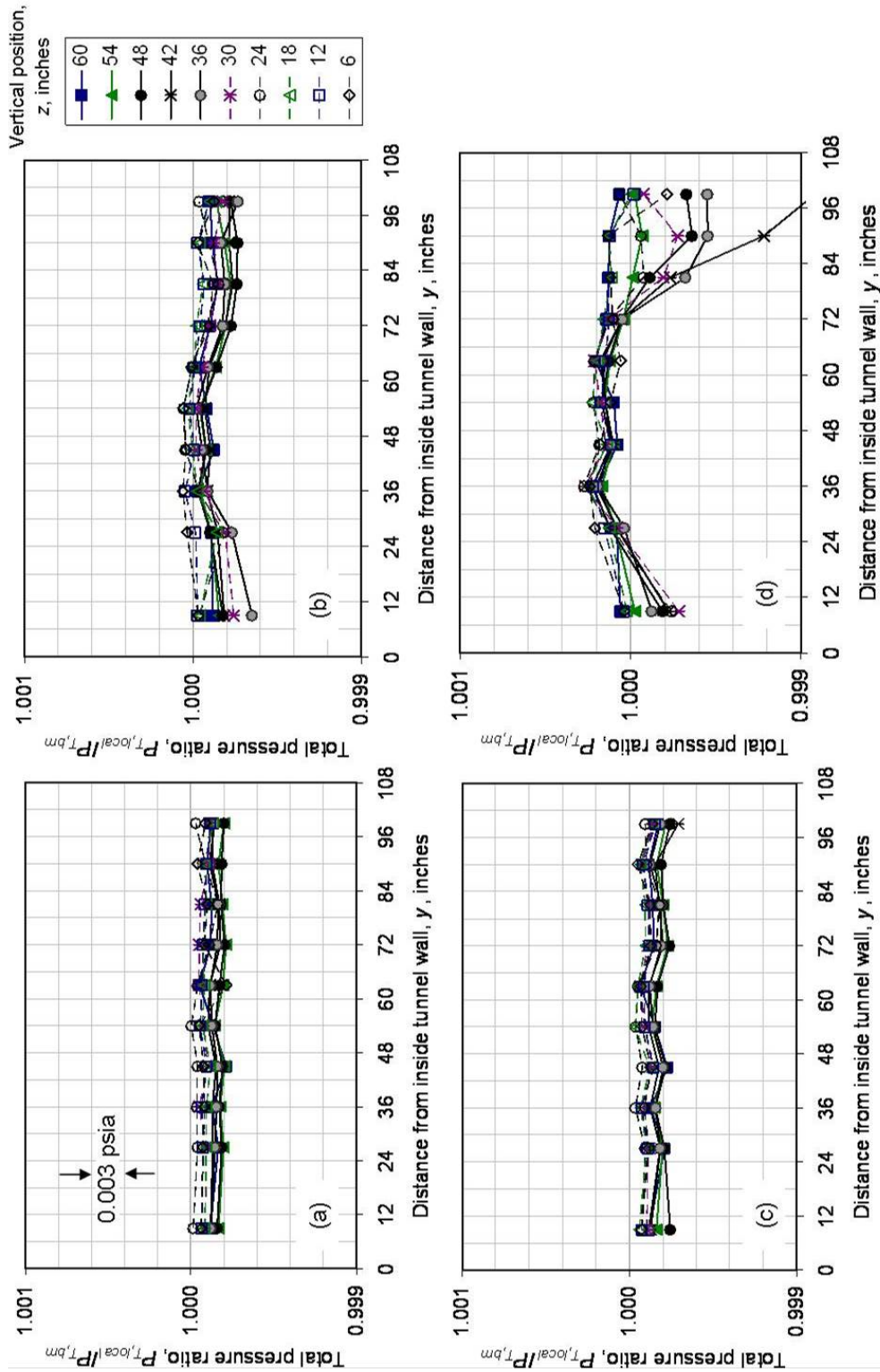


Figure 16.—Total pressure distribution data from the IRT test section. Data collected using the 9-ft survey rake mounted at 11 vertical positions over several tunnel runs. The test section total pressure data is normalized using the bellmouth total pressure measurement. Data from the 66-in. vertical position has been omitted due to boundary layer influence. Each y-axis grid (0.0002 total pressure ratio) represents approximately 0.003 psia. (a)  $U_{ts}=50$  mph (43 knots),  $P_{air}=0$  psig. (b)  $U_{ts}=50$  mph (43 knots),  $P_{air}=70$  psig. (c)  $U_{ts}=100$  mph (87 knots),  $P_{air}=0$  psig. (d)  $U_{ts}=100$  mph (87 knots),  $P_{air}=70$  psig.

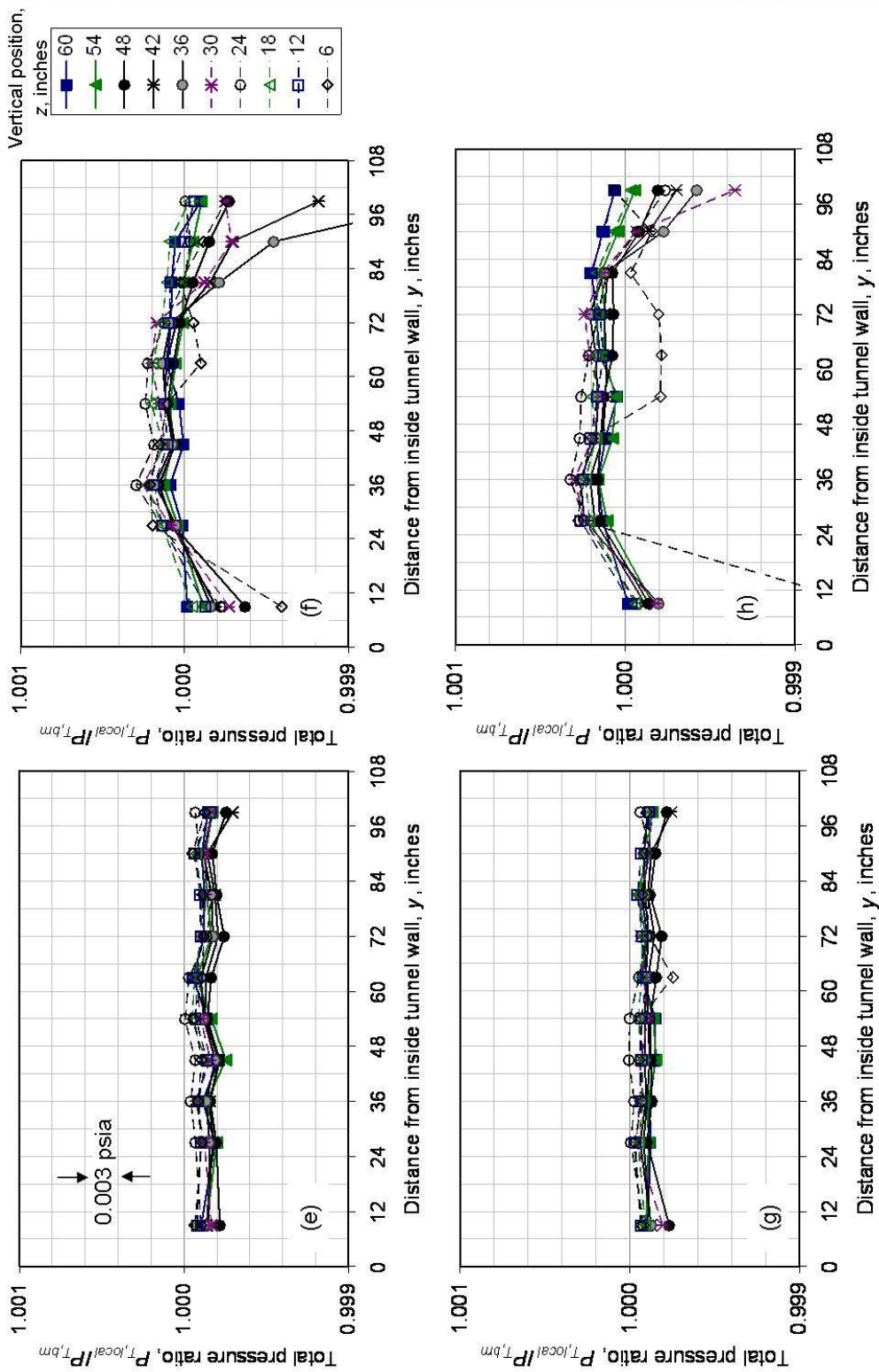


Figure 16.—Continued. (e)  $U_{is}=115$  mph (100 knots),  $P_{air}=0$  psig. (f)  $U_{is}=115$  mph (100 knots),  $P_{air}=70$  psig. (g)  $U_{is}=150$  mph (130 knots),  $P_{air}=0$  psig. (h)  $U_{is}=150$  mph (130 knots),  $P_{air}=70$  psig.

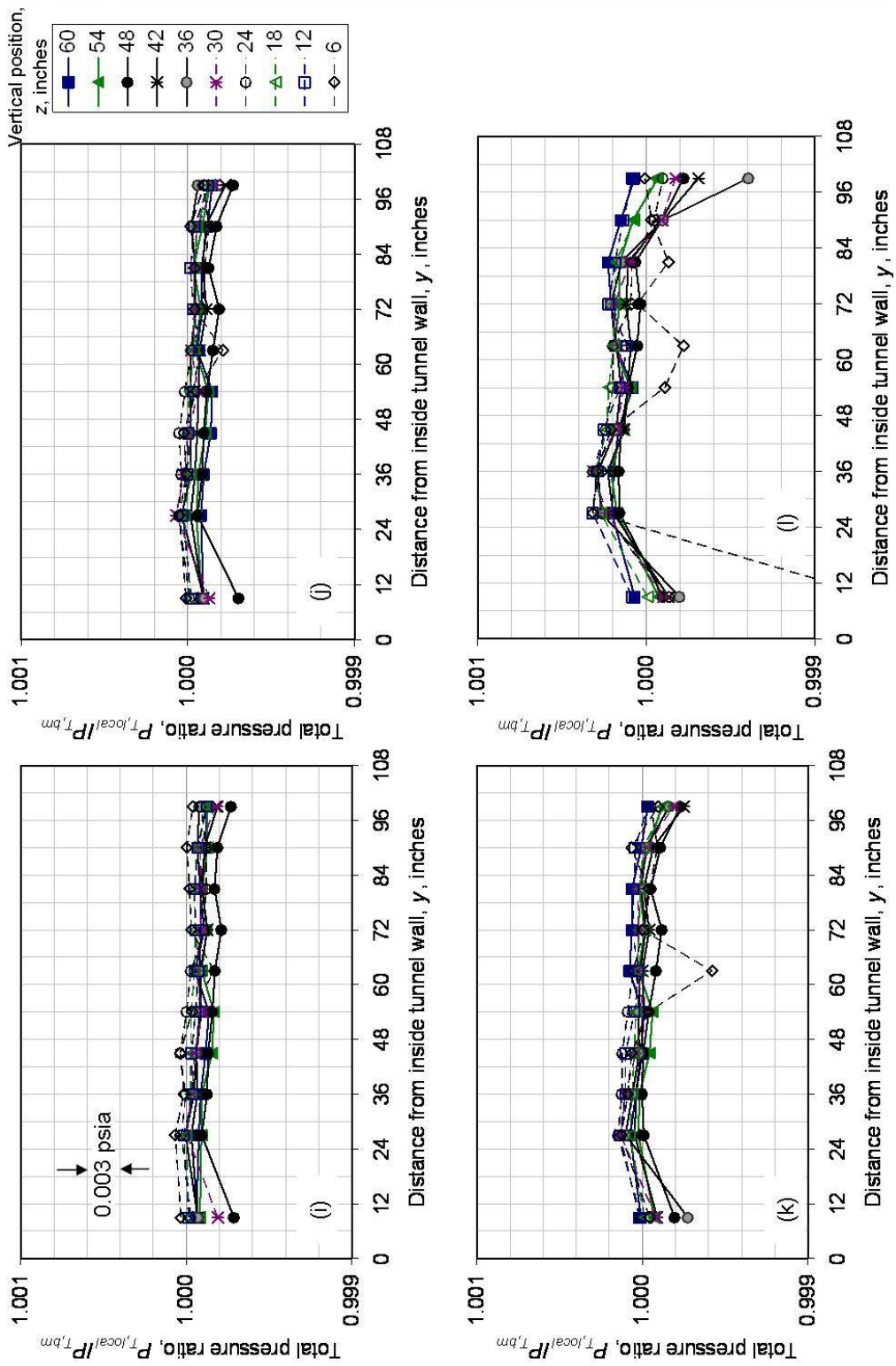


Figure 16.—Continued. (j)  $U_{is}=175$  mph (152 knots),  $P_{air}=0$  psig. (k)  $U_{is}=175$  mph (152 knots),  $P_{air}=5$  psig. (l)  $U_{is}=175$  mph (152 knots),  $P_{air}=175$  psig. (m)  $U_{is}=175$  mph (152 knots),  $P_{air}=70$  psig.

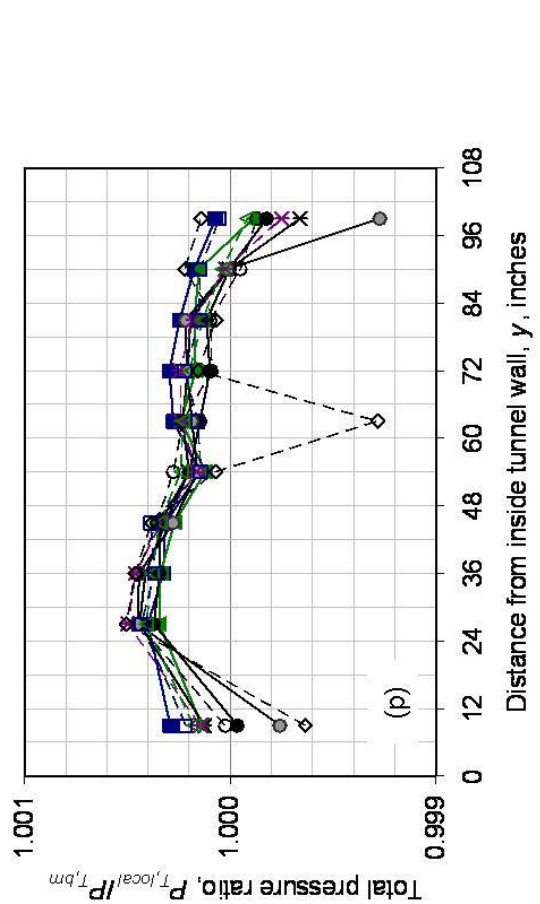
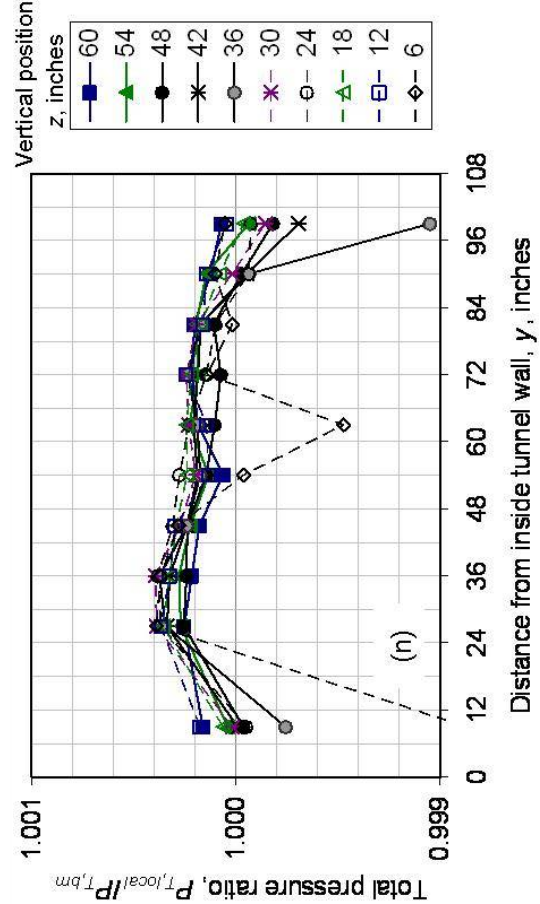
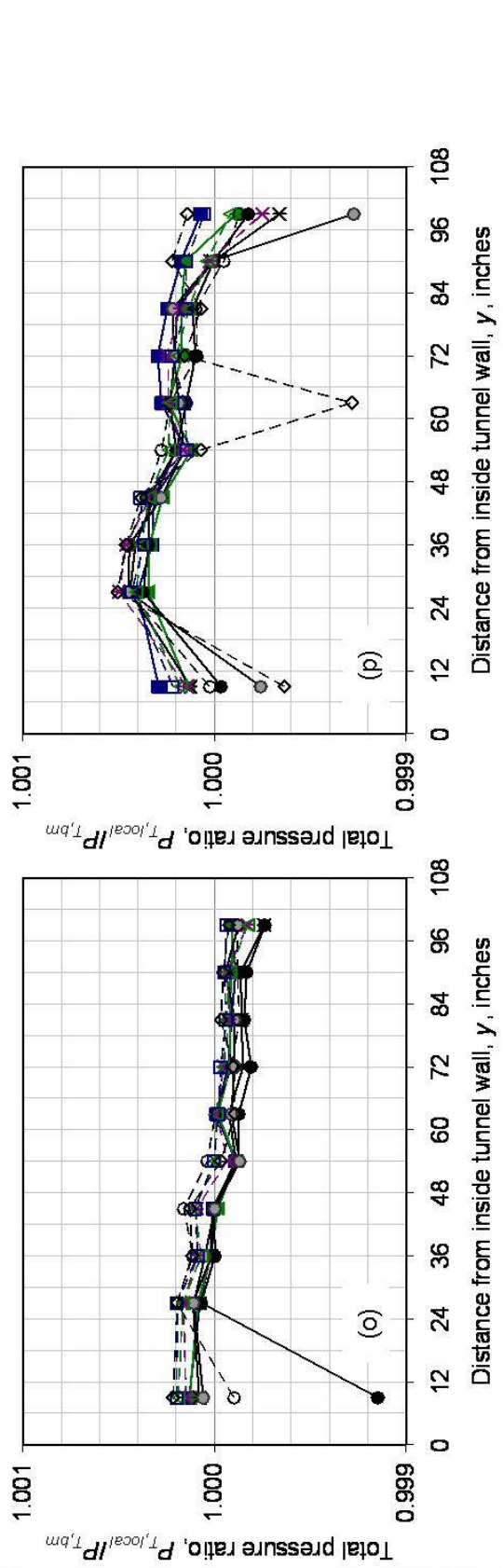
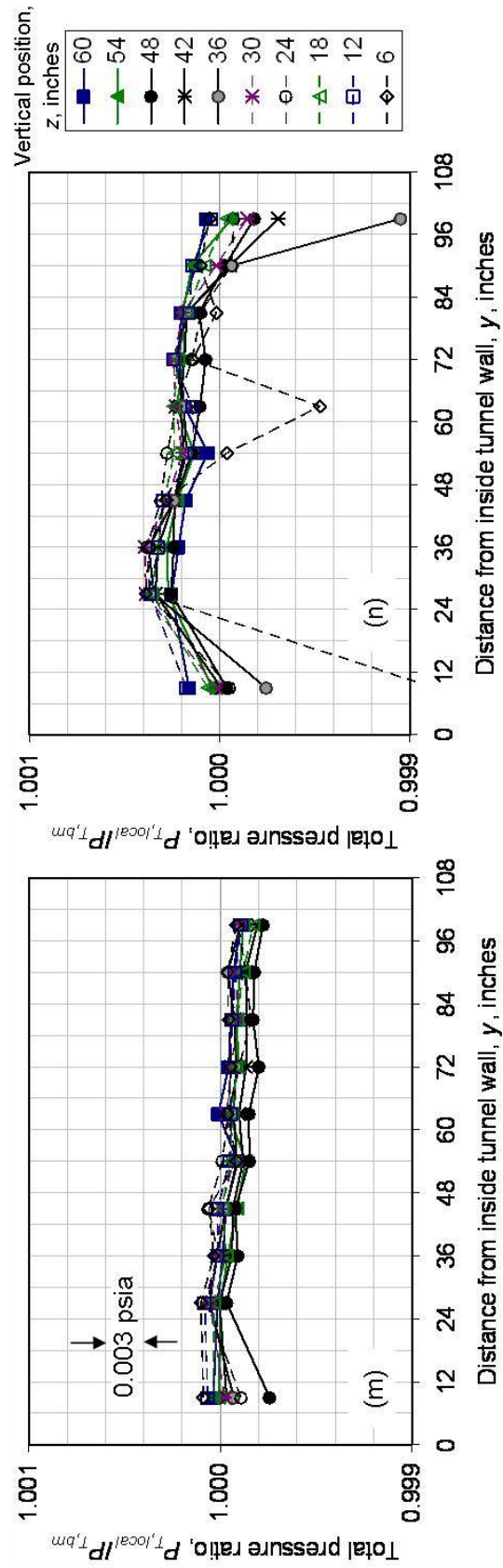


Figure 16.—Continued. (m)  $U_{ts}=200$  mph (174 knots),  $P_{air}=0$  psig. (n)  $U_{ts}=200$  mph (174 knots),  $P_{air}=70$  psig. (o)  $U_{ts}=250$  mph (217 knots),  $P_{air}=0$  psig. (p)  $U_{ts}=250$  mph (217 knots),  $P_{air}=70$  psig.

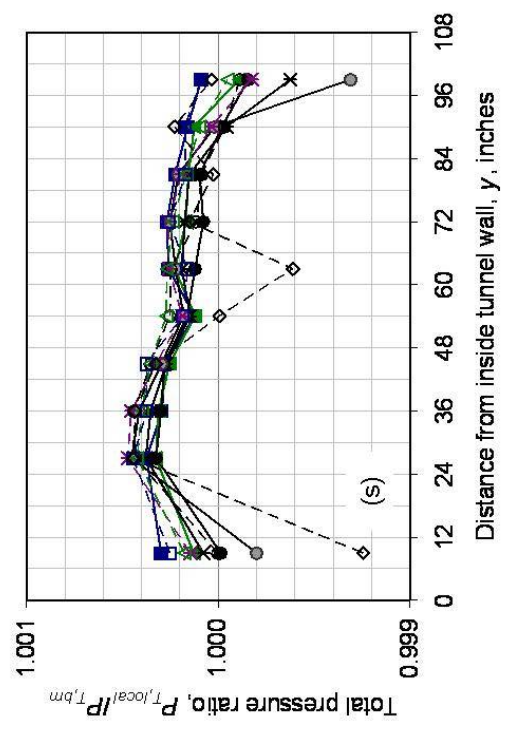
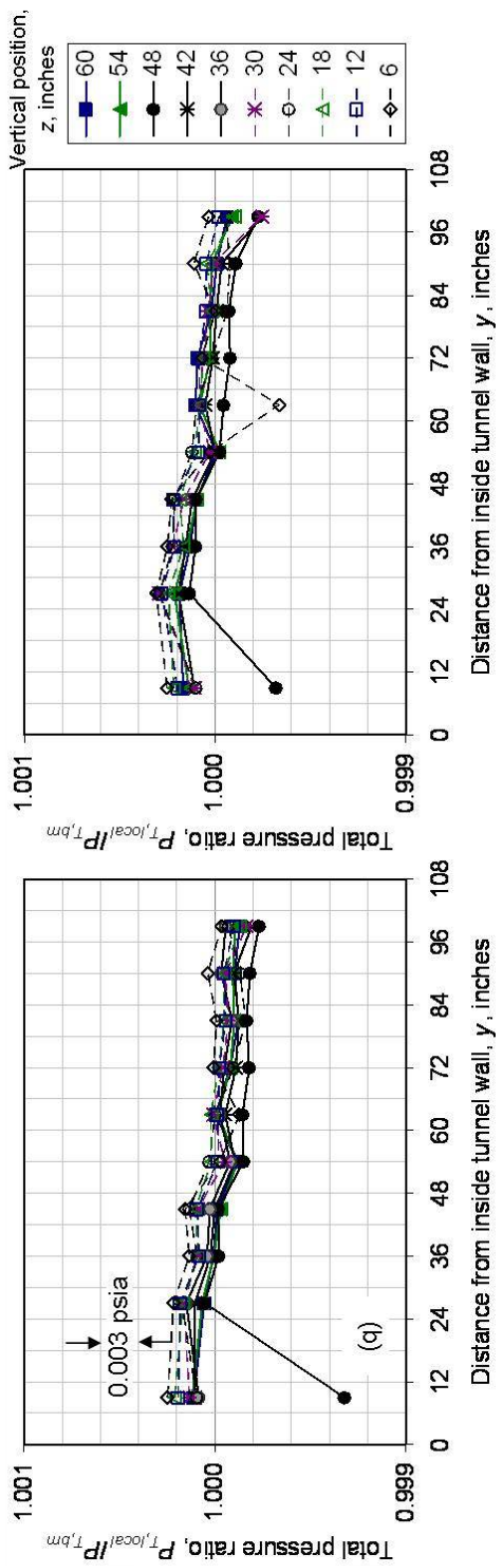


Figure 16.—Continued. (q)  $U_{ts}=225$  mph (195 knots),  $P_{air}=0$  psig. (r)  $U_{ts}=225$  mph (195 knots),  $P_{air}=20$  psig (no  $z=36$ -in. vertical position data). (s)  $U_{ts}=225$  mph (195 knots),  $P_{air}=70$  psig.

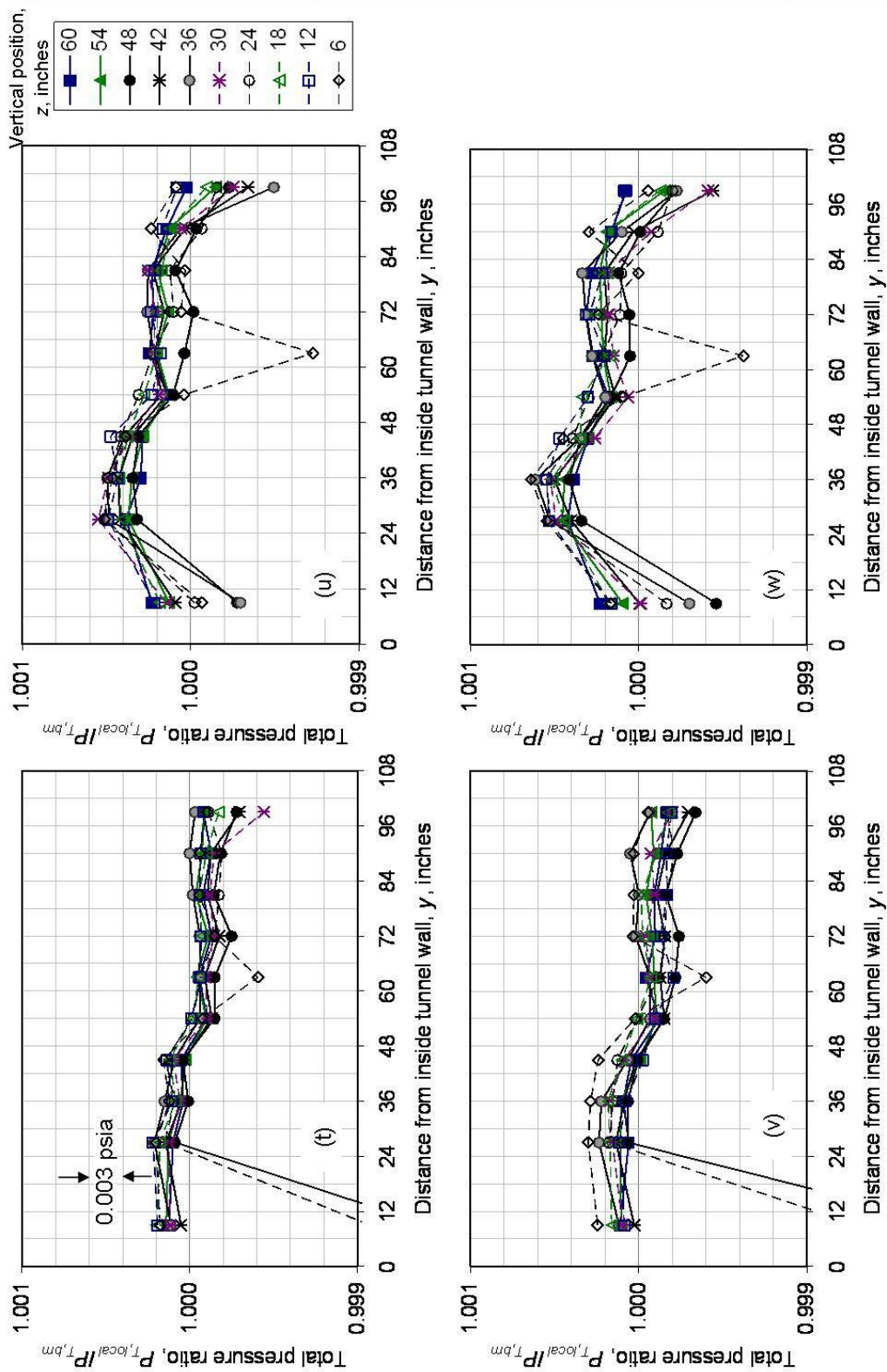


Figure 16.—Concluded. (t)  $U_{is}=300$  mph (261 knots),  $P_{air}=0$  psig. (u)  $U_{is}=300$  mph (261 knots),  $P_{air}=70$  psig. (v)  $U_{is}=350$  mph (304 knots),  $P_{air}=0$  psig. (w)  $U_{is}=350$  mph (304 knots),  $P_{air}=70$  psig.

## Mach Number

The Mach number ratio distribution data are shown in Figure 17. As was the case with the total pressure data, the Mach number measurements from the 9-ft survey rake mounted in the test section were normalized by the bellmouth Mach number so that the data could be combined to show the overall flow quality for a given test section condition. For each set of Mach number ratio data plots, an approximate delta Mach number ( $\Delta M$ ) was added to provide a gage of the absolute variation in the Mach number within the survey plane. Note that the y-axis scale is expanded to show flow field detail.

The overall Mach number variation for conditions with no spraybar air injection ( $P_{air} = 0$  psig) was 0.002 to 0.004, neglecting points near the test section surfaces that may have been affected by the boundary layer. The shape of the lateral distribution were consistent at each rake vertical position with slightly higher Mach numbers recorded nearer the outside test section wall and the variation was greater at the higher Mach number settings (note that the difference in Mach number from inside wall to outside wall was only 0.001 to 0.003).

Spraybar air injection did not have a significant effect on the Mach number distributions, particularly in the core of the test section. At the lowest airspeed settings, the spraybar air injection appeared to increase the boundary layer thickness near the test section walls (as was also seen in the total pressure data) resulting in lower Mach number readings at some rake positions for probes near the walls. For nominal airspeed settings of 200 mph (174 knots) and higher however, 70 psig spraybar air injection had little or no effect on the Mach number distribution data.

The Mach number distributions at the test section survey plane are very good over the entire operating range of the IRT, including those conditions with 70 psig spraybar air injection. Considering that there are no flow quality manipulators (i.e. screens or honeycomb) installed in the settling chamber upstream of the test section, the Mach number flow quality is remarkably good (the flat heat exchangers and D-corner turning vanes do have a positive effect on the test section flow quality, as described in Ref. 4).

## Total Temperature

For the icing tests that are conducted in the IRT, temperature is the most important of the aero-thermal measurements. Both the accuracy of the total temperature measurement and the uniformity of temperature in the test section are critical. Because of the critical nature of the temperature measurements, the IRT staff is always looking at ways to improve the quality of the total temperature data collected in the IRT and the overall flow quality in terms of the total temperature distributions in the test section. As mentioned above and in Reference 3, both the accuracy of the total temperature measurements and the test hardware used to survey the IRT test section were improved prior to the 2004 aero-thermal calibration. These improvements include upgrading the facility and calibration total temperature instrumentation from thermocouples to RTDs and using a dedicated total temperature survey tool, the 2-D RTD array, for test section measurements.

The total temperature setting in the IRT is controlled by the two flat heat exchangers located in the C-D leg of the tunnel loop (Figure 1). The 24 RTDs mounted on the leading edge of the D-corner turning vanes (Figure 14) are used to monitor the temperature uniformity of the air exiting the heat exchangers. The control system is used to vary the amount of coolant to each of the 8 heat exchanger zones in order to produce a uniform total temperature profile in D-corner. The goal is to control the temperature distribution to within  $\pm 0.5$  °C within the D-corner survey plane (this exceeds the goal set forth in Ref. 1 and listed in Table 4). Temperature conditions can be accurately set and controlled from about 4 to  $-30$  °C. The critical operating point for the IRT is  $U_{ts} = 230$  mph (200 knots) and  $T_{T,davg} = 0$  °C. Note that there were some points called out in the test matrix (Table 4) that required total temperature settings greater than 4 °C to achieve the desired static temperature. These conditions are beyond the effective controllable range of the IRT.

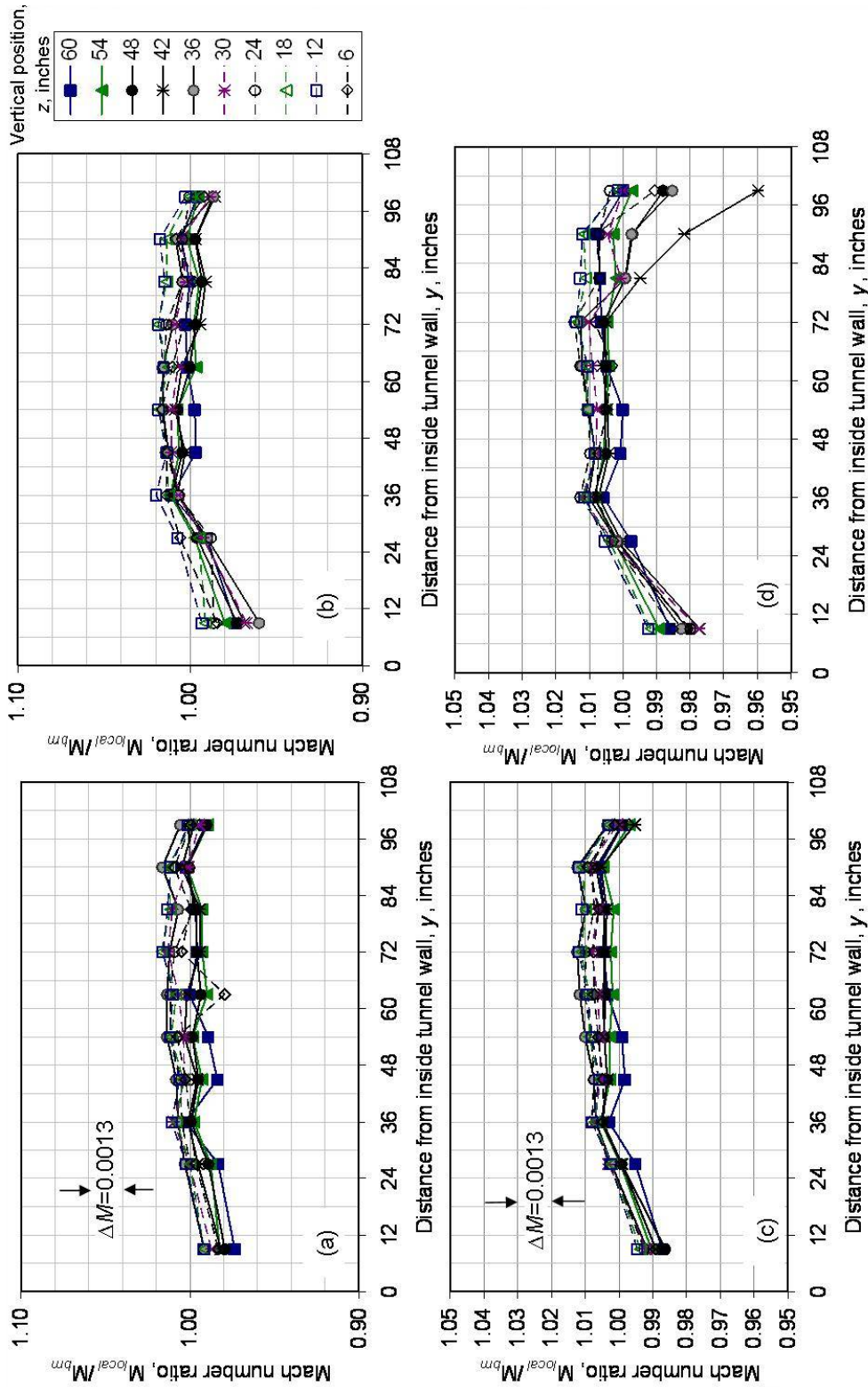


Figure 17.—Mach number distribution data from the IRT test section. Data collected using the 9-ft survey rake mounted at 11 vertical positions over several tunnel runs. The test section Mach number data was normalized using the bellmouth Mach number measurement. Data from the 66-in. vertical position was omitted due to boundary layer influence. Approximate Mach number delta is indicated for each test section setting. (a)  $U_{ts}=50$  mph,  $M_{ts}=0.066$ ,  $P_{air}=0$  psig. (b)  $U_{ts}=50$  mph,  $M_{ts}=0.066$ ,  $P_{air}=70$  psig. (c)  $U_{ts}=100$  mph,  $M_{ts}=0.066$ ,  $P_{air}=0$  psig. (d)  $U_{ts}=100$  mph,  $M_{ts}=0.133$ ,  $P_{air}=70$  psig.

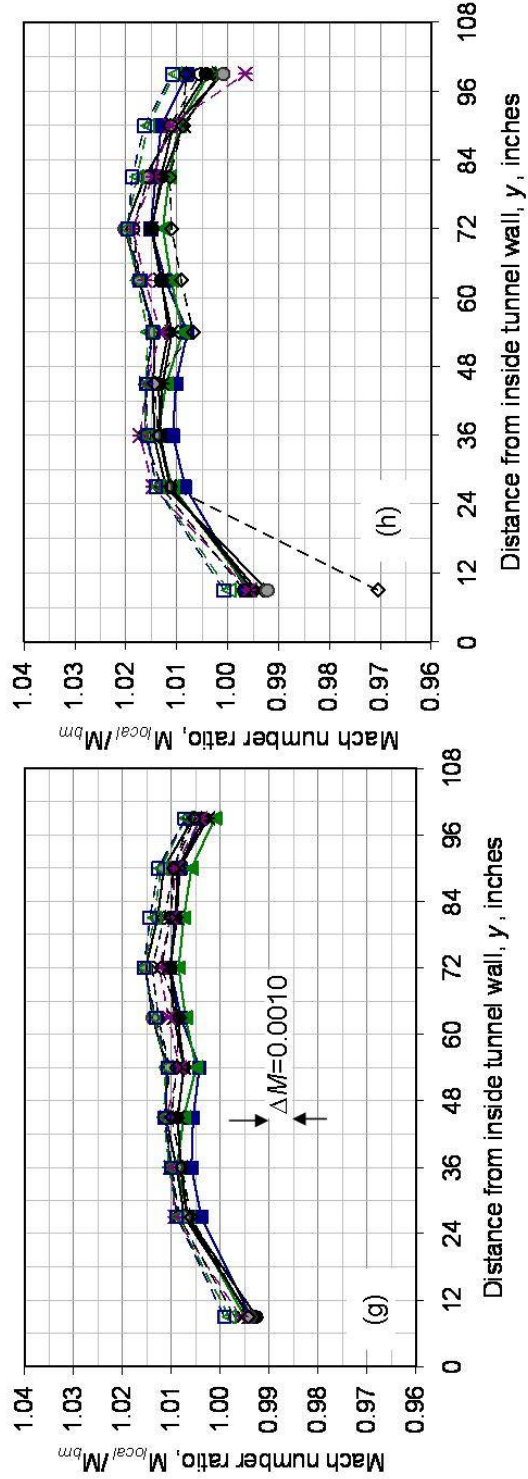
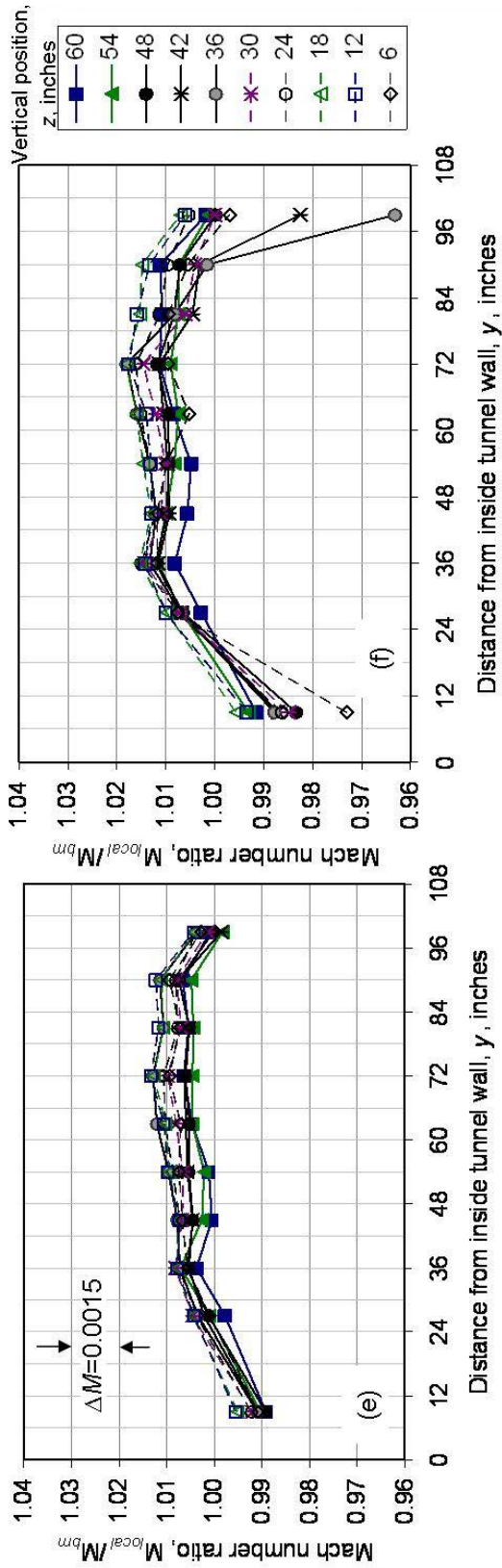


Figure 17.—Continued. (e)  $U_{ts}=115$  mph,  $M_{ts}=0.152$ ,  $P_{air}=0$  psig. (f)  $U_{ts}=115$  mph,  $M_{ts}=0.152$ ,  $P_{air}=70$  psig. (g)  $U_{ts}=150$  mph,  $M_{ts}=0.199$ ,  $P_{air}=0$  psig. (h)  $U_{ts}=150$  mph,  $M_{ts}=0.199$ ,  $P_{air}=70$  psig.

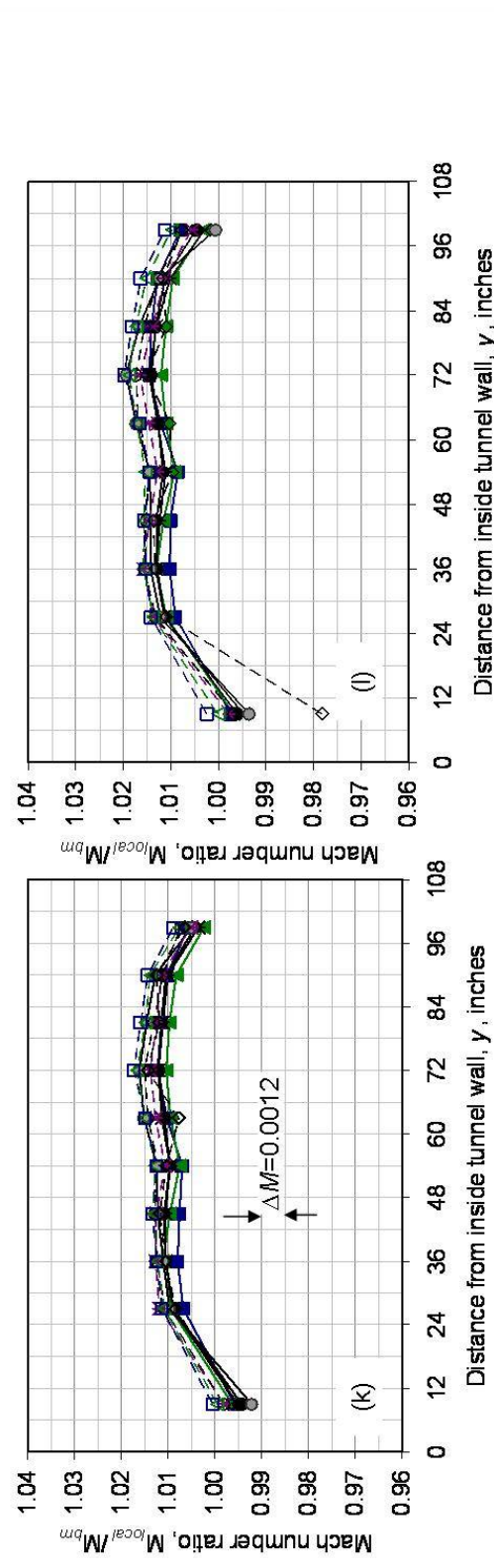
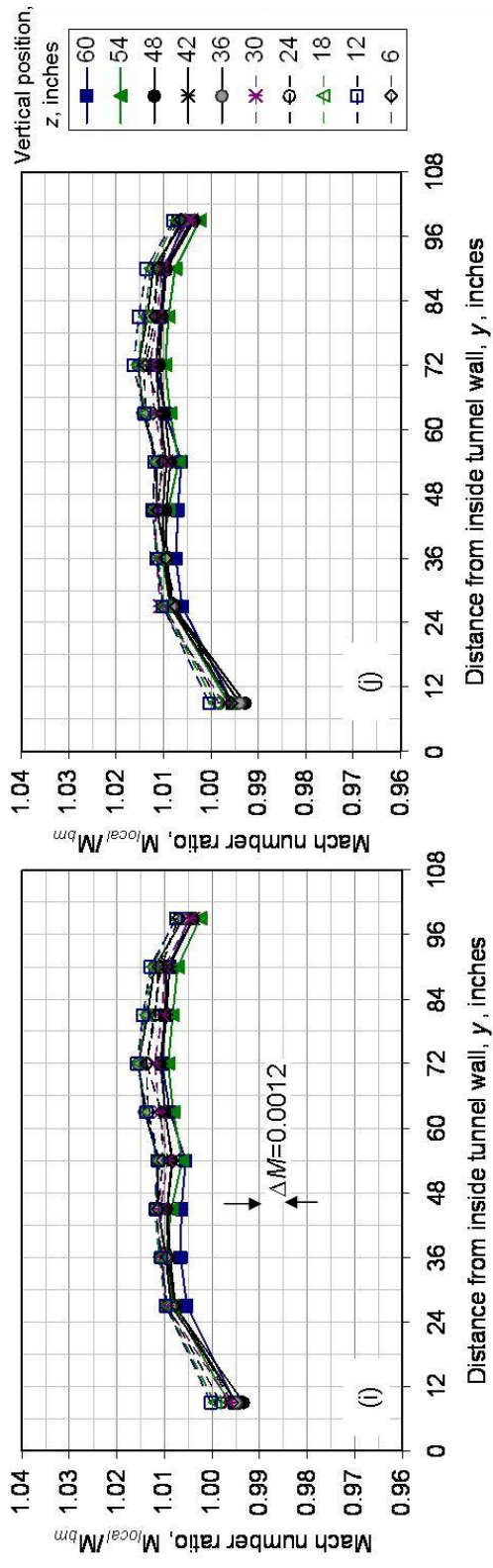


Figure 17.—Continued. (i)  $U_{ts}=175$  mph,  $M_{ts}=0.232$ ,  $P_{air}=0$  psig. (j)  $U_{ts}=175$  mph,  $M_{ts}=0.232$ ,  $P_{air}=5$  psig. (k)  $U_{ts}=175$  mph,  $M_{ts}=0.232$ ,  $P_{air}=20$  psig. (l)  $U_{ts}=175$  mph,  $M_{ts}=0.232$ ,  $P_{air}=70$  psig.

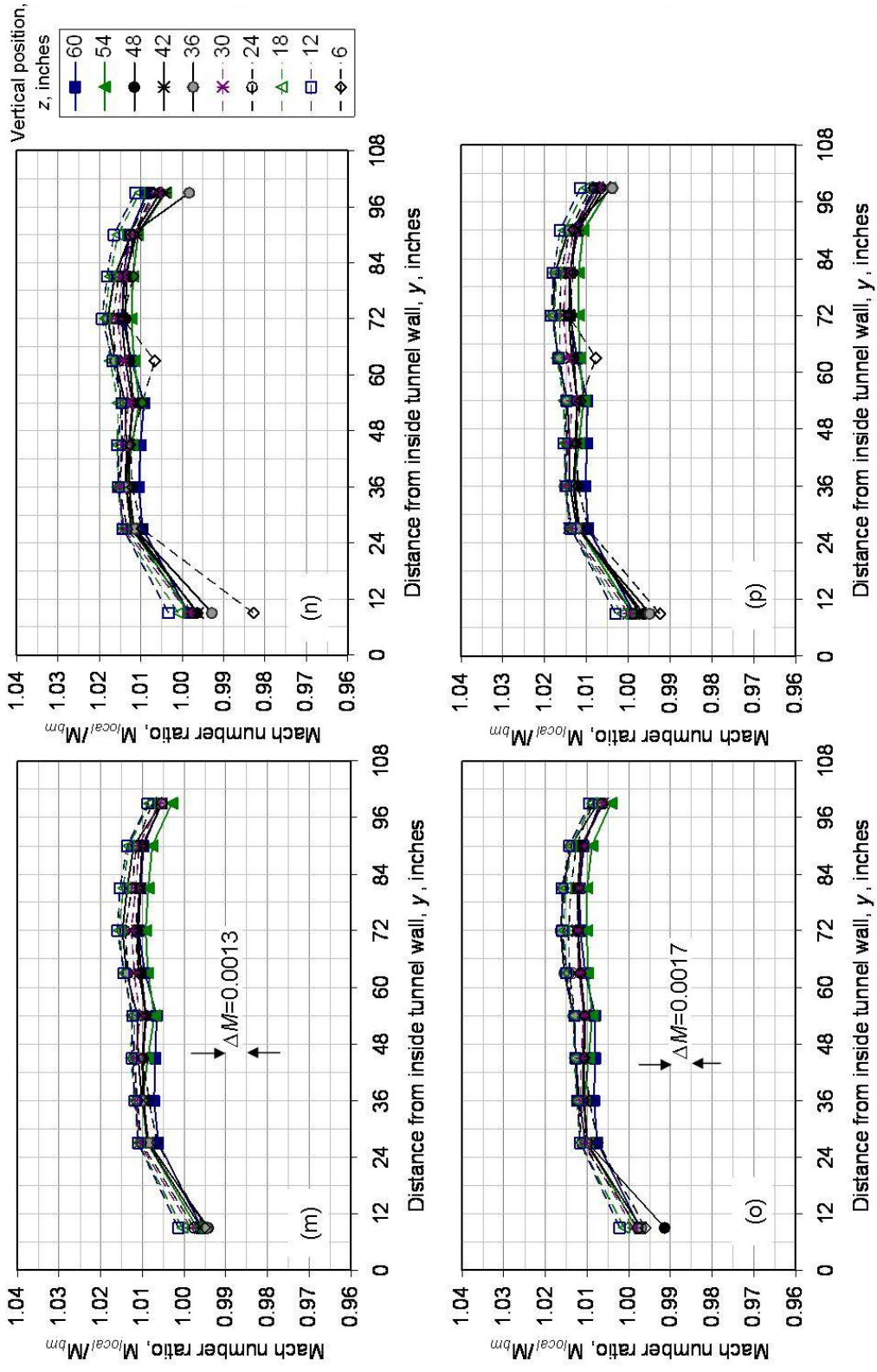


Figure 17.—Continued. (m)  $U_{IS}=200$  mph,  $M_{IS}=0.265$ ,  $P_{air}=0$  psig. (n)  $U_{IS}=200$  mph,  $M_{IS}=0.265$ ,  $P_{air}=70$  psig. (o)  $U_{IS}=250$  mph,  $M_{IS}=0.332$ ,  $P_{air}=0$  psig. (p)  $U_{IS}=250$  mph,  $M_{IS}=0.332$ ,  $P_{air}=70$  psig.

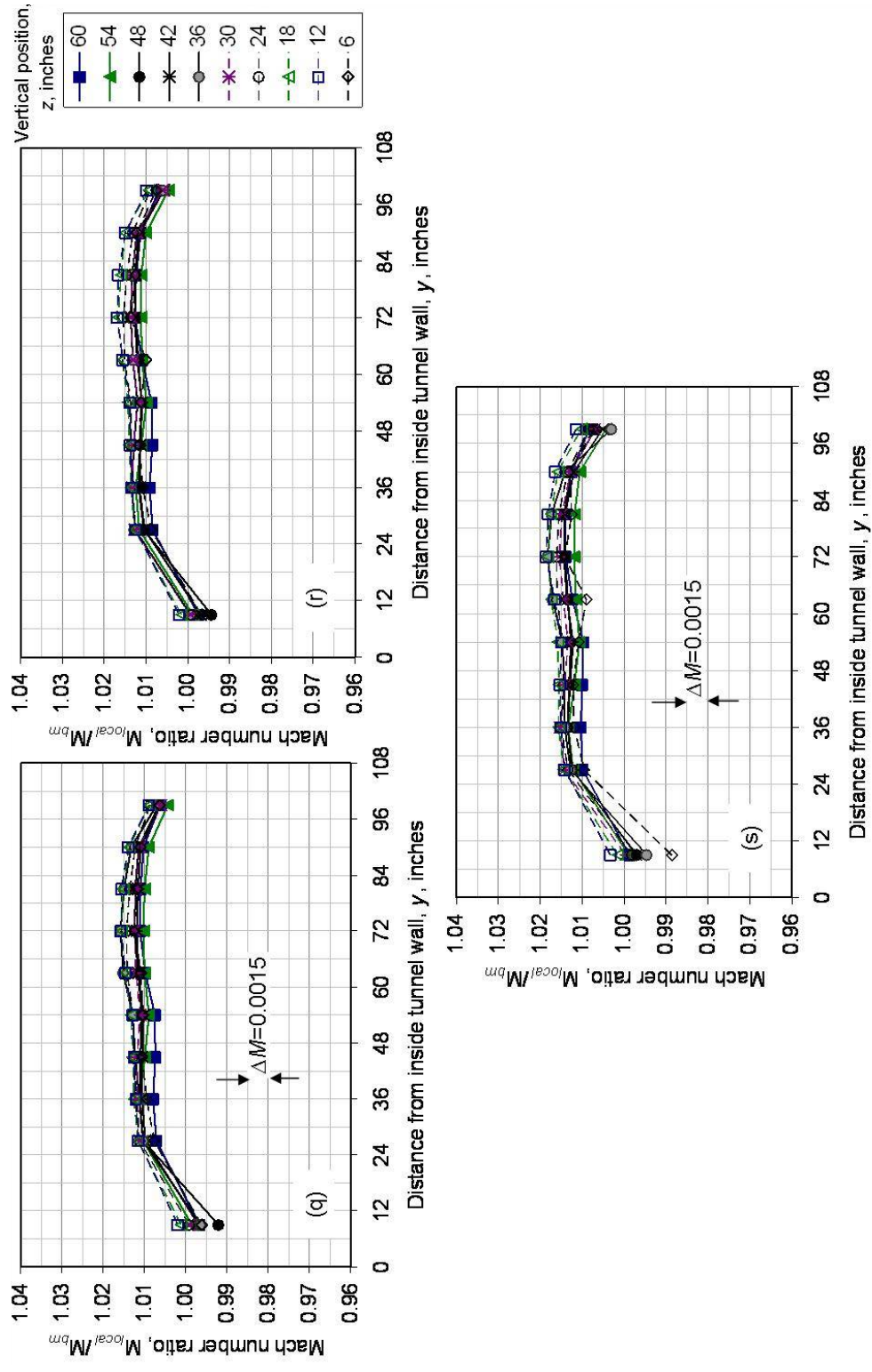


Figure 17.—Continued. (q)  $U_{ts}=225$  mph,  $M_{ts}=0.305$ ,  $P_{air}=0$  psig. (r)  $U_{ts}=225$  mph,  $M_{ts}=0.265$ ,  $P_{air}=20$  psig. (s)  $U_{ts}=225$  mph,  $M_{ts}=0.305$ ,  $P_{air}=70$  psi.

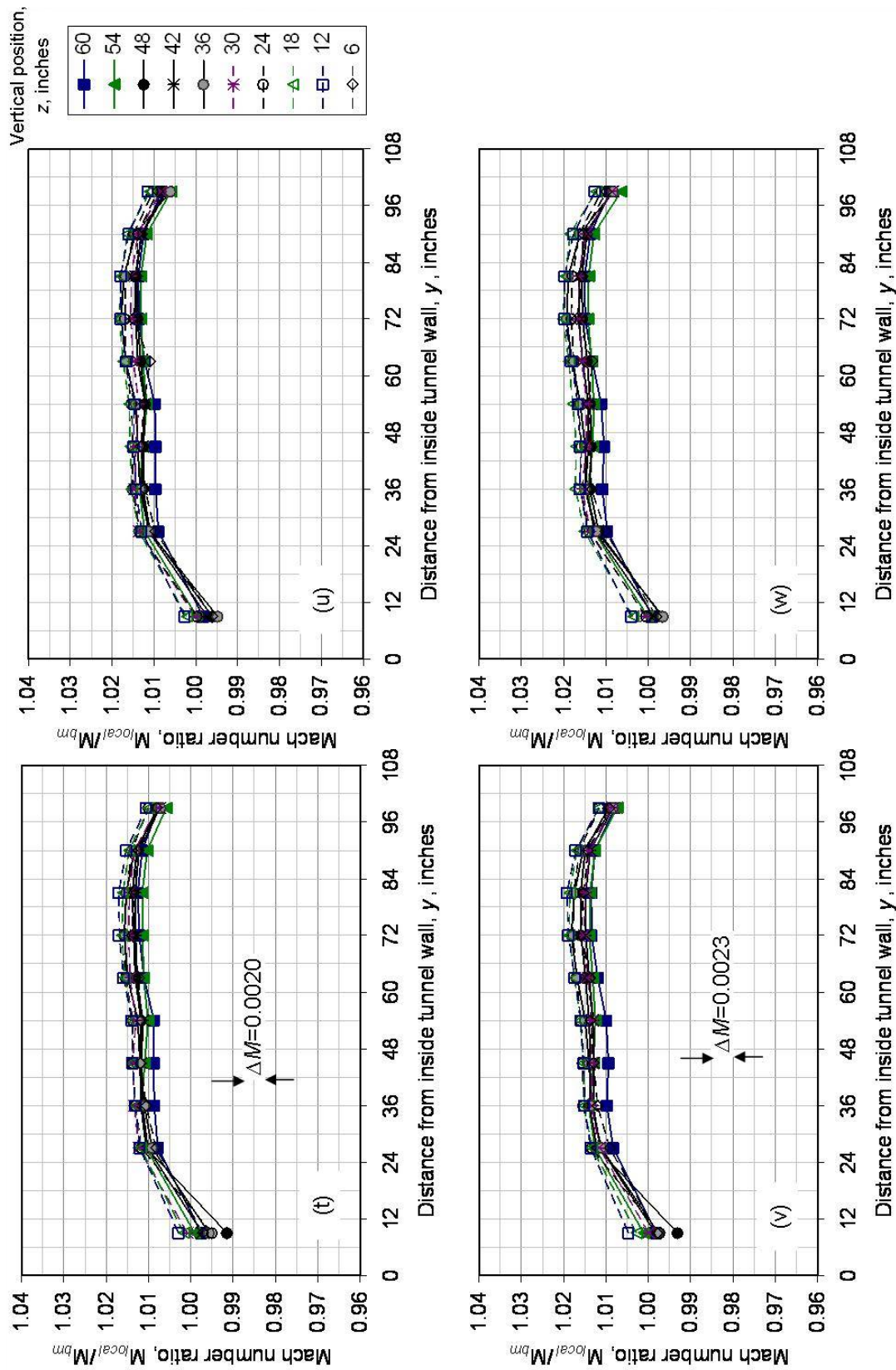


Figure 17.—Concluded. (t)  $U_{ts}=300$  mph,  $M_{ts}=0.399$ ,  $P_{air}=0$  psig. (u)  $U_{ts}=300$  mph,  $M_{ts}=0.399$ ,  $P_{air}=70$  psig. (v)  $U_{ts}=350$  mph,  $M_{ts}=0.464$ ,  $P_{air}=0$  psig. (w)  $U_{ts}=350$  mph,  $M_{ts}=0.464$ ,  $P_{air}=70$  psig.

Figure 18 shows the resulting uniformity of the D-corner total temperature for the settings used during the aero-thermal calibration. Note that for most all conditions below 3 °C the variation in D-corner total temperature readings are within or nearly within the goal. Exceptions are at very low temperatures and very low speeds where variations greater than  $\pm 1$  °C were recorded. The critical operating regime for the icing community is airspeed from 115 to 300 mph (100 to 260 knots) and temperatures from freezing to  $-20$  °C; for those settings the D-corner total temperature distribution was consistently within the  $\pm 0.5$  °C goal.

The test section total temperature data were collected using the 2-D RTD array. The total temperature distributions for each test condition are shown in Figure 19. The data in Figure 19 were sorted first by airspeed (lowest to highest) then by total temperature (highest to lowest) for each airspeed setting group. Each data plot in Figure 19 shows the test section total temperature distribution for a given airspeed, total temperature and spraybar air setting; that data are grouped by vertical height within each plot. Note that probe number 3 (top row of probes on the array, third from the inside test section wall) was inoperative for most of the test.

The following are general observations of the test section total temperature uniformity:

- D-corner total temperature settings greater than 3 °C ( $T_{T,davg} > 3$  °C).—These settings are warmer than the controlled operating range of the IRT heat exchange and therefore produce a much higher variation in the test section and D-corner total temperature distributions as compared to settings less than 3 °C (Figure 18 and Figure 19). The D-corner and test section total temperature gradient both show higher temperatures near the tunnel ceiling with a gradual decrease in temperature toward the floor for all conditions where  $T_{T,davg} > 3$  °C. As seen by the subsequent data plots, these “high temperature” settings are not indicative of the IRT total temperature flow quality at settings used for icing conditions.
- D-corner total temperature settings less than 3 °C ( $T_{T,davg} < 3$  °C).—For total temperature settings in the effective operating range of the heat exchangers (3 to  $-30$  °C), the total temperature variation in the core of the test section is reduced to 1 °C or less (the core of the test section is defined as the center 5- by 5-ft area). Many conditions show variation on the order of 0.5 °C (peak-to-peak).
- Nominal test section airspeed of 50 mph ( $U_{ts} = 50$  mph = 43 knots).—At the very low speed condition, the spraybar air injection has a significant effect on the test section total temperature distribution at all temperature settings. At  $P_{air} = 0$  psig, the distributions are uniform and show little variation over test section cross-section (horizontal and vertical distributions), generally on the order of 1 °C or less. Spraybar air is heated to nominally 80 °C at  $P_{air} = 70$  psig there is a noticeable horizontal gradient of about 2 °C across the test section (higher temperatures recorded near the outside wall) as well as vertical variation of about 2 °C.
- Temperature spikes near test section boundaries.—There are several instances of temperature spikes recorded near the test section floor or ceiling (probe vertical position of 9 and 63 in. above the floor, respectively). For example, there is a spike seen near the ceiling, 54 in. from the inside wall, at the  $U_{ts} = 50$  mph (43 knots); worst case is a 2 °C spike at  $T_{T,davg} = -5.4$  °C. Also, there is an occasional temperature spike at the floor, generally 72 in. from the inside wall at  $U_{ts}$  of 115 mph (100 knots) and higher. These spikes are near enough to the test section boundaries that they should not have any impact on the core flow temperature distributions.
- Primary operating range ( $115 < U_{ts} < 300$  mph,  $3 < T_{T,davg} < -20$  °C).—For all of the critical operating conditions (airspeed and total temperature combinations), the total temperature profiles in the core of the test section show very uniform conditions that meet the  $\pm 0.5$  °C goal. In fact, for many conditions, the total temperature variation in the core of the test section is 0.5 °C peak-to-peak for both spraybar air ( $P_{air}$ ) off and 70 psig conditions.
- Critical (freezing) conditions ( $T_{T,davg} = 0$  °C).—Temperature conditions at or about the freezing point of water are of critical importance in the aircraft icing community for all airspeed settings in

the IRT. These total temperature distributions in the IRT test section at freezing conditions are excellent; at all airspeed settings the variation in the core of the test section is less than the recommended goal of  $\pm 1$  °C stipulated in Reference 1 and for most cases meets the  $\pm 0.5$  °C goal used in the IRT.

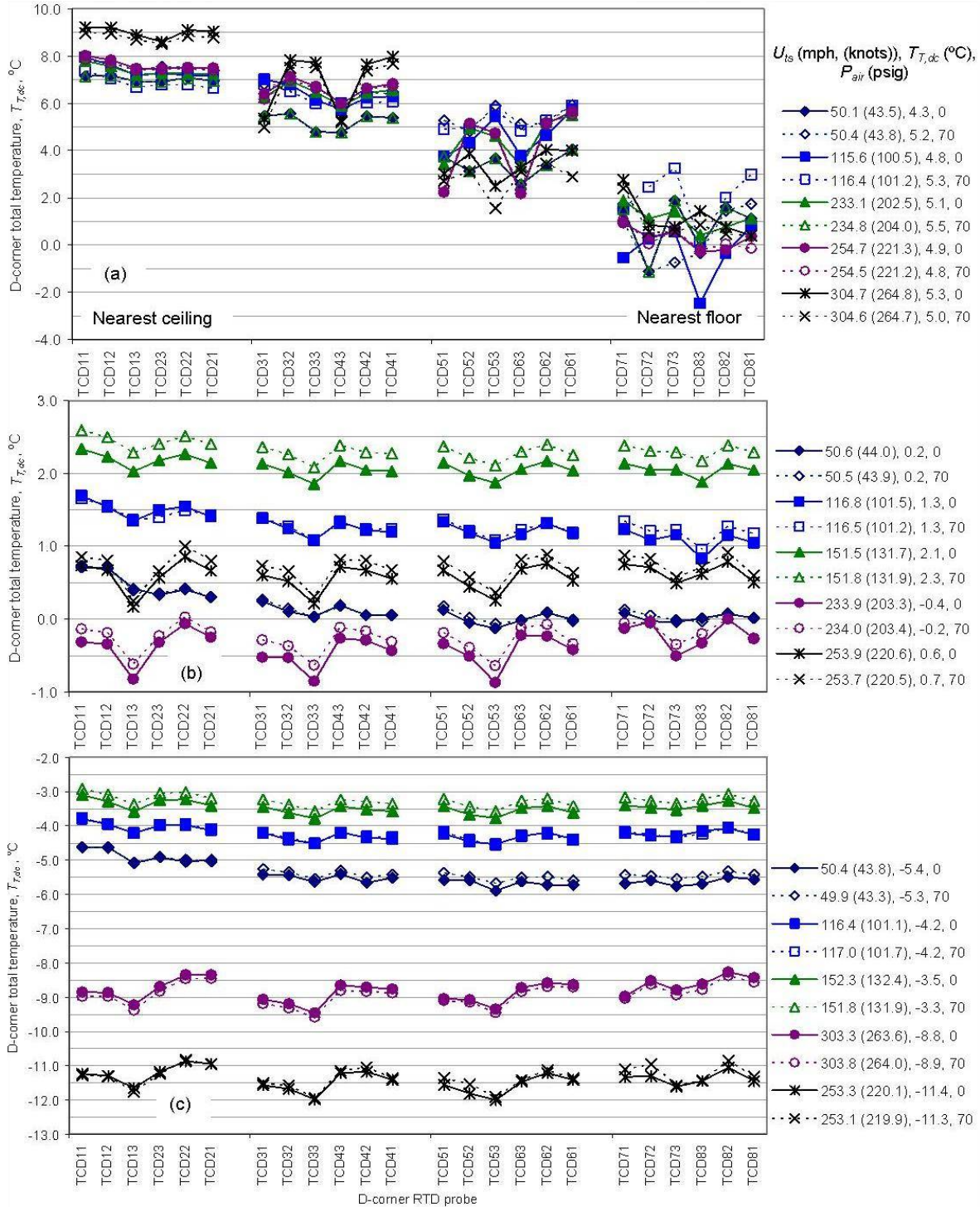


Figure 18.—Total temperature distribution along the D-corner turning vanes as measured by the D-corner RTD probes. See Figure 13 for location of probes relative to the heat exchanger. (a)  $T_{T,davg} > 4$  °C. (b)  $-0.5 > T_{T,davg} > -3$  °C. (c)  $-3 > T_{T,davg} > -9$  °C.

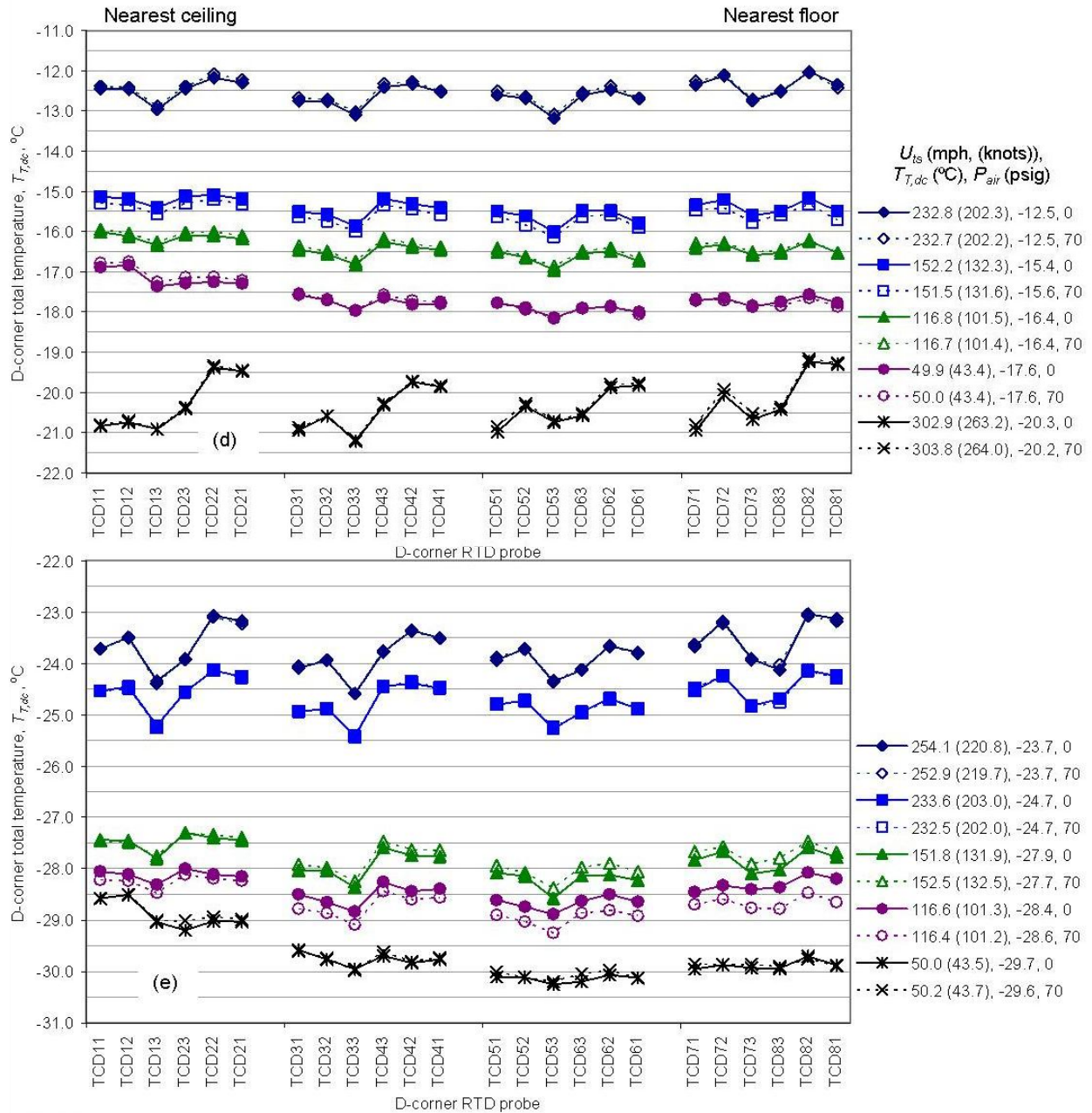


Figure 18.—Concluded. (d)  $-11 > T_{T,davg} > -22$  °C. (e)  $-22 > T_{T,davg} > -31$  °C.

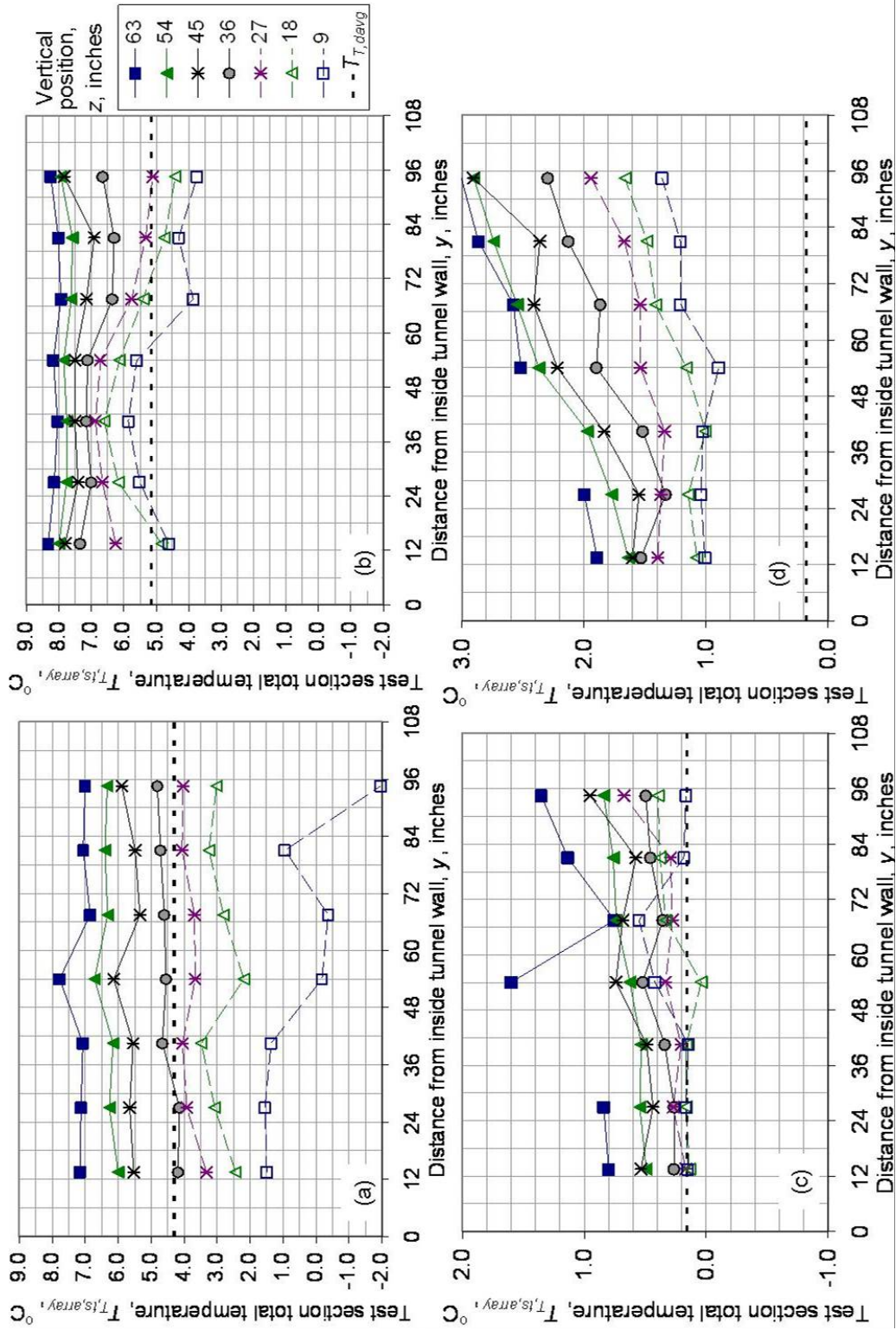


Figure 19.—IRT test section total temperature distribution data collected using the 2-D RTD Array (a)  $U_{is}=50.1$  mph (43.5 knots),  $T_{T,davg}=4.3$  °C,  $P_{air}=0$  psig. (b)  $U_{is}=50.4$  mph (43.8 knots),  $T_{T,davg}=5.2$  °C,  $P_{air}=70$  psig. (c)  $U_{is}=50.6$  mph (44.0 knots),  $T_{T,davg}=0.2$  °C,  $P_{air}=0$  psig. (d)  $U_{is}=50.5$  mph (43.9 knots),  $T_{T,davg}=0.2$  °C,  $P_{air}=70$  psig.

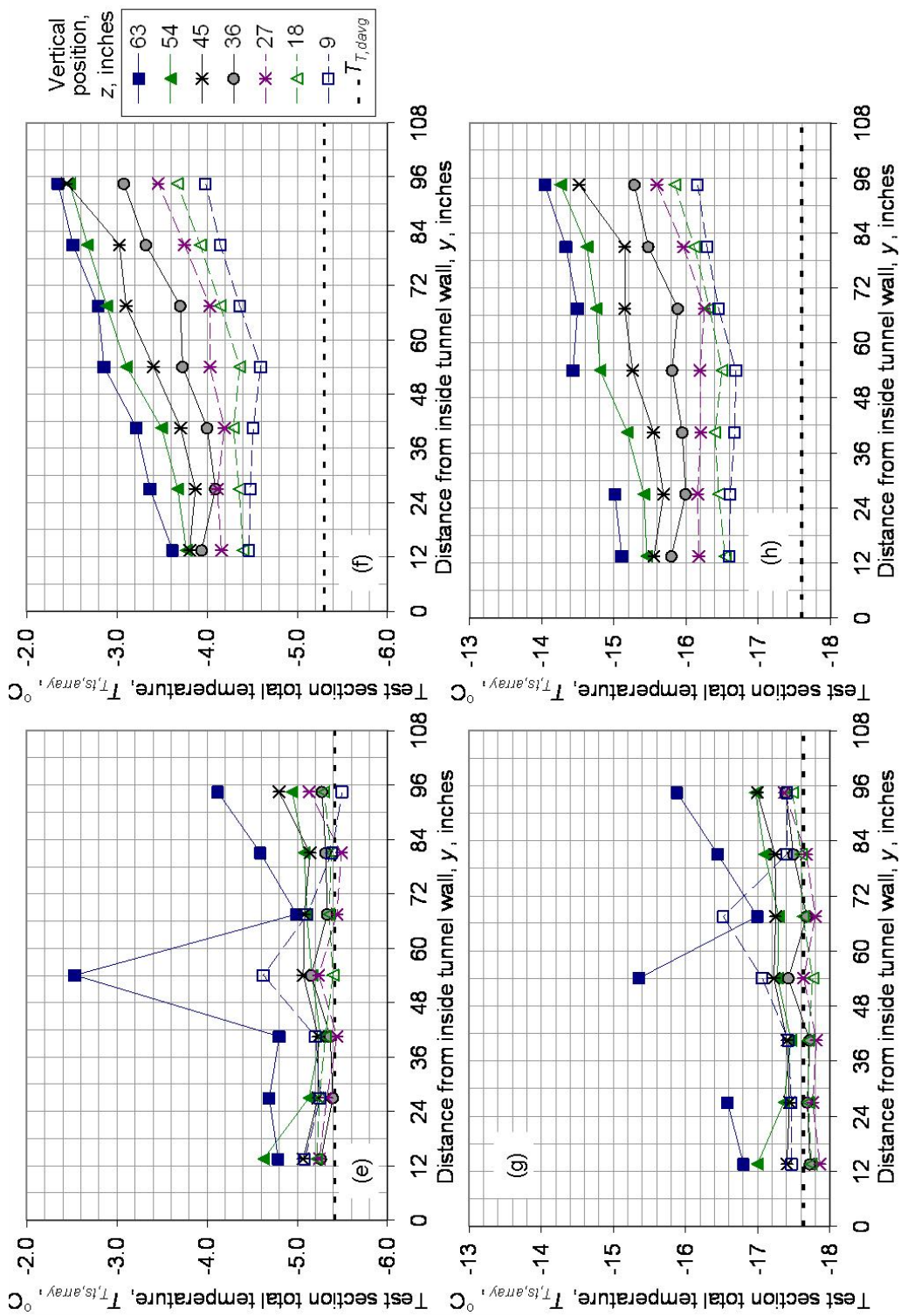


Figure 19.—Continued. (e)  $U_{Is}=50.4$  mph (43.8 knots),  $T_{T,davg}=-5.4$  °C,  $P_{air}=0$  psig. (f)  $U_{Is}=49.9$  mph (43.3 knots),  $T_{T,davg}=-5.3$  °C,  $P_{air}=0$  psig. (g)  $U_{Is}=49.9$  mph (43.4 knots),  $T_{T,davg}=-17.6$  °C,  $P_{air}=0$  psig. (h)  $U_{Is}=49.9$  mph (43.4 knots),  $T_{T,davg}=-17.6$  °C,  $P_{air}=70$  psig.

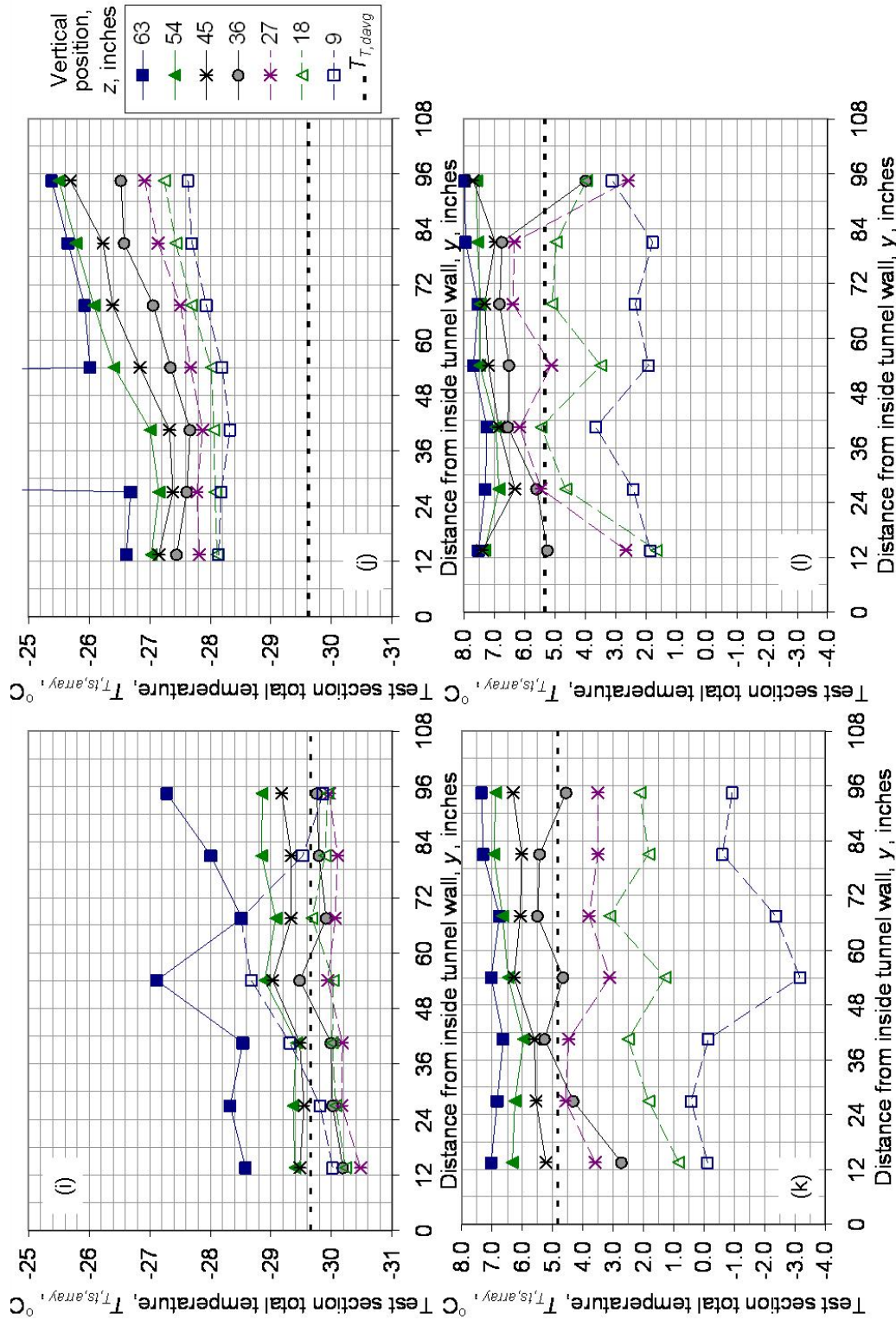


Figure 19.—Continued. (j)  $U_{is}=50.2$  mph (43.7 knots),  $T_{T, avg}=-29.6$  °C,  $P_{air}=70$  psig. (k)  $U_{is}=115.6$  mph (100.5 knots),  $T_{T, avg}=4.8$  °C,  $P_{air}=0$  psig. (l)  $U_{is}=50.0$  mph (43.5 knots),  $T_{T, avg}=-29.7$  °C,  $P_{air}=0$  psig. (m)  $U_{is}=116.4$  mph (101.2 knots),  $T_{T, avg}=5.3$  °C,  $P_{air}=70$  psig.

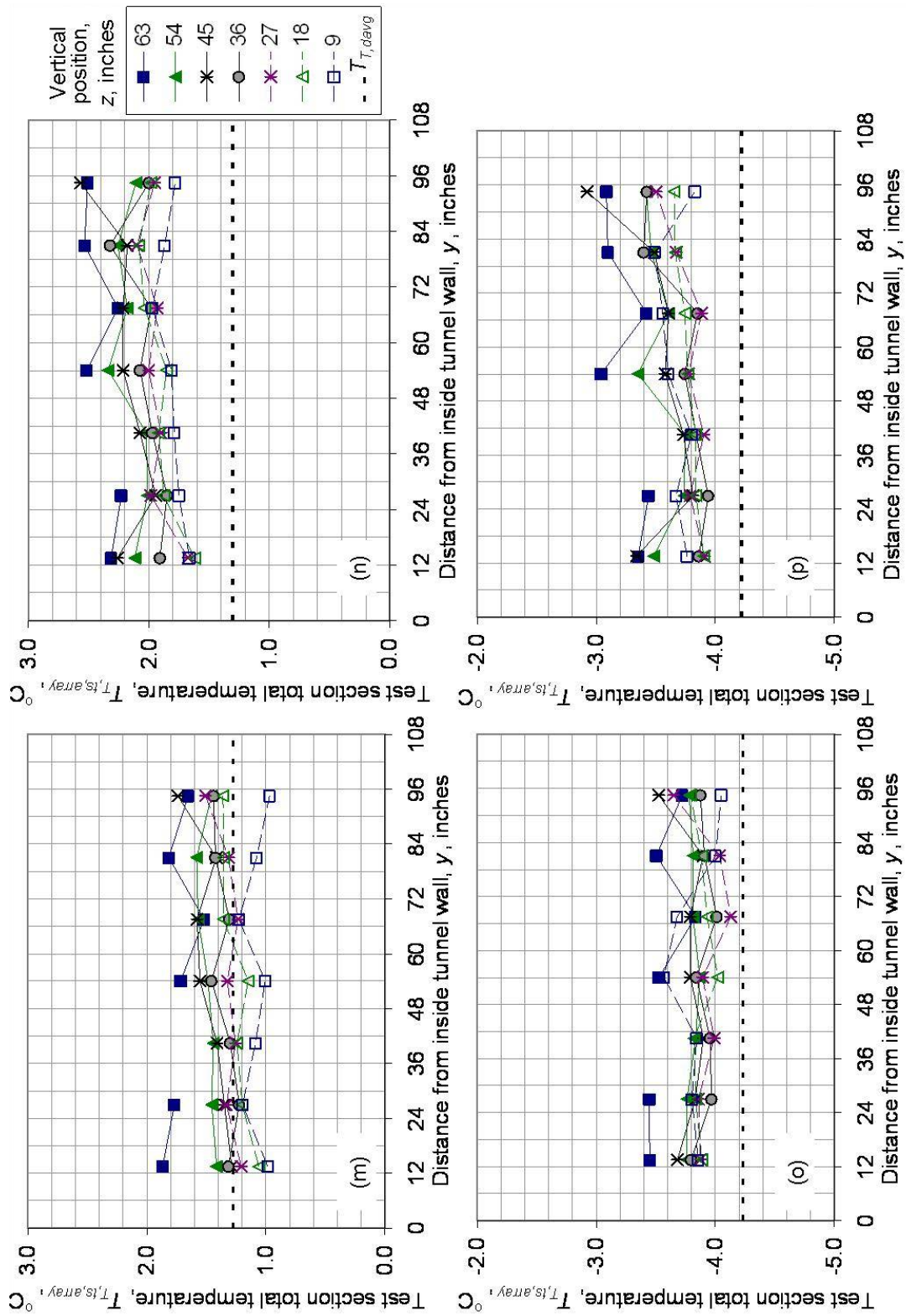


Figure 19.—Continued. (m)  $U_{ts}=116.8$  mph (101.5 knots),  $T_{T,davg}=1.3$  °C,  $P_{air}=0$  psig. (n)  $U_{ts}=116.5$  mph (101.2 knots),  $T_{T,davg}=1.3$  °C,  $P_{air}=70$  psig. (o)  $U_{ts}=116.4$  mph (101.1 knots),  $T_{T,davg}=-4.2$  °C,  $P_{air}=0$  psig. (p)  $U_{ts}=117.0$  mph (101.7 knots),  $T_{T,davg}=-4.2$  °C,  $P_{air}=70$  psig.

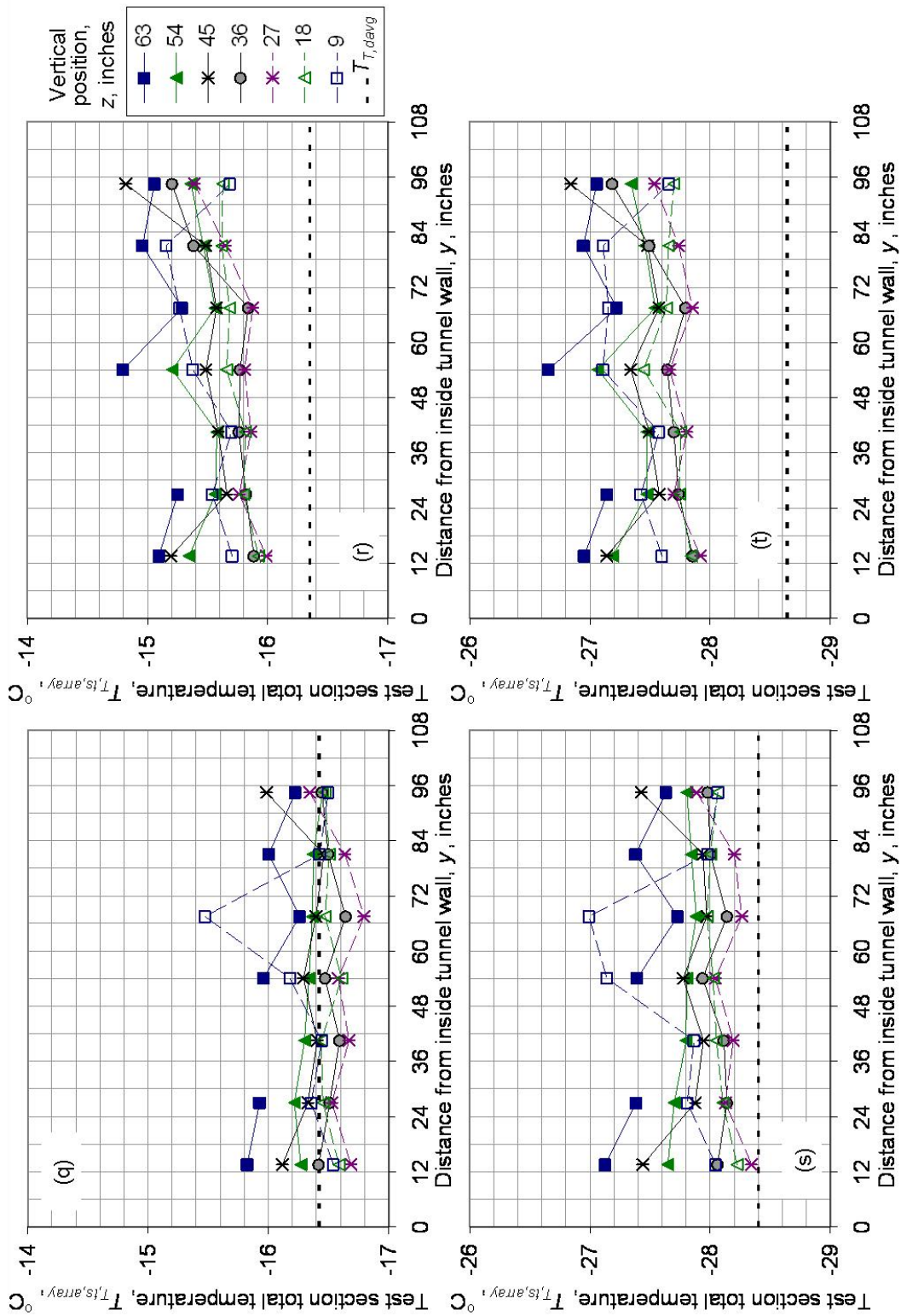


Figure 19.—Continued. (q)  $U_{ts}=116.8$  mph (101.5 knots),  $T_{T,davg}=-16.4$  °C,  $P_{air}=0$  psig. (r)  $U_{ts}=116.7$  mph (101.4 knots),  $T_{T,davg}=-16.4$  °C,  $P_{air}=70$  psig. (s)  $U_{ts}=116.6$  mph (101.3 knots),  $T_{T,davg}=-28.4$  °C,  $P_{air}=0$  psig. (t)  $U_{ts}=116.4$  mph (101.2 knots),  $T_{T,davg}=-28.6$  °C,  $P_{air}=70$  psig.

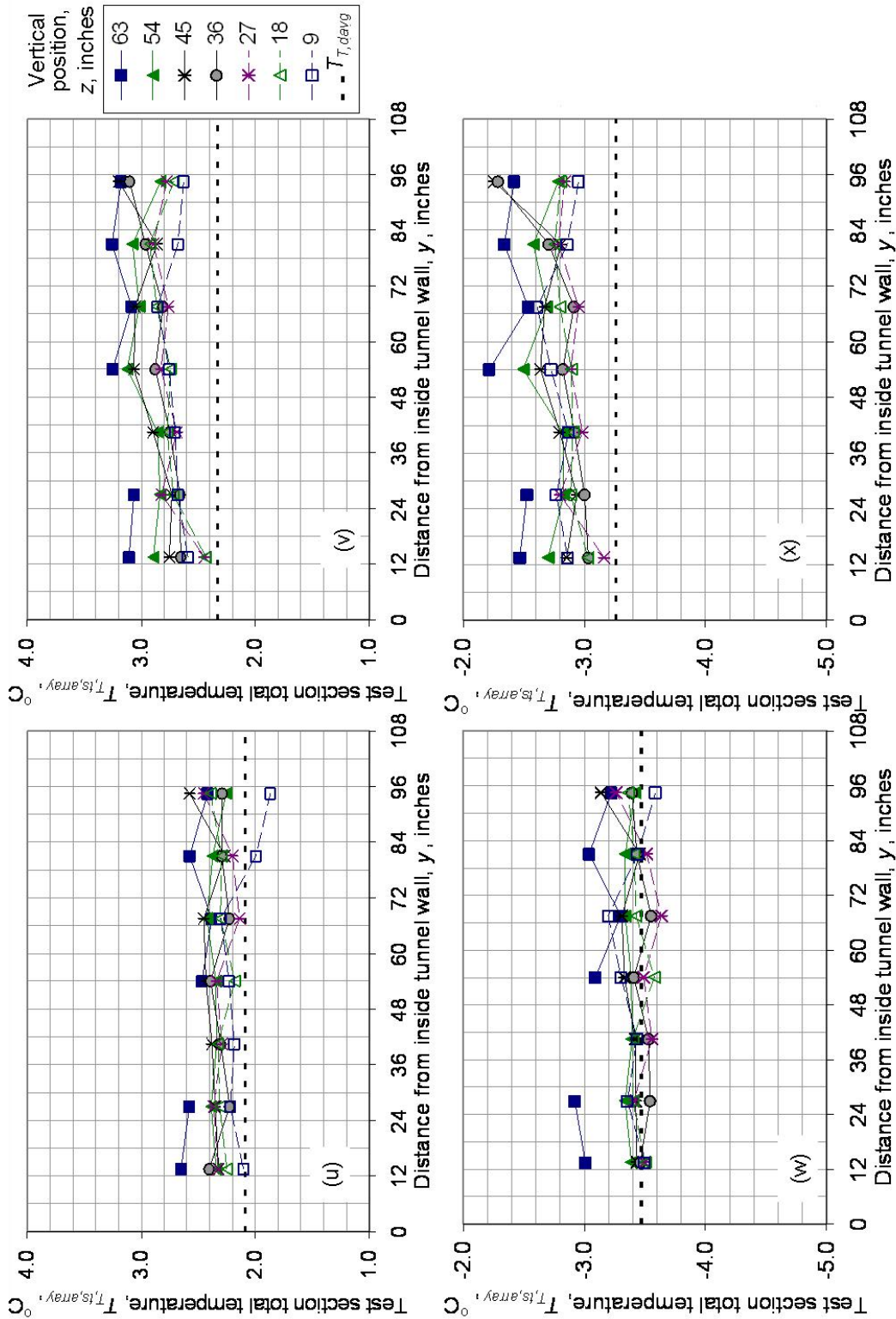


Figure 19.—Continued. (u)  $U_{ts}=151.5$  mph (131.7 knots),  $T_{T,devg}=2.1$  °C,  $P_{air}=0$  psig. (v)  $U_{ts}=151.8$  mph (131.9 knots),  $T_{T,devg}=2.3$  °C,  $P_{air}=70$  psig. (w)  $U_{ts}=152.3$  mph (132.4 knots),  $T_{T,devg}=-3.5$  °C,  $P_{air}=0$  psig. (x)  $U_{ts}=151.8$  mph (131.9 knots),  $T_{T,devg}=-3.3$  °C,  $P_{air}=70$  psig.

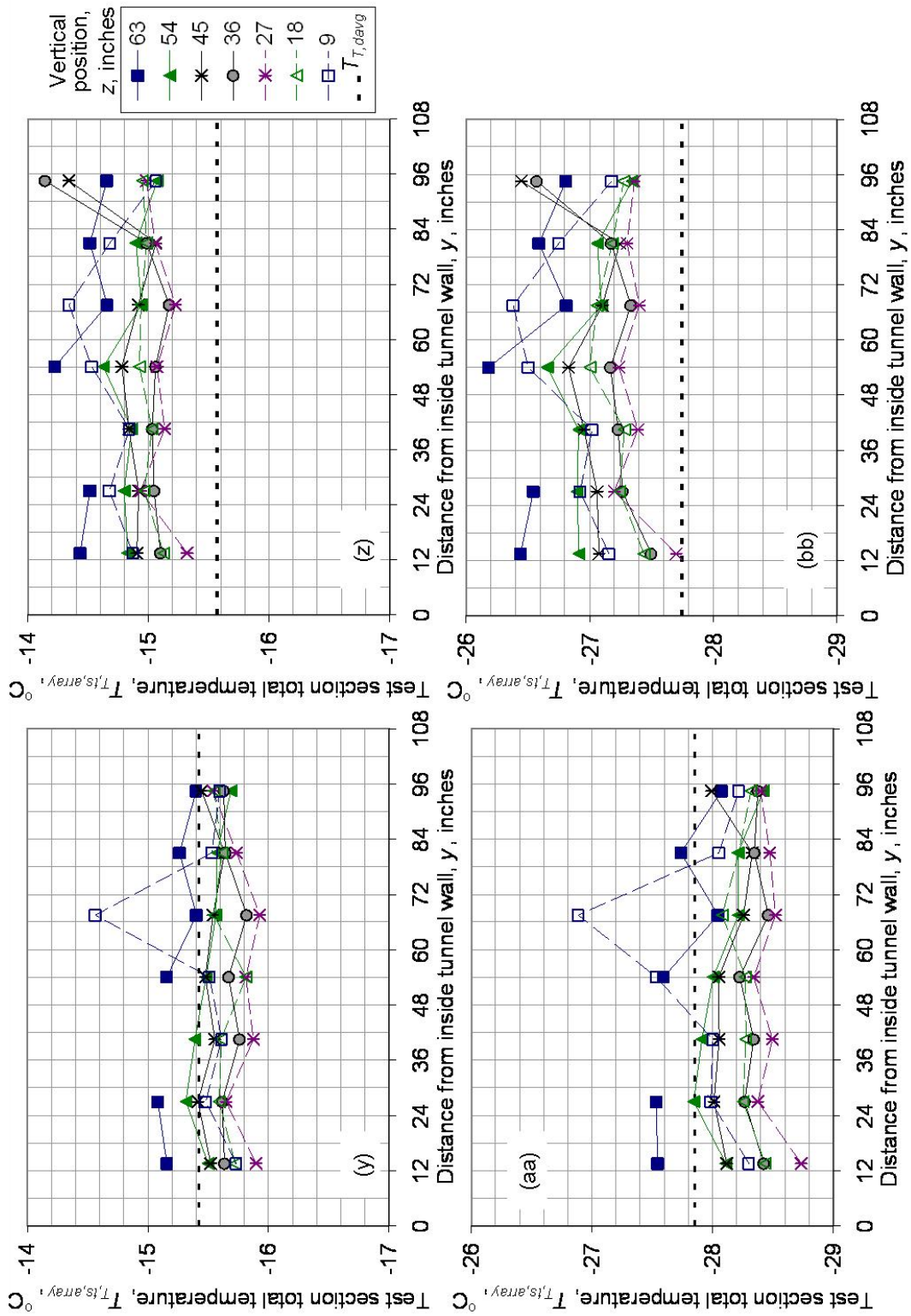


Figure 19.—Continued. (y)  $U_{IS}=152.2$  mph (132.3 knots),  $T_{T,davg}=-15.4$  °C,  $P_{air}=0$  psig. (z)  $U_{IS}=151.6$  mph (131.6 knots),  $T_{T,davg}=-15.6$  °C,  $P_{air}=70$  psig. (aa)  $U_{IS}=151.8$  mph (131.9 knots),  $T_{T,davg}=-27.9$  °C,  $P_{air}=0$  psig. (bb)  $U_{IS}=152.5$  mph (132.5 knots),  $T_{T,davg}=-27.7$  °C,  $P_{air}=70$  psig.

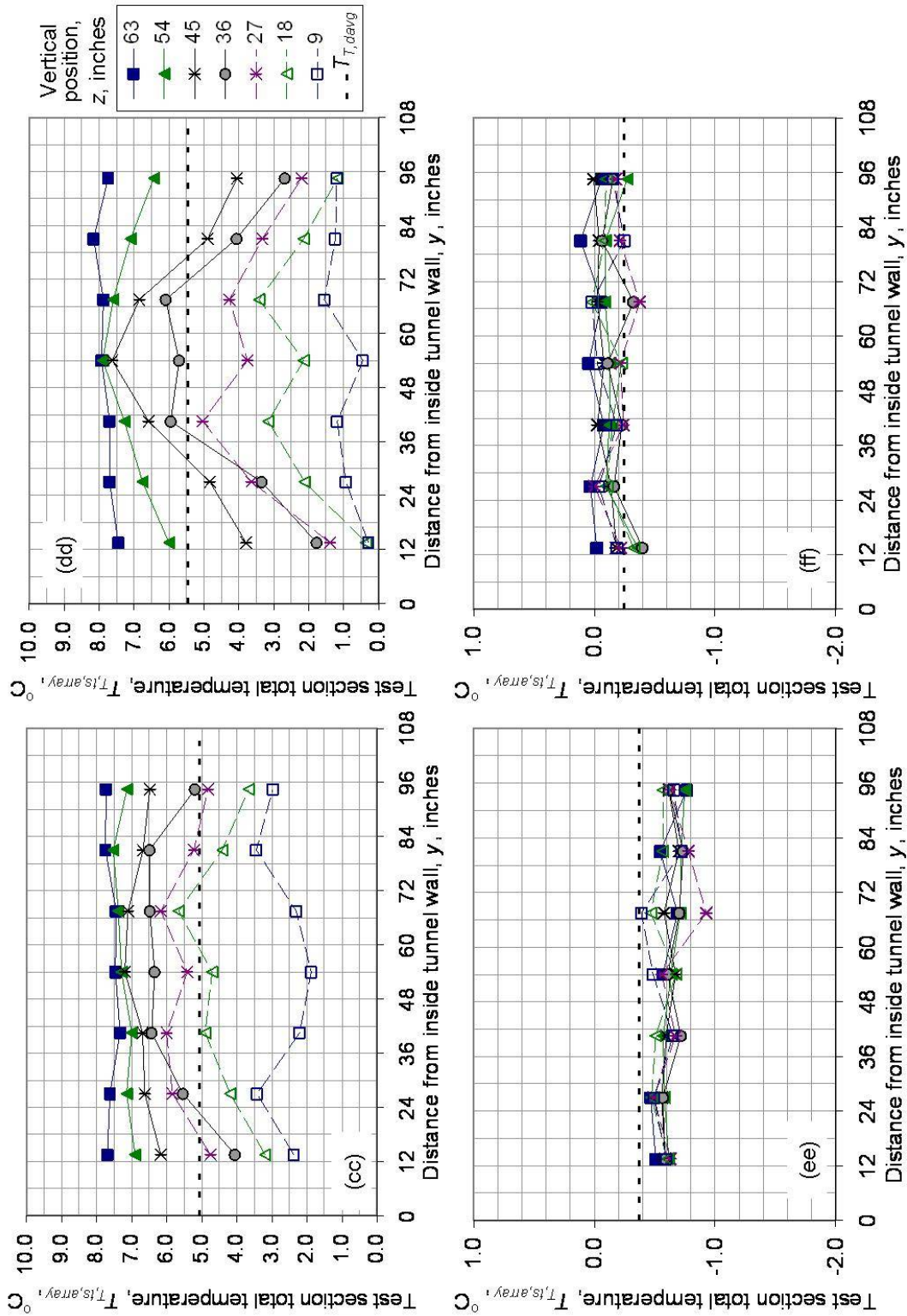


Figure 19.—Continued. (cc)  $U_{IS}=233.1$  mph (202.5 knots),  $T_{T,avg}=5.1$  °C,  $P_{air}=0$  psig. (dd)  $U_{IS}=234.8$  mph (204.0 knots),  $T_{T,avg}=5.5$  °C,  $P_{air}=70$  psig. (ee)  $U_{IS}=233.9$  mph (203.3 knots),  $T_{T,avg}=-0.4$  °C,  $P_{air}=0$  psig. (ff)  $U_{IS}=234.0$  mph (203.4 knots),  $T_{T,avg}=-0.2$  °C,  $P_{air}=70$  psig.

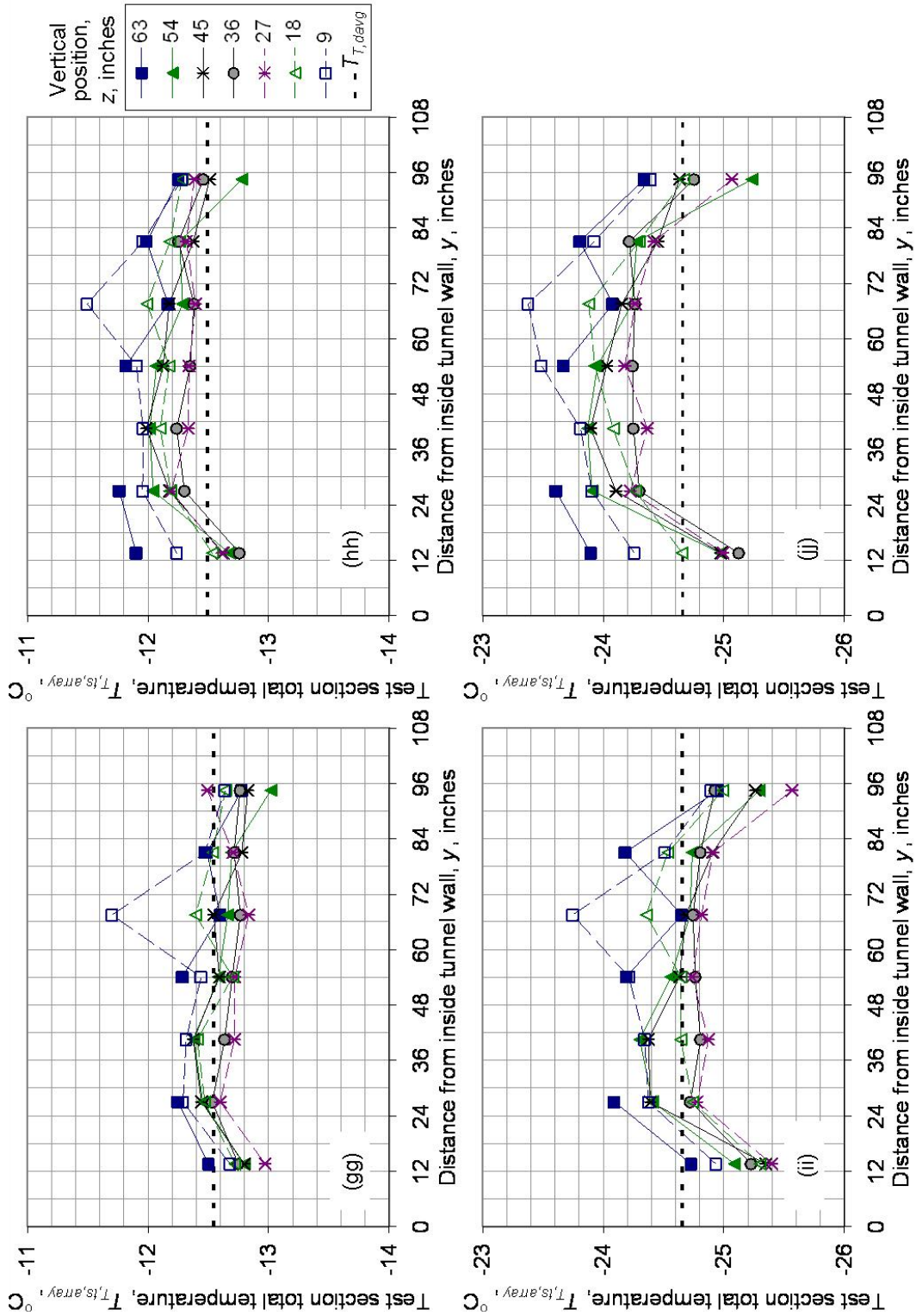


Figure 19.—Continued. (gg)  $U_{ts}=232.8$  mph (202.3 knots),  $T_{T,davg}=-12.5$  °C,  $P_{air}=0$  psig. (hh)  $U_{ts}=232.7$  mph (202.2 knots),  $T_{T,davg}=-12.5$  °C,  $P_{air}=70$  psig. (ii)  $U_{ts}=233.6$  mph (203.0 knots),  $T_{T,davg}=-24.7$  °C,  $P_{air}=0$  psig. (jj)  $U_{ts}=232.5$  mph (202.0 knots),  $T_{T,davg}=-24.7$  °C,  $P_{air}=70$  psig.

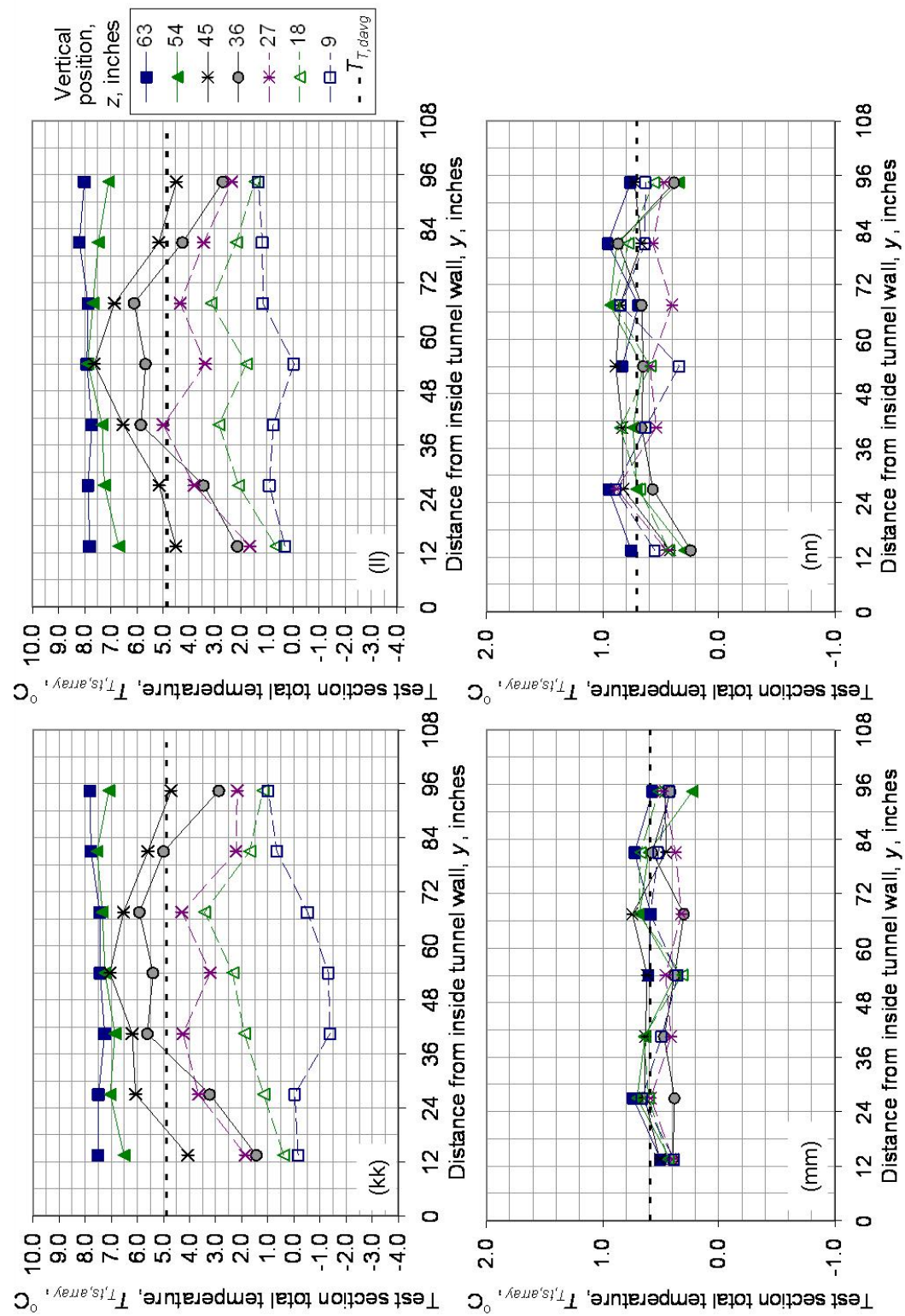


Figure 19.—Continued. (kk)  $U_{ts}=254.7$  mph (221.3 knots),  $T_{t,dev}=4.9$  °C,  $P_{air}=0$  psig. (ll)  $U_{ts}=254.5$  mph (221.2 knots),  $T_{t,dev}=4.8$  °C,  $P_{air}=70$  psig. (mm)  $U_{ts}=253.9$  mph (220.6 knots),  $T_{t,dev}=0.6$  °C,  $P_{air}=0$  psig. (nn)  $U_{ts}=253.7$  mph (220.5 knots),  $T_{t,dev}=0.7$  °C,  $P_{air}=70$  psig.

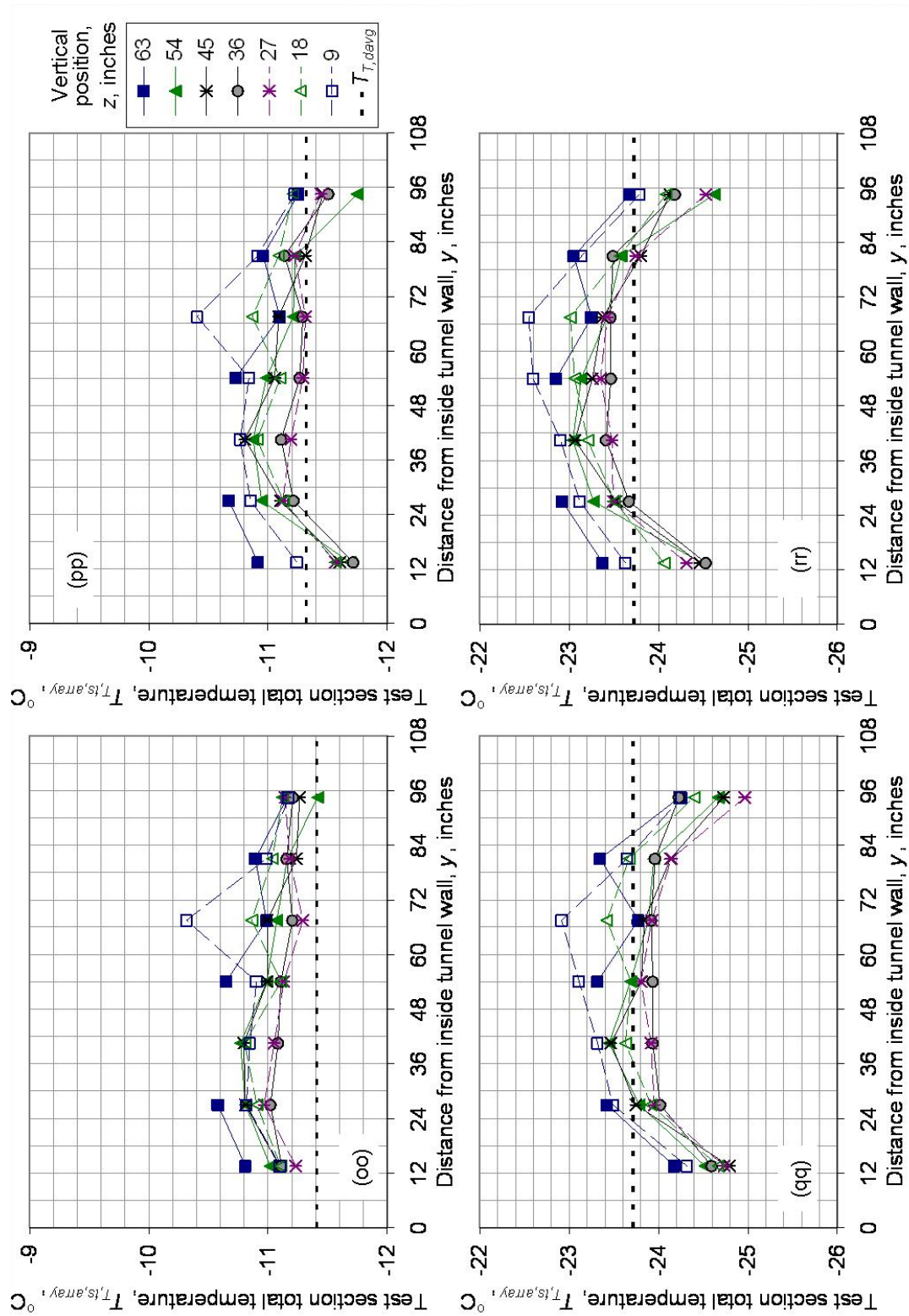


Figure 19.—Continued. (oo)  $U_{ts}=253.3$  mph (220.1 knots),  $T_{T,dev}=-11.4$  °C,  $P_{air}=0$  psig. (pp)  $U_{ts}=253.3$  mph (219.9 knots),  $T_{T,dev}=-11.3$  °C,  $P_{air}=70$  psig. (qq)  $U_{ts}=254.1$  mph (220.8 knots),  $T_{T,dev}=-23.7$  °C,  $P_{air}=0$  psig. (rr)  $U_{ts}=252.9$  mph (219.7 knots),  $T_{T,dev}=-23.7$  °C,  $P_{air}=70$  psig.

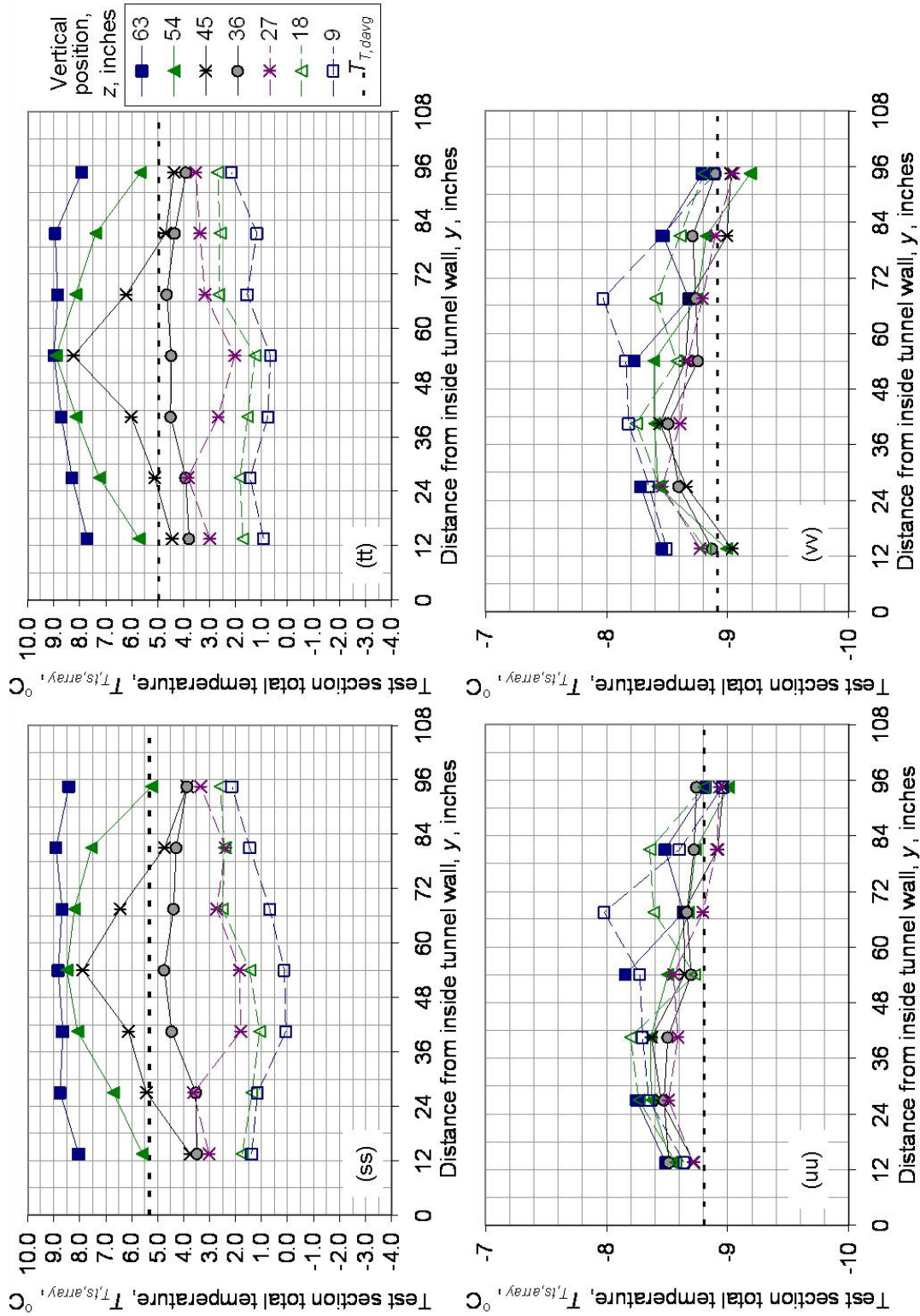


Figure 19.—Continued. (ss)  $U_{ts}=304.7$  mph (264.8 knots),  $T_{T, devg}=5.3$  °C,  $P_{air}=0$  psig. (tt)  $U_{ts}=304.6$  mph (264.7 knots),  $T_{T, devg}=5.0$  °C,  $P_{air}=70$  psig. (uu)  $U_{ts}=303.3$  mph (264.6 knots),  $T_{T, devg}=-8.8$  °C,  $P_{air}=0$  psig. (vv)  $U_{ts}=303.8$  mph (264.0 knots),  $T_{T, devg}=-8.9$  °C,  $P_{air}=70$  psig.

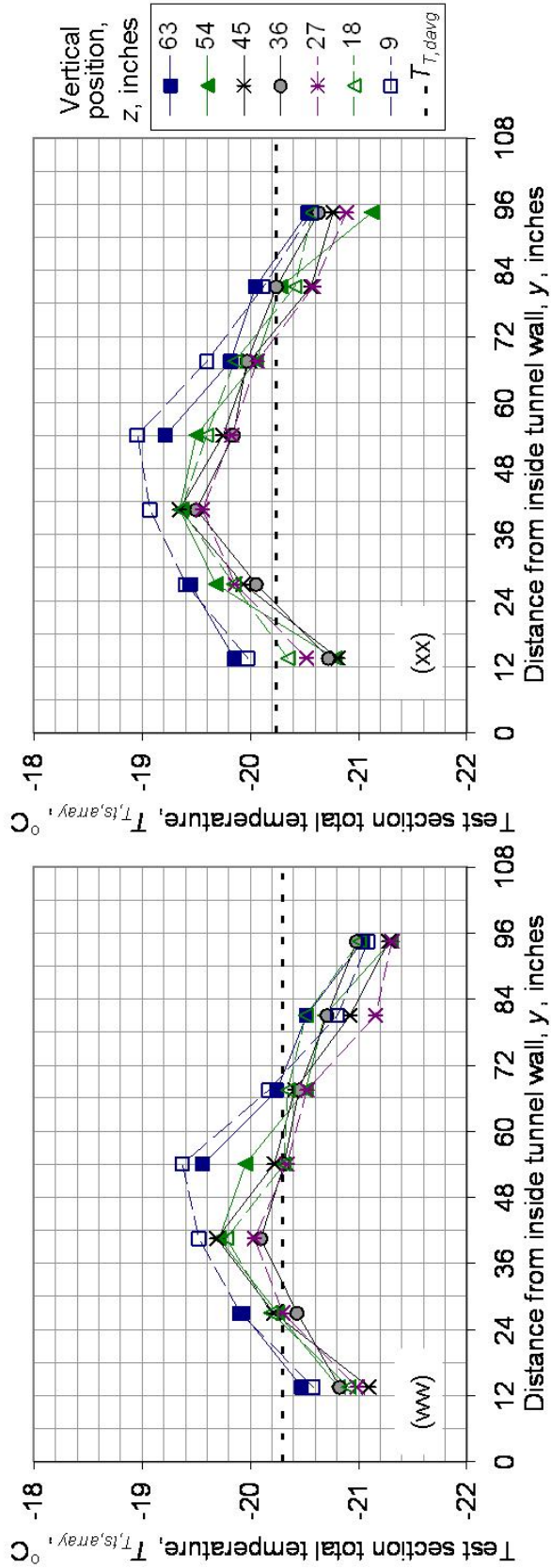


Figure 19.—Concluded. (ww)  $U_{ts}=302.9$  mph (263.2 knots),  $T_{T,avg}=-20.3$  °C,  $P_{air}=0$  psig. (xx)  $U_{ts}=303.8$  mph (264.0 knots),  $T_{T,avg}=-20.2$  °C,  $P_{air}=70$  psig.

## Flow Angularity

The test section flow angularity as measured by the 5-hole probes mounted on the 9-ft survey rake is shown in Figure 20. As described above, the 5-hole probes measure the pitch and yaw components of the flow angle and are then combined to produce the resultant flow vectors. The vectors shown in Figure 20 only reflect the magnitude and direction of the local air flow, but not airspeed. For the low speed test points ( $U_{ts}=50$  mph) the data from rake position 66-in. above the test section floor was deleted due to the low speeds measured at that location (the airspeeds were much lower than the calibrated range of the flow angle probes). Larger flow angles were consistently recorded near the test section ceiling which may be due to the suspected boundary layer interaction noted in Mach number and total pressure distribution data.

The flow angularity in the IRT test section generally meets the  $\pm 2^\circ$  goal stated in Reference 1 (Table 4), particularly in the core of the test section (roughly the center 4.5 by 3 ft area). In this central core area, the average flow angle vector magnitude is less than  $2^\circ$  for all conditions (including maximum spraybar air pressure) as shown in Figure 21. The average flow angle vector magnitude hovers between  $0.7^\circ$  and  $0.9^\circ$  over the entire airspeed range with no spraybar air injection ( $P_{air}=0$  psig). This data also indicates that there is a significant effect on the average flow angle vector magnitude at maximum spraybar air pressure ( $P_{air}=70$  psig) up to about  $U_{ts}=150$  mph. Above  $U_{ts}=150$  mph (130 knots), spraybar air pressure effect on the average flow angle vector magnitude is less than 0.1 degree between  $P_{air}=70$  and  $P_{air}=0$  psig. The limited data collected at lower spraybar air pressure settings ( $P_{air}=5$  and 20 psig) show no significant difference in average flow angle vector magnitude compared to spraybar air off ( $P_{air}=0$  psig).

Overall, the flow angularity in the IRT test section is acceptable for an icing facility and actually is not bad for a subsonic wind tunnel that does not have any flow straightening honeycomb in the settling chamber. Other than the vortices in the test section corners at low airspeed and high spraybar air settings, there are no obvious flow patterns shown in the vector data. Most of the variation in the flow angle orientation is probably due to disturbances generated by the spraybars (wakes).

## Turbulence

Thermal anemometry was used to measure the turbulence levels in the IRT test section. Three hot-wire probes were mounted on the 9-ft survey rake. The turbulence data is shown in Figure 22. The IRT will not have the low-turbulence levels of a wind tunnel used for aerodynamics testing due to the lack of flow manipulators like screens and honeycomb and due to the influence of the spraybars. In general, the axial turbulence varies between 0.2 and 1.0-percent with no air injection from the spraybar ( $P_{air} = 0$ ). The traverse turbulence is a little higher, ranging from 0.5 to 2.0-percent. Note also that the turbulence levels are higher near the test section centerline due to the wake from the spraybar centerline support. Higher turbulence levels were also recorded near the test section floor and ceiling, possible due to boundary layer effects. The injection of spraybar air has a significant effect on the test section turbulence, particularly at the lower airspeed settings.

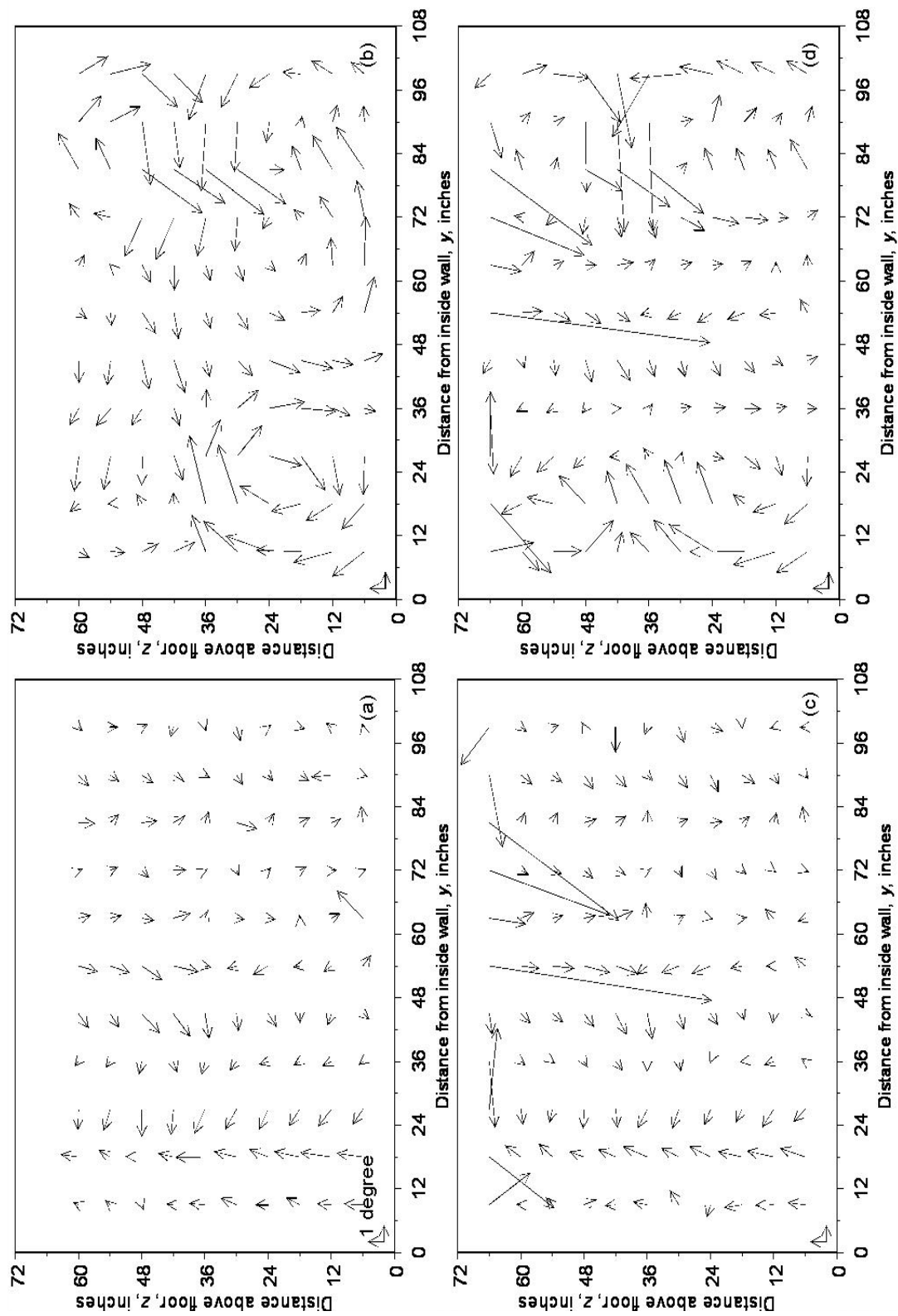


Figure 20.—Flow angle data from the IRT test section collected using the 9-ft survey rake mounted at 11 vertical positions over several tunnel runs. Nominal conditions are used to denote each data set. (a)  $U_{ts}=50$  mph (43 knots),  $P_{air}=0$  psig. (b)  $U_{ts}=50$  mph (43 knots),  $P_{air}=70$  psig. (c)  $U_{ts}=100$  mph (87 knots),  $P_{air}=0$  psig. (d)  $U_{ts}=100$  mph (87 knots),  $P_{air}=70$  psig.

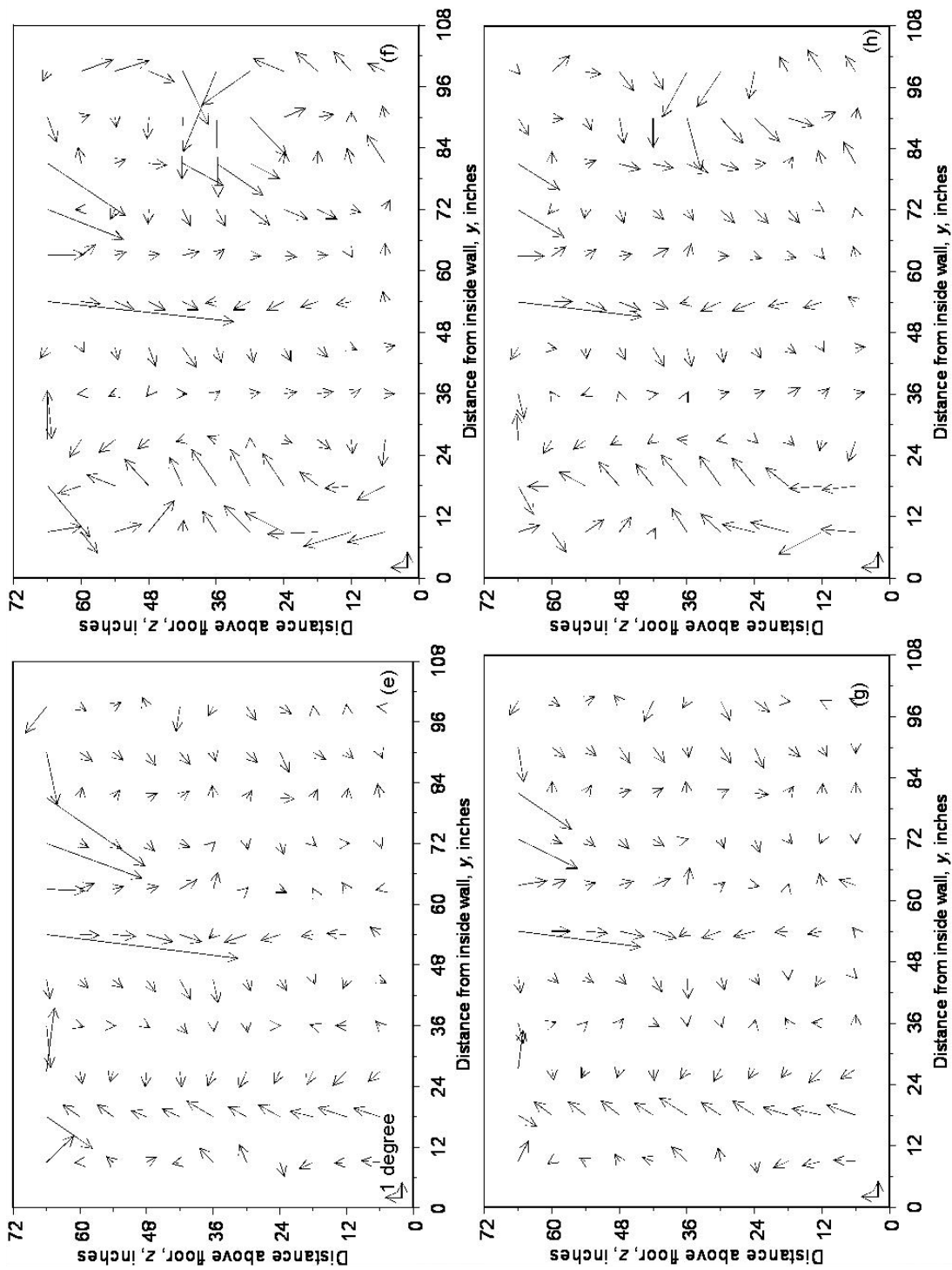


Figure 20.—Continued. (e)  $U_{IS}=115$  mph (100 knots),  $P_{air}=0$  psig. (f)  $U_{IS}=115$  mph (100 knots),  $P_{air}=70$  psig. (g)  $U_{IS}=150$  mph (130 knots),  $P_{air}=0$  psig. (h)  $U_{IS}=150$  mph (130 knots),  $P_{air}=70$  psig.

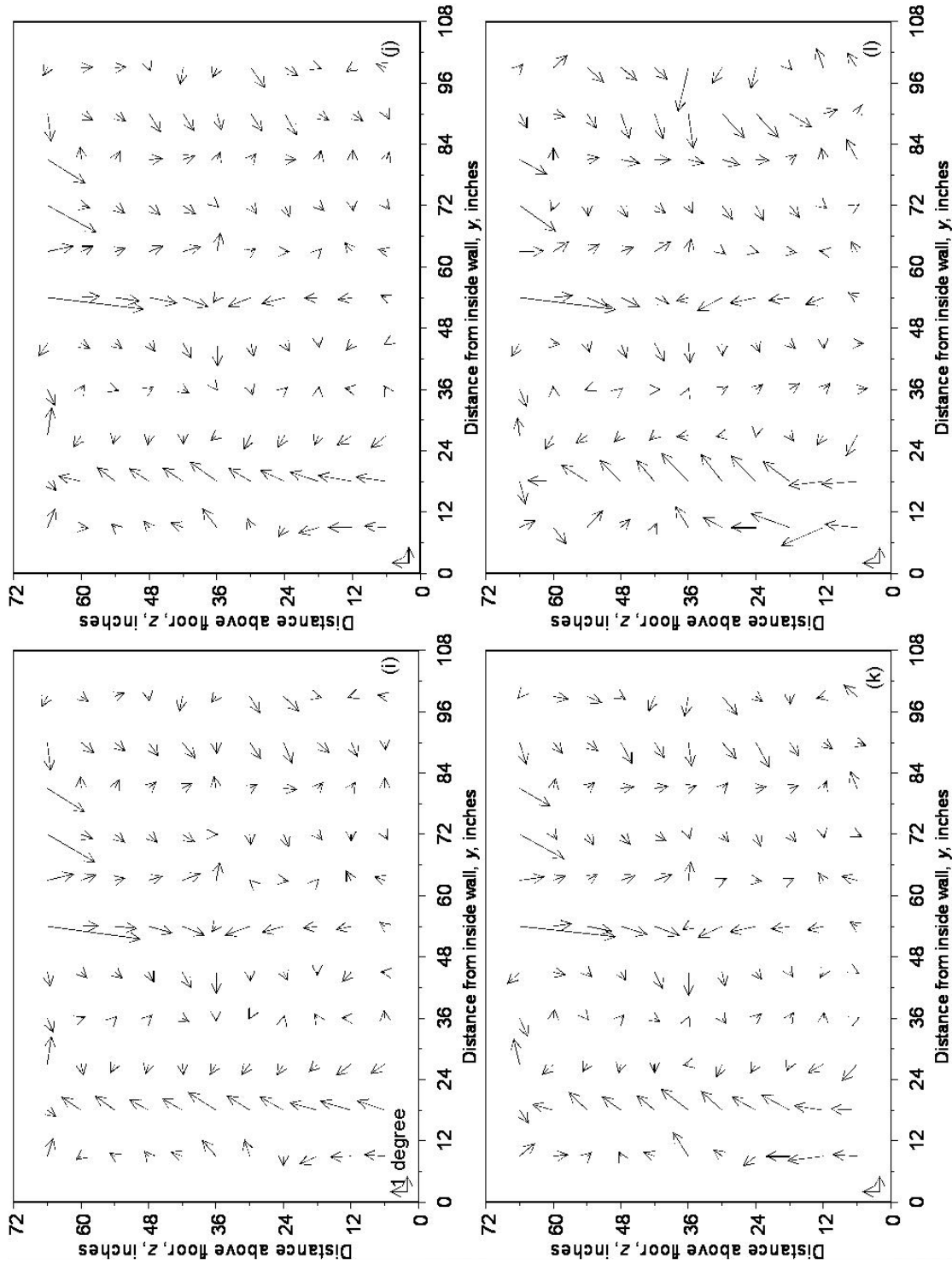


Figure 20.—Continued. (j)  $U_s=175$  mph (152 knots),  $P_{air}=0$  psig. (k)  $U_s=175$  mph (152 knots),  $P_{air}=5$  psig. (l)  $U_s=175$  mph (152 knots),  $P_{air}=70$  psig. (m)  $U_s=152$  knots,  $P_{air}=70$  psig.

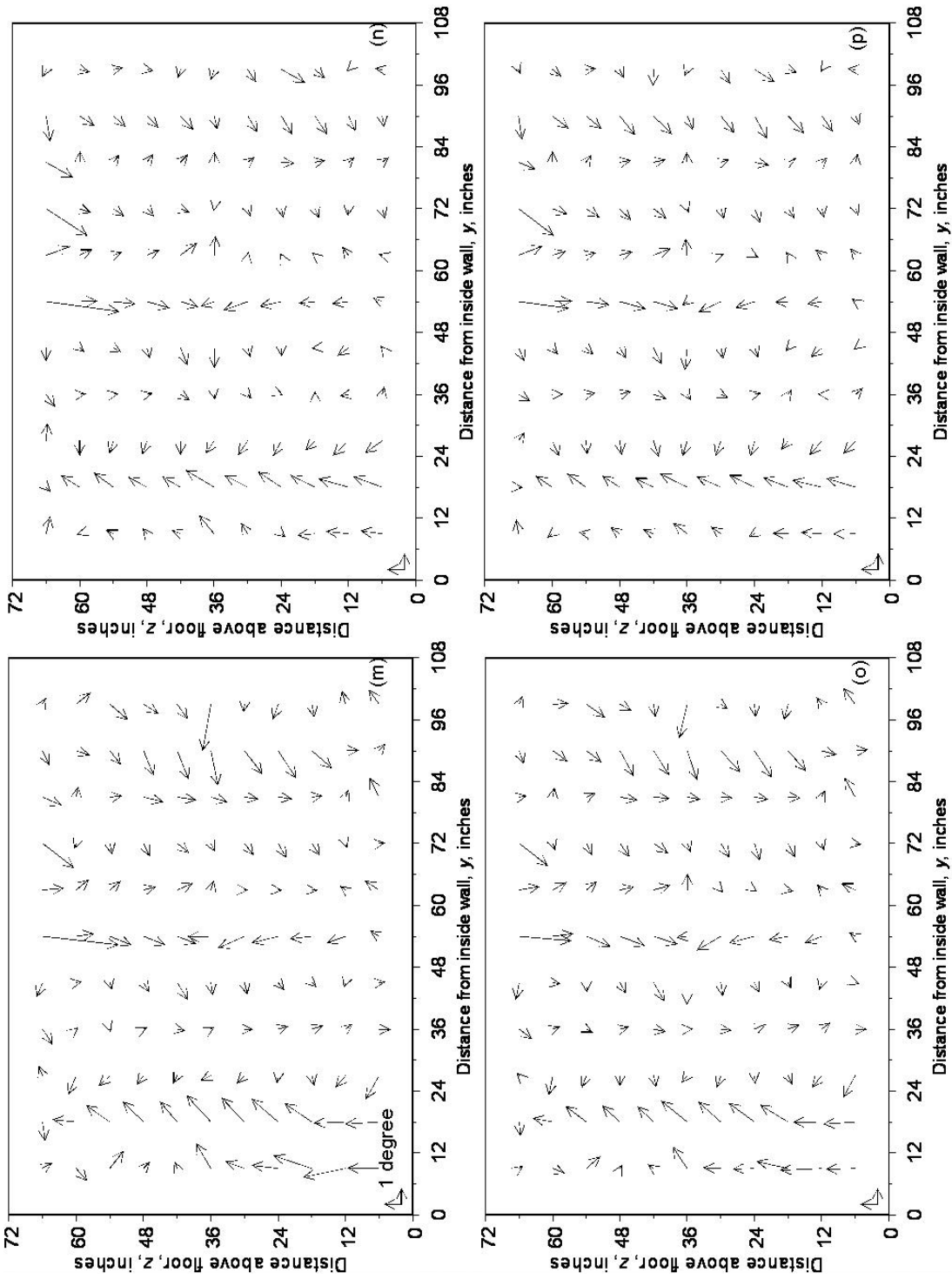


Figure 20.—Continued. (m)  $U_{fs}=200$  mph (174 knots),  $P_{air}=0$  psig. (n)  $U_{fs}=200$  mph (174 knots),  $P_{air}=70$  psig. (o)  $U_{fs}=250$  mph (217 knots),  $P_{air}=0$  psig. (p)  $U_{fs}=250$  mph (217 knots),  $P_{air}=70$  psig.

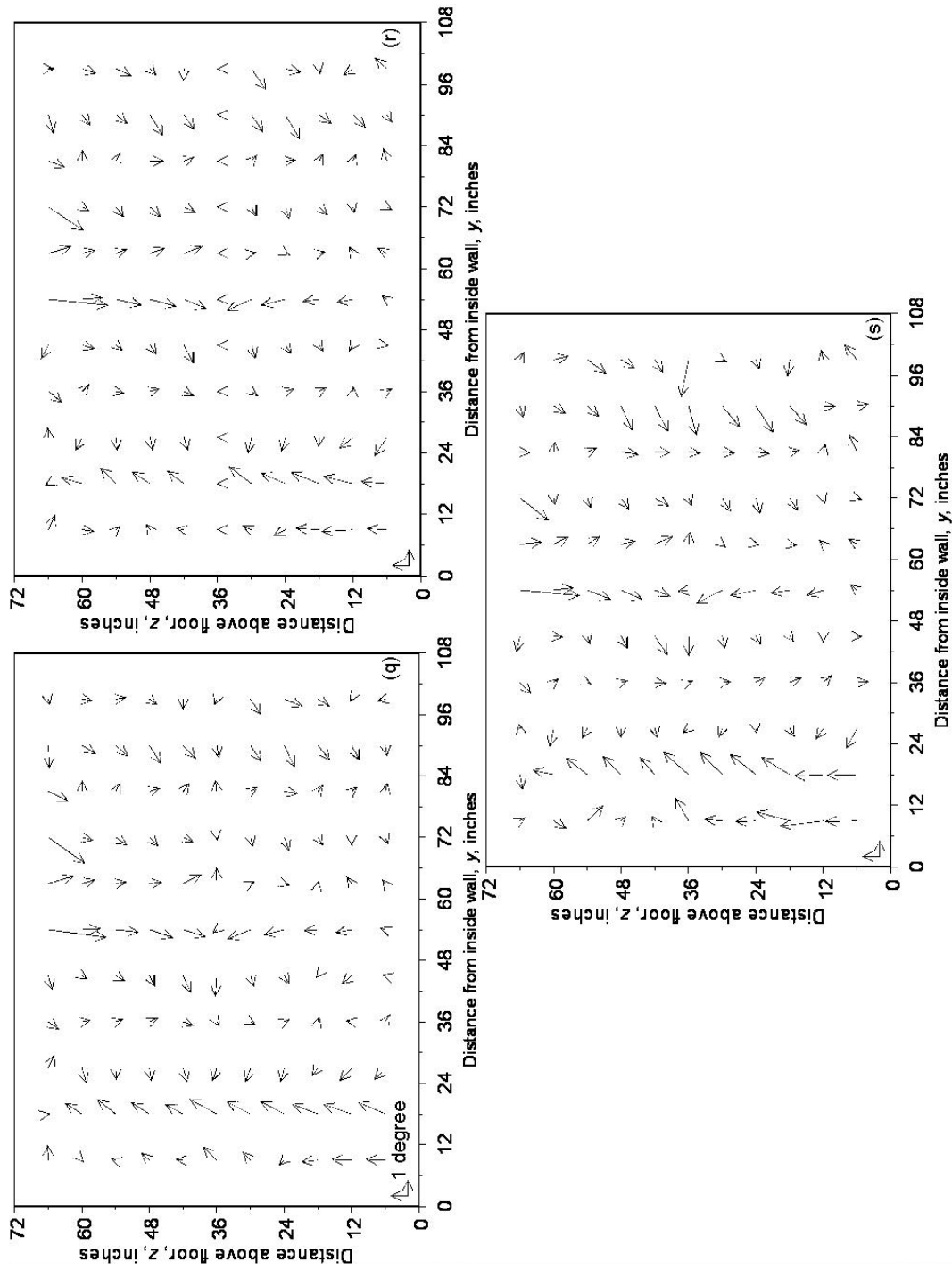


Figure 20.—Continued. (q)  $U_{is}=225$  mph (195 knots),  $P_{air}=0$  psig. (r)  $U_{is}=225$  mph (195 knots),  $P_{air}=20$  psig. (s)  $U_{is}=225$  mph (195 knots),  $P_{air}=70$  psig.

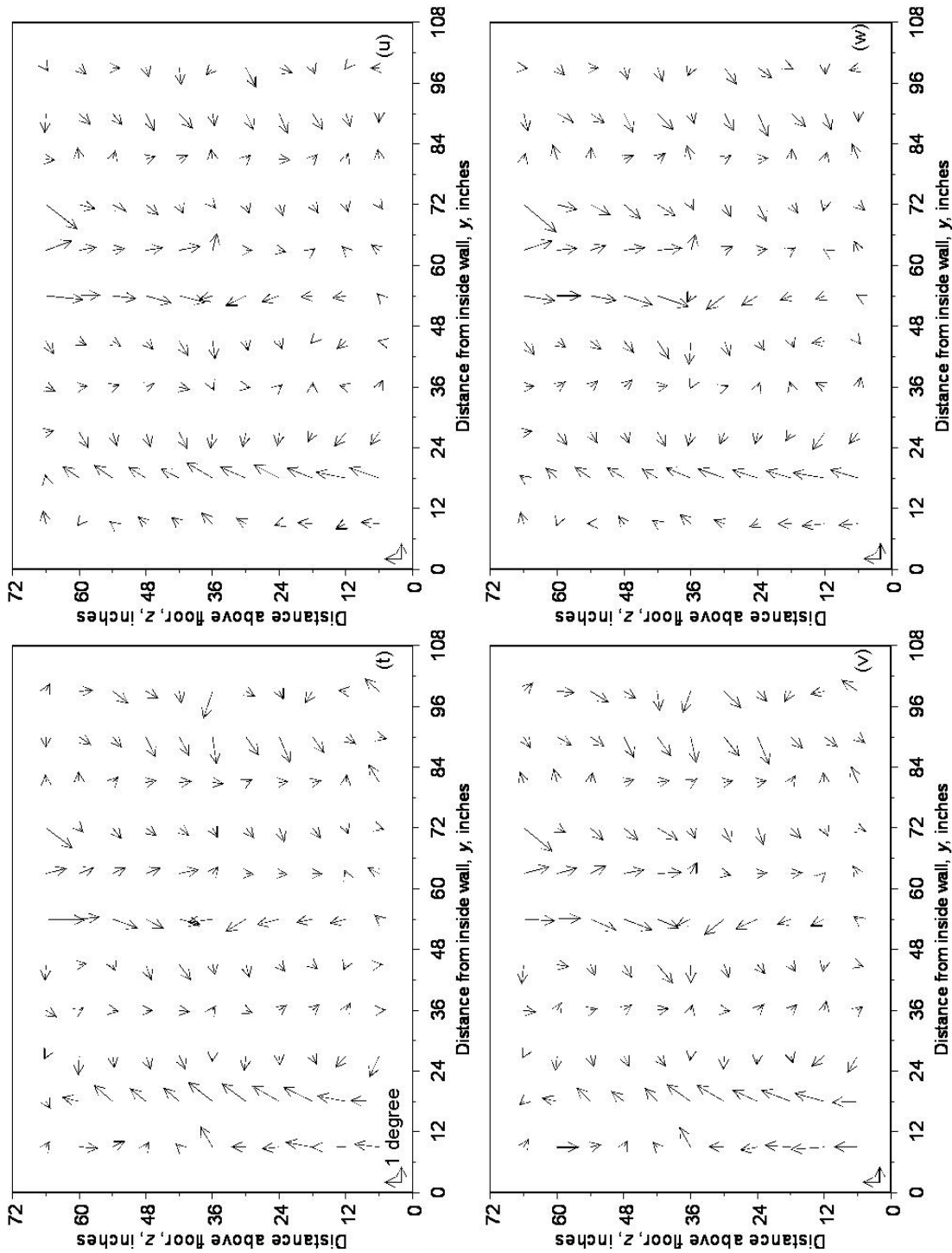


Figure 20.—Concluded. (t)  $U_{fs}=300$  mph (261 knots),  $P_{air}=0$  psig. (u)  $U_{fs}=300$  mph (261 knots),  $P_{air}=70$  psig. (v)  $U_{fs}=350$  mph (304 knots),  $P_{air}=0$  psig. (w)  $U_{fs}=350$  mph (304 knots),  $P_{air}=70$  psig.

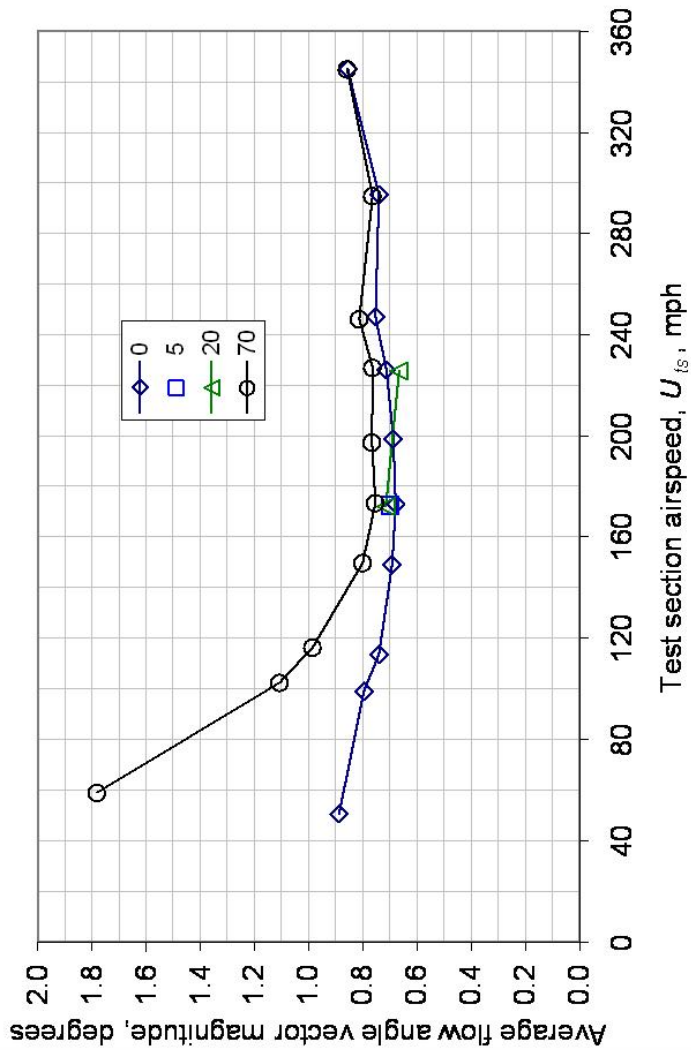


Figure 21.—Average flow angularity vector magnitude in the core (center 4.5- by 3- ft area) of the IRT test section at various  $P_{air}$  settings.

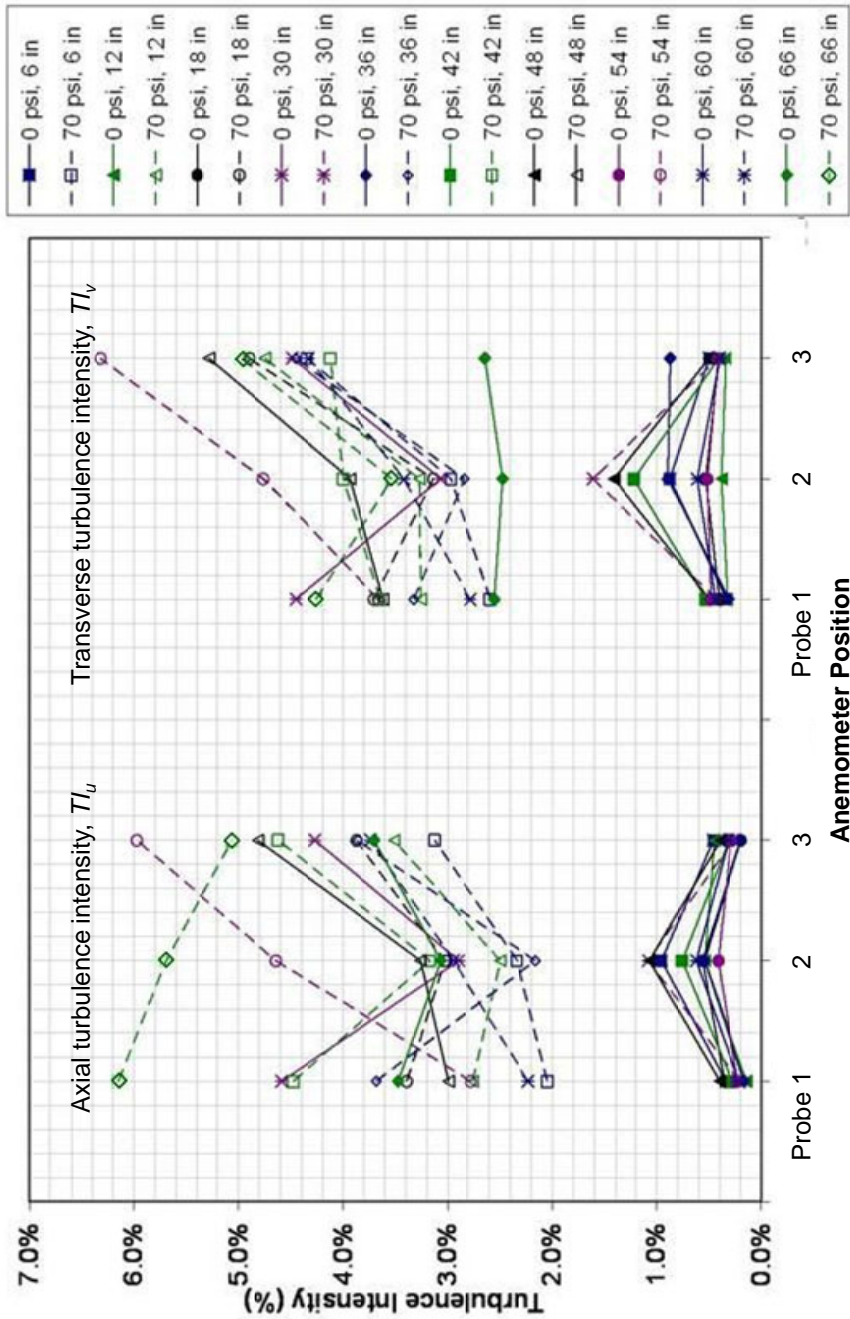


Figure 22.—Summary of the axial and transverse turbulence levels in the IRT test section as measured by probes mounted on the 9-ft survey rake. The probes were arrayed laterally across the span of the rake as follows: Probe 1 was 31.8 in. from the inside wall, probe 2 was 53.7 in. and probe 3 was 76.2 in. (a) Test section airspeed of 50 mph

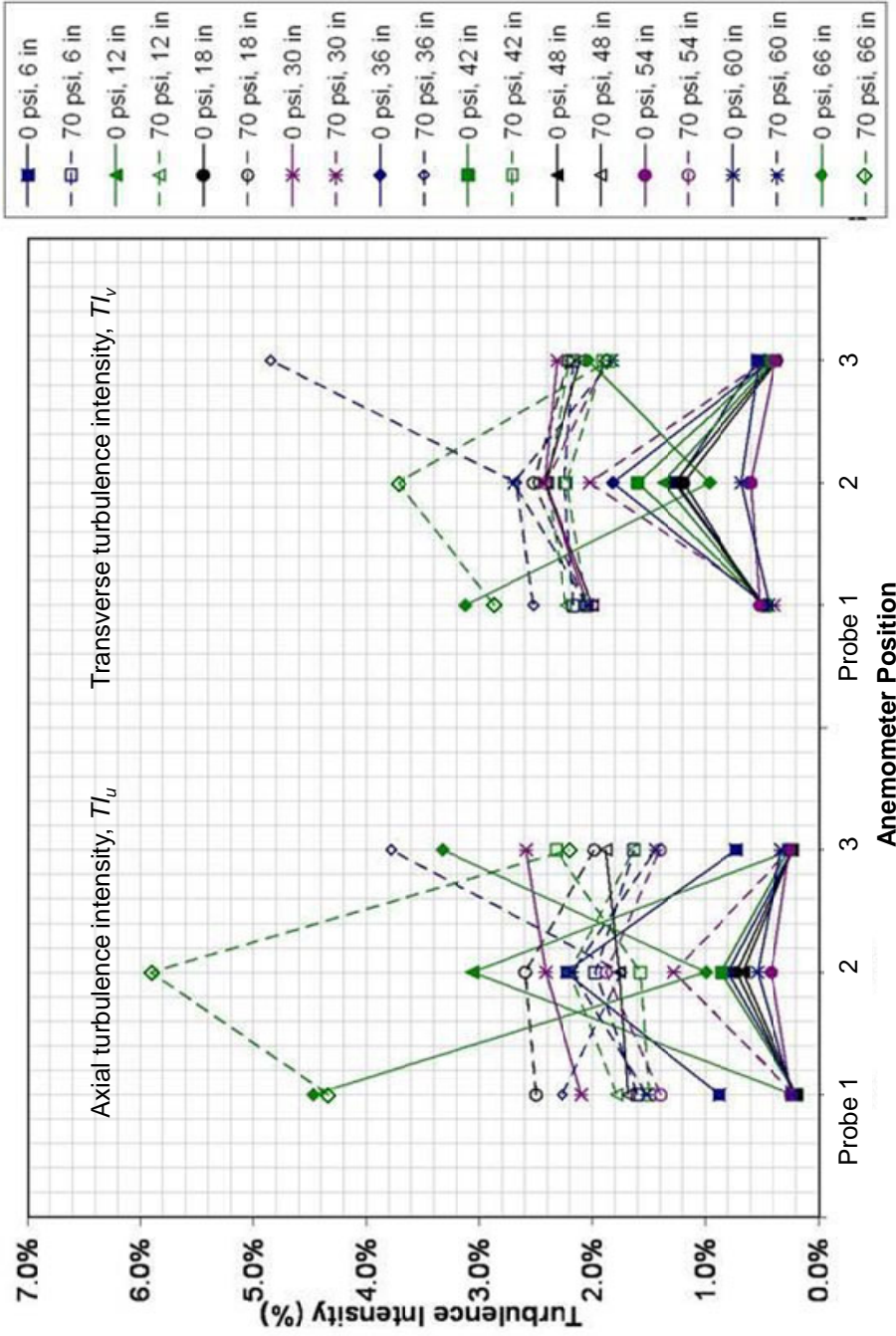


Figure 22.—Continued. (b) 100 mph

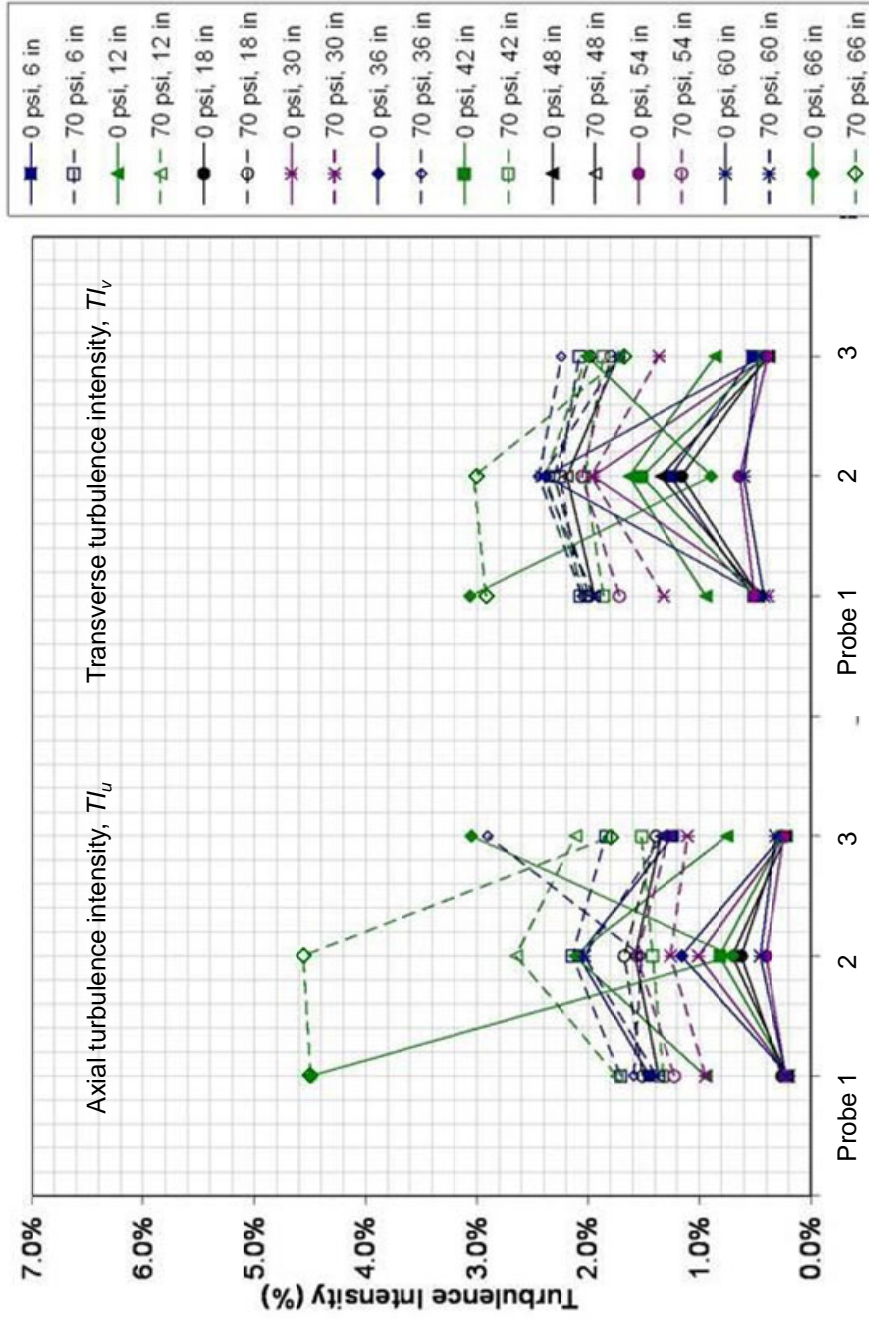


Figure 22.—Continued. (c) 115 mph

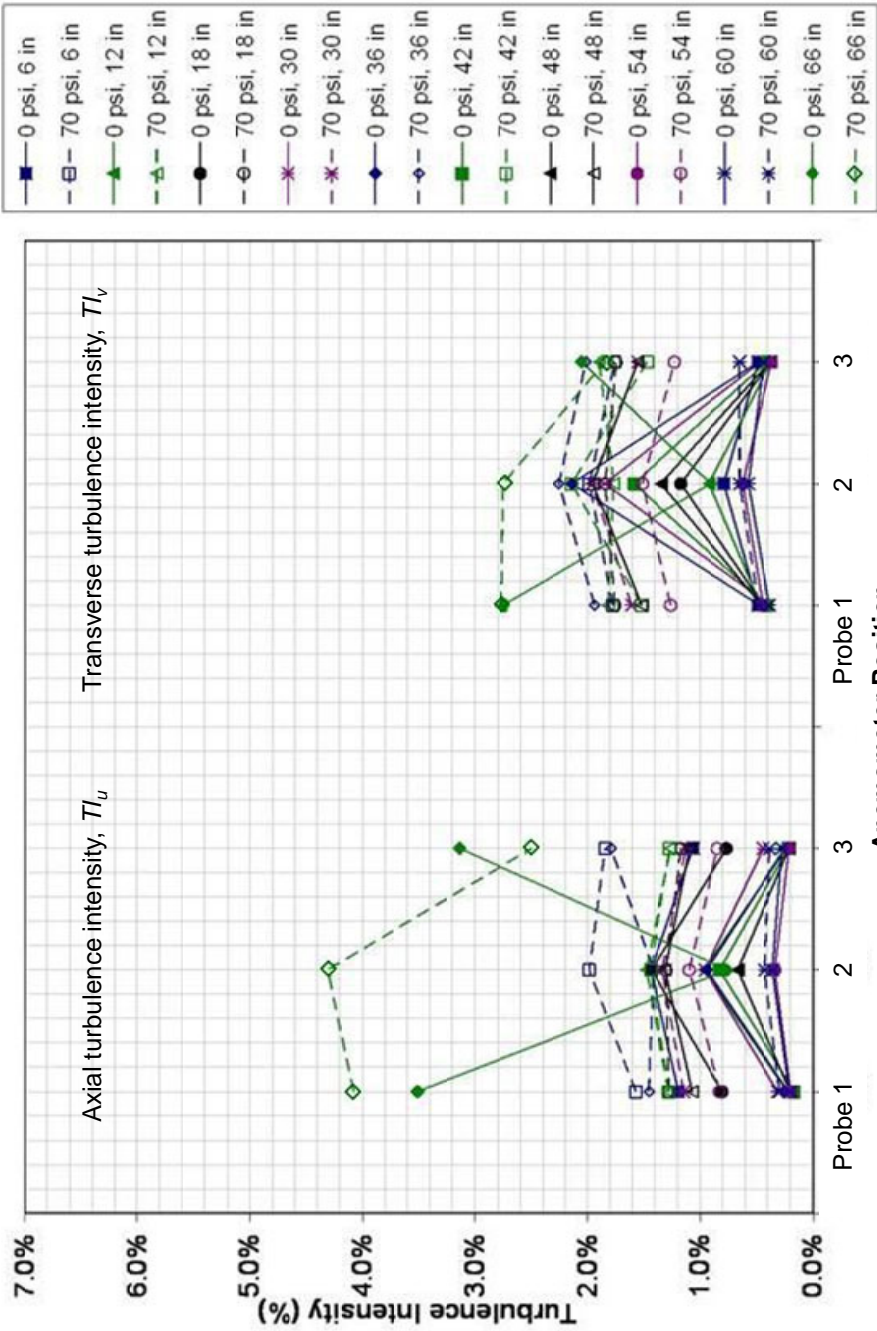


Figure 22.—Continued. (d) 150 mph

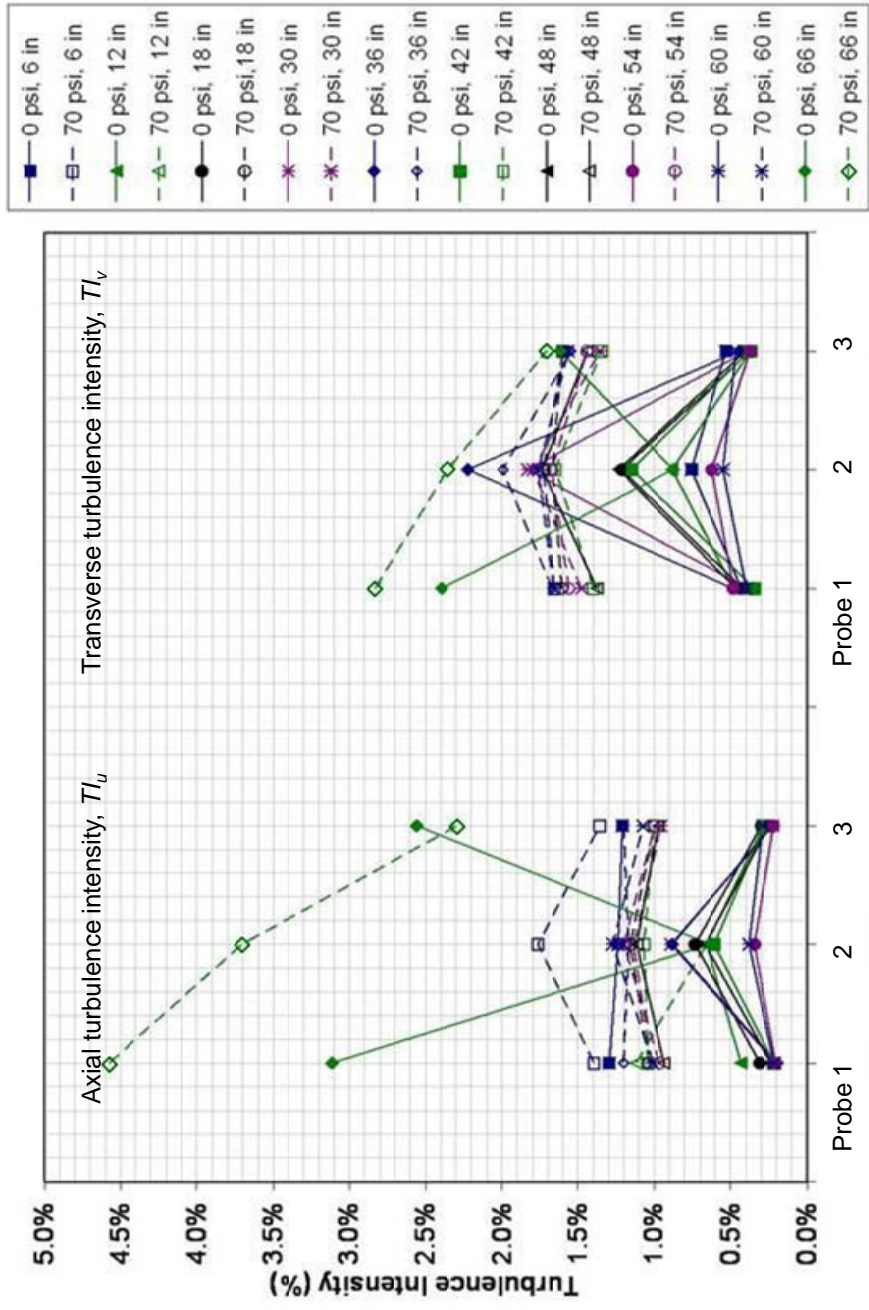


Figure 22.—Continued. (e) 175 mph, 0 and 70 psi.

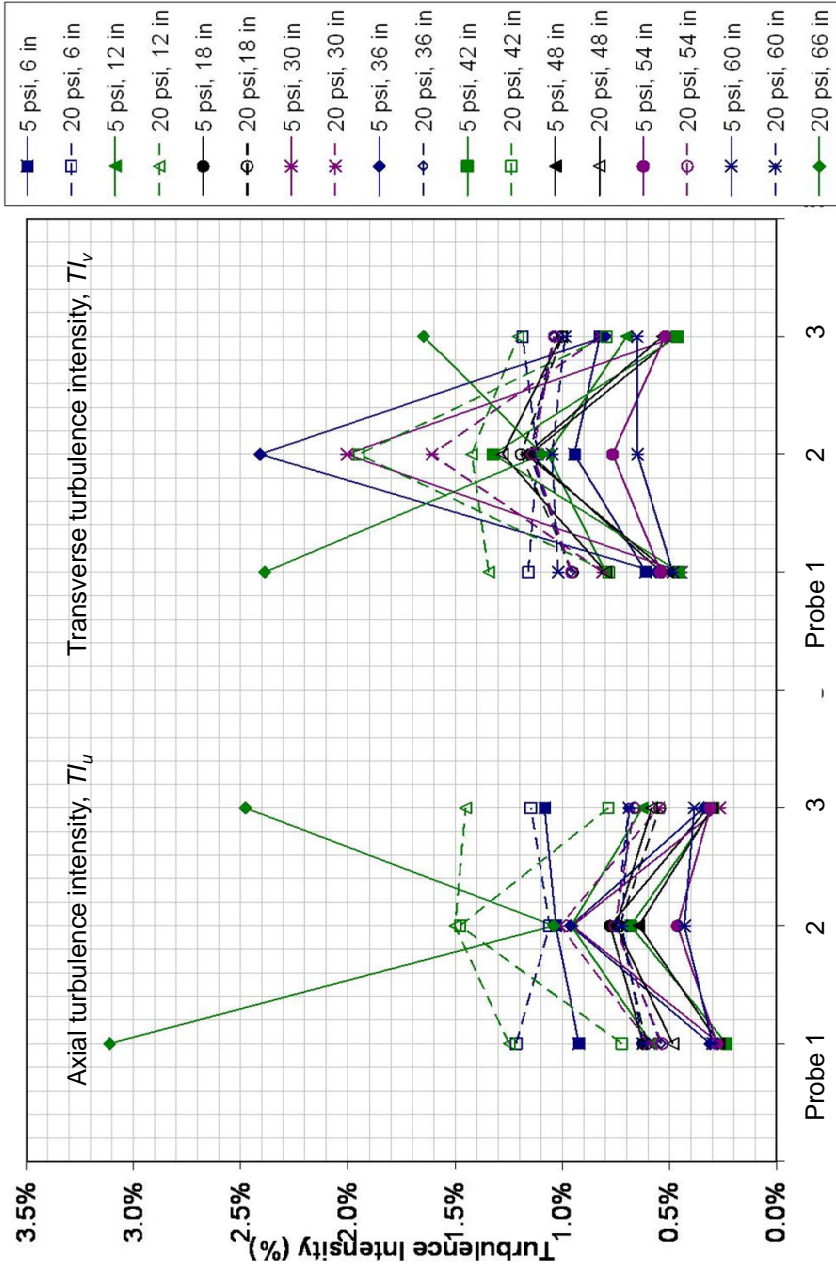


Figure 22.—Continued. (f) 175 mph, 5 and 20 psi.

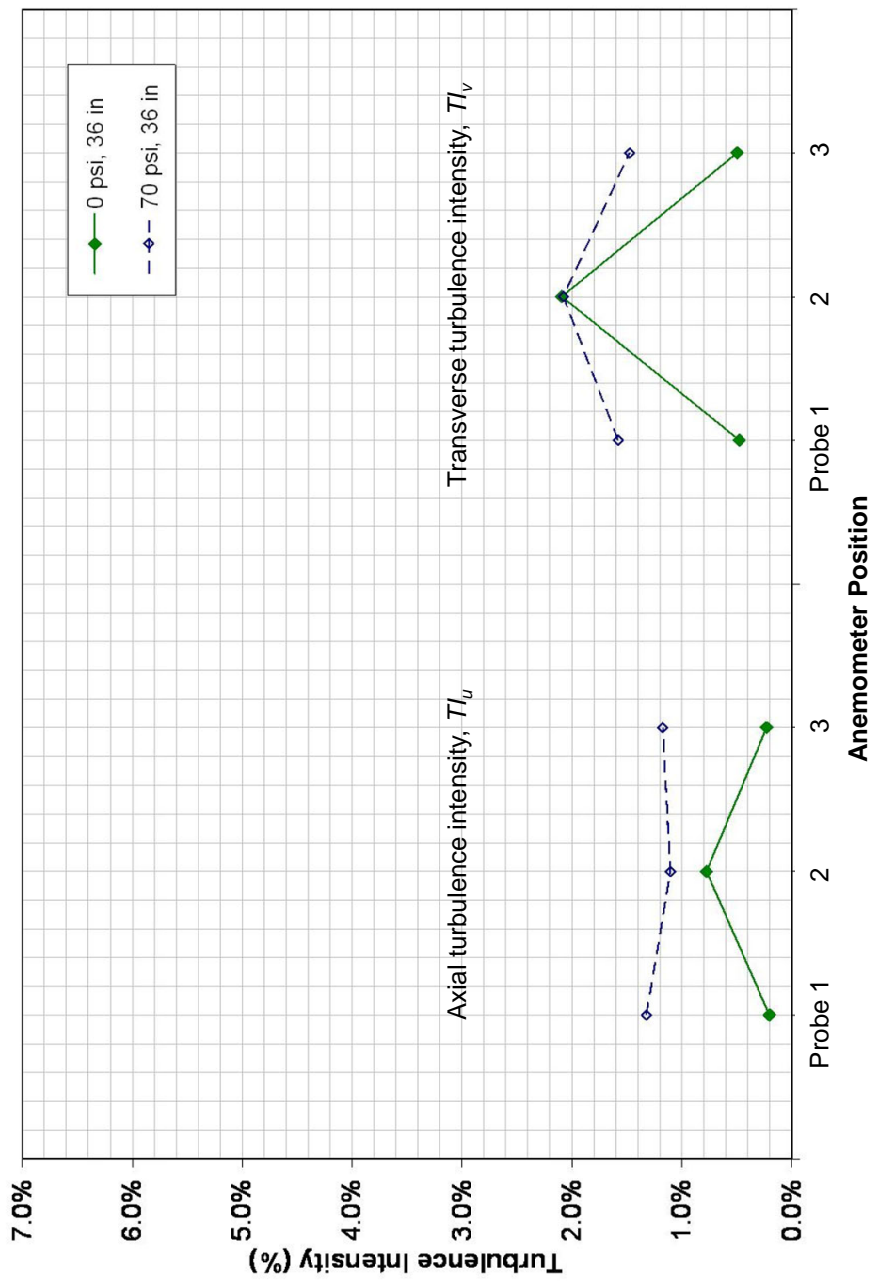


Figure 22.—Concluded. (g) 200 mph.

## Summary of Test Results

Aero-thermal calibration testing was completed following facility modifications to the NASA Glenn Icing Research Tunnel. The original inlet guide vanes upstream of the IRT drive fan were replaced due to the age and structural concerns. The new inlet guide vanes were designed to provide more efficient operation of the IRT. During January 2004 a full aero-thermal calibration was completed to fully assess the impact of the new inlet guide vanes on the IRT test section calibration and flow quality. An interim calibration was completed in January 2005. The following were the primary accomplishments and results from the 2004 to 2005 aero-thermal calibration test entries in the IRT.

From the January 2004 full aero-thermal calibration:

- Completed the planned test matrix that covered the entire operating of the IRT (airspeed, temperature and spraybar air injection).
- From the collected data set, a new set of aero-thermal calibration curves were constructed. These calibration curves provided an accurate characterization of the IRT aero-thermal test section conditions over the operation range of the facility.
- The data set also provided a detailed flow field map of the aero-thermal flow quality in the IRT test section.

In addition to providing a general check of the IRT aero-thermal operation and calibration, the data collected during the January 2005 interim aero-thermal calibration provided an improved total temperature calibration model.

## Recommendations

The following recommendations were developed following each calibration test entry. Some of the recommendations from the 2004 test were implemented during the 2005 test.

- Following the 2004 test, it was noted that the aero-thermal calibration curves should be refined to better model the affects of the spraybar air. This was implemented in the calibration curves developed following the 2005 interim calibration.
- During the 2004 calibration, there some test conditions that required additional stabilization time, particularly in terms of total temperature. It was recommended that a means of monitoring the stability of the total temperature setting was needed to ensure steady test conditions. The facility electrical engineers developed a graphical representation that monitored the real-time, running average and standard deviation in the D-corner temperature measurements to monitor data stability. This was implemented for the 2005 testing.
- The data collected in 2004 and 2005 showed that spraybar air injected into the airstream has a very noticeable effect on the test section operating conditions as the low speed settings (less than 100 knots). Additional testing is needed to determine (1) the test section airspeed at which spraybar air pressure no longer has a significant effect and (2) the minimum spraybar air pressure that causes a noticeable effect at the low speed settings.

## Appendix A.—Uncertainty Estimates

This analysis was conducted based on the AIAA Standard “Assessment of Experimental Uncertainty with Application to Wind Tunnel Testing” and its companion Guide, References 12 and 13.

### A.1 General Uncertainty Analysis

The accuracy of a measurement is the true value in relation to the measured value. In experimentation, the true value is unknown. Therefore, the uncertainty of the measured value is determined using the bias and precision errors. The bias error is the fixed or constant error that occurs with each measurement, while the precision error is the random or repeatability error.

General uncertainty analysis (Ref. 14) uses the experimental result,  $r$ , with variables up to  $X_J$  as seen in Equation (A1)

$$r = r(X_1, X_2, \dots, X_J) \quad (\text{A1})$$

The general uncertainty equation takes the form seen in Equation (A2) with the expanded form shown as

$$U_r = \left[ \sum_{i=1}^J \theta_i^2 U_{X_i}^2 \right]^{1/2} \quad (\text{A2})$$

$$U_r = \left[ \left( \frac{\partial r}{\partial X_1} U_{X_1} \right)^2 + \left( \frac{\partial r}{\partial X_2} U_{X_2} \right)^2 + \dots + \left( \frac{\partial r}{\partial X_J} U_{X_J} \right)^2 \right]^{1/2} \quad (\text{A3})$$

In this analysis, the uncertainties of the velocity, Mach number, and flow angularity were determined with respect to total temperature, total pressure and static pressure. Additionally, the pressure measurement uncertainty was determined with respect to the Escort D+ data acquisition system for the IRT facility, including the pressure transducer and amplifier.

### A.2 Hardware RTD Temperature Uncertainty

The individual component uncertainties were reviewed for the RTD total temperature probe system. Uncertainty values are given in Table A.1. The component uncertainties were calculated using a root-sum-squared (RSS) technique which is a method of determining errors.

$$RSS = \sqrt{a^2 + b^2 + c^2} \quad (\text{A4})$$

The component uncertainties calculated using the RSS technique yielded a system uncertainty of  $\pm 0.10$  °C for a probe that had been individually calibrated for flow recovery and  $\pm 0.16$  °C for a probe that had not been individually calibrated for flow recovery. The uncertainties associated with the RTD probes are more than an order of magnitude improvement over the uncertainty estimate for the thermocouples on the 9-ft survey rake. The system uncertainty associated with the 9-ft survey rake is  $\pm 1.1$  °C.<sup>4,5</sup> The RSS computations for the RTD probes are show below:

For probes that were tested for total temperature flow recovery:

$$RSS = \sqrt{(0.030^2 + 0.080^2 + 0.006^2 + 0.026^2 + 0.040^2 + 0.030^2)} = \pm 0.10 \text{ °C}$$

For probes using average flow recovery coefficients:

$$RSS = \sqrt{(0.030^2 + 0.080^2 + 0.006^2 + 0.026^2 + 0.040^2 + 0.123^2)} = \pm 0.16 \text{ } ^\circ\text{C}$$

TABLE A.1.—RTD TOTAL TEMPERATURE PROBE SYSTEM COMPONENT UNCERTAINTIES.

Component uncertainty, $^\circ\text{C}$	Component description
$\pm 0.030$	RTD capsule, 0.01% DIN curve
$\pm 0.080$	RTD temperature transmitter
$\pm 0.006$	Resistor to convert transmitter 4 to 20 mA output to DC V (USF 240 250 $\Omega$ 0.01% 2 ppm/ $^\circ\text{C}$ )
$\pm 0.026$	Escort data system analog to digital conversion error
$\pm 0.040$	Flow recovery reference temperature measurement error (jet plenum reference)
$\pm 0.030$	Flow recovery curve uncertainty (individual probe cal)
$\pm 0.123$	Flow recovery curve uncertainty (probe not calibrated for flow recovery, average coefficients)

### A.3 Hardware Pressure Uncertainty

#### A.3.1 Total Pressure

Two pitot-static probes, one mounted on the IRT test section vertical north wall and the other on the vertical south wall, are used to measure total and differential pressure. The total pressure is measured using a 0- to 20-psia Setra Model 270 transducer (Setra Systems, Inc., Boxborough, MA), and the differential pressure is measured using a 0- to 3-psid Setra Model 239 transducer.

The IRT facility data acquisition system utilized the ESCORT D+ with 470 Neff amplifier system and the Setra Model 270 pressure transducer for the total pressure measurement.

The calculations shown below detail the bias error of the system.

$$B = \pm \sqrt{B1^2 + B2^2 + B3^2 + B4^2 + B5^2 + B6^2 + B7^2 + B8^2 + B9^2}$$

$$B = \pm \sqrt{(0.002)^2 + (0.010)^2 + (0.001)^2 + (0.001)^2 + (0.010)^2 + (0.004)^2 + (0.001)^2}$$

$$B = \pm 0.0149 \text{ psia}$$

TABLE A.2.—TOTAL PRESSURE COMPONENT BIAS UNCERTAINTIES

Component uncertainty, psia	Component description
$\pm 0.002$	Cal Lab calibration error
$\pm 0.010$	Non-linearity
$\pm 0.001$	Thermal Zero shift
$\pm 0.001$	Thermal span shift
$\pm 0.010$	Neff gain accuracy
$\pm 0.004$	Neff non-linearity
$\pm 0.000$	Channel-to-channel offset
$\pm 0.000$	Common mode voltage
$\pm 0.001$	Digitizing Error

Precision error

$$S = \pm \sqrt{S1^2 + S2^2 + S3^2 + S4^2 + S5^2 + S6^2}$$

$$S = \pm \sqrt{(0.002)^2 + (0.002)^2 + (0.001)^2 + (0.004)^2 + (0.003)^2 + (0.002)^2}$$

$$S = \pm 0.0117 \text{ psia}$$

TABLE A.3.—TOTAL PRESSURE COMPONENT PRECISION UNCERTAINTIES

Component uncertainty, psia	Component description
±0.002	Repeatability
±0.002	Hysteresis
±0.001	Excitation voltage effect
±0.004	Neff Gain Stability
±0.003	Zero Stability
±0.002	Noise

Total pressure measurement uncertainty

$$U_{RSS} = \pm \sqrt{(B)^2 + \left(\frac{2S}{\sqrt{N}}\right)^2} \quad (A5)$$

$$U_{RSS} = U_{P_T} = \pm 0.027741 \text{ psia}$$

$$U\% = (U_{RSS}/P_T) = (U_{P_T}/P_T) = 0.001387 = 0.13\%$$

### A.3.2 Dynamic Pressure

Equation (A6) was found using the Ames Tables (4) and assuming an isentropically perfect gas.

$$q = P_T \frac{\gamma}{2} M^2 \left(1 + \frac{\gamma-1}{2} M^2\right)^{-\frac{\gamma}{\gamma-1}} \quad (A6)$$

$$\frac{\partial q}{\partial P_T} = \frac{\gamma M^2}{2 \left(\left(\frac{\gamma-1}{2}\right) M^2 + 1\right)^{\frac{\gamma}{\gamma-1}}} \quad (A7)$$

$$\frac{\partial q}{\partial M} = \frac{\gamma M P_T}{\left(\left(\frac{\gamma-1}{2}\right) M^2 + 1\right)^{\frac{\gamma}{\gamma-1}}} - \frac{\gamma^2 M^3 P_T \left(\frac{\gamma-1}{2}\right)}{(\gamma-1) \left(\left(\frac{\gamma-1}{2}\right) M^2 + 1\right)^{\frac{\gamma}{\gamma-1}+1}} \quad (A8)$$

$$U_q = \left[ \left(\frac{\partial q}{\partial P_T} U_{P_T}\right)^2 + \left(\frac{\partial q}{\partial M} U_M\right)^2 \right]^{\frac{1}{2}} \quad (A9)$$

$$U_q = \left[ \frac{\gamma^2 M^4 U_{P_T}^2}{4 \left(\left(\frac{\gamma-1}{2}\right) M^2 + 1\right)^{\frac{2\gamma}{\gamma-1}}} + \left( \frac{\gamma M P_T}{\left(\left(\frac{\gamma-1}{2}\right) M^2 + 1\right)^{\frac{\gamma}{\gamma-1}}} - \frac{\gamma^2 M^3 P_T \left(\frac{\gamma-1}{2}\right)}{(\gamma-1) \left(\left(\frac{\gamma-1}{2}\right) M^2 + 1\right)^{\frac{\gamma}{\gamma-1}+1}} \right) U_M^2 \right]^{\frac{1}{2}} \quad (A10)$$

### A.3.3 Static Pressure

Using the Ames Tables (4) and assuming an isentropically perfect gas.

$$P_S = P_T \left( 1 + \frac{\gamma-1}{2} M^2 \right)^{\frac{-\gamma}{\gamma-1}} \quad (\text{A11})$$

$$\frac{\partial P_S}{\partial P_T} = \frac{1}{\left( \left( \frac{\gamma-1}{2} \right) M^2 - 1 \right)^{\frac{\gamma}{\gamma-1}}} \quad (\text{A12})$$

$$\frac{\partial P_S}{\partial M} = \frac{2\gamma M P_T \left( \frac{\gamma-1}{2} \right)}{(\gamma-1) \left( \left( \frac{\gamma-1}{2} \right) M^2 - 1 \right)^{\frac{\gamma}{\gamma-1}+1}} \quad (\text{A13})$$

$$U_{P_S} = \left[ \left( \frac{\partial P_S}{\partial P_T} U_{P_T} \right)^2 + \left( \frac{\partial P_S}{\partial M} U_M \right)^2 \right]^{\frac{1}{2}} \quad (\text{A14})$$

$$U_{P_S} = \left[ \frac{U_{P_T}^2}{\left( \left( \frac{\gamma-1}{2} \right) M^2 + 1 \right)^{\frac{2\gamma}{\gamma-1}}} + \frac{4\gamma^2 M^2 P_T^2 U_M^2 \left( \frac{\gamma-1}{2} \right)^2}{\left( \left( \frac{\gamma-1}{2} \right) M^2 + 1 \right)^{\frac{2\gamma}{\gamma-1}+2} (\gamma-1)^2} \right]^{\frac{1}{2}} \quad (\text{A15})$$

### A.4 Airspeed Calculations

Using the velocity equation, Equation (A16), the speed of sound equation, Equation (A18), and the isentropic identity shown, Equation (A19), the velocity was solved for

$$V = M \cdot a \quad (\text{A16})$$

$$M = \left[ \left( \frac{2}{\gamma-1} \right) \left[ \left( \frac{P_T}{P_S} \right)^{\left( \frac{\gamma-1}{\gamma} \right)} - 1 \right] \right]^{\frac{1}{2}} \quad (\text{A17})$$

$$a = \sqrt{\gamma RT} \quad (\text{A18})$$

$$\frac{T}{T} = \left( \frac{P_S}{P_T} \right)^{\left( \frac{\gamma-1}{\gamma} \right)} \quad (\text{A19})$$

$$V = \left[ \left( \frac{2}{\gamma - 1} \right) \gamma R T_T \left[ \left( \frac{P_T}{P_S} \right)^{\frac{\gamma - 1}{\gamma}} - 1 \right] \right]^{\frac{1}{2}} \quad (\text{A20})$$

The general expression for uncertainty is given by Equation (A21).  $U_{T_T}$ , is the uncertainty in total temperature,  $U_{P_S}$ , is the uncertainty in static pressure, and  $U_{P_T}$ , is the uncertainty in total pressure.

$$U_V = \left[ \left( \frac{\partial V}{\partial T_T} U_{T_T} \right)^2 + \left( \frac{\partial V}{\partial P_S} U_{P_S} \right)^2 + \left( \frac{\partial V}{\partial P_T} U_{P_T} \right)^2 \right]^{\frac{1}{2}} \quad (\text{A21})$$

To produce algebraic simplification, the uncertainty expression is divided by  $V^2$  and shown below.

$$\left[ \frac{U_V}{V} \right]^2 = \left[ \frac{1}{V} \frac{\partial V}{\partial T_T} U_{T_T} \right]^2 + \left[ \frac{1}{V} \frac{\partial V}{\partial P_S} U_{P_S} \right]^2 + \left[ \frac{1}{V} \frac{\partial V}{\partial P_T} U_{P_T} \right]^2 \quad (\text{A22})$$

Taking the partial derivative of the velocity equation with respect to total temperature,  $T_T$ , static pressure,  $P_S$ , and total pressure,  $P_T$ , the uncertainty of velocity is seen in Equation (A26).

$$\frac{\partial V}{\partial T_T} = \frac{\frac{1}{2} \gamma R \left( \frac{2}{\gamma - 1} \right)^{\frac{1}{2}} \left[ \left( \frac{P_T}{P_S} \right)^{\frac{\gamma - 1}{\gamma}} - 1 \right]^{\frac{1}{2}}}{(\gamma R T_T)^{\frac{1}{2}}} \quad (\text{A23})$$

$$\frac{\partial V}{\partial P_S} = - \frac{0.5 P_T \left( \frac{2}{\gamma - 1} \right)^{\frac{1}{2}} \left( \frac{P_T}{P_S} \right)^{\frac{\gamma - 1}{\gamma} - 1} (\gamma - 1)}{\gamma P_S^2 \left[ \left( \frac{P_T}{P_S} \right)^{\frac{\gamma - 1}{\gamma}} - 1 \right]^{\frac{1}{2}}} \quad (\text{A24})$$

$$\frac{\partial V}{\partial P_T} = \frac{0.5 \left( \frac{2}{\gamma - 1} \right)^{\frac{1}{2}} \left( \frac{P_T}{P_S} \right)^{\frac{\gamma - 1}{\gamma} - 1} (\gamma - 1) (\gamma R T_T)^{\frac{1}{2}}}{\gamma P_S \left[ \left( \frac{P_T}{P_S} \right)^{\frac{\gamma - 1}{\gamma}} - 1 \right]^{\frac{1}{2}}} \quad (\text{A25})$$

$$U_V = \left[ \frac{0.25\gamma^2 R^2 U_T^2 \left( \frac{2}{\gamma-1} \right) \left( \left( \frac{P_T}{P_S} \right)^{\frac{\gamma-1}{\gamma}} - 1 \right)}{(\gamma R T_T)} + \frac{0.25 U_{P_T}^2 \left( \frac{2}{\gamma-1} \right) \left( \frac{P_T}{P_S} \right)^{\frac{2(\gamma-1)-2}{\gamma}} (\gamma-1)^2 (\gamma R T_T)}{\gamma^2 P_S^2 \left( \left( \frac{P_T}{P_S} \right)^{\frac{\gamma-1}{\gamma}} - 1 \right)} + \frac{0.25 P_T^2 U_{P_S}^2 \left( \frac{2}{\gamma-1} \right) \left( \frac{P_T}{P_S} \right)^{\frac{2(\gamma-1)-2}{\gamma}} (\gamma-1)^2 (\gamma R T_T)}{\gamma^2 P_S^4 \left( \left( \frac{P_T}{P_S} \right)^{\frac{\gamma-1}{\gamma}} - 1 \right)} \right]^{\frac{1}{2}} \quad (\text{A26})$$

## A.5 Mach Number Calculations

Using the MuPAD feature in the symbolic toolbox in Matlab the partial derivatives for Mach number were solved for and are shown in Equation (A27) and (A28).

$$\frac{\partial M}{\partial P_T} = \frac{\left( \frac{P_T}{P_S} \right)^{\frac{\gamma-1}{\gamma} - 1}}{\gamma P_S \left( \left( \frac{P_T}{P_S} \right)^{\frac{\gamma-1}{\gamma}} - 1 \right)^{\frac{1}{2}}} \quad (\text{A27})$$

$$\frac{\partial M}{\partial P_S} = - \frac{P_T \left( \frac{P_T}{P_S} \right)^{\frac{\gamma-1}{\gamma} - 1}}{\gamma P_S^2 \left( \left( \frac{P_T}{P_S} \right)^{\frac{\gamma-1}{\gamma}} - 1 \right)^{\frac{1}{2}}} \quad (\text{A28})$$

The partial derivatives were then plugged back into Equation (A3) yielding the following for the uncertainty for Mach.

$$U_M = \left[ \frac{U_{P_T}^2 \left( \frac{P_T}{P_S} \right)^{\frac{2(\gamma-1)-2}{\gamma}}}{\gamma P_S^2 \left( \left( \frac{P_T}{P_S} \right)^{\frac{\gamma-1}{\gamma}} - 1 \right)} + \frac{P_T^2 U_{P_S}^2 \left( \frac{P_T}{P_S} \right)^{\frac{2(\gamma-1)-2}{\gamma}}}{\gamma P_S^4 \left( \left( \frac{P_T}{P_S} \right)^{\frac{\gamma-1}{\gamma}} - 1 \right)} \right]^{\frac{1}{2}} \quad (\text{A29})$$

## A.6 Flow Angle Calculations

The flow angle calculations are completed utilizing the 9-ft rake flow angularity probes. Figure 6 in the main body of the document illustrates the locations and descriptions of each of the pressure orifices. Equations (A31) and (A32) are the equations used to calculate pitch and yaw utilizing the flow angularity probes.

$$P_{1-4,avg} = \frac{P_1 + P_2 + P_3 + P_4}{4} \quad (\text{A30})$$

$$\alpha = K0A + K1A \frac{(P_3 - P_1)}{(P_5 - P_{1-4,avg})} + POFF + DPOFF \quad (A31)$$

$$\beta = K0B + K2B \frac{(P_4 - P_2)}{(P_5 - P_{1-4,avg})} + YOFF + DYOFF \quad (A32)$$

The partials of the pitch and yaw equations were taken with respect to P1 through P5 and plugged into the uncertainty equations. Equation (A33) is the uncertainty equation for pitch, and Equation (A34) is the uncertainty equation for yaw.

$$U_{Pitch} = \left( U_{P1}^2 \left( \frac{K1A}{\frac{P_1}{4} + \frac{P_2}{4} + \frac{P_3}{4} + \frac{P_4}{4} - P_5} - \frac{K1A(P_1 - P_3)}{4 \left( \frac{P_1}{4} + \frac{P_2}{4} + \frac{P_3}{4} + \frac{P_4}{4} - P_5 \right)^2} \right)^2 + U_{P3}^2 \left( \frac{K1A}{\frac{P_1}{4} + \frac{P_2}{4} + \frac{P_3}{4} + \frac{P_4}{4} - P_5} - \frac{K1A(P_1 - P_3)}{4 \left( \frac{P_1}{4} + \frac{P_2}{4} + \frac{P_3}{4} + \frac{P_4}{4} - P_5 \right)^2} \right)^2 + \frac{K1A^2 U_{P2}^2 (P_1 - P_3)^2}{16 \left( \frac{P_1}{4} + \frac{P_2}{4} + \frac{P_3}{4} + \frac{P_4}{4} - P_5 \right)^4} + \frac{K1A^2 U_{P4}^2 (P_1 - P_3)^2}{16 \left( \frac{P_1}{4} + \frac{P_2}{4} + \frac{P_3}{4} + \frac{P_4}{4} - P_5 \right)^4} + \frac{K1A U_{P5}^2 (P_1 - P_3)^2}{16 \left( \frac{P_1}{4} + \frac{P_2}{4} + \frac{P_3}{4} + \frac{P_4}{4} - P_5 \right)^4} \right)^{0.5} \quad (A33)$$

$$U_{Yaw} = \left( U_{P2}^2 \left( \frac{K2B}{\frac{P_1}{4} + \frac{P_2}{4} + \frac{P_3}{4} + \frac{P_4}{4} - P_5} - \frac{K1A(P_2 - P_4)}{4 \left( \frac{P_1}{4} + \frac{P_2}{4} + \frac{P_3}{4} + \frac{P_4}{4} - P_5 \right)^2} \right)^2 + U_{P4}^2 \left( \frac{K2B}{\frac{P_1}{4} + \frac{P_2}{4} + \frac{P_3}{4} + \frac{P_4}{4} - P_5} - \frac{K2B(P_2 - P_4)}{4 \left( \frac{P_1}{4} + \frac{P_2}{4} + \frac{P_3}{4} + \frac{P_4}{4} - P_5 \right)^2} \right)^2 + \frac{K2B^2 U_{P1}^2 (P_2 - P_4)^2}{16 \left( \frac{P_1}{4} + \frac{P_2}{4} + \frac{P_3}{4} + \frac{P_4}{4} - P_5 \right)^4} + \frac{K2B^2 U_{P3}^2 (P_2 - P_4)^2}{16 \left( \frac{P_1}{4} + \frac{P_2}{4} + \frac{P_3}{4} + \frac{P_4}{4} - P_5 \right)^4} + \frac{K2B U_{P5}^2 (P_2 - P_4)^2}{16 \left( \frac{P_1}{4} + \frac{P_2}{4} + \frac{P_3}{4} + \frac{P_4}{4} - P_5 \right)^4} \right)^{0.5} \quad (A34)$$

Utilizing the following inputs from the 2004 data set RDG 1530, the following uncertainties were determined. The inputs and the uncertainties calculated for the single data point are shown in Table A.4.

TABLE A.4.—FACILITY UNCERTAINTIES

Input		Uncertainties	
Total Pressure (psi)	14.315	Total Pressure (psia)	0.027741
Static Pressure (psi)	12.258	Total Temperature (°C/R)	0.16/0.08889
K0A	-0.1682	Static Pressure (psia)	0.0411
K1A	12.1366	Mach Number	0.0061
K0B	0.5052	Dynamic Pressure	0.0582
K2B	11.9173	Velocity (ft/sec)	6.7359
		Pitch (degrees)	0.0435
		Yaw (degrees)	0.0427



## Appendix B.—RTD Probe Flow Recovery Coefficients

Table B.1 contains the total temperature flow recovery curve fit coefficients for each of the RTD probes used on the 2-D RTD Array. The corrected total temperature measurement for a given probe is determined from the following equation

$$T_{T,local} = (C_0 + C_1 \cdot M_{ts} + C_2 \cdot M_{ts}^2) \cdot T_{T,array}$$

where  $T_{T,array}$  is the total temperature measured by the RTD probe and  $T_{T,local}$  is the corrected local total temperature.

TABLE B.1.—FLOW RECOVERY CORRECTION COEFFICIENTS FOR THE RTD PROBES MOUNTED ON THE 2-D RTD ARRA.

Probe Serial Number	$C_2$	$C_1$	$C_0$
1	$5.681198 \times 10^{-3}$	$8.859325 \times 10^{-4}$	1.0
2	$7.608867 \times 10^{-3}$	$5.487745 \times 10^{-6}$	1.0
3	$6.518485 \times 10^{-3}$	$2.305113 \times 10^{-4}$	1.0
4	$6.562552 \times 10^{-3}$	$9.399041 \times 10^{-4}$	1.0
5	$5.788899 \times 10^{-3}$	$6.373217 \times 10^{-4}$	1.0
6	$6.482487 \times 10^{-3}$	$1.749681 \times 10^{-4}$	1.0
7	$1.011491 \times 10^{-2}$	$-1.646186 \times 10^{-3}$	1.0
8	$5.661808 \times 10^{-3}$	$5.089893 \times 10^{-4}$	1.0
9	$6.506136 \times 10^{-3}$	$4.493981 \times 10^{-4}$	1.0
10	$5.600892 \times 10^{-3}$	$5.937824 \times 10^{-4}$	1.0
11	$6.159188 \times 10^{-3}$	$7.799326 \times 10^{-4}$	1.0
12	$4.848719 \times 10^{-3}$	$1.197796 \times 10^{-3}$	1.0
13	$5.634439 \times 10^{-3}$	$1.523486 \times 10^{-4}$	1.0
14	$5.412994 \times 10^{-3}$	$1.068442 \times 10^{-3}$	1.0
15	$6.099340 \times 10^{-3}$	$6.670401 \times 10^{-4}$	1.0
16	$5.399611 \times 10^{-3}$	$6.660572 \times 10^{-4}$	1.0
17	$6.631578 \times 10^{-3}$	$6.137670 \times 10^{-4}$	1.0
18	$6.718590 \times 10^{-3}$	$6.487126 \times 10^{-4}$	1.0
19	$4.910175 \times 10^{-3}$	$8.683076 \times 10^{-4}$	1.0
20	$6.384046 \times 10^{-3}$	$6.479808 \times 10^{-4}$	1.0
21	$6.823889 \times 10^{-3}$	$3.565925 \times 10^{-4}$	1.0
22	$5.007236 \times 10^{-3}$	$1.218866 \times 10^{-3}$	1.0
23	$6.436245 \times 10^{-3}$	$5.701839 \times 10^{-4}$	1.0
Average	$6.881316 \times 10^{-3}$	$1.490507 \times 10^{-4}$	1.0



## Appendix C.—Calculated Test Section Conditions

The following set of equations is used to compute the test section flow conditions based on the calibrated test section conditions. The calibrated test section conditions are static pressure,  $P_{S,ts}$ , Mach number,  $M_{ts}$  and total temperature,  $T_{T,ts}$ . For all calculations,  $\gamma=1.4$  and  $R=1716$  ft-lb/(slug·°R). English units are used for all calculations; however some units conversions are required to provide operating conditions in the units desired by the aircraft icing community.

The first parameter calculated is the test section total pressure,  $P_{T,ts}$ . The ratio of static to total pressure is determined from calibrated Mach number found in Reference 9 as Equation 44.

$$P_{rat,ts} = \frac{P_{S,ts}}{P_{T,ts}} = \left(1 + \frac{M_{ts}^2}{5}\right)^{-7/2}$$

The total pressure is then calculated using the pressure ratio and the calibrated static pressure. Note that the units used in the calculation are psf.

$$P_{T,ts} = \left(\frac{P_{T,ts}}{P_{S,ts}}\right) \cdot P_{S,ts} = \frac{P_{S,ts}}{P_{rat,ts}}$$

The test section static temperature,  $T_{S,ts}$ , is calculated, in °R, as shown below using Reference 9, Equation 43

$$T_{S,ts} = \frac{T_{T,ts}}{1 + 0.2 \cdot M_{ts}^2}$$

Test section airspeed  $U_{ts}$  in ft/sec, is determined from the definition of Mach number,  $M=V/a$ . Solving for  $V$  and substituting the definition for the speed of sound produces the following equation

$$U_{ts} = M_{ts} \cdot a_{ts} = M_{ts} \sqrt{\gamma \cdot R \cdot T_{S,ts}}$$

Many of the IRT test customers are used to working with airspeed in knots, so the following unit conversion is needed

$$U_{ts}(\text{knots}) = 0.592484 \cdot U_{ts}(\text{ft/sec})$$

The test section Reynolds number is calculated beginning with determining the air density

$$\rho_{ts} = \frac{P_{S,ts}}{R \cdot T_{S,ts}}$$

The test section air viscosity,  $\mu_{ts}$  in units of slugs/(ft·sec), is determined from the following equation

$$\mu_{ts} = 2.270 \frac{T_{S,ts}^{1.5}}{T_{S,ts} + 198.6} \cdot 10^{-8}$$

These parameters are used in the Reynolds number, ( $10^6/\text{ft}$ ),  $Re_{ts}$ , equation seen below

$$\text{Re}_{ts} = \frac{\rho_{ts} U_{ts} l}{\mu_{ts}}$$

In this equation, the characteristic length,  $l$ , is equal to 1 ft. The test section Reynolds number can also be calculated based on test article dimension (i.e., chord length)

$$\text{Re}_c = \text{Re}_{ts} \cdot c_x$$

Table C.1 summarizes the inputs, calibrated test section conditions and calculated test section conditions as in this report. The program name column lists the variable names for each parameter as they appear in the computer subroutine IRTAT. At present, the parameter name and program names do not exactly match because the parameter naming nomenclature has been updated to be consistent with naming recommendations, detailed in Reference 2. The program names will eventually be updated to be consistent with the naming recommendations. Also, note that  $P_{air}$  was added as an input to IRTAT as part of revision 6.

TABLE C.1.—SUMMARY OF THE PARAMETERS USED TO DETERMINE THE TEST SECTION AERO-THERMAL CONDITIONS IN THE IRT

Parameter	Program Name	Description	Units	Source
Average Bellmouth and D-Corner Conditions				
$P_{T,bm}$	POBM	Bellmouth total pressure	psia	Input
$\Delta P_{bm}$	DPBM	Bellmouth delta-pressure	psia	Input
$P_{S,bm}$	PSBM	Bellmouth static pressure	psia	Input
$T_{T,davg}$	TODC	D-Corner total temperature	°C	Input
$P_{rat,bm}$	PRATBM	Ratio of bellmouth static to total pressure	none	Calculated
$M_{bm}$	MBM	Bellmouth Mach number	None	Calculated
$P_{air}$	SBAIRP	Spraybar air pressure	psig	Input
Test Section Conditions—Calibrated Parameters				
$P_{S,ts}$	PSTS	Test section static pressure	psia	Calibration
$M_{ts}$	MTS	Test section Mach number	none	Calibration
$T_{T,ts}$	TOTSC TOTSF TOTS	Total temperature	°C °F R	Calibration (Units) (Units)
Test Section Conditions—Calculated Parameters				
$P_{rat}$	PRAT	Ratio of static to total pressure	none	Calculated
$P_{T,ts}$	POTS	Test section total pressure	psia	Calculated
$T_{S,ts}$	TSTS	Static temperature	°R	Calculated
$U_{ts}$	VTS VTSK	Airspeed	ft/sec knots	Calculated (units)
$\rho_{ts}$	RHOTS	Air density	slugs/ft <sup>3</sup>	Calculated
$\mu_{ts}$	MUTS	Air viscosity	slugs/(ft sec)	Calculated
$\text{Re}_{ts}$	REFT	Reynolds number	10 <sup>6</sup> /ft	Calculated
$\text{Re}_{cx}$	RECX	Reynolds number based on model length	10 <sup>6</sup> /ft	Calculated
$\gamma$	GAMMA	Ratio of specific heats = 1.4	none	constant
$R$	R	Gas constant = 1716	lbf-ft/(slug°R)	Constant
$c_x$	CX	Model chord or other critical dimension	feet	PARAM File input

## Appendix D.—2005 Interim Aero-Thermal Calibration of the IRT

As mentioned in the Introduction section, there are three basic levels of calibration used in the IRT, full, interim and check calibrations. Full and interim calibrations occur in pairs and are designed to provide a level of redundancy to ensure consistent operation of the facility. The full and interim calibrations occur either following a facility modification or every 5 years if there are no facility modifications. The information in this appendix will provide the final test documentation of the 2005 interim calibration of the IRT including the test matrix, test conditions, data and results.

An interim calibration uses the same hardware as a full calibration, namely the 9-ft survey rake and the 2-D RTD array. For the 2005 interim calibration, testing using the 9-ft survey rake was completed in January (January 18, 2005), however, the total temperature calibration measurements using the RTD array was not conducted and completed until April (April 1 and April 4, 2005). The time between the 9-ft rake and RTD array testing was used for icing cloud calibration and diagnostics.

The test matrices for the 2005 interim calibration are given in Table D.1 and Table D.2. These test matrices were designed to:

- Complete data collection to check the total and static pressure calibration relationships and the centerline flow quality using the 9-ft survey rake at the test section centerline at the turntable station.
- Complete data collection to check the total temperature calibration relationship and flow field surveys using a two-dimensional array of RTDs. The 2005 test matrix differs from the 2004 full calibration by the addition of a spraybar air pressure setting of  $P_{air} = 40$  psig. The addition was made to begin a sensitivity study of the spraybar air pressure on the aero-thermal characteristics of the test section calibration and flow quality.

In addition to the fundamental aero-thermal calibration goals, the 2005 interim calibration was used to conduct temperature stability studies between the D-corner and test section. The primary concern was the overall stability and settling time required to achieve uniform total temperature distribution in D-Corner and the test section. The 2-D RTD array was used to monitor the test section temperature distribution in conjunction with the D-Corner RTDs. The D-Corner RTDs are facility instrumentation mounted on the leading edge of the D-Corner turning vanes. The objective of the surveys was to document the settling/stability characteristics to the total temperature profiles in D-Corner and the test section and to determine guidelines for IRT operation to insure a uniform and stable total temperature in both D-Corner and the test section. The Escort system, the facility data acquisition and display system, was used to monitor the standard deviation of the D-Corner total temperature,  $\sigma_{TT,DC}$ , and the time variation in the D-Corner average temperature,  $\Delta \overline{T}_{DC}$ . Details and results of the temperature stability study are given in (Ref. 3).

TABLE D.1.—TEST MATRIX FOR THE IRT AERO-THERMAL CALIBRATION USING THE 9-ft SURVEY RAKE (2005 INTERIM CALIBRATION).

Rake height, $Y$ , in.	Total Temperature, $T_{Tavg}$ , °C	Test Section Airspeed, $U_{ts}$ , knots	Spraybar air pressure, $P_{air}$ , psig
36	5	0, 43, 65, 87, 100, 130, 152, 173, 200, 217, 240, 260, 282, 304, 339	0
36	5	0, 43, 65, 87, 100, 130, 152, 173, 200, 217, 240, 260, 282, 304, 339	40
36	5	0, 43, 65, 87, 100, 130, 152, 173, 200, 217, 240, 260, 282, 304, 339	70

TABLE D.2.—TEMPERATURE CALIBRATION TEST MATRIX  
USING THE 2-D RTD ARRAY (2005 INTERIM CALIBRATION).

Test section static temperature, $T_{S,ts}$ , °C	Test section airspeed, $U_{ts}$ , knots	D-corner total temperature, $T_{T,davg}$ , °C	Spraybar air pressure, $P_{air}$ , psig	Test section static temperature, $T_{S,ts}$ , °C	Test section airspeed, $U_{ts}$ , knots	D-corner total temperature, $T_{T,davg}$ , °C	Spraybar air pressure, $P_{air}$ , psig
-30	43	-29.8	0, 40, 70	-5.6	43	-5.3	0, 40, 70
-30	100	-28.7	0, 40, 70	-5.6	100	-4.2	0, 40, 70
-30	130	-27.8	0, 40, 70	-5.6	130	-3.3	0, 40, 70
-30	200	-24.5	0, 40, 70	-5.6	200	-0.3	0, 40, 70
-30	217	-23.8	0, 40, 70	-5.6	217	0.7	0, 40, 70
-30	304	-17.8	0, 40, 70	0	43	0.2	0, 40, 70
-17.8	43	-17.6	0, 40, 70	0	100	1.3	0, 40, 70
-17.8	100	-16.4	0, 40, 70	0	130	2.2	0, 40, 70
-17.8	130	-15.6	0, 40, 70	-0.6	200	4.7	0, 40, 70
-17.8	200	-12.5	0, 40, 70	-1.7	217	4.6	0, 40, 70
-17.8	217	-11.6	0, 40, 70	-7.2	304	4.9	0, 40, 70
-17.8	304	-5.6	0, 40, 70	4.4	43	4.7	0, 40, 70
				3.3	100	4.7	0, 40, 70

## D.1 Total Temperature Calibration

The total temperature calibration relationship is one of a set of three calibrations used to fully define the aero-thermal operating conditions in the IRT test section (the other two calibration relationships are static pressure and Mach number). The total temperature calibration simply relates the test section total temperature measured by the 2-D RTD (average of 49 measurements) array to the total temperature measured in D corner (average of 24 measurements). Prior to 2005, a single curve-fit was used to represent the total temperature calibration across the operating range of the IRT. This single curve-fit did not include data collected at low airspeed with the spray bar air turned on due to the amount of scatter in these data relative to the data collected at higher airspeeds.

During the 2005 interim calibration, an analysis was done to determine if a family of calibration curves was needed for the total temperature to account for airspeed and spraybar air pressure effects. The final conclusion was that there is a break-point between 50 and 100 knots such that above 100 knots, spraybar air pressure no longer has a significant effect on the total temperature calibration. The result was to create a set of four calibration curves, one for airspeeds greater than 50 knots and three for airspeed less than 50 knots based on the spraybar air pressure setting (0, 40 or 70 psig). The resulting total temperature calibration curves are shown in Figure D.1. Table D.3 provides the details for the calculation of the calibrated test section total temperature from the measured D-corner total temperature. In order to provide some degree of vernier on the spraybar air pressure at the low speed conditions, the slope and intercept from each of the low speed calibration curve-fits were plotted against the spraybar air pressure so that calibration curve coefficients could be estimated for other spraybar air settings (Figure D.2). The resulting curve-fit equations for estimating  $C_{TT,0}$  and  $C_{TT,1}$  for  $U_{ts} < 50$  knots are listed below.

For all  $P_{air}$  settings not specifically listed in Table D.3:

$$C_{TT,0} = 0.06550710 + 0.01720280 \cdot P_{air} + 0.00004323 \cdot P_{air}^2$$

For  $0 < P_{air} < 40$  psig:

$$C_{TT,1} = 0.98917044 - 0.00001881 \cdot P_{air}$$

For  $40 < P_{air} < 70$  psig:

$$C_{TT,1} = 0.99428850 - 0.00014676 \cdot P_{air}$$

These calculated values for  $C_{TT,0}$  and  $C_{TT,1}$  are then used in the calibration equation (Table D.3) to determine  $T_{T,ts}$  at the low speed conditions.

Based on the 2005 interim calibration, the subroutine used to determine the aero-thermal operating conditions in the test section (IRTAT) was updated (revision 6, dated April 11, 2005). The changes were the inclusion of the spraybar air pressure,  $P_{air}$ , as an input to IRTAT (the computer code name used was SBAIRP) and to generalize the equation for calibrated test section total temperature

$$T_{T,ts} = C_{TT,0} + C_{TT,1} \cdot T_{T,davg}$$

Where  $C_{TT,0}$  and  $C_{TT,1}$  are determined as defined above and in Table D.3.

TABLE D.3.—GENERAL EQUATION AND CURVE FIT COEFFICIENTS USED IN THE CALCULATION OF THE CALIBRATED TEST SECTION TOTAL TEMPERATURE.

$T_{T,ts} = C_{TT,0} + C_{TT,1} \cdot T_{T,davg}$			
Test section airspeed, $U_{ts}$ , knots	Spraybar air pressure, $P_{air}$ , psig	Curve fit intercept term, $C_{TT,0}$ , °C	Curve fit slope term, $C_{TT,1}$ , °C/°C
> 50	≥ 0	-0.19470324	0.99014859
< 50	0	0.06550710	0.98917044
< 50	40	0.82278309	0.98841811
< 50	70	1.48151795	0.98401532

## D.2 Flow Quality Comparison

The interim calibration data are also used to check the consistency in the test section flow quality from the previous full aero-thermal calibration. For most of the flow quality parameters this becomes a comparison of centerline data since the 9-ft survey rake is only mounted on centerline for the interim calibration; however, for total temperature the entire test section cross section is compared as the RTD array provides complete coverage during both the interim and full calibrations.

Figure D.3 shows the centerline Mach number comparison data for the 2004 full aero-thermal calibration and the 2005 interim aero-thermal calibration. The Mach number data collected from the 9-ft survey rake were normalized by the bellmouth Mach number. Data were also included to show the spraybar air injection effects. The y-axis scale on the Mach number ratio plots was expanded to show very minute detail in the flow field. A  $\Delta M$  band was added to each plot to show the absolute variation in the data.

In general, there is no significant difference in the centerline Mach number ratio distributions between the 2004 and 2005 calibration tests. For most every case there is nearly an exact match core portion of the test section between the data in the sets from each year for the Mach number and spraybar air setting. There are two points of slight difference between the 2004 and 2005 data. First is near the inside test section wall where the 2004 data is consistently lower than the 2005 data. However, the difference is only 0.001 to 0.003 in Mach number. The other area is in the right-center of the test section (60 to 90 in. from the inside wall) where the 2004 data is slightly higher than the 2005 data, but again by only 0.001 to 0.003 Mach number. Overall, the 2005 data shows a flatter Mach number profile for all test conditions.

Total temperature survey data measured using the 2-D RTD Array is shown in Figure D.4. In general the trends in the total temperature data are fairly consistent between the 2004 and 2005 tests. There is some improvement seen in the temperature distributions in terms of reduced spread in the data measured during the 2005 test, particularly at lower airspeed settings. Since there were not changes to the tunnel, this improvement is attributed primarily to allowing more time for the temperature conditions to stabilize. Figure D.5 compares the standard deviation in the total temperature measurements over the survey plane. This data also indicates little difference between the 2004 and 2005 data sets, except again for the low speed settings.

Figure D.6 shows the resultant flow angle vectors collected using the 9-ft survey rake at 36-in. above the test section floor (centerline). This data provides a comparison between the 2004 and 2005 test results over the airspeed range of the IRT and at spraybar air pressure settings of 0 and 70 psig; in addition,  $P_{air}$  of 40 psig data collected in 2005 is also included.

A qualitative inspection of the flow angularity data indicates no significant differences in test section flow quality between 2004 and 2005, although the flow angle vector magnitude does appear larger in the 2005 data. In general, both the magnitude and direction of the flow angularity vectors is consistent between the 2004 and 2005 data for like test conditions, particularly for airspeed settings of 100 knots and higher. There are some noticeable differences in the flow angle vectors at the lower airspeed settings (below 100 knots), but at these low airspeeds, the flow angle probes are not as accurate.

To provide a more qualitative comparison, average values and standard deviations were computed for the pitch and yaw flow angle components (Figure D.7 and Figure D.8). The data were reviewed first by using the entire data set (11 points across the test section) then by looking only at the core data (the seven center probes along the survey line). The following points were drawn from the comparison of the average pitch and yaw flow angle data (Figure D.7):

- The average yaw angle data is repeatable across the IRT airspeed range for both the spraybar air off and 70 psig pressure settings. Even the large yaw angles recorded at the low airspeeds with the spraybar air pressure at 70 psig show a close match between the 2004 and 2005 tests.
- The core data indicates that the average yaw angle is about  $-0.02^\circ$  for airspeed settings of 100 knots and higher for both the 2004 and 2005 data.
- There is a mismatch in the average pitch flow angle magnitude between the 2004 and 2005 tests seen in both the full-span and core data sets. The core data from 2004 indicate that the average pitch flow angle is about  $0.1^\circ$  over the airspeed range; however the 2005 data shows that the average pitch angle increases from about  $0.1^\circ$  at 100 knots to about  $0.5^\circ$  at 300 knots. The cause for this change in average pitch angle was not determined.
- Spraybar air effects do not have a significant effect on the average flow angle values (pitch or yaw angles) for airspeeds of 130 knots and higher.

Evaluation of the standard deviation in the flow angle data indicates that there were no significant changes in the amount of variation in the pitch and yaw flow angle distribution between 2004 and 2005. The pitch and yaw standard deviations from 2004 and 2005 are very consistent over the airspeed range of the IRT (Figure D.8). These data also indicate for most the cases; the variation in flow angle is much lower in the core of the test section. This is particularly true for the yaw angle data with the spraybar air pressure set at 70 psig and the pitch angle data with the spraybar air off. The yaw angle deviation with spraybar air off is essentially the same for the full-span and core data.

Comparison of turbulence measurements made in 2004 and 2005 are shown in Figure D.9. Similar turbulence levels and trends over the airspeed range are noted between the two data sets. The only discrepancy is at the lowest airspeed setting with spraybar air injection, where the 2005 measurements indicated a much higher turbulence level.

### D.3 Calibration Curve Comparison

Figure D.10 shows the aero-thermal calibration curves with flow field data from the centerline of the test section from both the 2004 and 2005 tests. The calibration curves were developed based on the 2004 data. The flow field data is the average of the center seven probes on the 9-ft survey rake with the rake positioned at the test section centerline (vertical height of 36 in. above the test section floor). There is a very favorable comparison for all three calibration curves (Mach number, static pressure and total temperature). Figure D.10(c) also provides a comparison to the total temperature calibration curves based on the 2004 and 2005 calibrations. The 2004 calibration curve was based on entire data set (covered the entire airspeed range), while the 2005 calibration uses a family of curves to model the total temperature and take into account changes in the model over the airspeed range. For simplicity, only the 2005 total temperature calibration curve for airspeed greater than 50 knots is included in the comparison.

o

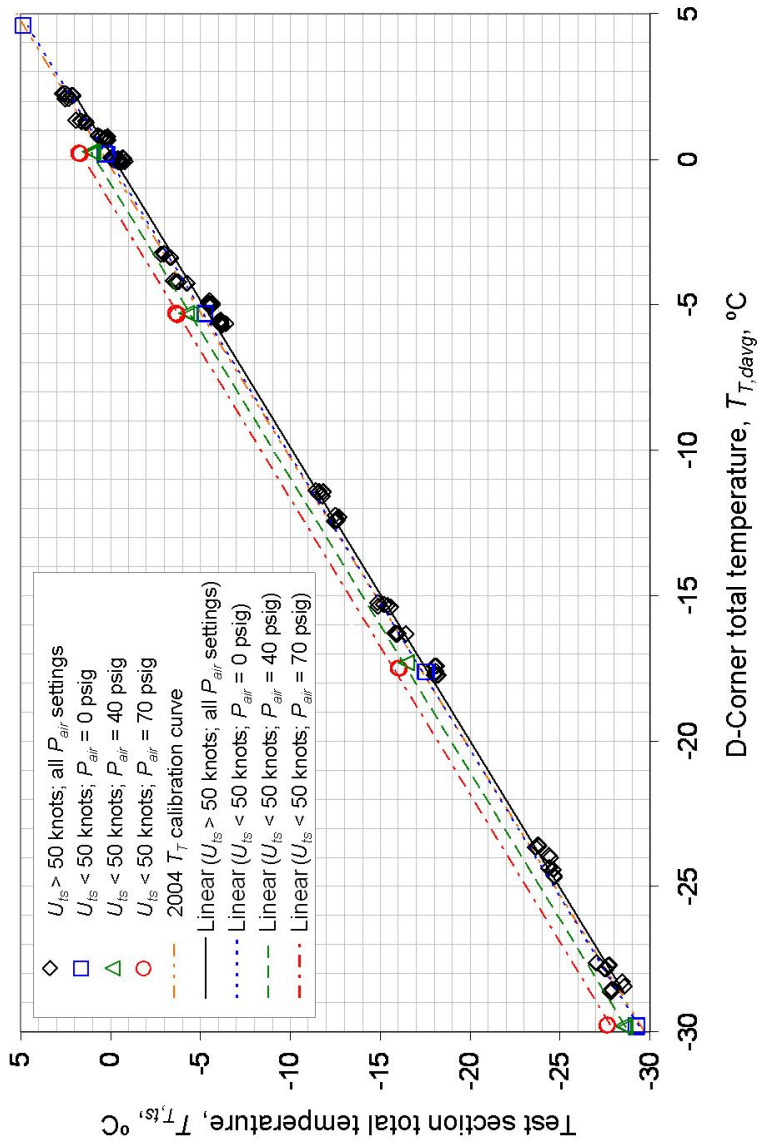


Figure D.1.—Total temperature calibration curves for the IRT based on the 2005 aero-thermal interim calibration data.

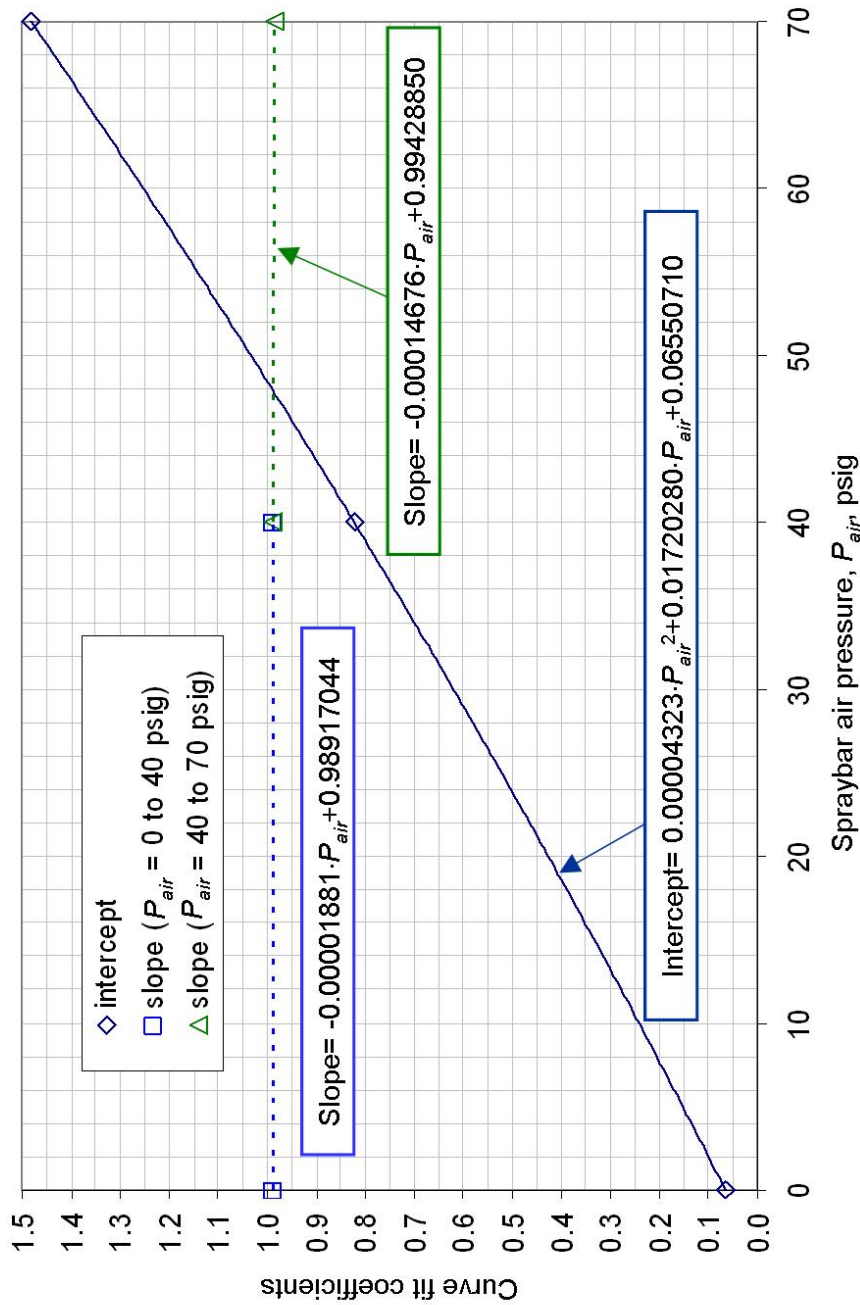


Figure D.2.—Total temperature calibration curve coefficients for  $U_{ts} < 50$  knots. This information is used to interpolate slope and intercept values for spray bar air pressure settings between 0 and 40 and between 40 and 70 psig.

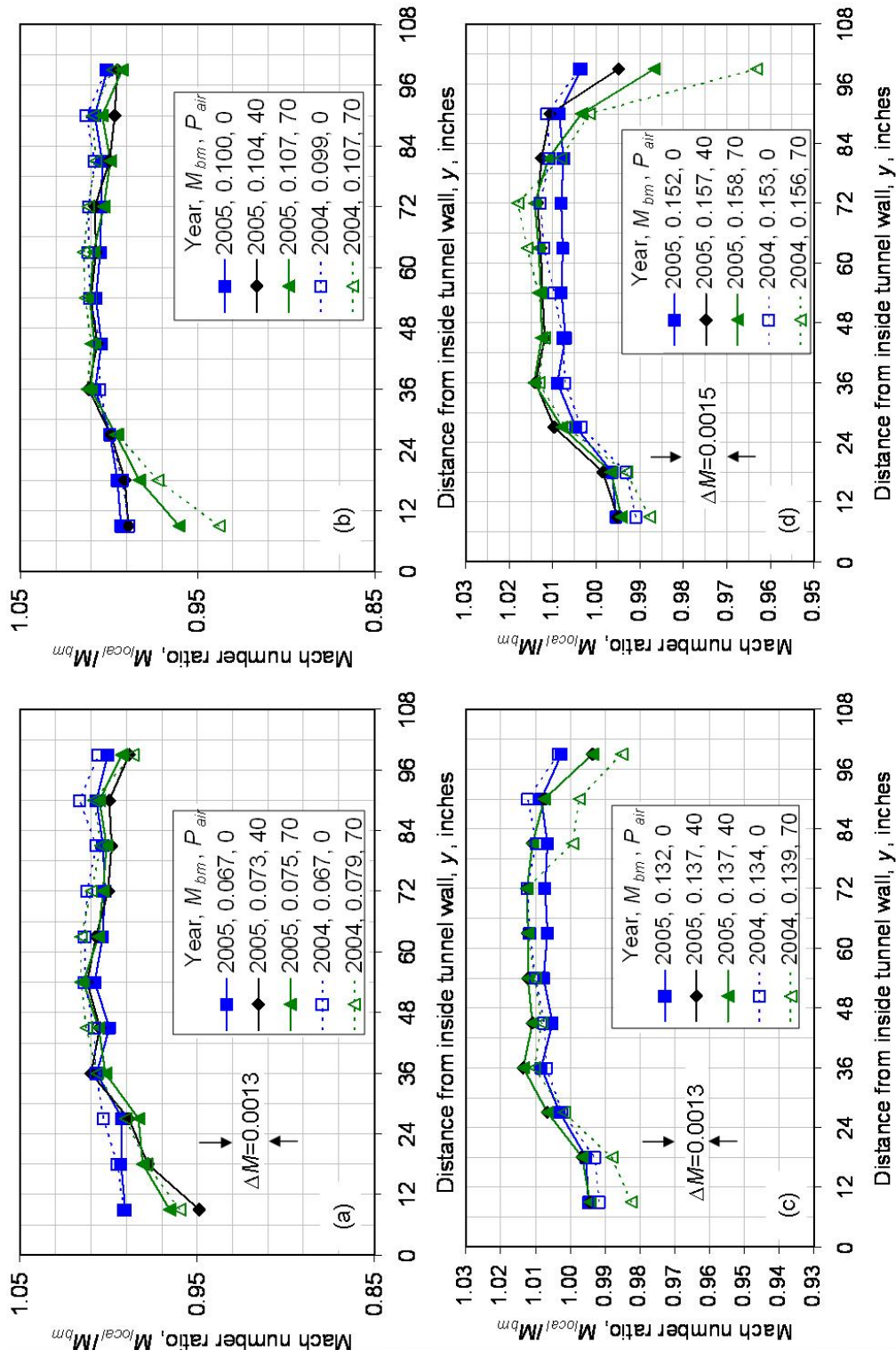
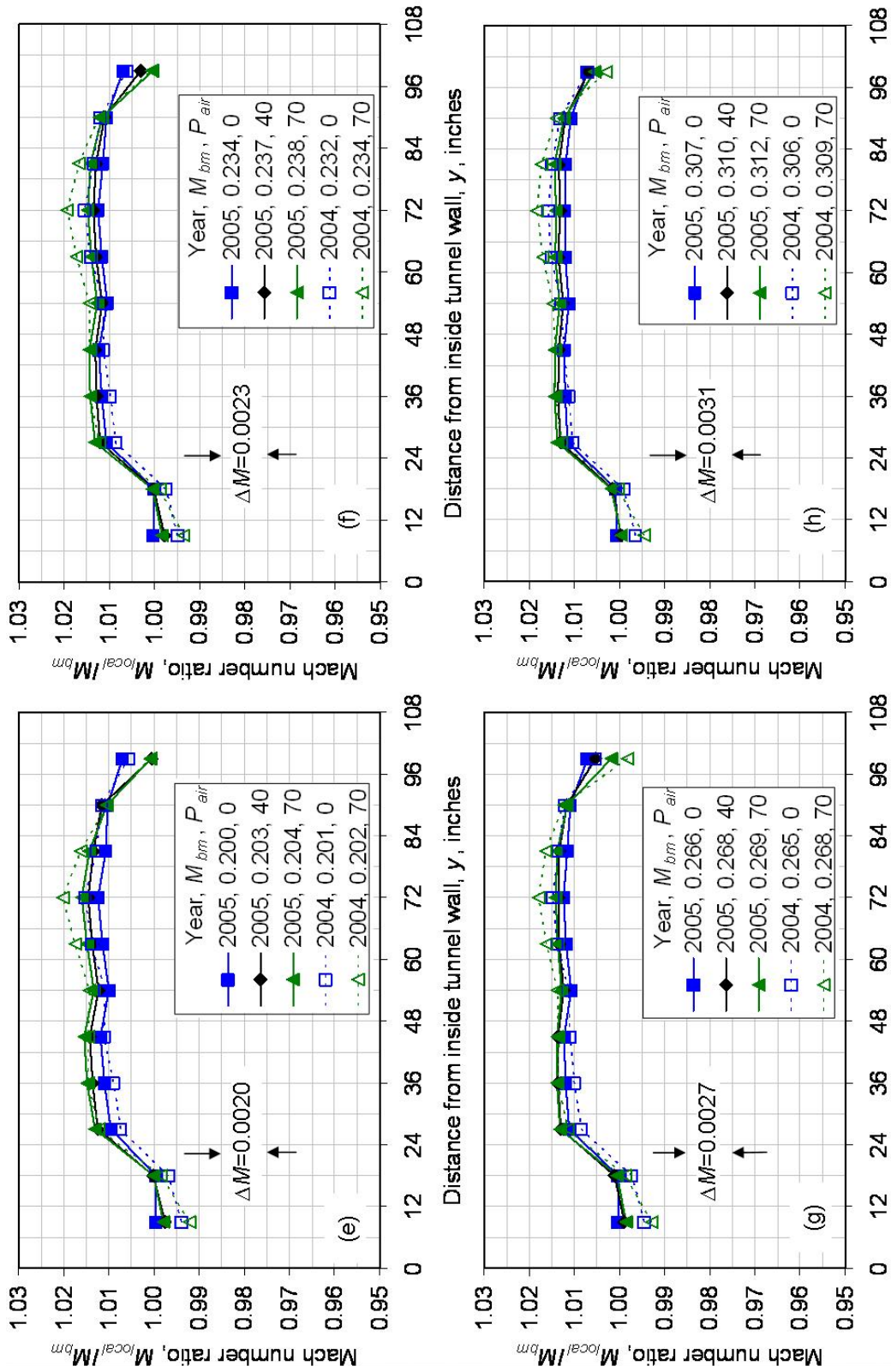


Figure D.3.—Comparison of Mach number ratio distribution data across the tunnel at test section centerline. (a)  $M_{nom} = 0.066$ ,  $U_{nom} = 43$  knots. (b)  $M_{nom} = 0.100$ ,  $U_{nom} = 65$  knots. (c)  $M_{nom} = 0.133$ ,  $U_{nom} = 87$  knots. (d)  $M_{nom} = 0.152$ ,  $U_{nom} = 100$  knots.



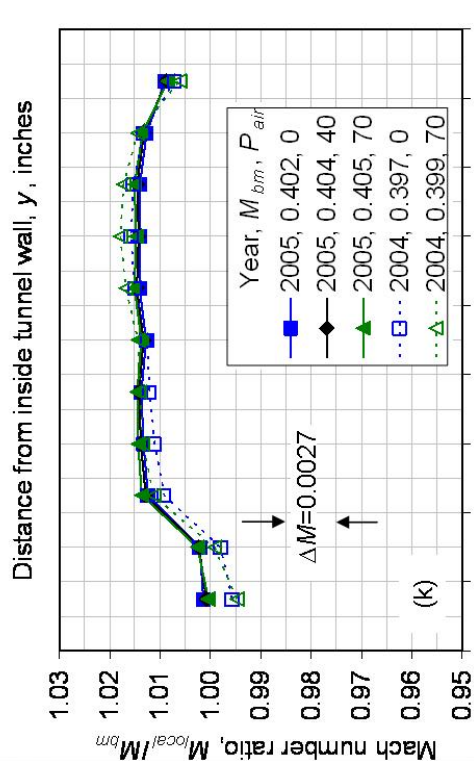
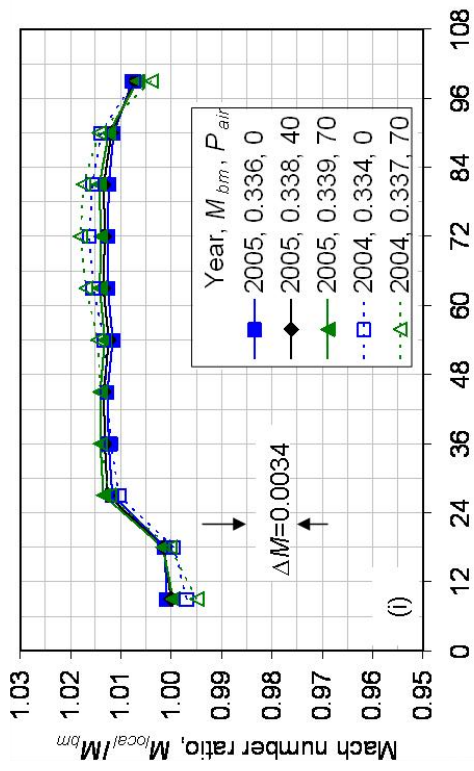
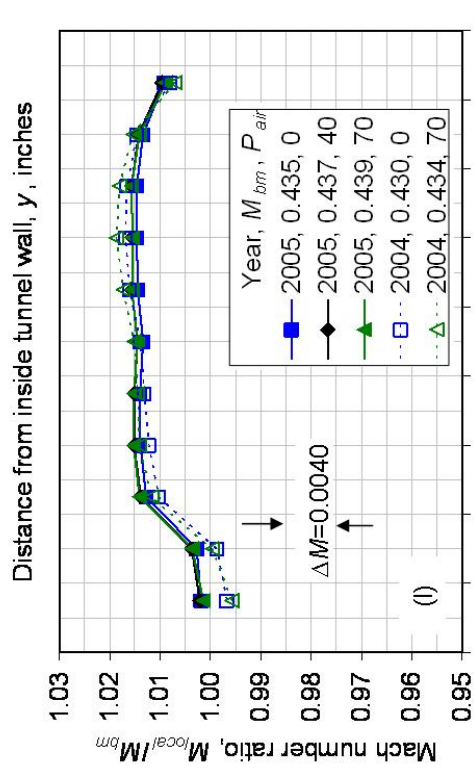
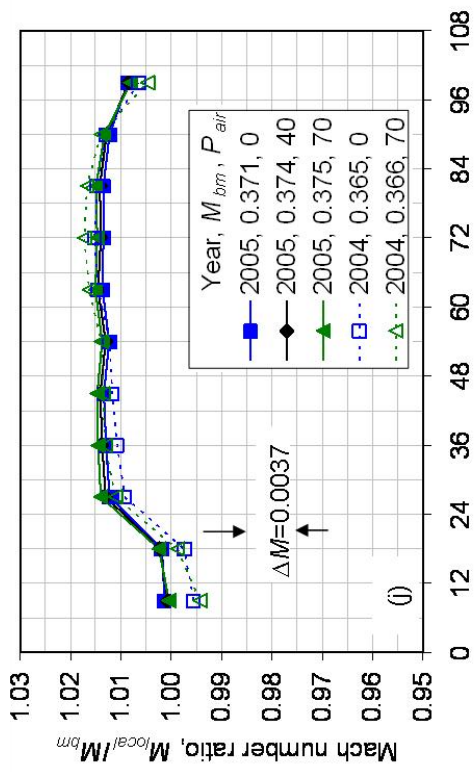


Figure D.3.—Continued. (i)  $M_{nom}=0.336$ ,  $U_{nom}=220$  knots. (j)  $M_{nom}=0.370$ ,  $U_{nom}=240$  knots. (k)  $M_{nom}=0.402$ ,  $U_{nom}=260$  knots. (l)  $M_{nom}=0.435$ ,  $U_{nom}=280$  knots.

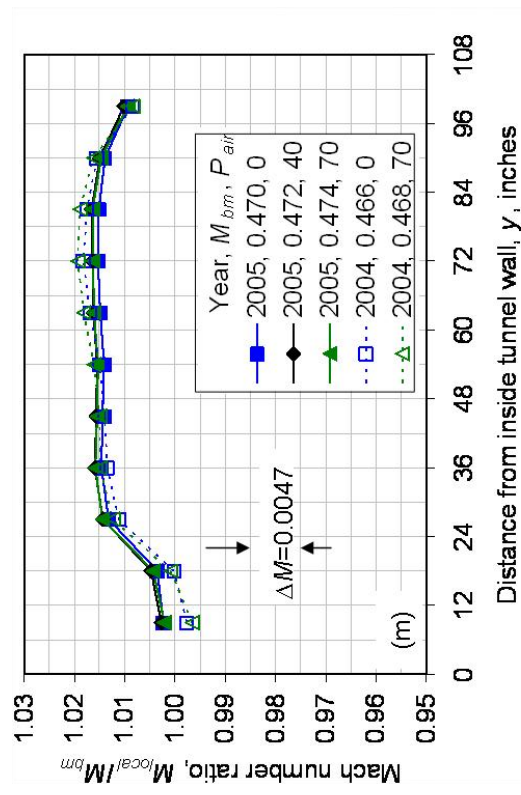


Figure D.3.—Concluded. (m)  $M_{nom} = 0.470$ ,  $U_{nom} = 300$  knots.

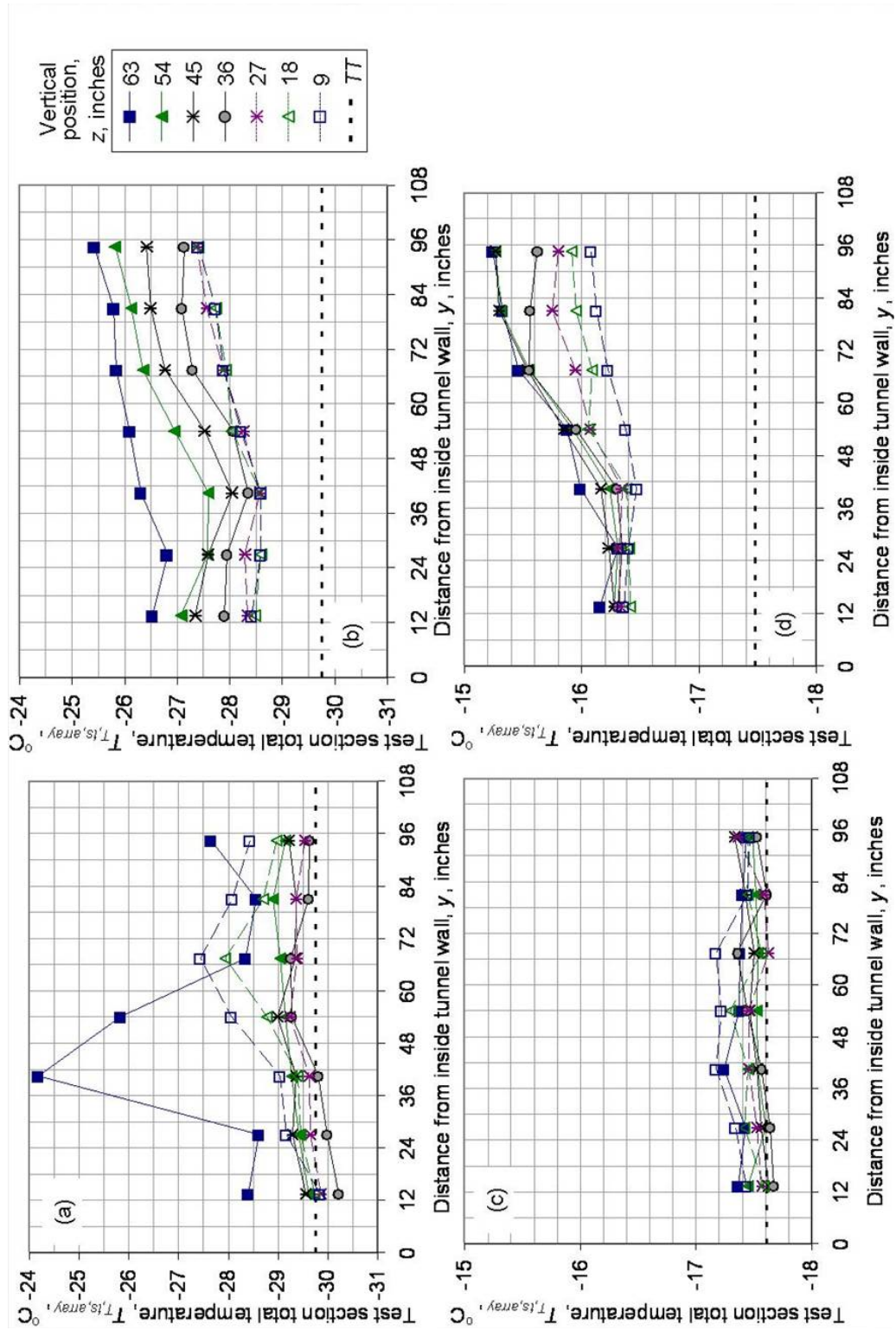


Figure D.4.—IRT test section total temperature distribution data collected using the 2-D RTD Array. (a)  $U_{is}=49.02$  mph (42.6 knots),  $T_{T, \text{avg}}=-29.8$  °C,  $P_{air}=0$  psig. (b)  $U_{is}=55.2$  mph (48.0 knots),  $T_{T, \text{avg}}=-29.8$  °C,  $P_{air}=70$  psig. (c)  $U_{is}=49.14$  mph (42.7 knots),  $T_{T, \text{avg}}=-17.6$  °C,  $P_{air}=0$  psig. (d)  $U_{is}=54.89$  mph (47.7 knots),  $T_{T, \text{avg}}=-17.5$  °C,  $P_{air}=70$  psig.

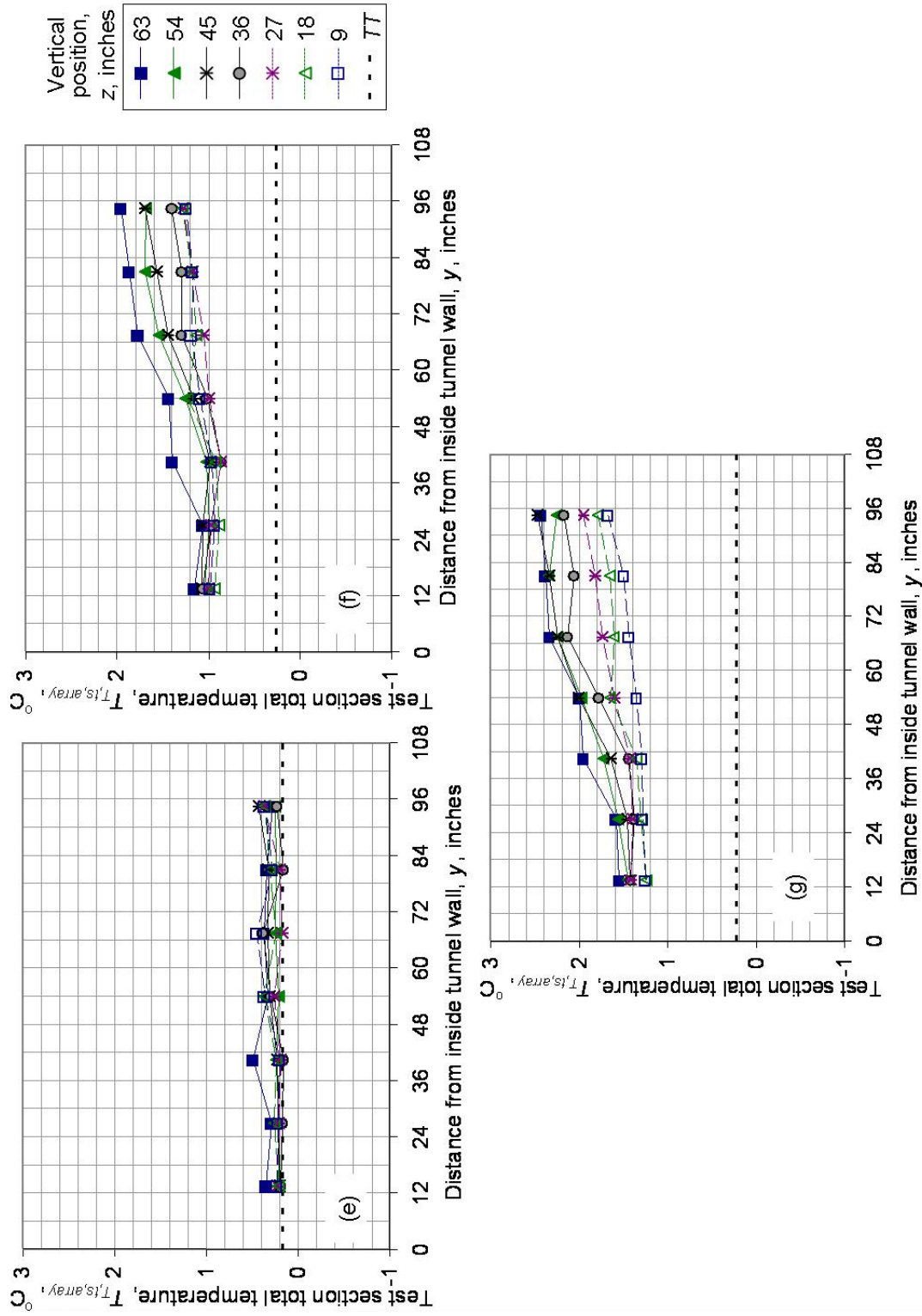


Figure D.4.—Continued. (e)  $U_{is}=49.71$  mph (43.2 knots),  $T_{T,devg}=0.2$  °C,  $P_{air}=70$  psig. (f)  $U_{is}=49.94$  mph (43.4 knots),  $T_{T,devg}=0.3$  °C,  $P_{air}=40$  psig. (g)  $U_{is}=49.59$  mph (43.1 knots),  $T_{T,devg}=0.2$  °C,  $P_{air}=70$  psig.

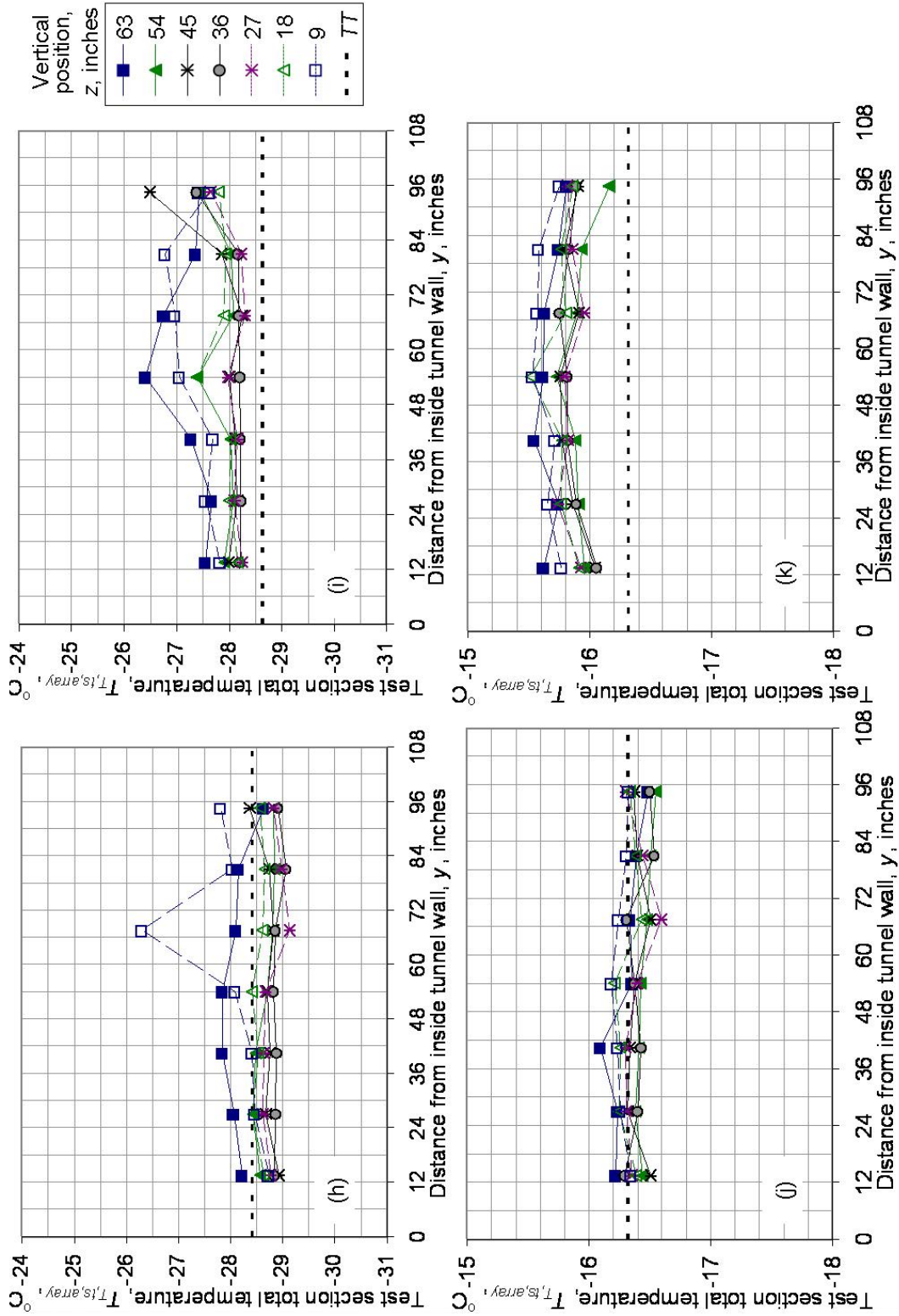


Figure D.4.—Continued. (h)  $U_{ts}=116.46$  mph (101.2 knots),  $T_{T, avg}=-28.4$  °C,  $P_{air}=0$  psig. (i)  $U_{ts}=116.46$  mph (101.2 knots),  $T_{T, avg}=-16.3$  °C,  $P_{air}=0$  psig. (j)  $U_{ts}=118.76$  mph (103.2 knots),  $T_{T, avg}=-28.4$  °C,  $P_{air}=70$  psig. (k)  $U_{ts}=118.30$  mph (102.8 knots),  $T_{T, avg}=-16.3$  °C,  $P_{air}=70$  psig.

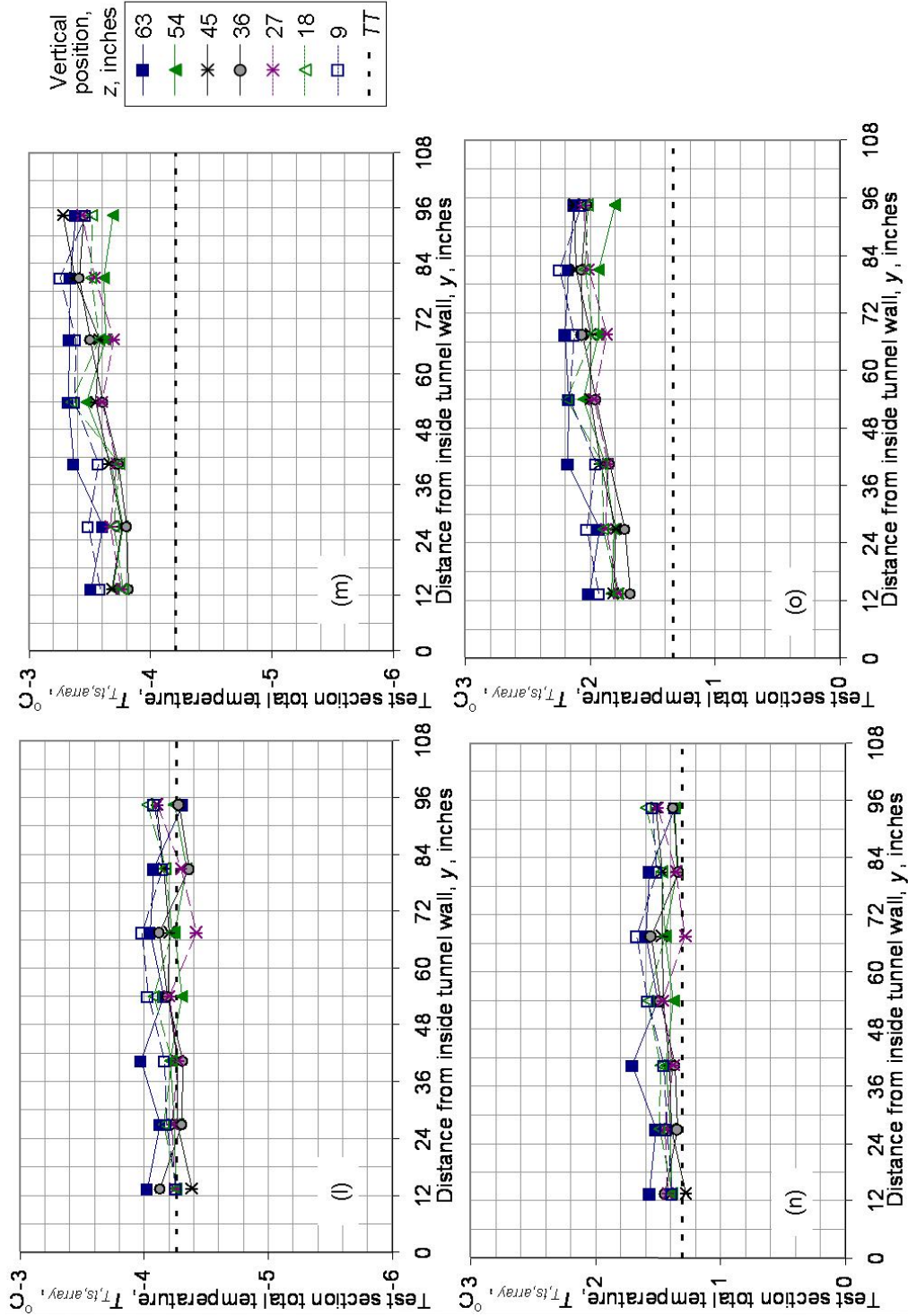


Figure D.4.—Continued. (l)  $U_{ts}=116.57$  mph (101.3 knots),  $T_{T,davg}=-4.3$  °C,  $P_{air}=0$  psig. (m)  $U_{ts}=116.80$  mph (101.5 knots),  $T_{T,davg}=-4.2$  °C,  $P_{air}=70$  psig. (n)  $U_{ts}=116.34$  mph (101.1 knots),  $T_{T,davg}=1.3$  °C,  $P_{air}=0$  psig. (o)  $U_{ts}=116.34$  mph (101.1 knots),  $T_{T,davg}=1.3$  °C,  $P_{air}=70$  psig.

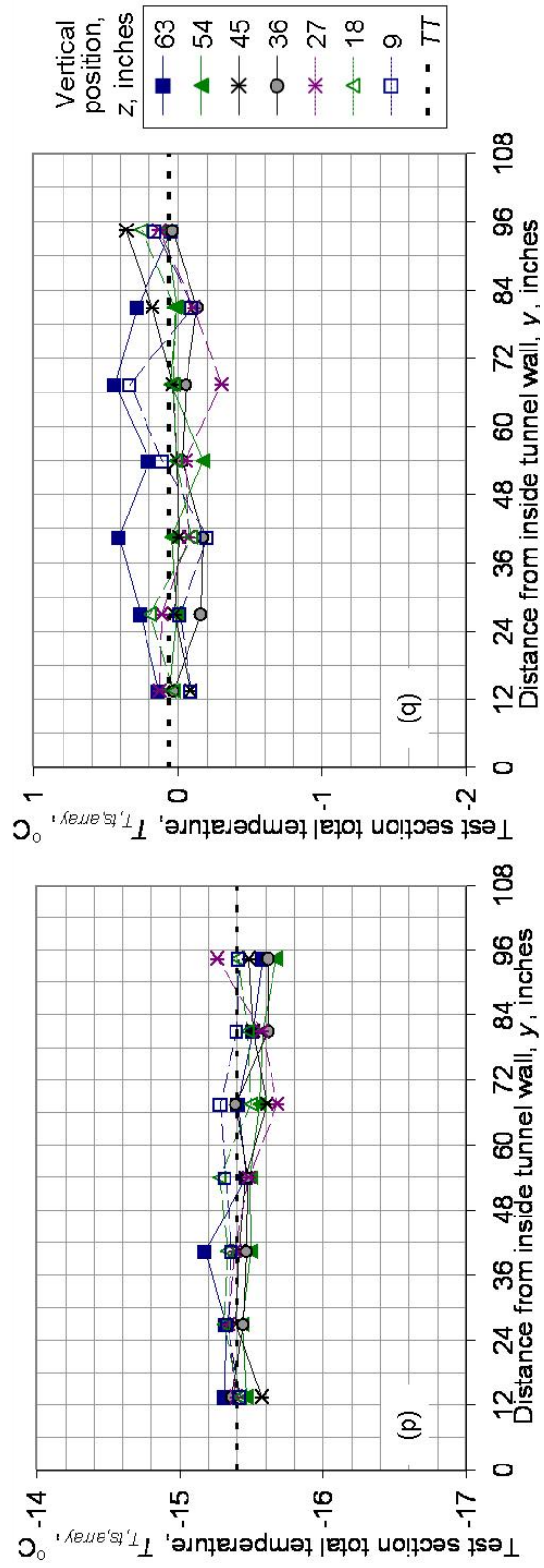


Figure D.4.—Continued. (p)  $U_{ts}=151.91$  mph (132.01 knots),  $T_{T,davg}=-15.4$  °C,  $P_{air}=0$  psig. (q)  $U_{ts}=174.53$  mph (151.6 knots),  $T_{T,davg}=0.06$  °C,  $P_{air}=0$  psig.

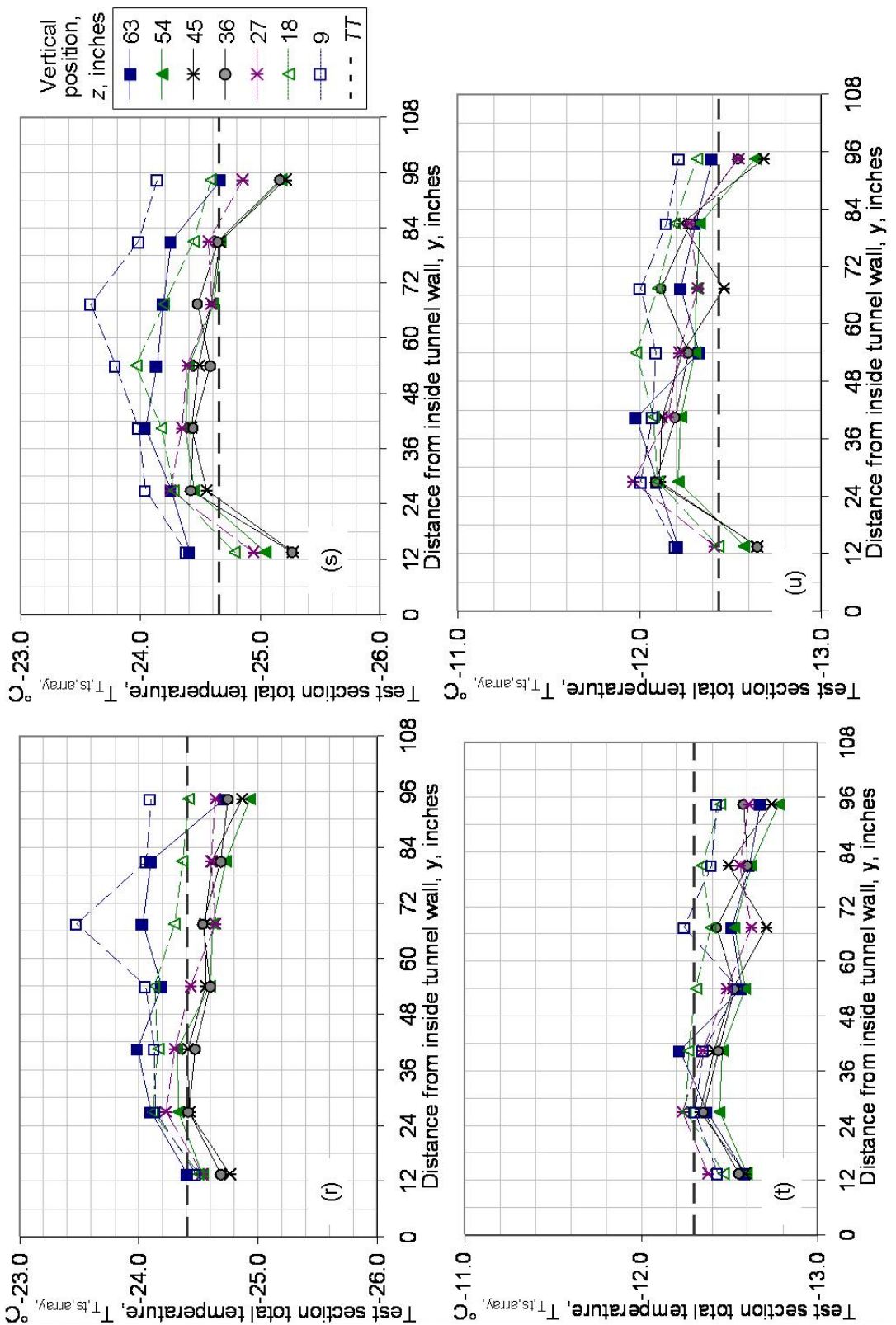


Figure D.4.—Continued. (r)  $U_{ts}=233.38$  mph (202.8 knots),  $T_{T,devg}=-24.4$  °C,  $P_{air}=0$  psig. (s)  $U_{ts}=233.61$  mph (203.0 knots),  $T_{T,devg}=-24.7$  °C,  $P_{air}=70$  psig. (t)  $U_{ts}=235.10$  mph (204.3 knots),  $T_{T,devg}=-12.3$  °C,  $P_{air}=0$  psig. (u)  $U_{ts}=234.87$  mph (204.1 knots),  $T_{T,devg}=-12.4$  °C,  $P_{air}=70$  psig.

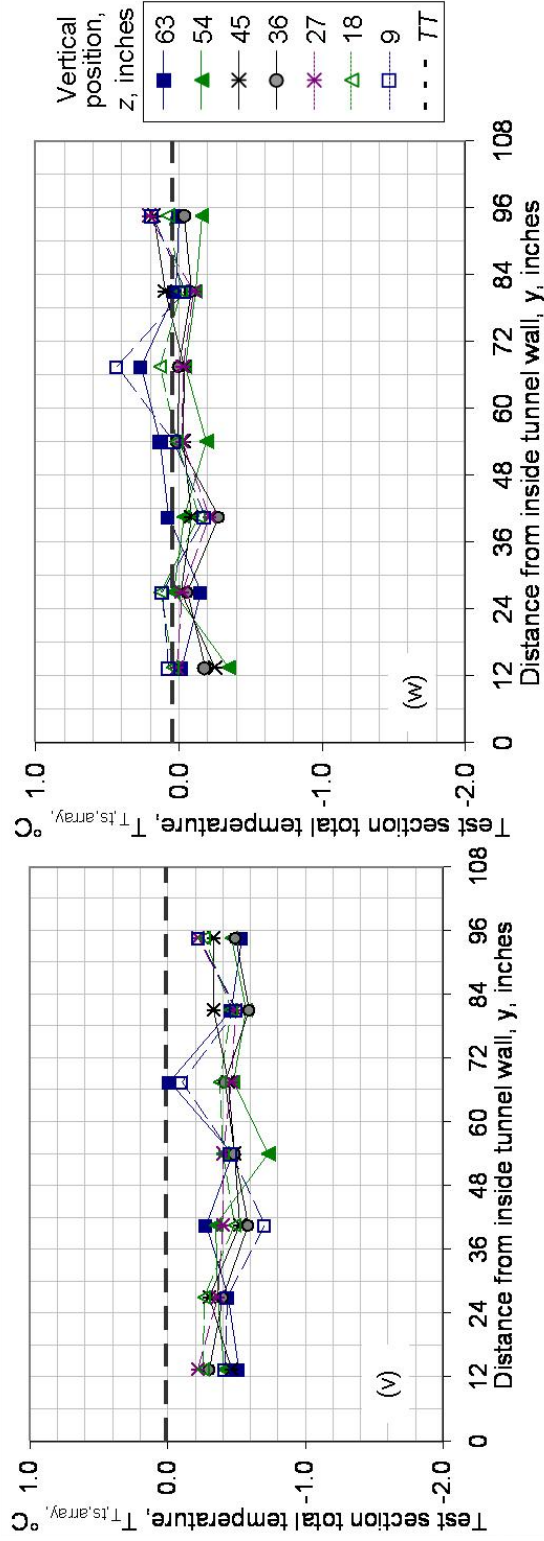


Figure D.4.—Continued. (v)  $U_{is}=230.5$  mph (200.3 knots),  $T_{T,devg}=0.0$  °C,  $P_{air}=0$  psig. (w)  $U_{is}=231.19$  mph (200.9 knots),  $T_{T,devg}=0.0$  °C,  $P_{air}=70$  psig.

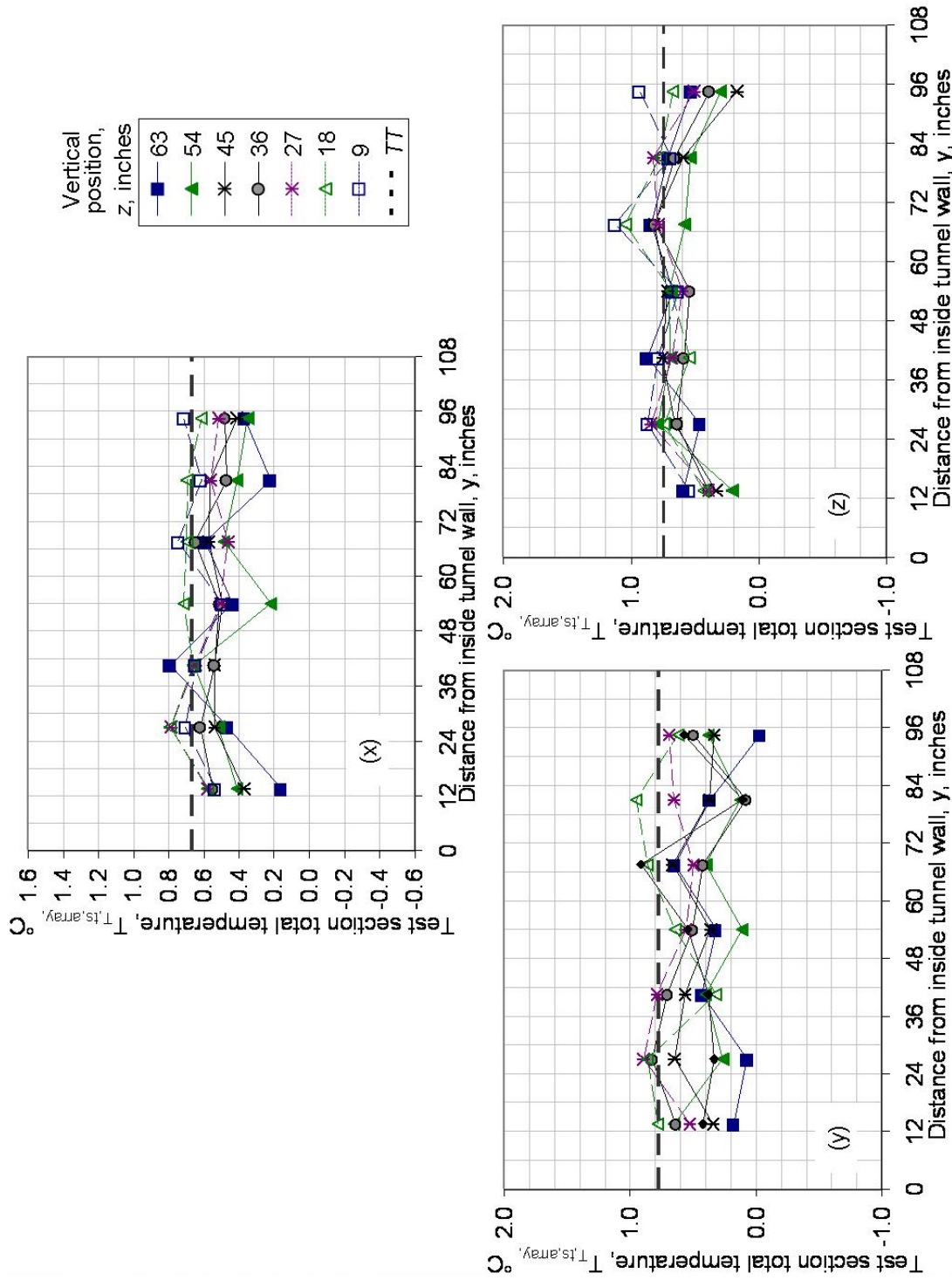


Figure D.4.—Continued. (x)  $U_{ts}=253.11$  mph (219.95 knots),  $T_{r,davg}=0.67$  °C,  $P_{air}=0$  psig. (y)  $U_{ts}=292.07$  mph (253.8 knots),  $T_{r,davg}=0.8$  °C,  $P_{air}=0$  psig. (z)  $U_{ts}=291.61$  mph (253.4 knots),  $T_{r,davg}=0.7$  °C,  $P_{air}=70$  psig.

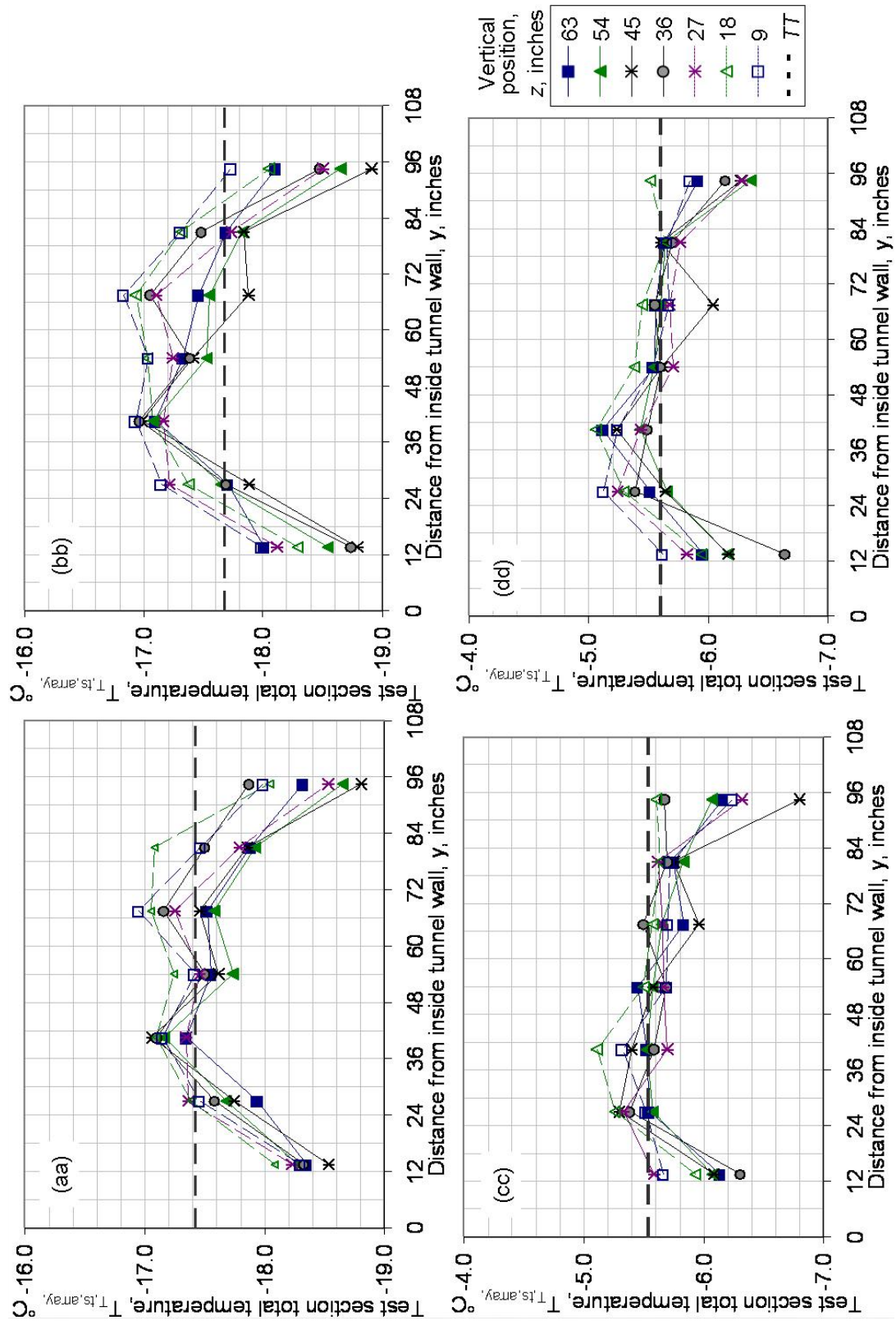


Figure D.4.—Concluded. (aa)  $U_{is}=338.33$  mph (294.0 knots),  $T_{T,davg}=-17.4$  °C,  $P_{air}=0$  psig. (bb)  $U_{is}=338.1$  mph (293.8 knots),  $T_{T,davg}=-17.7$  °C,  $P_{air}=70$  psig. (cc)  $U_{is}=338.9$  mph (294.5 knots),  $T_{T,davg}=-5.5$  °C,  $P_{air}=0$  psig. (dd)  $U_{is}=339.6$  mph (295.1 knots),  $T_{T,davg}=-5.6$  °C,  $P_{air}=70$  psig.

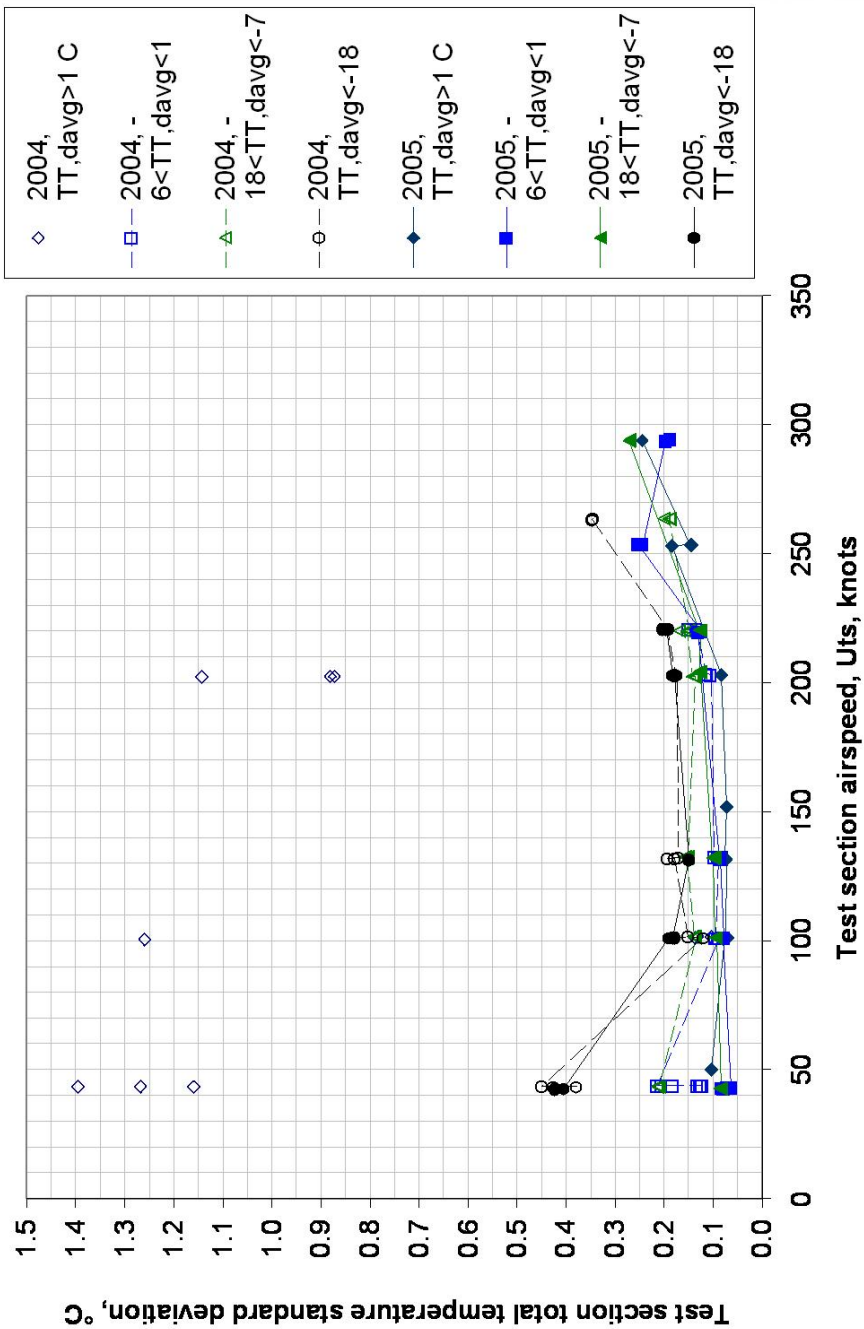


Figure D.5.—IRT test section total temperature standard deviation data collected using the 2-D RTD Array at the center line of the RTD Array.

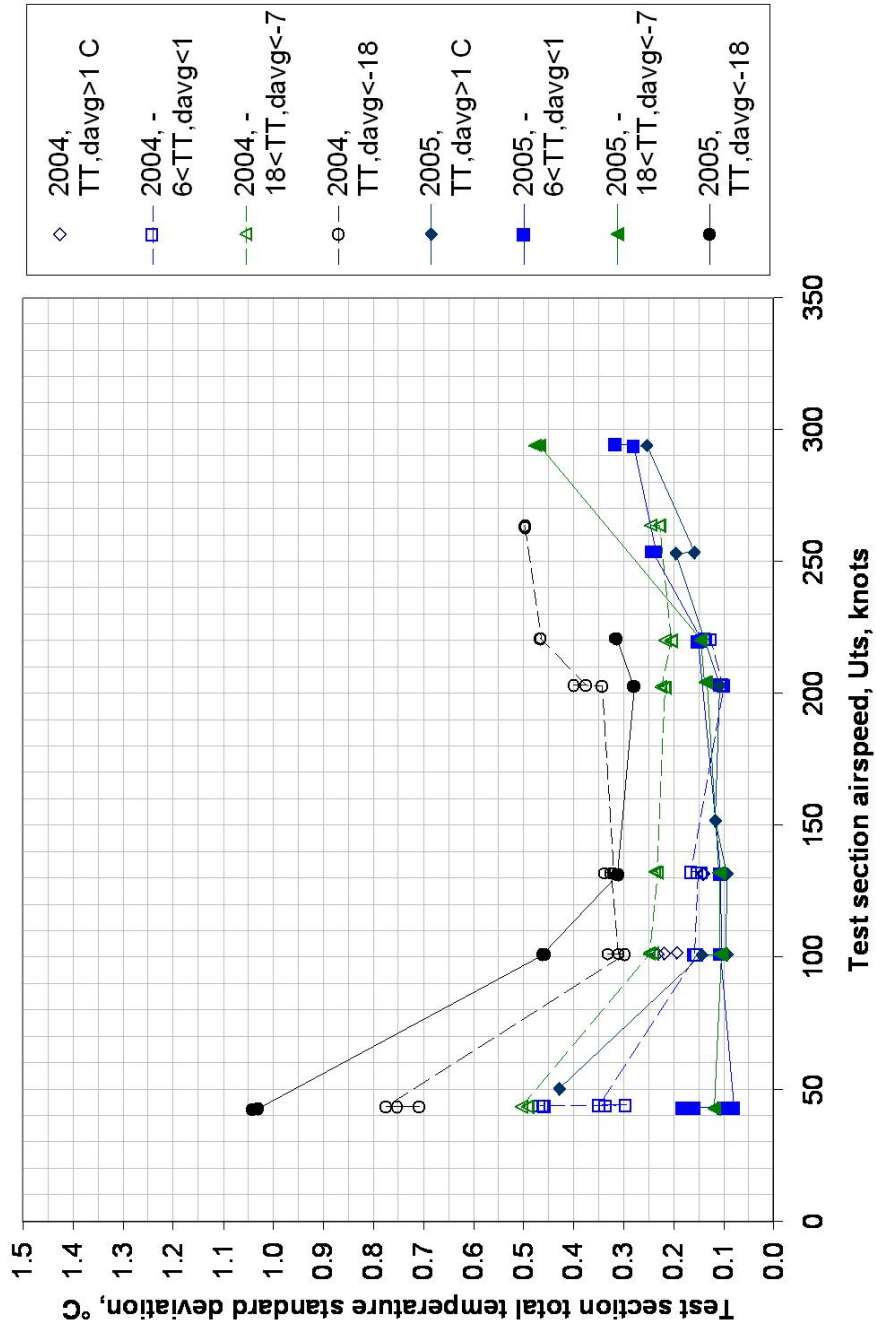


Figure D.5.—Concluded. IRT test section total temperature standard deviation data collected using the 2-D RTD Array for the full RTD Array.

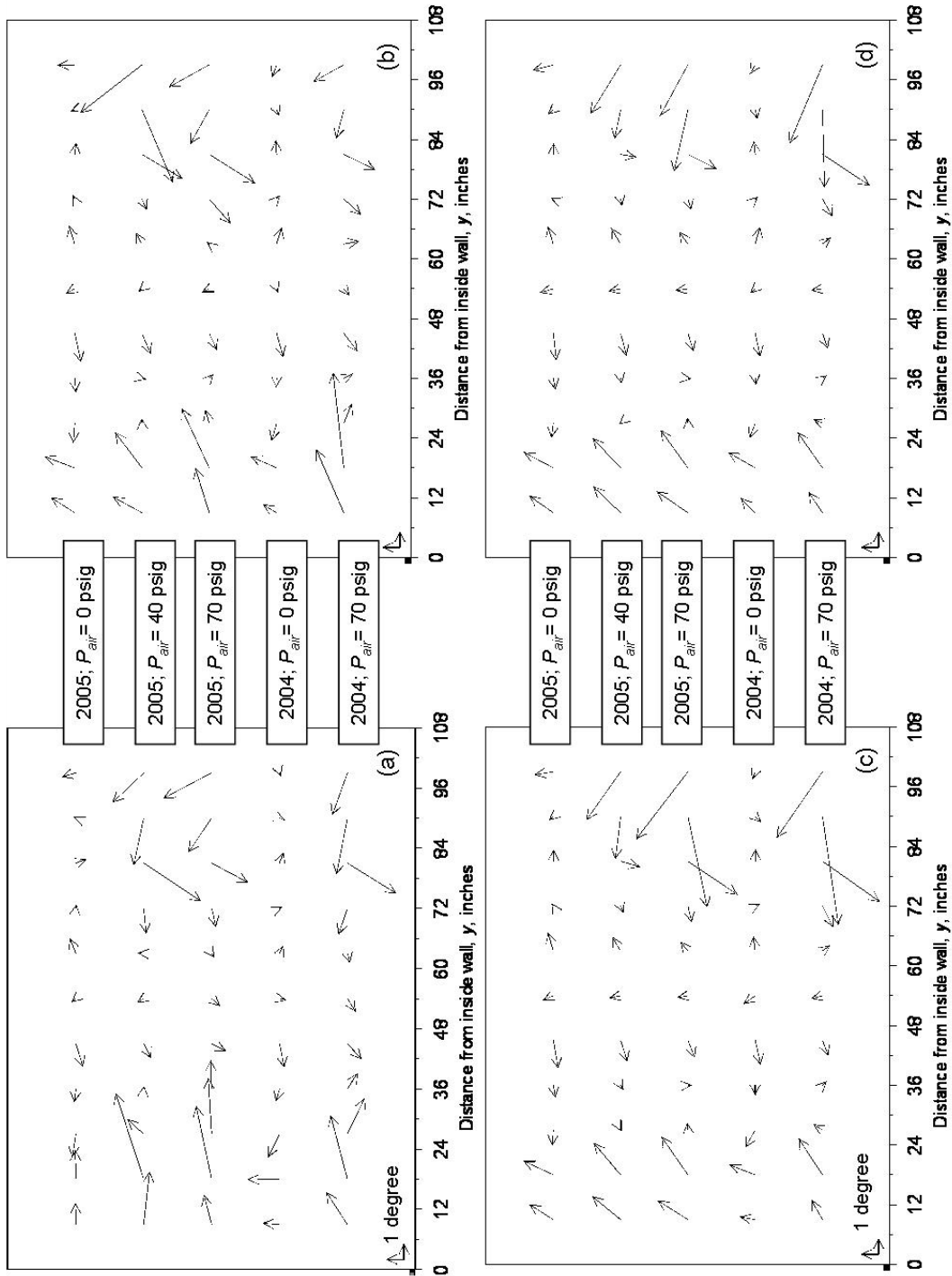


Figure D.6.—Comparison of test section centerline flow angularity vectors from the 2004 full calibration and 2005 interim calibration at various  $P_{air}$  settings. (a)  $M_{nom} = 0.066$ ,  $V_{nom} = 43$  knots. (b)  $M_{nom} = 0.100$ ,  $V_{nom} = 65$  knots. (c)  $M_{nom} = 0.133$ ,  $V_{nom} = 87$  knots. (d)  $M_{nom} = 0.152$ ,  $V_{nom} = 100$  knots.

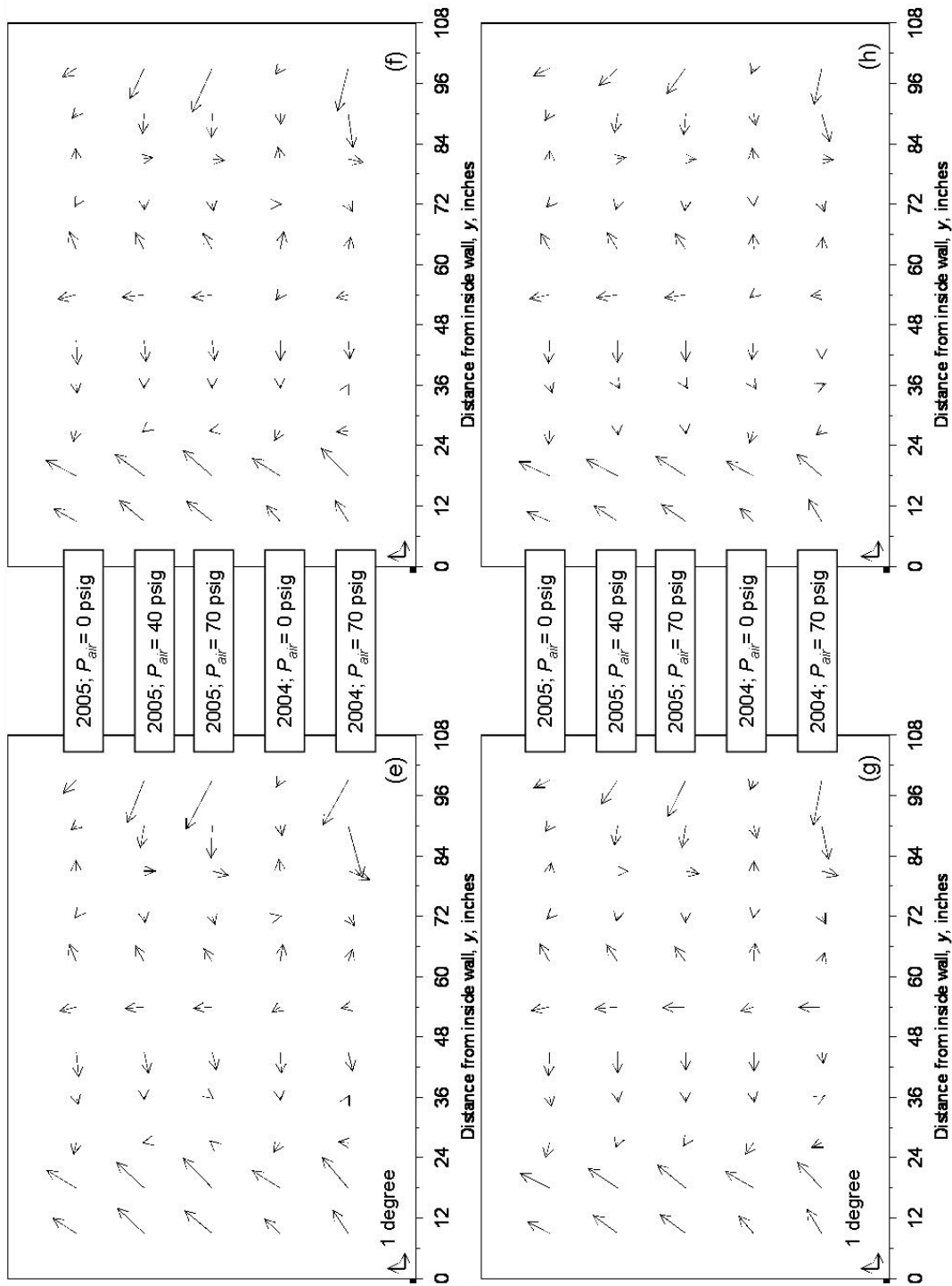


Figure D.6.—Continued. (e)  $M_{nom} = 0.200$ ,  $V_{nom} = 130$  knots. (f)  $M_{nom} = 0.234$ ,  $V_{nom} = 150$  knots. (g)  $M_{nom} = 0.266$ ,  $V_{nom} = 178$  knots. (h)  $M_{nom} = 0.306$ ,  $V_{nom} = 200$  knots.

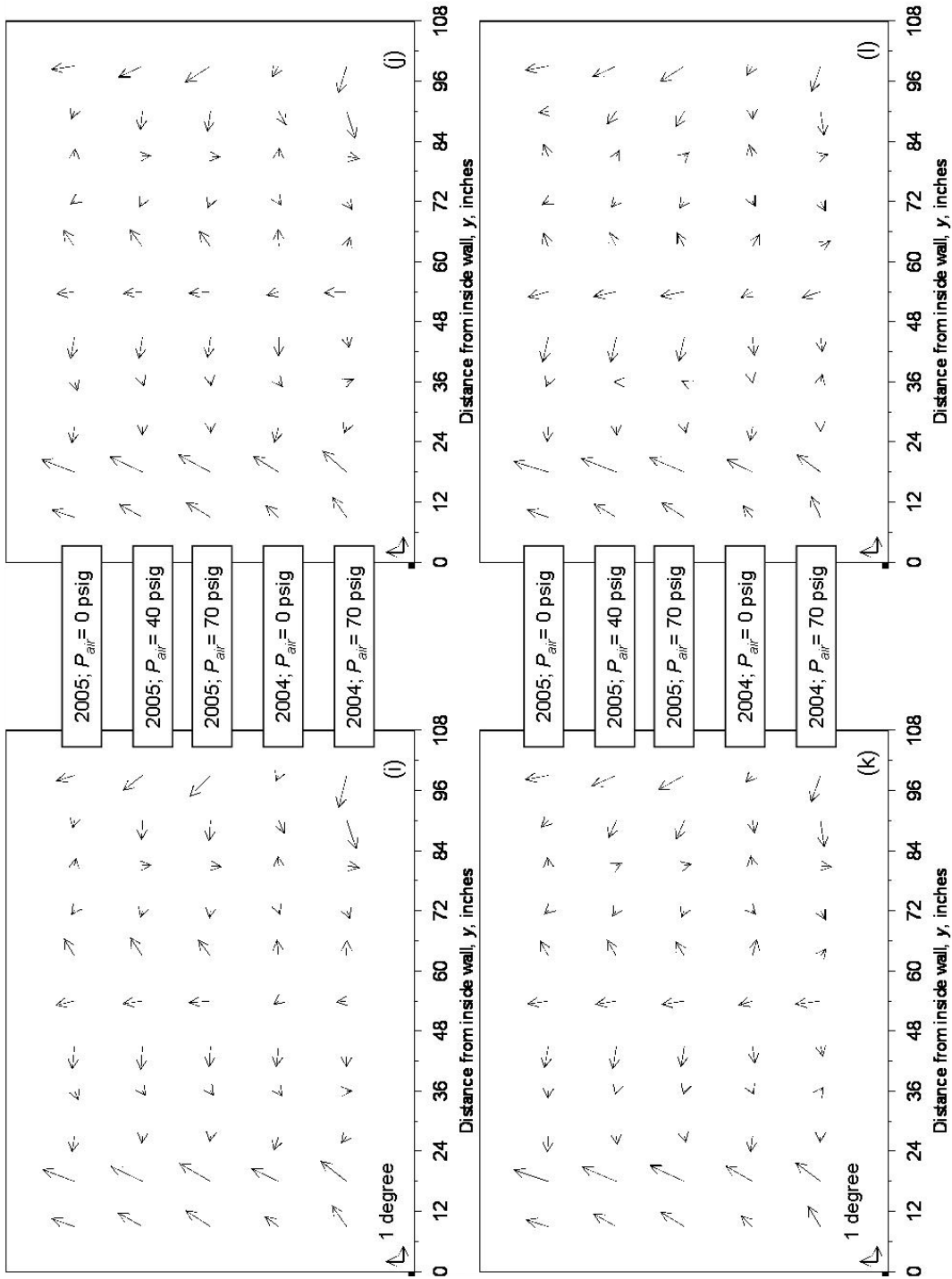


Figure D.6.—Continued. (i)  $M_{nom} = 0.336$ ,  $V_{nom} = 220$  knots. (j)  $M_{nom} = 0.370$ ,  $V_{nom} = 240$  knots. (k)  $M_{nom} = 0.402$ ,  $V_{nom} = 260$  knots. (l)  $M_{nom} = 0.435$ ,  $V_{nom} = 280$  knots.

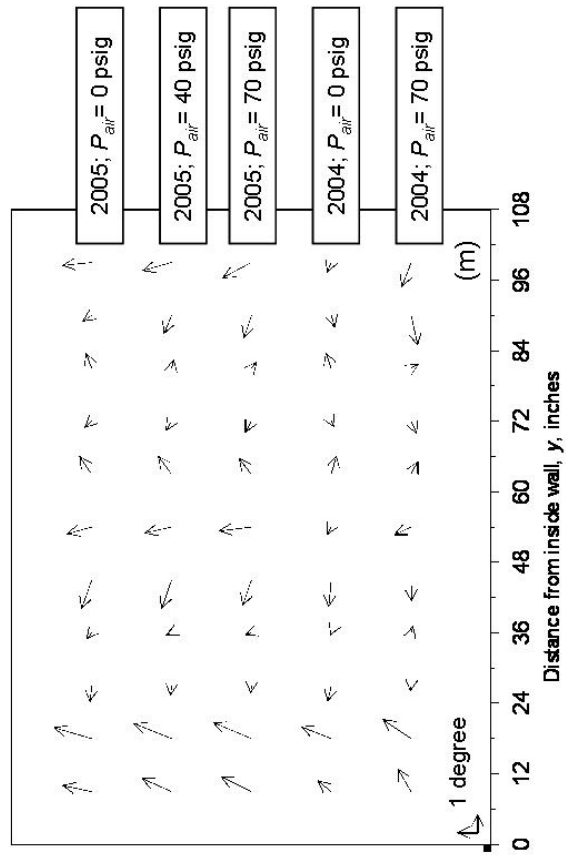


Figure D.6.—Concluded. (m)  $M_{nom} = 0.470$ ,  $V_{nom} = 300$  knots.

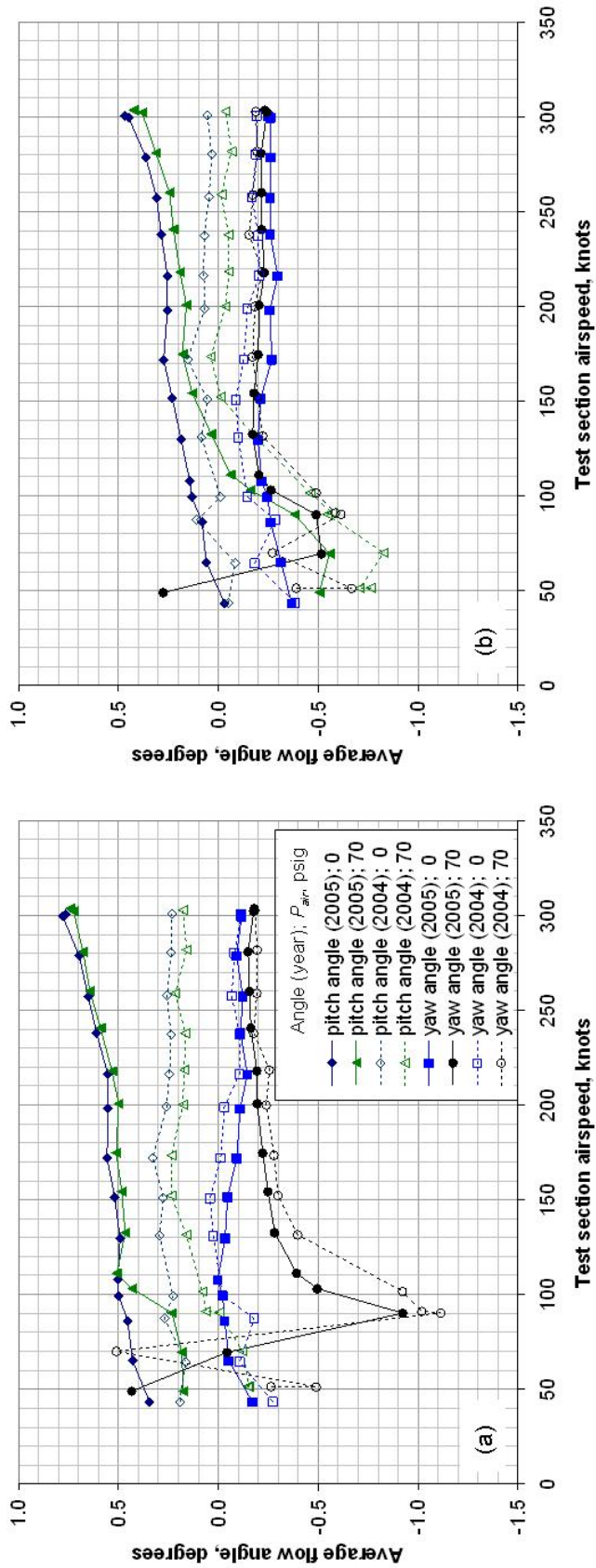


Figure D.7.—Comparison of average data from flow angularity measurements made in the IRT test section (horizontal survey at centerline) during the 2004 and 2005 test entries. (a) Full-span data (all eleven probes included). (b) Core data (center seven probes only).

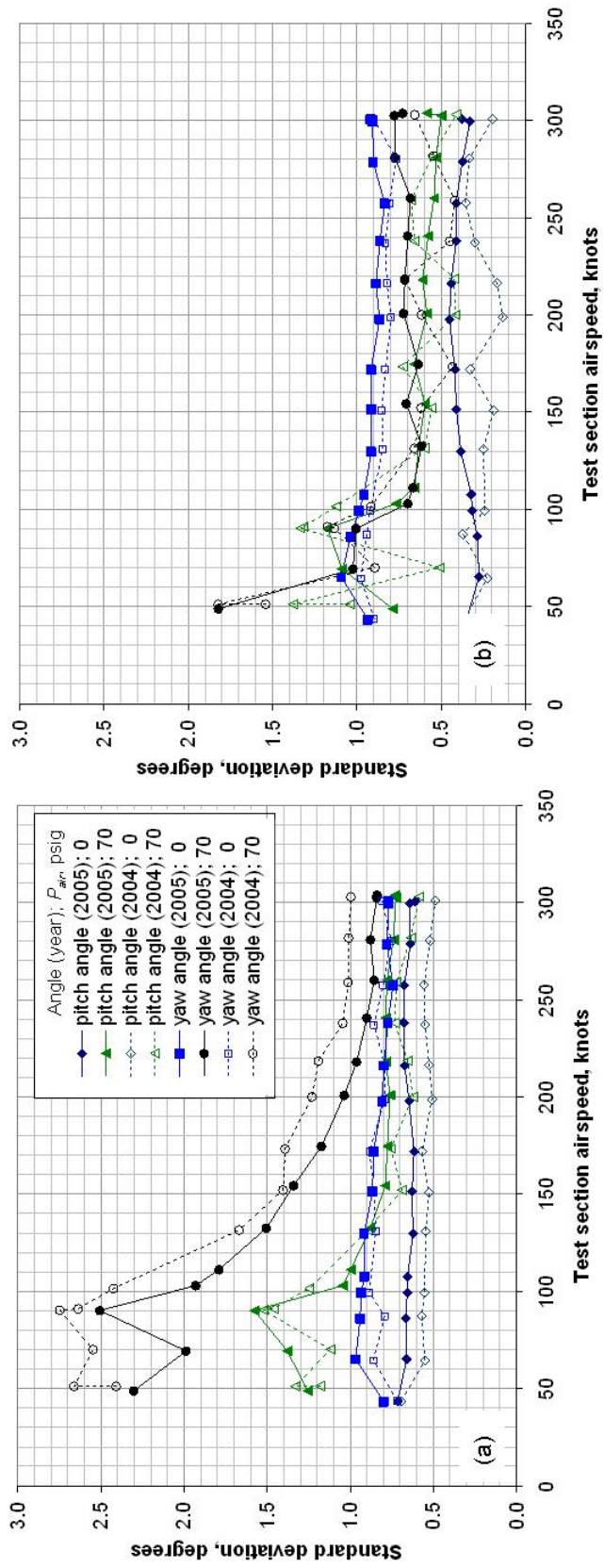


Figure D.8.—Comparison of standard deviation data from flow angularity measurements made in the IRT test section (horizontal survey at centerline) during the 2004 and 2005 test entries. (a) Full-span data (all eleven probes included). (b) Core data (center seven probes only).

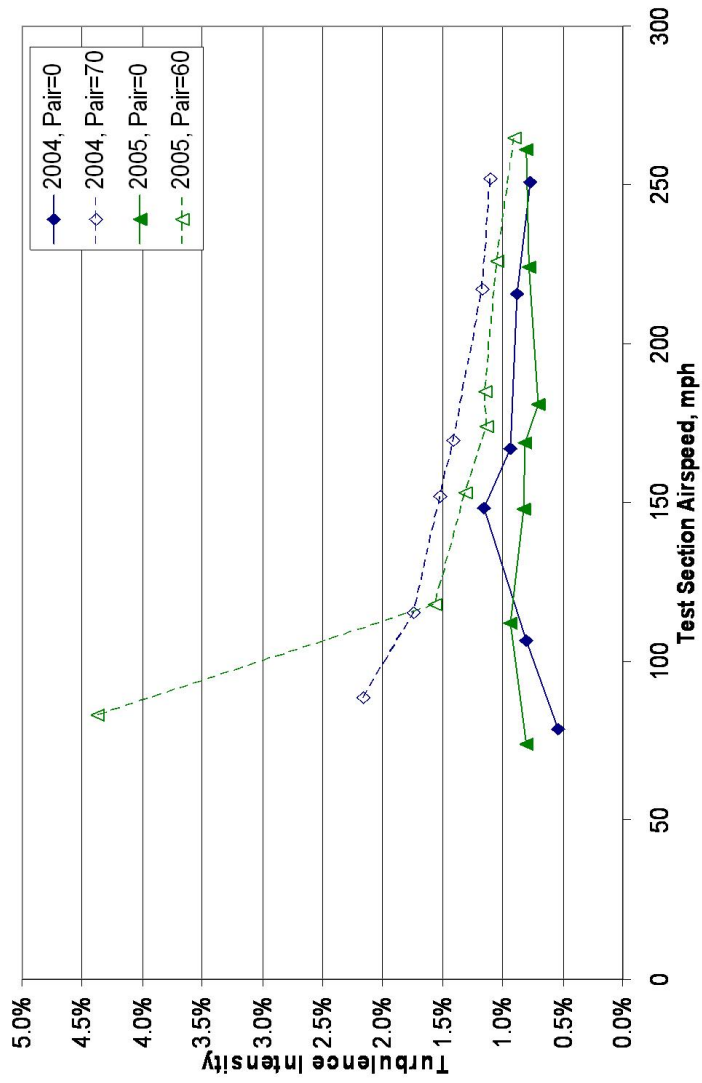


Figure D.9.—Comparison of 2004 and 2005 turbulence data (horizontal survey at centerline).

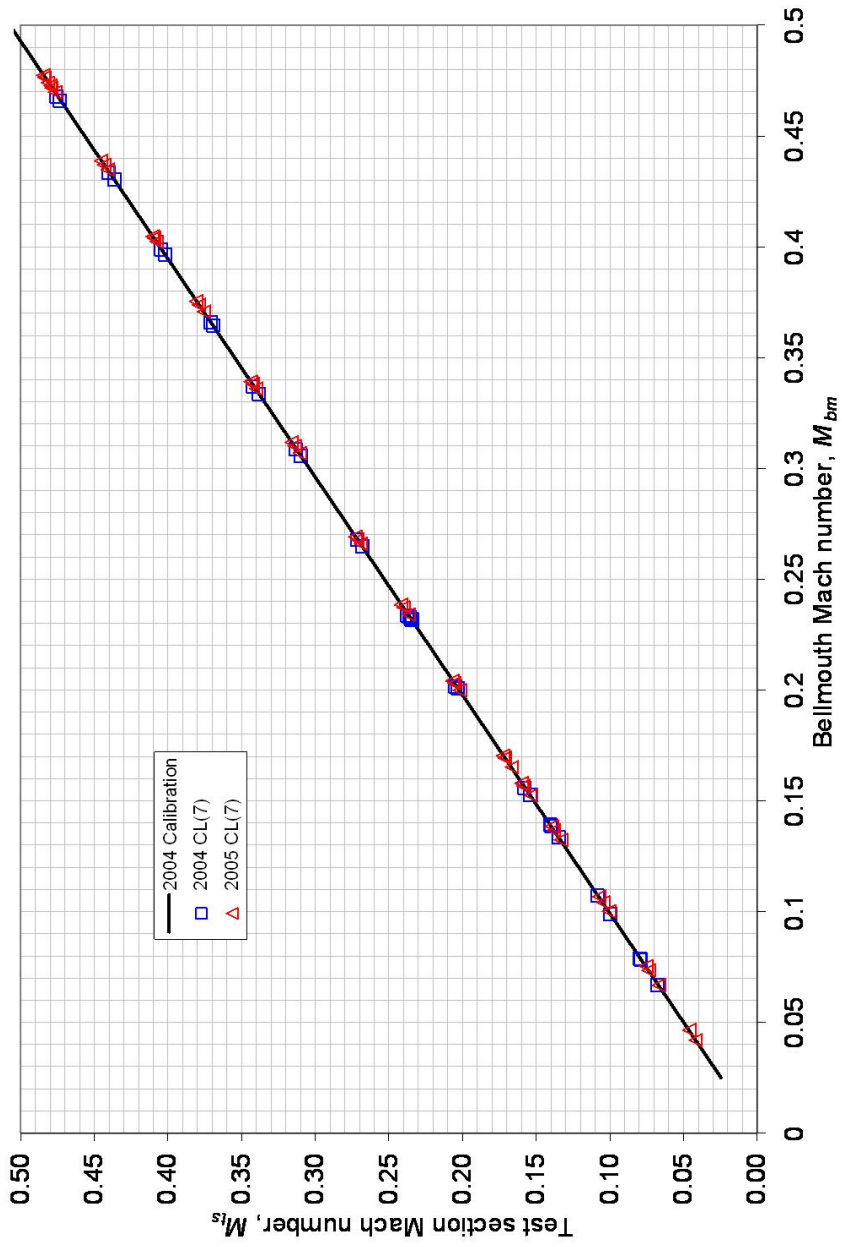


Figure D.10.—Comparison of the aero-thermal calibration curves created based on the 2004 and 2005 test results.  
 (a): Mach number calibration curve comparison with 2004 and 2005 test data.

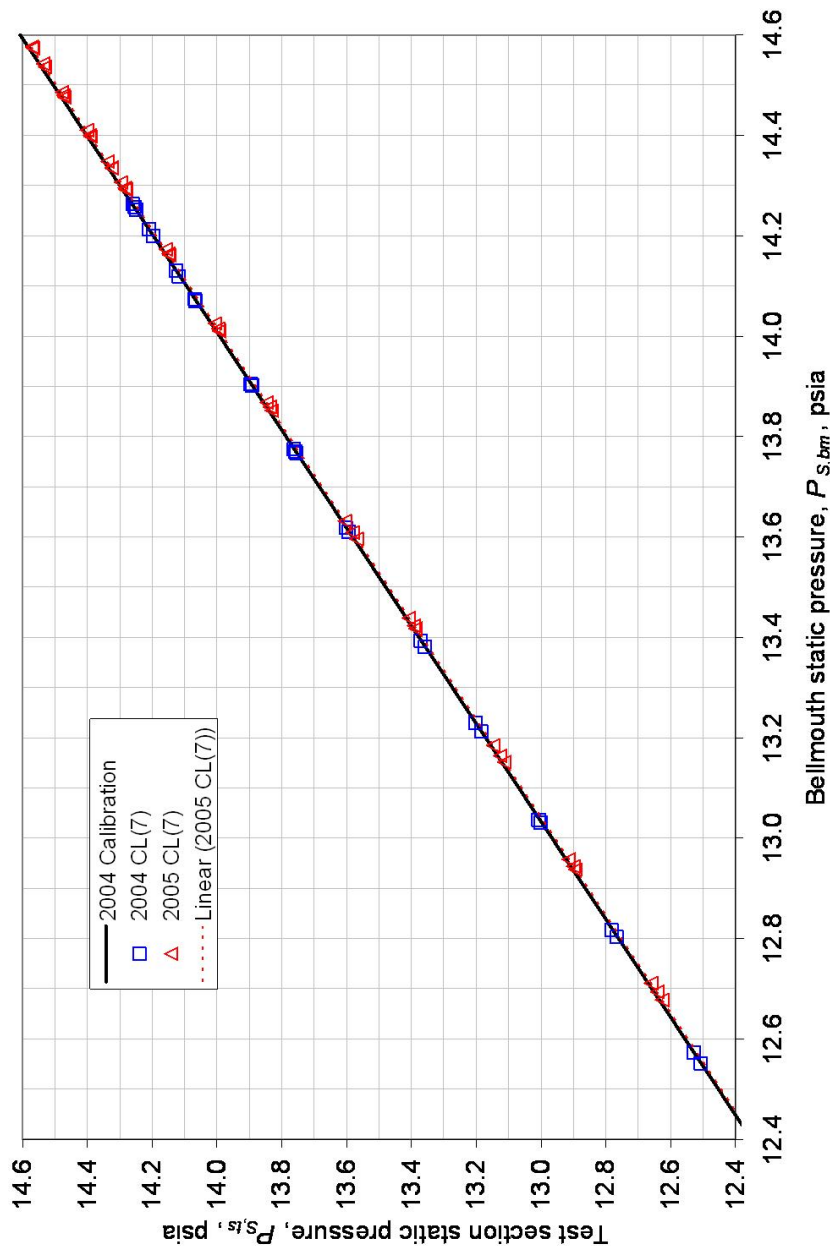


Figure D.10.—Continued. (b) Static Pressure calibration curves for the IRT based on the 2004 and 2005 calibration data.

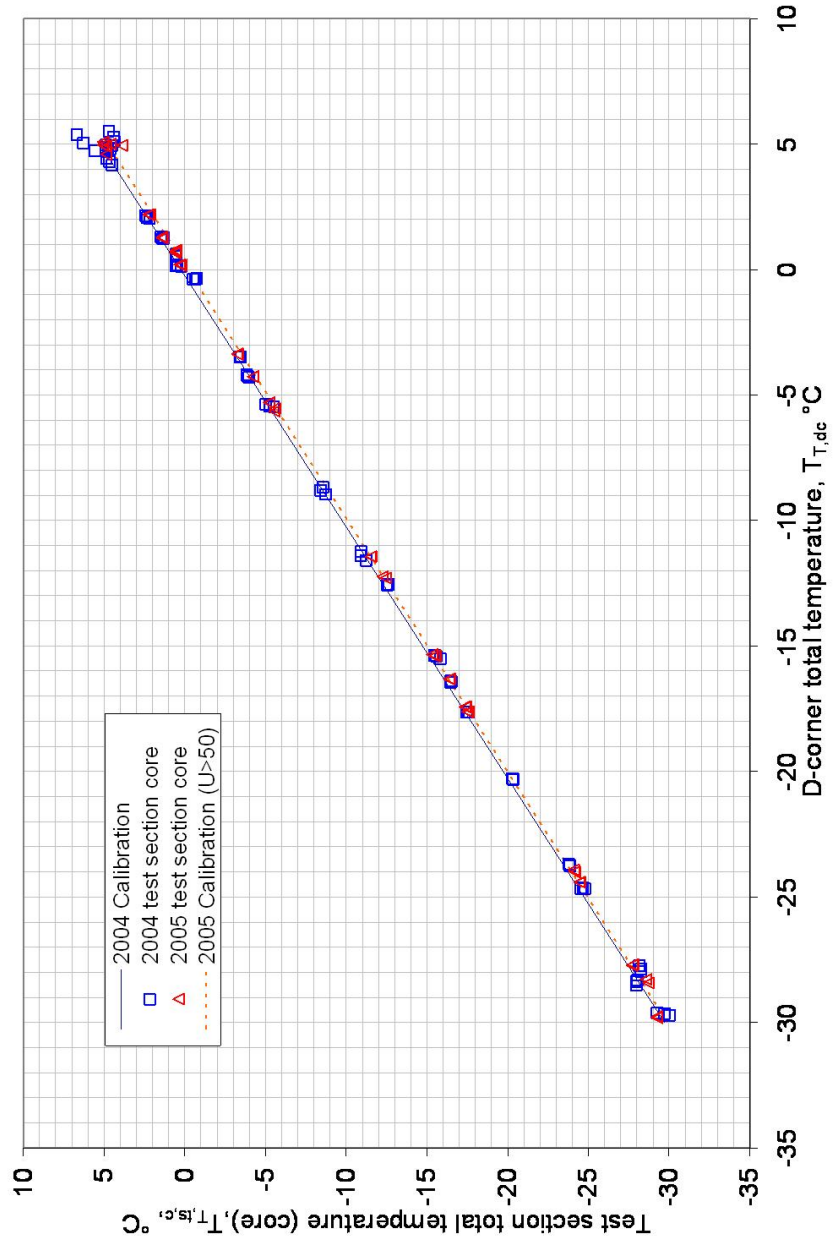


Figure D.10.—Concluded. (c) Total temperature calibration curves for the IRT based on the 2004 and 2005 calibration data.

## References

1. "Calibration and Acceptance of Icing Wind Tunnels," SAE Standards ARP5905, 2003.
2. "Calibration of Subsonic and Transonic Wind Tunnels," AIAA Recommended Practice R-093-2003, 2003.
3. Arrington, E.A. and Gonzalez, J.C., "Improvements to the Total Temperature Calibration of the NASA Glenn Icing Research Tunnel," NASA/CR-2005-213875, AIAA-2005-4276.
4. Gonzalez, J.C., Arrington, E.A., and Curry III, M.R., "Aero-Thermal Calibration of the NASA Glenn Icing Research Tunnel (2000 Tests)," NASA/CR-2001-210685, AIAA-2001-0233, 2001.
5. Leary, William M., "We Freeze to Please: A History of NASA's Icing Research Tunnel and the Quest for Flight Safety," NASA/SP-2002-4226, 2002.
6. Irvine, T.B., Kevdžija, S.L., Sheldon, D.W. and Spera, D.A., "Overview of the Icing and Flow Quality Improvements Program for the NASA Glenn Icing Research Tunnel," AIAA-2001-0229, 2001.
7. Soeder, R.H., Sheldon, D.W., Ide, R.F., Spera, D.A. and Andracchio, C.R., "NASA Glenn Icing Research Tunnel User Manual," NASA/TM-2003-212004, 2003.
8. Gonzalez, J.C., Arrington, E.A., "Five-Hole Flow Angle Probe Calibration for the NASA Glenn Icing Research Tunnel," NASA/CR-1999-202330, AIAA-96-2201, 1999.
9. Ames Aeronautical Laboratory: "Equations, Tables and Charts for Compressible Flow," NASA TR-1135 (NASA TN-1428), 1953.
10. Gonzalez, J.C., and Arrington, E.A., "Aerodynamic Calibration of the NASA Lewis Icing Research Tunnel (1997 Tests)," NASA/CR-2001-210809, AIAA-98-0633, 2001.
11. Bruun, H.H.: Hot-Wire Anemometry, Principles and Signal Analysis, Oxford University Press, 1999.
12. Assessment of Experimental Uncertainty with Application to Wind Tunnel Testing. Reston, VA, American Institute of Aeronautics and Astronautics, 1999. AIAA S-071A-1999.
13. Assessing Experimental Uncertainty - Supplement to AIAA S-071A-1999. Reston, VA, American Institute of Aeronautics and Astronautics, 2003. AIAA G-045-2003.
14. Coleman, H.W. and Steele, W.G. Experimentation and Uncertainty Analysis for Engineers. New York, Wiley, 1989.

REPORT DOCUMENTATION PAGE			Form Approved OMB No. 0704-0188		
<p>The public reporting burden for this collection of information is estimated to average 1 hour per response, including the time for reviewing instructions, searching existing data sources, gathering and maintaining the data needed, and completing and reviewing the collection of information. Send comments regarding this burden estimate or any other aspect of this collection of information, including suggestions for reducing this burden, to Department of Defense, Washington Headquarters Services, Directorate for Information Operations and Reports (0704-0188), 1215 Jefferson Davis Highway, Suite 1204, Arlington, VA 22202-4302. Respondents should be aware that notwithstanding any other provision of law, no person shall be subject to any penalty for failing to comply with a collection of information if it does not display a currently valid OMB control number.</p> <p>PLEASE DO NOT RETURN YOUR FORM TO THE ABOVE ADDRESS.</p>					
<b>1. REPORT DATE (DD-MM-YYYY)</b> 01-07-2010		<b>2. REPORT TYPE</b> Final Contractor Report		<b>3. DATES COVERED (From - To)</b>	
<b>4. TITLE AND SUBTITLE</b> Aero-Thermal Calibration of the NASA Glenn Icing Research Tunnel (2004 and 2005 Tests)			<b>5a. CONTRACT NUMBER</b> NAS3-00145; NNC05CA95C		
			<b>5b. GRANT NUMBER</b>		
			<b>5c. PROGRAM ELEMENT NUMBER</b>		
<b>6. AUTHOR(S)</b> Arrington, E., Allen; Pastor, Christine, M.; Gonzalez, Jose, C.; Curry, Monroe, R., III			<b>5d. PROJECT NUMBER</b>		
			<b>5e. TASK NUMBER</b>		
			<b>5f. WORK UNIT NUMBER</b> WBS 122711.03.07.03.02		
<b>7. PERFORMING ORGANIZATION NAME(S) AND ADDRESS(ES)</b> Sierra Lobo, Inc. Cleveland, Ohio 44135			<b>8. PERFORMING ORGANIZATION REPORT NUMBER</b> E-17310		
<b>9. SPONSORING/MONITORING AGENCY NAME(S) AND ADDRESS(ES)</b> National Aeronautics and Space Administration Washington, DC 20546-0001			<b>10. SPONSORING/MONITOR'S ACRONYM(S)</b> NASA		
			<b>11. SPONSORING/MONITORING REPORT NUMBER</b> NASA/CR-2010-216733		
<b>12. DISTRIBUTION/AVAILABILITY STATEMENT</b> Unclassified-Unlimited Subject Category: 09 Available electronically at <a href="http://gltrs.grc.nasa.gov">http://gltrs.grc.nasa.gov</a> This publication is available from the NASA Center for AeroSpace Information, 443-757-5802					
<b>13. SUPPLEMENTARY NOTES</b>					
<b>14. ABSTRACT</b> A full aero-thermal calibration of the NASA Glenn Icing Research Tunnel was completed in 2004 following the replacement of the inlet guide vanes upstream of the tunnel drive system and improvement to the facility total temperature instrumentation. This calibration test provided data used to fully document the aero-thermal flow quality in the IRT test section and to construct calibration curves for the operation of the IRT. The 2004 test was also the first to use the 2-D RTD array, an improved total temperature calibration measurement platform.					
<b>15. SUBJECT TERMS</b> Wind tunnel; Calibration; Flow quality					
<b>16. SECURITY CLASSIFICATION OF:</b>			<b>17. LIMITATION OF ABSTRACT</b>  UU	<b>18. NUMBER OF PAGES</b> 125	<b>19a. NAME OF RESPONSIBLE PERSON</b> STI Help Desk (email:help@sti.nasa.gov)
<b>a. REPORT</b> U	<b>b. ABSTRACT</b> U	<b>c. THIS PAGE</b> U			<b>19b. TELEPHONE NUMBER (include area code)</b> 443-757-5802



